



E-ISSN 2667-5846

EXPERIMED

Volume **14** Issue **3** December 2024

experimed.istanbul.edu.tr



ISTANBUL
UNIVERSITY
PRESS

EXPERIMED

INDEXING AND ABSTRACTING

Web of Science – Emerging Sources Citation Index

Scopus

ULAKBIM TR Index

Web of Science - Biological Abstracts

Web of Science - BIOSIS Previews

Chemical Abstracts Service (CAS)

EBSCO - Central & Eastern European Academic Source

SOBIAD

EXPERIMED

OWNER

Prof. Dr. Gunnur DENİZ

Department of Immunology, Istanbul University, Aziz Sancar Institute of Experimental Medicine, Istanbul, Türkiye

RESPONSIBLE MANAGER

Prof. Dr. Bedia ÇAKMAKOĞLU

Department of Molecular Medicine, Istanbul University, Aziz Sancar Institute of Experimental Medicine, Istanbul, Türkiye

CORRESPONDENCE ADDRESS

Istanbul University, Aziz Sancar Institute of Experimental Medicine,
Vakıf Gureba Avenue, 34093, Çapa, Fatih, Istanbul, Türkiye
Phone: +90 (212) 414 22 29
E-mail: experimed@istanbul.edu.tr

PUBLISHER

Istanbul Üniversitesi Yayınevi / Istanbul University Press
Istanbul University Central Campus,
34452 Beyazıt, Fatih / Istanbul, Türkiye
Phone: +90 (212) 440 00 00

Authors bear responsibility for the content of their published articles.

The publication language of the journal is English.

This is a scholarly, international, peer-reviewed and open-access journal published triannually in April, August and December.

Publication Type: Periodical

EXPERIMED

EDITORIAL MANAGEMENT BOARD

Editor-in-Chief

Prof. Dr. Bedia CAKMAKOGLU

Department of Molecular Medicine, Istanbul University, Aziz Sancar Institute of Experimental Medicine, Istanbul, Türkiye – bedia@istanbul.edu.tr

Co-Editors-in-Chief

Prof. Dr. Umut Can KUCUKSEZER

Department of Immunology, Istanbul University, Aziz Sancar Institute of Experimental Medicine, Istanbul, Türkiye – uksezer@istanbul.edu.tr

Assoc. Prof. Vuslat YILMAZ

Department of Neuroscience, Istanbul University, Aziz Sancar Institute of Experimental Medicine, Istanbul, Türkiye – vuslat.yilmaz@istanbul.edu.tr

Managing Editor

Prof. Dr. Sema Sirma EKMEKCI

Department of Genetics, Istanbul University, Aziz Sancar Institute of Experimental Medicine, Istanbul, Türkiye – sirmasem@istanbul.edu.tr

Editorial Management Board Members

Dr. Canan Aysel ULUSOY

Department of Neuroscience, Istanbul University, Aziz Sancar Institute of Experimental Medicine, Istanbul, Türkiye – canan.ulusoym@istanbul.edu.tr

Dr. Baris ERTUGRUL

Department of Molecular Medicine, Istanbul University, Aziz Sancar Institute of Experimental Medicine, Istanbul, Türkiye – baris.ertugrul@istanbul.edu.tr

Ethical Editor

Prof. Dr. Elif OZKOK

Department of Neuroscience, Istanbul University, Aziz Sancar Institute of Experimental Medicine, Istanbul, Türkiye – eozykok@istanbul.edu.tr

Section Editors

Assoc. Prof. Sinem BIRELLER

Department of Biochemistry, Faculty of Pharmacy, Acıbadem Mehmet Ali Aydınlar University, Istanbul, Türkiye – sinem.bireller@acibadem.edu.tr

Assoc. Prof. Ferda PACAL

Department of Lab Animal Science, Istanbul University, Aziz Sancar Institute of Experimental Medicine, Istanbul, Türkiye – ferda.pacal@istanbul.edu.tr

Assoc. Prof. Ali Cihan TASKIN

Department of Lab Animal Science, Istanbul University, Aziz Sancar Institute of Experimental Medicine, Istanbul, Türkiye – ataskin@istanbul.edu.tr

Assoc. Prof. Dr. Timur Hakan BARAK

Department of Pharmacognosy, Faculty of Pharmacy, Acıbadem Mehmet Ali Aydınlar University, Istanbul, Türkiye - timur.barak@acibadem.edu.tr

Language Editors

Elizabeth Mary EARL

Department of Foreign Languages, Istanbul University, Istanbul, Türkiye – elizabeth.earl@istanbul.edu.tr

Statistics Editor

Sevda OZEL YILDIZ

Department of Biostatistic, Istanbul Medical Faculty, Istanbul University, Istanbul, Türkiye – sevda@istanbul.edu.tr

EXPERIMED

EDITORIAL BOARD

Aziz SANCAR (Honorary Member)

Department of Biochemistry and Biophysics, University of North Carolina School of Medicine, Chapel Hill, North Carolina, USA – aziz_sancar@med.unc.edu

Abid HUSSAINI

Department of Pathology and Cell Biology, Columbia University, Taub Institute, New York, USA – abid.hussaini@columbia.edu

Ahmet GUL

Department of Internal Medicine, Istanbul University School of Medicine, Istanbul, Turkiye – agul@istanbul.edu.tr

Ali Onder YILDIRIM

Department of Lung Biology and Diseases, Helmholtz Zentrum München, München, Germany – oender.yildirim@helmholtz-muenchen.de

Batu ERMAN

Department of Molecular Biology, Genetics and Bioengineering, Sabanci University, Istanbul, Turkiye – batu.erman@boun.edu.tr

Çagla EROGLU

Department of Cell Biology, Duke University, North Carolina, USA – cagla.eroглу@duke.edu

Ebba LOHMANN

Department of Neurodegenerative Diseases, Tübingen University, Tübingen, Germany – ebba.lohmann@uni-tuebingen.de

Elif APOHAN

Department of Biology, İnönü University, Malatya, Turkiye – elif.apohan@inonu.edu.tr

Erdem TUZUN

Department of Neuroscience, Istanbul University, Aziz Sancar Institute of Experimental Medicine, Istanbul, Turkiye – erdem.tuzun@istanbul.edu.tr

Gokçe TORUNER

Department of Hematology, MD Anderson Cancer Center, Houston, Texas, USA – gatoruner@mdanderson.org

Gunnur DENİZ

Department of Immunology, Istanbul University, Aziz Sancar Institute of Experimental Medicine, Istanbul, Turkiye – gdeniz@istanbul.edu.tr

Gurol TUNCMAN

Department of Genetics and Complex Diseases, Harvard University, Massachusetts, USA – gtuncman@hsph.harvard.edu

Hannes STOCKINGER

Molecular Immunology Unit, Vienna School of Medicine, Pathophysiology Center, Vienna, Austria – hannes.stockinger@medunivien.ac.at

Hesenov Muşviq CƏLALOĞLU

Department of General Surgery, Azerbaijan Medical University, Baku, Azerbaijan - hesenov@amu.edu.az

Rukset ATTAR

Department of Obstetrics and Gynecology, Yeditepe University, Istanbul, Turkiye – rattar@yeditepe.edu.tr

Ihsan GURSEL

Department of Molecular Biology and Genetics, Bilkent University, Ankara, Turkiye – ihsangursel@bilkent.edu.tr

Melih ACAR

Texas University Pediatric Research Institute, Dallas, Texas, USA – melihacar@gmail.com

Numan OZGEN

Department of Pathology and Immunology, Baylor University School of Medicine, Texas, USA – numan.oezguen@bcm.edu

Serhat PABUCCUOĞLU

Department of Reproduction & Artificial Insemination, Istanbul University-Cerrahpaşa School of Veterinary, Istanbul, Turkiye – serpab@iuc.edu.tr

Suhendan EKMEKÇIOĞLU

MD Anderson Cancer Center, Texas University, Houston, Texas, USA – sekmekcioglu@mdanderson.org

Yusuf BARAN

Department of Molecular Biology and Genetics, İzmir Institute of Technology, İzmir, Turkiye – yusufbaran@iyte.edu.tr

EXPERIMED

CONTENTS

REVIEW ARTICLES

- 131 **Advanced Targeted Therapeutic Strategies for Glioblastoma Multiforme: Bevacizumab and Its Emerging Nanotechnology-Based Interventions**
Zeynep Birsu Cincin, Soner Sahin

ORIGINAL ARTICLES

- 139 **Virulence Factor of *Porphyromonas gingivalis* Disrupts Intestinal Oxidative Status and Acetylcholinesterase Activity in Rotenone-Exposed Zebrafish**
Ipek Islek, Merih Beler, Ismail Unal, Derya Cansiz, Ebru Emekli-Alturfan, Kemal Naci Kose
- 146 **Effects of o-tDCS and tDCS on Maximal Grip Strength**
Sercan Seker, Gaye Eskicioglu, Zeynep Kucuk, Sacit Karamursel
- 154 **Evaluation of the Molecular Effects of the Anticancer Adjuvant Valproic Acid on HEK293T Cells**
Hazal Banu Olgun Celebioglu, Yeliz Ekici, Abdullah Yilmaz, Feyza Nur Tuncer
- 161 **Epigenetic Signatures in Ovarian Cancer to Determine Potential Diagnostic/Prognostic Biomarkers**
Tugce Senturk Kirmizitas, Servet Tunoglu, Jean Helmijr, Samet Topuz, Maurice Jansen, Tuba Gunel
- 174 **Identification of Peptides Binding Specifically to Colon Cancer Cells through Phage Display Peptide Library Screening**
Deniz Sahin, Zeynep Kanlidere, Bariscan Ekal, Berkehur Abayli, Yordan Hayat, Ece Selcuk
- 183 **Metabolomic Profiling and Biological Activities of Cell-Free Supernatants of *Bacillus* sp. Isolates: Antibacterial, Antibiofilm, and Anti-quorum Sensing Activities**
Gamze Benli Yardimci, Ekrem Murat Gonulalan, Nurnehir Baltaci Bozkurt, Emirhan Nemitlu, Engin Kocak, Mujde Eryilmaz
- 194 **Development of Natural Castile Soaps from Vegetable Oils**
Gokhan Ozokan, Abdulkirim Bilginer
- 203 **Impact of the COVID-19 Pandemic on the Distribution of Viral Pathogens Involved in Febrile Seizures**
Emel Eksi-Alp, Gizem Dikencik-Cuceloglu, Aytac Goktug, Mahmut Firat Halici, Gulser Esen Besli, Eda Kepenekli
- 210 **Could Increased *Glp1r* Expression via Sitagliptin in the GLP-1/GLP-1 Receptor Axis in the Diet-Induced Obesity Rat Model be Important in Liver Metabolism?**
Neslihan Cevik, Gulper Nacarkahya, Serkan Gurgul, Cem Horozoglu
- 215 **Determining Prostate Cancer-Related Pathways and the Role of the *RPH3AL* Gene**
Didem Seven, Omer Faruk Bayrak

Advanced Targeted Therapeutic Strategies for Glioblastoma Multiforme: Bevacizumab and Its Emerging Nanotechnology-Based Interventions

Zeynep Birsu Cincin¹ , Soner Sahin² 

¹Department of Medical Biochemistry, Faculty of Medicine, Istanbul Nisantasi University, Istanbul, Turkiye

²Department of Neurosurgery, Faculty of Medicine, Istanbul Nisantasi University, Istanbul, Turkiye

ORCID ID: Z.B.C. 0000-0001-6948-5382; S.S. 0000-0001-9391-8088

Cite this article as: Cincin ZB, Sahin S. Advanced targeted therapeutic strategies for glioblastoma multiforme: bevacizumab and its emerging nanotechnology-based interventions. *Experimed* 2024; 14(3): 131-138.

ABSTRACT

Bevacizumab is an important treatment for glioblastoma multiforme (GBM), especially after surgery, radiation, and chemotherapy, but it has not yet been successfully used to treat recurrent or progressive tumors. Bevacizumab is a humanized monoclonal antibody that targets vascular endothelial growth factor A and inhibits neovascularization. Bevacizumab works by cutting off the blood supply to the tumor, thus alleviating symptoms and enhancing quality of life in situations where standard therapies have failed. Nonetheless, the effect of bevacizumab on the overall survival of patients with GBM was modest. Resistance ultimately occurs through the activation of alternative angiogenesis pathways or tumor evolution, including remodeling of the microenvironment and extracellular matrix. In response to these drawbacks, new strategies are under investigation, focusing on drug delivery systems based on nanotechnology. These include bevacizumab-loaded nanoparticles that cross the blood-brain barrier with greater efficiency, allowing for direct drug delivery to the tumor. Synergistic therapies using bevacizumab and classical chemotherapeutic agents or immunomodulatory therapies in these nanoparticle systems have shown promise in improving therapeutic potency by simultaneously targeting multiple tumor pathways or mechanisms, as demonstrated preclinically. Further development of these novel delivery approaches could lead to a more robust therapeutic paradigm for GBM, improving survival and quality of life for patients affected by this complex disease.

Keywords: Glioblastoma, bevacizumab, nanotechnology, tumor resistance

INTRODUCTION

Glioblastoma multiforme (GBM) is a highly aggressive primary malignant brain tumor of the highest grade (1). Standard treatment protocols and conventional immunotherapy are ineffective as they fail to meaningfully improve the long-term survival of GBM patients (2). Bevacizumab, a monoclonal antibody that inhibits vascular endothelial growth factor (VEGF), has shown some improvement in progression-free survival (PFS) in GBM patients, but due to poor overall survival, there is no standard definition of its effectiveness (3). We discuss the responsiveness of bevacizumab in GBM, the causes of immune escape, and future therapeutic approaches for

progressive GBM, including nanotechnology. Currently approved therapeutic strategies and subsequent lines of systemic treatments using emerging scientific advances in targeted therapies will also be discussed.

Characteristic Properties of GBM

GBM is the most aggressive type of malignant brain tumor, and it is characterized by local invasion, extreme treatment resistance, and high lethality (1). Due to its biological characteristics, it is highly invasive and can infiltrate normal adjacent brain tissue via numerous pathways, and almost all patients with this tumor are resistant to conventional therapies (2). The rapidly growing nature of GBM allows

Corresponding Author: Soner Sahin **E-mail:** sahin.soner@nisantasi.edu.tr

Submitted: 26.10.2024 **Revision Requested:** 13.11.2024 **Last Revision Received:** 24.11.2024 **Accepted:** 02.12.2024 **Published Online:** 11.12.2024



Content of this journal is licensed under a Creative Commons Attribution-NonCommercial 4.0 International License.

for a more aggressive invasion, and it can rapidly infiltrate the normal brain tissue that surrounds it, often traveling to sites in the contralateral hemisphere. Changes in cell mobility allow the GBM to travel through brain tissue along the perivascular spaces and white matter tracts (3). In contrast to most cancers, GBM is not associated with classical metastatic spread. Its invasive behavior also seems to trigger major changes in the adjacent connective tissues, which contain a nonspecific fibrous tissue encapsulating the tumor nodule (4). Such extreme heterogeneity at the cellular and molecular levels is one of the main reasons for the rapid spread of GBM (Table 1).

“GBM heterogeneity” refers to the different traits of cancer cells, which can have various genetic profiles and show various responses to treatment in different tumor areas, making it difficult to target them all the same way (5). Transcriptional and mutational profiles characteristic for different tumors and even parts of the same tumor have led to the subdivision of GBM tumors into major subtypes, primarily proneural, classical, and mesenchymal (6-7). In addition, single-cell RNA sequencing (scRNA-seq) identified multiple GBM transcriptional states, such as oligodendrocyte progenitor-like, neural progenitor-like, astrocyte-like, and mesenchymal-like, that can change during tumor evolution (6-7).

The growth of GBM is further supported by the induction of angiogenesis, which provides an ever-present supply of oxygen and nutrients (8). Low oxygen levels in the tumor microenvironment (TME) drive the secretion of angiogenic

factors like VEGF from surrounding stroma to sustain angiogenesis and aid the escape or re-entry of tumor cells through the bloodstream (9). Mutations in the epidermal growth factor receptor (EGFR) gene, deletions in the phosphatase and tensin homolog (PTEN) tumor suppressor gene, and activation of the PI3K/AKT/mTOR signaling pathway are genetic and molecular changes that promote relentless growth of GBM and invasion to surrounding tissues (10). Furthermore, proteolytic enzymes such as matrix metalloproteinases (MMPs) secreted by GBM cells degrade the extracellular matrix (ECM), which breaks down tissue barriers and aids tumor spread (Figure 1).

Treating GBM is also made more difficult by the blood-brain barrier (BBB) and blood-tumor barrier (BTB). The BBB normally prevents most therapeutic agents from entering the brain, resulting in an anatomically and physiologically immune-privileged site that often impedes therapy with immunotherapies (11). Although the BTB formed around the GBM may be more penetrable than the BBB, this irregular permeability restricts effective drug transport. As a result, this immune-privileged niche can reduce the surveillance of immune activity and promote the escape of GBM from defense via host immunity, further supporting tumor expansion (12-13). In conjunction with the intrinsic cellular heterogeneity of GBM, these barriers render its effective treatment exceedingly difficult (Figure 2).

Table 1. The mechanisms and clinical implications of the spread of GBM

Spread Factor	Mechanism	Clinical Implications
Invasiveness	GBM cells infiltrate surrounding brain tissue	Makes surgical and localized treatment less effective
Glioma Stem Cells	Treatment-resistant stem-like cells drive growth and spread	Leads to high recurrence and treatment resistance
Angiogenesis	Formation of new blood vessels to support tumor growth	Supports sustained tumor growth and distant spread within the brain
Genetic Alterations	Mutations in EGFR, PTEN and PI3K/AKT/mTOR pathways	Drives aggressive proliferation and spread
ECM Degradation	Degradation of extracellular matrix by MMP enzymes	Allows tumor cells to invade adjacent tissues
Immune Evasion	Immune system suppression due to the brain's immune-privileged environment	Limits the body's natural ability to fight the tumor
Tumor Heterogeneity	Genetic diversity among tumor cells enables survival and spread	Results in poor treatment response and recurrence
Resistance to Apoptosis	Resistance to programmed cell death (apoptosis)	Prolongs tumor cell survival and promotes invasion
Tumor Microenvironmental Interaction	GBM interacts with surrounding cells and immune responses to enhance spread	Creates a supportive environment for further invasion and growth

(Created in <https://BioRender.com>).

GBM: Glioblastoma multiforme; EGFR: Epidermal growth factor receptor; PTEN: Phosphatase and tensin homolog; ECM: Extracellular matrix; MMP: Matrix metalloproteinases.

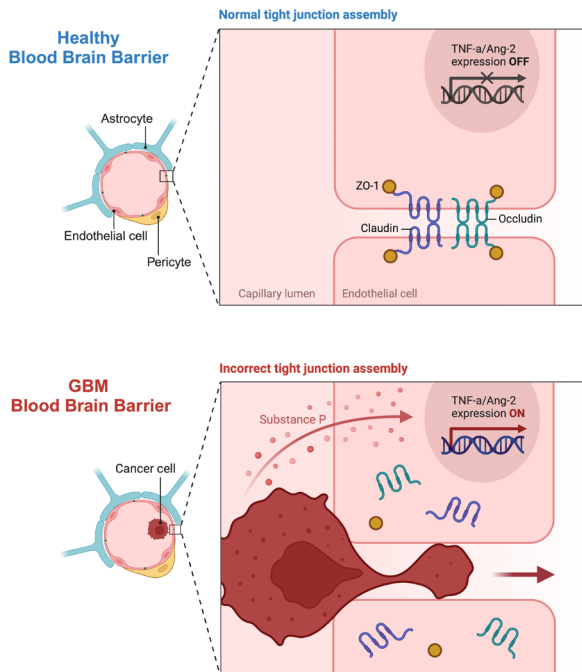


Figure 1. The structure of the BBB in normal brain tissue and the GBM.

The upper panel represents a healthy BBB, which is characterized by normal tight junction assembly between endothelial cells. Tight junction proteins (ZO-1, Claudin and Occludin) maintain the integrity of the barrier and thus prevent unwanted crossing of material from blood to the brain. The synthesis of pro-inflammatory factors such as TNF- α and Ang-2, is inhibited, and tight junction formation is maintained. The lower panel depicts the effect of brain tumors on BBB permeability, depicting the aberrant tight junction assembly. This permeability allows substances such as substance P to infiltrate the brain, as tumor cells disrupt tight junction proteins. The pro-inflammatory factors TNF- α and Ang-2 stimulate barrier disruption, which ultimately promotes tumor cell infiltration and metastasis. This leakiness of a dysfunctional BBB facilitates the transference of cancer cells and toxic elements across the BBB, thereby promoting glioma growth and invasive progression in the brain (Created in <https://BioRender.com>).

BBB: Blood–brain barrier; GBM: Glioblastoma multiforme; TNF- α : Tumor necrosis factor alpha; Ang-2: Angiotensin-2.

GBM cells create apoptosis-resistance mechanisms that enable cells to survive despite the invasion of neighboring tissues (14). Additionally, GBM cells also affect adjacent cells and the immune system to form a protective niche for unrestricted tumor growth. This variability and evolutionary liability makes it improbable that a single treatment modality can be designed, emphasizing the need for therapies that take into account genetic, cellular, and environmental diversity in GBM (15).

Current Treatment Modalities for GBM

Due to the aggressive properties of GBM and the hindrance caused by BBB in drug penetration, GBM treatment involves a multimodal approach (16). These methods are referred to as the first treatment for GBM, which consists mainly of surgery, radiotherapy, chemotherapy, and targeted therapy (17).

Temozolomide (TMZ) is an oral chemotherapeutic agent that inhibits the replication of cancer cells by acting on their DNA (18). It is usually administered in conjunction with radiotherapy as one of the first lines of standard treatment for GBM. It plays a role in front-line therapy due to its capacity to partially penetrate the BBB, whereby it can affect tumor cells within the brain (19). Nonetheless, TMZ penetrates the barrier incompletely, and its efficacy is limited, whereas GBM is often accompanied by the development of resistance dynamics. Although TMZ is effective for treating newly diagnosed GBM, its long-term effects are often abrogated by cell resistance to drug-mediated cytotoxicity and limited brain penetration (20).

The role of TMZ in PFS and overall survival (OS) in GBM has been disputed for years, especially when it comes to the long-term effects of TMZ on survival (18-20). TMZ has shown efficacy in PFS. Many trials have demonstrated that the combination of concomitant radiation with TMZ is associated with a longer time to progression in patients with newly diagnosed GBM. Nevertheless, the median time to PFS for patients on TMZ is relatively short; typically within the 6–9 month range (18-20). This means that although the drug delays tumor growth for a period, it does not prevent the disease from progressing. Furthermore, the role of TMZ in improving OS is controversial. Although TMZ has been demonstrated to prolong OS compared with other therapeutic regimens, the impact is modest. When TMZ with radiation is used, for example, the median OS usually is on the order of 14–16 months (18-20). The question of whether TMZ is effective against OS remains open, even more so in cases of relapsing GBM after this treatment when the disease frequently develops resistance to the drug.

Bevacizumab, a targeted agent, is capable of inhibiting VEGF, a major force promoting tumor angiogenesis (21). Bevacizumab inhibits the process of angiogenesis by blocking VEGF, limiting tumor blood supply to naturally reduce tumor size and decrease the symptoms of edema. Bevacizumab is mainly used for recurrent GBM after the first-line treatment, such as surgery, radiotherapy, and TMZ, has failed, especially in advanced-stage symptom control, contributing to brain edema or other neurological deficits (22). Bevacizumab leads to a relative prolongation of PFS; however, its effect on OS remains unclear and has been debated in GBM. Eventually, treatment fails because of the inevitable resistance to bevacizumab (21-22). Further studies are needed to elucidate the underlying mechanisms and to develop new methods of drug delivery to enhance efficacy and reduce resistance.

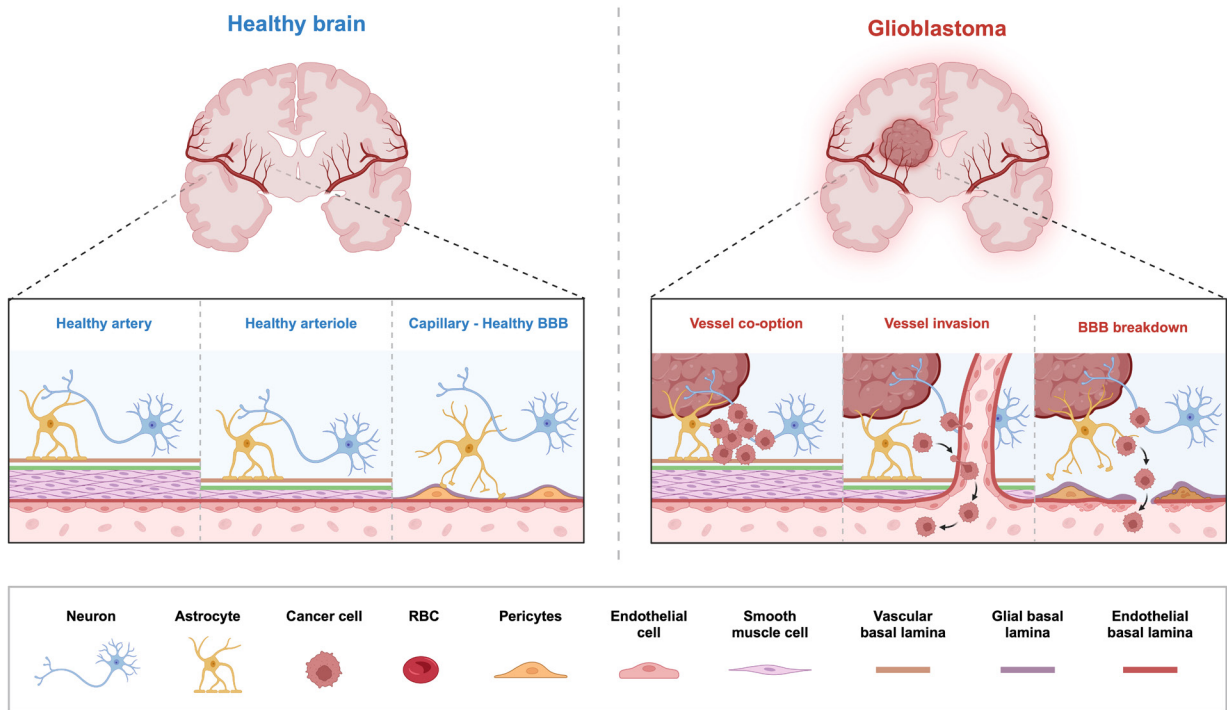


Figure 2. Neuropathological illustration comparing vascular structures in healthy brain versus GBM-invaded brain tissue. The schematic representation illustrates the differences between normal brain vasculature and the pathological vascular microenvironment in GBM. In a normal brain, the BBB provides a protective layer that prevents unwanted components from entering the brain. This barrier involves the cooperation of several key cells, including neurons, astrocytes, pericytes, and endothelial cells. The left column depicts a normal brain with preserved BBB structures where pericytes, astrocytes, and endothelial cells maintain healthy arteries, arterioles, and capillaries supported by neurons. A GBM-invaded brain is depicted on the right panel, with vessel co-option (black arrow), vessel invasion (white arrows), and BBB breakdown as hallmarks of cancer progression. Some of these alterations in pathology enable infiltration into surrounding brain tissue and destruction of the BBB; both allow for expansion and dissemination of GBM. By contrast, in GBM, cancer cells derange this organization via vessel co-option (tumor cells use pre-existing blood vessels), followed by infiltration of tumor cells into the vascular wall, and ultimately BBB disruption. These adaptations allow cancer cells to metastasize, modify blood circulation, and provide nutrients and oxygen to the tumor. BBB dysfunction hampers effective treatment delivery by hindering therapeutic agents from reaching the tumor site, which causes GBM to exhibit an aggressive phenotype and exhibit resistance to conventional therapies (Created in <https://BioRender.com>).

BBB: Blood–brain barrier; GBM: Glioblastoma multiforme; RBC: Red blood cell.

Bevacizumab as a Targeted Therapeutic Agent

Bevacizumab blocks VEGF-mediated invasion and spread (Figure 2). The importance of these results lies in the possible integration of bevacizumab with other therapies targeting invasion and metastasis. Furthermore, emerging preclinical evidence suggests that bevacizumab may affect tumor metabolism. These results are noteworthy because GBM cells mostly use glucose for energy and often exhibit a glycolytic phenotype, even in oxygen-rich environments (23). Moreover, GBM cells can effectively metabolize lactate (24). Researchers have reported that the antiangiogenic drug bevacizumab

worsens hypoxic stress by stopping the growth of new blood vessels and changing how tumor cells use energy. When bevacizumab is mixed with metabolic drugs that stop glycolysis, biological treatment may be more effective (23-24).

Although bevacizumab mainly antagonizes VEGF-A, emerging evidence implicates other pathways in its effects (25). Bevacizumab enhances the tumor microenvironment and inhibits the infiltration of regulatory T cells and myeloid-derived suppressor cells into tumors. While current immunotherapies, like anti-PD-1 and anti-CTLA-4, use counter-immunity (PD-L1 or CTLA-4) to make the “counter-immune” agents less efficient,

if bevacizumab can clear these immune-suppressing cells, they may enhance their effectiveness by allowing more of them to survive (26). In addition, the mobilization of ECM is an important physiological action of bevacizumab. VEGF is an established mediator of ECM degradation and allows tumors to infiltrate normal tissue (27).

Clinical Significance of Bevacizumab in GBM

Bevacizumab is widely used because it effectively reduces peritumoral edema, headache, and seizures caused by high intracranial pressure (27). The FDA has approved bevacizumab for treating recurrent GBM. This approach not only reduced the need for corticosteroids but also likely aided for treating neurological symptoms in a group in which these issues substantially affected their quality of life (28). However, its limited impact on OS constrains the advantages of bevacizumab in enhancing PFS (27-28). In response to this issue, researchers have conducted clinical trials that combine bevacizumab with other medications to enhance its efficacy. Researchers may use immune checkpoint inhibitors such as nivolumab and ipilimumab, combined with bevacizumab, can enhance the presence of CD8⁺ effector T cells and lymphoid structures inside tumors. This treatment may provide therapeutic effects (29).

Bevacizumab alters the tumor microenvironment and may increase immunotherapy efficiency by promoting immune surveillance and cytotoxicity against tumor cells. This mechanism could further enhance the synergy of combination therapy with anti-PD-L1 agents (27-29). This has also led to clinical trials of the wide range of antiangiogenic combinations that are currently under investigation aiming at targeting certain angiogenic pathways to possibly bypass resistance to anti-VEGF therapies (30). Other pro-angiogenic factors, such as fibroblast growth factor (FGF) and platelet-derived growth factor (PDGF), have received attention as possibly having greater importance in stimulating angiogenesis than VEGF alone (27-30). Investigators have also been investigating the use of bevacizumab combined with agents that inhibit the hepatocyte growth factor (HGF) or insulin-like growth factor 1 (IGF1) pathways to optimize treatment. However, the emergence of resistance of some tumor cells to bevacizumab and other targeted therapies is still unknown (27-30). Several recent studies have focused on targeting bevacizumab via nanotechnology to further its site-specific therapeutic use and prolong its therapeutic effect (31). Nanocarriers such as liposomes, polymeric nanoparticles (NPs), and exosome-based systems help increase drug proximity to tumors (32). This might increase the life span of patients without increasing poor PFS or OS rates. To enhance immune activity and limit resistance, the use of checkpoint inhibitors with bevacizumab has been explored (32).

Integrating Bevacizumab with Nanotechnology for GBM Treatment

One of the most utilized nanotechnological approaches is the design of NPs that are denoted as a suitable solution to the

hard-line penetration of conventional drugs due to the dual enhancement of passive and active delivery of them to GBM tumor cells (33). The most inspiring point is that intravenously injected NPs can be easily homed specifically to the brain by navigating through the BBB. From the tumor angiogenesis environment, NPs serve as main actors in the multi-targeted intervention of GBM tumor cells, as well as tumor angiogenesis and vessel barriers (34). To form a mononuclear phagocyte system and secrete cytokines, it is a routine process that various inorganic and organic substances are encapsulated onto the surface of NPs, mainly smoothing the phagocytosis of macrophages, elongating the period of the biological circulation of NPs, and enhancing delivery to the brain, improving BBB penetration and permeability (33-34).

Many types of NPs have shown wonderful application in the imaging department, particularly gadolinium, gold NPs, and carbon-based materials, offering MRI, CT, and fluorescence-mediated imaging of GBM (33-34). Furthermore, it is worth noting that the application of cell membrane-camouflaged NPs can surmount the barriers of the BBB and BTB in tumor cells (35).

Recent studies have shown big steps forward in using nanotechnology to make bevacizumab more effective in treating GBM, especially in getting past the BBB, which is a major problem for drugs that are meant to target the brain (Figure 2). Using gold NPs (AuNPs) with bevacizumab makes the BBB more permeable, which helps target tumors and boosts anticancer effects at the same time (36). Bevacizumab-coated NPs concentrate around the tumor, reducing contact with healthy tissue and improving the drug's therapeutic effectiveness (37). Researchers have found that adding bevacizumab to a nanoparticle delivery system makes other drugs work better at stopping the growth of new blood vessels and the immune system's response to them. Graphene quantum dots (GQDs) have the potential to improve drug delivery via photothermal effects (38). This results from their capacity to augment membrane permeability and promote the infiltration of medications into cells. This comprehensive approach may substantially impede tumor progression while minimizing the negative effects often associated with systemic therapies. Ultrasonic technology and nanoparticle therapeutics are being studied together in new clinical studies to determine how they can work better together to pass the BBB.

Initial research suggests that this approach improves drug delivery and alters the tumor microenvironment to promote immune system recognition. This is a notable progression in the immunotherapeutic treatment of GBM (39). Technologies such as biodegradable hydrogel systems and implanted devices that provide bevacizumab locally and continuously may be used. These technologies provide increased concentrations of medication at the tumor location, possibly improving patient outcomes over time and extending PFS (40). These strategies are important for treating GBM because they allow the creation of platforms for multifunctional NPs that can target,

transport, and change the immune system. These are crucial for addressing the complexity and resistance mechanisms of GBM (39-40).

Clinical Trials

Ongoing studies are exploring the existence of biomarkers predictive of clinical response to bevacizumab, which may lead to a more personalized treatment strategy for GBM (41). High VEGF levels, tumor hypoxia, and certain genotypes of FGF have been proposed as biomarkers for predicting the response to treatment with bevacizumab, which allows researchers and clinicians to personalize therapeutic regimens according to individual tumor characteristics to improve efficacy (42). Various combinations of bevacizumab with immune checkpoint inhibitors, as well as molecularly targeted drugs, are currently being investigated in clinical trials to enhance treatment outcomes for GBM (42). Co-therapy with inhibitors of the PI3K/AKT/mTOR pathway, which is frequently altered in GBM, has shown promise in preclinical models, thereby appearing to represent a potential approach for further inhibition of pathophysiological processes enabled by bevacizumab therapy (43). Alternative studies suggest improved responses from combining radiation or agents that inhibit DNA damage repair pathways with bevacizumab to take advantage of the intrinsic sensitivity of GBM cells and minimize other patterns of resistance, a common obstacle in long-term therapy with bevacizumab (44). Additionally, several new drug delivery systems based on nanotechnology have been developed to enhance the efficacy and safety profile of bevacizumab (45). Improvements in nanoparticle design have been reported to enable targetable, locus targeted delivery of therapeutic agents like bevacizumab with reduced systemic exposure and increased tumor vulnerability (46). Nanoparticle platforms capable of crossing the BBB to enable simultaneous delivery of multiple therapies on one platform are also in development. Targeting multiple pathways and conveying better bioactivity of bevacizumab using these platforms can lessen treatment resistance by providing an innovative strategy to overcome the multifactorial nature of GBM.

CONCLUSION

Bevacizumab continues to be a crucial antiangiogenic treatment for GBM, showing improvements in symptomatic and PFS. Given that bevacizumab failed to extend survival, phase II investigations into combination therapies and innovative drug delivery methods are needed. These investigations must focus on non-VEGF-driven pathways that are unaffected by VEGF suppression. For many years, nanotechnology-based delivery methods have provided an effective solution to these issues, allowing targeted and controlled bevacizumab release with minimal systemic adverse effects (47). Adding bevacizumab to immunotherapy and molecularly targeted treatments or improving the nanoparticle delivery system might improve GBM treatment work better (48).

We anticipate that discovery will stimulate significant future molecular research in GBM, perhaps leading us to overcome this fatal disease. We anticipate that the creation of tumor-specific therapy vectors using bevacizumab will enhance the prognosis and survival rates of individuals afflicted with these lethal illnesses in the coming decade (49). This suggests that further research is required to determine the optimal combination of treatment modalities and to identify potential biomarkers that could predict patient outcomes. This may enhance the beneficial effects of bevacizumab in patients (50).

Peer-review: Externally peer-reviewed.

Author Contributions: Conception/Design of Study – Z.B.C., S.S.; Data Acquisition – Z.B.C., S.S.; Data Analysis/Interpretation – Z.B.C., S.S.; Drafting Manuscript – Z.B.C., S.S.; Critical Revision of Manuscript – Z.B.C., S.S.; Final Approval and Accountability – Z.B.C., S.S.

Conflict of Interest: The authors declared that they have no competing interests

Financial Disclosure: The authors declared that this study has received no financial support

REFERENCES

1. Lan Z, Li X, Zhang X. Glioblastoma: An update in pathology, molecular mechanisms and biomarkers. *Int J Mol Sci* 2024; 25(5): 3040.
2. Bou-Gharios J, Noël G, Burckel H. Preclinical and clinical advances to overcome hypoxia in glioblastoma multiforme. *Cell Death Dis* 2024; 15(7): 503.
3. Aghajani M, Jalilzadeh N, Aghebati-Maleki A, Yari A, Tabnak P, Mardi A, et al. Current approaches in glioblastoma multiforme immunotherapy. *Clin Transl Oncol* 2024; 26(7): 1584-612.
4. Shahcheraghi SH, Alimardani M, Lotfi M, Uversky VN, Guetchueng ST, Palakurthi SS, et al. Advances in glioblastoma multiforme: Integrating therapy and pathology perspectives. *Pathol Res Pract* 2024; 257: 155285.
5. Lorimer I. Modeling glioblastoma. *eLife* 2024; 13: e100824.
6. Wu H, Guo C, Wang C, Xu J, Zheng S, Duan J, et al. Single-cell RNA sequencing reveals tumor heterogeneity, microenvironment, and drug-resistance mechanisms of recurrent glioblastoma. *Cancer Sci* 2023; 114(6): 2609-21.
7. Tomar MS, Kumar A, Srivastava C, Shrivastava A. Elucidating the mechanisms of Temozolomide resistance in gliomas and the strategies to overcome the resistance. *Biochim Biophys Acta Rev Cancer* 2021; 1876(2): 188616.
8. Cortes Ballen AI, Amosu M, Ravinder S, Chan J, Derin E, Slika H, et al. Metabolic reprogramming in glioblastoma multiforme: A review of pathways and therapeutic targets. *Cells* 2024; 13(18): 1574.
9. Sarkar S, Patranabis S. Immunomodulatory signalling networks in glioblastoma multiforme: a comprehensive review of therapeutic approaches. *Hum Cell* 2024; 37(5): 1355-1377.
10. Barzegar Behrooz A, Talaie Z, Jusheghani F, Łos MJ, Klönisch T, Ghavami S. Wnt and PI3K/Akt/mTOR survival pathways as therapeutic targets in glioblastoma. *Int J Mol Sci* 2022; 23(3): 1353.

11. Jena L, McErlean E, McCarthy H. Delivery across the blood-brain barrier: nanomedicine for glioblastoma multiforme. *Drug Deliv Transl Res* 2020; 10(2): 304-18.
12. Song X, Qian H, Yu Y. Nanoparticles mediated the diagnosis and therapy of glioblastoma: bypass or cross the blood-brain barrier. *Small* 2023; 19(45): e2302613.
13. Pearson JRD, Cuzzubbo S, McArthur S, Durrant LG, Adhikaree J, Tinsley CJ, et al. Immune escape in glioblastoma multiforme and the adaptation of immunotherapies for treatment. *Front Immunol* 2020; 11: 582106.
14. Tang W, Fan W, Lau J, Deng L, Shen Z, Chen X. Emerging blood-brain-barrier-crossing nanotechnology for brain cancer theranostics. *Chem Soc Rev* 2019; 48(11): 2967-3014.
15. Kılıç T, Yıldırım Ö, Şahin S, Pamir MN. Glial tümörlerin anjiogenezini. *Türk Neurosurg* 2005; 15(1): 1-9.
16. Michaelsen SR, Staberg M, Pedersen H, Jensen KE, Majewski W, Broholm H, et al. VEGF-C sustains VEGFR2 activation under bevacizumab therapy and promotes glioblastoma maintenance. *Neuro Oncol* 2018; 20(11): 1462-74.
17. Diaz RJ, Ali S, Qadir MG, De La Fuente MI, Ivan ME, Komotar RJ. The role of bevacizumab in the treatment of glioblastoma. *J Neurooncol* 2017; 133(3): 455-67.
18. Arora H, Mammi M, Patel NM, Zyfi D, Dasari HR, Yunusa I, et al. Dexamethasone and overall survival and progression free survival in patients with newly diagnosed glioblastoma: a meta-analysis. *J Neurooncol* 2024; 166(1): 17-26.
19. Pasupuleti V, Vora L, Prasad R, Nandakumar DN, Khatri DK. Glioblastoma preclinical models: strengths and weaknesses. *Biochim Biophys Acta Rev Cancer* 2024; 1879(1): 189059.
20. Reardon DA, Brandes AA, Omuro A, Mulholland P, Lim M, Wick A, et al. Effect of nivolumab vs bevacizumab in patients with recurrent glioblastoma: The CheckMate 143 phase 3 randomized clinical trial. *JAMA Oncol* 2020; 6(7): 1003-10.
21. Tsien CI, Pugh SL, Dicker AP, Raizer JJ, Matuszak MM, Lallana EC, et al. NRG Oncology/RTOG1205: A randomized phase II trial of concurrent bevacizumab and reirradiation versus bevacizumab alone as treatment for recurrent glioblastoma. *J Clin Oncol* 2023; 41(6): 1285-95.
22. Tamura R, Tanaka T, Ohara K, Miyake K, Morimoto Y, Yamamoto Y, et al. Persistent restoration to the immunosupportive tumor microenvironment in glioblastoma by bevacizumab. *Cancer Sci* 2019; 110(2): 499-508.
23. De Leo A, Ugolini A, Yu X, Scirocchi F, Scocozza D, Peixoto B, et al. Glucose-driven histone lactylation promotes the immunosuppressive activity of monocyte-derived macrophages in glioblastoma. *Immunity* 2024; 57(5): 1105-23.e8.
24. Rashidi A, Billingham LK, Zolp A, Chia TY, Silvers C, Katz JL, et al. Myeloid cell-derived creatine in the hypoxic niche promotes glioblastoma growth. *Cell Metab* 2024; 36(1): 62-77.e8.
25. Stadlbauer A, Roessler K, Zimmermann M, Buchfelder M, Kleindienst A, Doerfler A, et al. Predicting glioblastoma response to bevacizumab through MRI biomarkers of the tumor microenvironment. *Mol Imaging Biol* 2019; 21(4): 747-57.
26. Fathi M, Razavi SM, Sojoodi M, Ahmadi A, Ebrahimi F, Namdar A, et al. Targeting the CTLA-4/B7 axes in glioblastoma: Preclinical evidence and clinical interventions. *Expert Opin Ther Targets* 2022; 26(11): 949-61.
27. de Cristo Soares Alves A, Lavayen V, de Fraga Dias A, Bruinsmann FA, Scholl JN, Cé R, et al. EGFRvIII peptide nanocapsules and bevacizumab nanocapsules: A nose-to-brain multitarget approach against glioblastoma. *Nanomedicine (Lond)* 2021; 16(20): 1775-90.
28. Cai Q, Li X, Xiong H, Fan H, Gao X, Vemireddy V, et al. Optical blood-brain-tumor barrier modulation expands therapeutic options for glioblastoma treatment. *Nat Commun* 2023; 14(1): 4934.
29. Mauldin IS, Jo J, Wages NA, Yogendran LV, Mahmutovic A, Young SJ, et al. Proliferating CD8+ T cell infiltrates are associated with improved survival in glioblastoma. *Cells* 2021; 10(12): 3378.
30. Jimenez-Pascual A, Mitchell K, Siebzehrnubli FA, Lathia JD. FGF2: A novel druggable target for glioblastoma? *Expert Opin Ther Targets* 2020; 24(4): 311-8.
31. Singh RR, Mondal I, Janjua T, Popat A, Kulshreshtha R. Engineered smart materials for RNA based molecular therapy to treat glioblastoma. *Bioact Mater* 2023; 33: 396-423.
32. Wiwatchitawee K, Quarterman JC, Geary SM, Salem AK. Enhancement of therapies for glioblastoma (GBM) using nanoparticle-based delivery systems. *AAPS PharmSciTech* 2021; 22(2): 71.
33. Ruiz-Garcia H, Ramirez-Loera C, Malouff TD, Seneviratne DS, Palmer JD, Trifiletti DM. Novel strategies for nanoparticle-based radiosensitization in glioblastoma. *Int J Mol Sci* 2021; 22(18): 9673.
34. Lakshmi BA, Kim YJ. Modernistic and emerging developments of nanotechnology in glioblastoma-targeted theranostic applications. *Int J Mol Sci* 2022; 23(3): 1641.
35. Jena L, McErlean E, McCarthy H. Delivery across the blood-brain barrier: Nanomedicine for glioblastoma multiforme. *Drug Deliv Transl Res* 2020; 10(2): 304-18.
36. She L, Su L, Liu C. Bevacizumab combined with re-irradiation in recurrent glioblastoma. *Front Oncol* 2022; 12: 961014.
37. Uddin MS, Mamun AA, Alghamdi BS, Tewari D, Jeandet P, Sarwar MS, et al. Epigenetics of glioblastoma multiforme: From molecular mechanisms to therapeutic approaches. *Semin Cancer Biol* 2022; 33: 100-20.
38. Cui X, Huo D, Wang Q, Wang Y, Liu X, Zhao K, et al. RUNX1/NPM1/H3K4me3 complex contributes to extracellular matrix remodeling via enhancing FOSL2 transcriptional activation in glioblastoma. *Cell Death Dis* 2024; 15(1): 98.
39. Mahmoud AB, Ajina R, Aref S, Darwish M, Alsayb M, Taher M, et al. Advances in immunotherapy for glioblastoma multiforme. *Front Immunol* 2022; 13: 944452.
40. Friedman HS, Prados MD, Wen PY, Mikkelsen T, Schiff D, Abrey LE, et al. Bevacizumab alone and in combination with irinotecan in recurrent glioblastoma. *J Clin Oncol* 2023; 41(32): 4945-52.
41. Collado J, Boland L, Ahrendsden JT, Miska J, Lee-Chang C. Understanding the glioblastoma tumor microenvironment: leveraging the extracellular matrix to increase immunotherapy efficacy. *Front Immunol* 2024; 15: 1336476.
42. Chamrath S, Mekala JR. Functional importance of glucose transporters and chromatin epigenetic factors in glioblastoma multiforme (GBM): possible therapeutics. *Metab Brain Dis* 2023; 38(5): 1441-69.
43. Abdi F, Arkan E, Eidzadeh M, Valipour E, Naseryeh T, Gamizgy YH, et al. The possibility of angiogenesis inhibition in cutaneous melanoma by bevacizumab-loaded lipid-chitosan nanoparticles. *Drug Deliv Transl Res* 2023; 13(2): 568-79.
44. Khan MA, Kalsoom S, Ayub AR, Ilyas M, Hassan N, Irshad K, et al. Host-guest coupling to potentially increase the bio-accessibility of 1-(2-chloroethyl)-3-cyclohexyl-1-nitrosourea by nanocarrier graphyne for brain tumor therapy, a comprehensive quantum mechanics study. *J Mol Graph Model* 2023; 123: 108517.
45. Tensaouti F, Desmoulin F, Gilhodes J, Roques M, Ken S, Lotterrie JA, et al. Is pre-radiotherapy metabolic heterogeneity of glioblastoma predictive of progression-free survival? *Radiother Oncol* 2023; 183: 109665.

46. Liang HT, Mizumoto M, Ishikawa E, Matsuda M, Tanaka K, Kohzuki H, et al. Peritumoral edema status of glioblastoma identifies patients reaching long-term disease control with specific progression patterns after tumor resection and high-dose proton boost. *J Cancer Res Clin Oncol* 2021; 147(12): 3503-16.
47. Brown CE, Rodriguez A, Palmer J, Ostberg JR, Naranjo A, Wagner JR, et al. Off-the-shelf, steroid-resistant, IL13R α 2-specific CAR T cells for treatment of glioblastoma. *Neuro Oncol* 2022; 24(8): 1318-30.
48. Jo J, Wen PY. Antiangiogenic therapy of high-grade gliomas. *Prog Neurol Surg* 2018; 31: 180-99.
49. Kim MM, Umemura Y, Leung D. Bevacizumab and glioblastoma: Past, present, and future directions. *Cancer J* 2018; 24(4): 180-6.
50. Carvalho B, Lopes JM, Silva R, Peixoto J, Leitão D, Soares P, et al. The role of c-Met and VEGFR2 in glioblastoma resistance to bevacizumab. *Sci Rep* 2021; 11: 6067.

Virulence Factor of *Porphyromonas gingivalis* Disrupts Intestinal Oxidative Status and Acetylcholinesterase Activity in Rotenone-Exposed Zebrafish

Ipek Islek¹, Merih Beler², Ismail Unal², Derya Cansiz³, Ebru Emekli-Alturfan⁴, Kemal Naci Kose⁵

¹Department of Periodontology, Institute of Health Sciences, Marmara University, Istanbul, Turkiye

²Department of Biochemistry, Institute of Health Sciences, Marmara University, Istanbul, Turkiye

³Department of Biochemistry, Faculty of Medicine, Medipol University, Istanbul, Turkiye

⁴Department of Biochemistry, Faculty of Dentistry, Marmara University, Istanbul, Turkiye

⁵Department of Periodontology, Faculty of Dentistry, Marmara University, Istanbul, Turkiye

ORCID ID: I.I. 0000-0002-6012-270X; M.B. 0000-0002-3828-4630, I.U. 0000-0002-8664-3298; D.C. 0000-0002-6274-801X; E.E.A. 0000-0003-2419-8587; K.N.K. 0000-0002-0423-8011

Cite this article as: Islek I, Beler M, Unal I, Cansiz D, Emekli-Alturfan E, Kose KM. Virulence factor of *Porphyromonas gingivalis* disrupts intestinal oxidative status and acetylcholinesterase activity in rotenone-exposed zebrafish. Experimed 2024; 14(3): 139-145.

ABSTRACT

Objective: *Porphyromonas gingivalis* (*P. gingivalis*) is a major pathogenic bacterium in periodontal disease and is associated with neurodegenerative diseases. One of the most destructive endotoxins of *P. gingivalis* is gingipain. Our objective was to show the impact of gingipain on acetylcholinesterase (AChE) activity and oxidative status in the intestinal tissues of zebrafish exposed to rotenone.

Materials and Methods: Zebrafish were grouped as; control group (C), gingipain-injected group (G), rotenone-exposed group (R), gingipain-injected and rotenone-exposed group (G+R) (n=15). At the end of 4 weeks, spectrophotometric analyses were performed to evaluate the oxidative status and AChE activity in the intestinal tissues.

Results: Intestinal lipid peroxidation (LPO) levels were higher in the G group than in the C group. Gingipain injection significantly reduced the activities of AChE and superoxide dismutase (SOD). In the R group, there were significant elevations in SOD, nitric oxide (NO), glutathione-S-transferase (GST), and AChE activities compared with those in the C group. In the G+R group, LPO, NO, SOD, and GST activities were reduced compared with the R group.

Conclusion: Our results show that gingipain dysregulated AChE activity and the oxidant-antioxidant balance in rotenone-exposed zebrafish, demonstrating its possible role in gut dysbiosis, neuroinflammation, and Parkinson's disease.

Keywords: *Porphyromonas gingivalis*, gingipain, zebrafish, rotenone, oxidative stress, acetylcholinesterase

INTRODUCTION

Approximately 11.2% of the world's population is affected by periodontitis, which is a disease characterized by the destruction of the tissues that surround the teeth (1). *Porphyromonas gingivalis* (*P. gingivalis*) is a key pathogen for periodontitis progression and has many virulence factors,

including fimbriae, lipopolysaccharide (LPS), capsule, and cysteine proteases to overcome the host defense.

Gingipain, cysteine proteinases from the trypsin-like enzyme family, are destructive virulence factors of *P. gingivalis*. They are categorized into two main groups: lysine-specific gingipain (Kgp) and arginine-specific

Corresponding Author: Kemal Naci Kose **E-mail:** kemkose@superonline.com

Submitted: 21.03.2024 **Revision Requested:** 16.04.2024 **Last Revision Received:** 25.04.2024 **Accepted:** 13.05.2024



Content of this journal is licensed under a Creative Commons Attribution-NonCommercial 4.0 International License.

gingipain (RgpA, RgpB) (2). They execute a significant portion of the proteolytic activity that *P. gingivalis* utilizes in periodontal tissues to overcome the host defense. They negatively affect the functioning of extracellular matrix components, disrupt the structure of cell metalloproteinases, and dysregulate the host defense. The release of various compounds into the extracellular matrix is facilitated by gingipain by breaking down collagen and proteins in the cell structure, contributing to the nutrition and proliferation of bacteria. They reduce the effects of immune cells by causing impairment in T cell receptors, such in CD4⁺ and CD8⁺ T cells, to overcome the host's immune response (2).

The detrimental consequences of *P. gingivalis* and gingipain are not limited to periodontal tissues. *P. gingivalis* and its endotoxins can disseminate to various organs through circulation and the digestive tract, thereby contributing to the progression and severity of many diseases, including cardiovascular diseases, diabetes mellitus, rheumatoid arthritis, and neurodegenerative diseases (3, 4). For instance, *P. gingivalis* was detected in a study examining post-mortem brain tissue samples from individuals with Alzheimer's disease (3). Moreover, gingipain was identified in the plasma samples of Parkinson's disease (PD) patients (5).

Among neurodegenerative diseases, PD ranks as one of the most prevalent globally. Its characteristic feature is the deterioration of dopamine-producing neurons, subsequently affecting many dopamine-required motor and non-motor functions in the body. Dysfunctions of the gastrointestinal system are prevalent non-motor symptoms of PD, and some recent research suggests that PD progression has been linked with changes in intestinal homeostasis through a structure of neurons named the enteric nervous system (ENS) (6).

The sophisticated neuronal network located along the lining of the gastrointestinal tract (GIT) is known as the ENS, also frequently called "the second brain". It has essential functions for maintaining homeostasis in GIT by regulating various processes, including secretion, peristalsis, and absorption (7). During these processes, a diverse intestinal microbial community produces chemicals that modulate ENS activity and contribute to proper digestion. There are constant molecular interactions between the ENS and the central nervous system (CNS) through hormones, vagus nerve, immune cells and neurotransmitters like acetylcholine and dopamine. This interconnection between these two systems is frequently termed the "gut-brain axis" (6).

Acetylcholine (ACh) is a neurotransmitter and a neuromodulator that regulates dopamine, serotonin, and other neuro hormones for a balanced cholinergic system in the CNS. In addition, ACh has an anti-inflammatory function via the "cholinergic anti-inflammatory pathway" which involves the inhibition of pro-inflammatory cytokines. ACh plays an essential role in ENS functioning by signaling digestive enzyme secretion, promoting peristalsis, and smooth muscle contraction. Acetylcholinesterase (AChE) is an enzyme that regulates

ACh levels by modulating its activity and contributes to the maintenance of proper intestinal function (8). Imbalances in ACh/AChE activities have been linked with irritable bowel syndrome (IBS) and inflammatory bowel disease, highlighting their importance in maintaining intestinal homeostasis (9).

Disturbances in intestinal homeostasis, such as dysbiosis in microbial composition, can lead to increased reactive oxygen species (ROS) levels and cause oxidative stress in the GIT. The changes within the oxidant-antioxidant molecules alter the oxidative balance and affect intestinal homeostasis. Recently, there has been an increasing amount of attention in studies that focus on the possible connection between disturbances in the gut microenvironment and neurodegenerative diseases via the gut-brain axis. Accordingly, recent research has indicated that pathological changes associated with PD can also be present in the enteric nervous system, contributing to disease progression (6).

The research focused on revealing the underlying mechanisms of PD is continuing with human and animal studies. Zebrafish is an exotic freshwater fish that is a preferred model for PD studies because of its similarities to the human immune system and the well-characterized dopaminergic system. Rotenone, a member of the rotenoid family of chemicals, is one of the most commonly used neurotoxins for inducing PD in animals (10). It accumulates in neurons and inhibits mitochondrial complex I, which elevates ROS levels and leads to neuron dysfunction. When zebrafish are exposed to rotenone, their dopaminergic neurons are damaged, resulting in reduced dopamine levels, impaired motor function, behavioral abnormalities, and intestinal dysfunction associated with PD (10). In recent years, it has been proposed that *P. gingivalis* along with its virulence factors, especially gingipain, may change the gut microbiota and possibly be related to neurodegeneration via the gut-brain axis. To elucidate the impact of gingipain on intestinal homeostasis and to understand its link to neurodegenerative diseases, we directly administered gingipain during rotenone exposure in a zebrafish model. Our study evaluated gingipain's effect on the gut AChE activity and oxidant-antioxidant status in rotenone-exposed zebrafish.

MATERIALS AND METHODS

Animal Experiments

The experiments conducted in this study followed the guidelines outlined by the European Communities Council Directive of November 24, 1986 (86/609/EEC). The study's techniques were approved by the Animal Care and Use Committee of Marmara University (17.2022mar). The standards of Animal Research: Reporting of *in vivo* experiments were followed, and every attempt was made to use the fewest number of animals in the study as possible.

AB/AB strain, male/female, wild type, 4-6 months old, healthy zebrafish (*Danio rerio*) were maintained in an aquarium setup (ZebTEC, Italy) that was adjusted to 27–28 ± 1°C under a 14/10

h light/dark period. The fish were given flake fish food (20 mg) twice daily (Tetramine, Germany). Sixty adult zebrafish were divided into four groups randomly. The groups were assigned as follows: Control (C); Gingipain (G); Rotenone (R); Gingipain + Rotenone, (G+R) (n=15 each) groups. To replicate the systemic inflammatory effect of periodontitis, zebrafish in the G group received 93 nmol/L gingipain (MyBioSource, United States, Recombinant *P. gingivalis* Gingipain, RgpA, MBS969681) injections intraperitoneally. Gingipain concentration was established by our research group's previous study (11). The

injections were administered by the same researcher and performed once every 7 days for 4 weeks. In 5 L of aquarium water, the R group was exposed to a mixture of 5 µg/L rotenone (Sigma, United States) and dimethyl sulfoxide (0.1%) (Sigma, United States), based on our group's prior studies (12). Fish in the G+R group underwent intraperitoneal injections of gingipain (93 nmol/L), and were exposed to rotenone (5µg/L). The zebrafish in the control group were injected intraperitoneally with 5 µL phosphate-buffered saline to mimic the stress caused by the injection procedure in the experimental groups.

During the injection process, zebrafish were anaesthetized via rapid cooling for 10 seconds. Subsequently, the fish were positioned ventral side up in a groove on a wet sponge, and the related agent was injected intraperitoneally using a Hamilton injector. Water tanks and exposure solutions were refreshed every 48 h. After 4 weeks, the fish were sedated through rapid cold exposure, and euthanized by decapitation. Intestinal samples were obtained, and stored at -20°C for future analyses. The biochemical and data analyses were performed by blinded researchers.

Biochemical Analyses

Zebrafish intestinal tissues were homogenized to create 10% homogenates. After following centrifugation, the resulted supernatant was isolated, and prepared for biochemical analysis. The Lowry et al. approach was used to measure total protein levels, and the outcomes were expressed as a Unit per protein (13). A byproduct of lipid peroxidation (LPO), malondialdehyde levels, were assessed using the technique described by Yagi (14). Quantities of nitric oxide (NO) were assessed by the approach of Miranda et al. (15). Superoxide dismutase (SOD) activity was evaluated using a photo-oxidation reaction (16). The Habig & Jacoby technique was used to measure glutathione-S-transferase (GST) enzyme activity at 340 nm (17). The activity of acetylcholinesterase (AChE) was determined by following Ellman et al.'s protocol (18).

Statistical Analyses

Statistical power analysis was used to establish the sample size, with an emphasis on identifying small effects. GraphPad Prism 9.0 software (GraphPad Software, United States) was utilised for statistical analysis, and the outcomes were presented as the mean ± standard deviation. Dunn's multiple comparison tests were used after the Kruskal-Wallis test to compare the data. A p-value of less than 0.05 (p<0.05) was selected for determining statistical significance.

RESULTS

Results of the Biochemical Analyses

Gingipain injection significantly increased intestinal LPO levels compared with the C, R, and G + R groups. In comparison with the G, R, and control groups, the LPO levels of the G + R group were significantly decreased (Figure 1A).

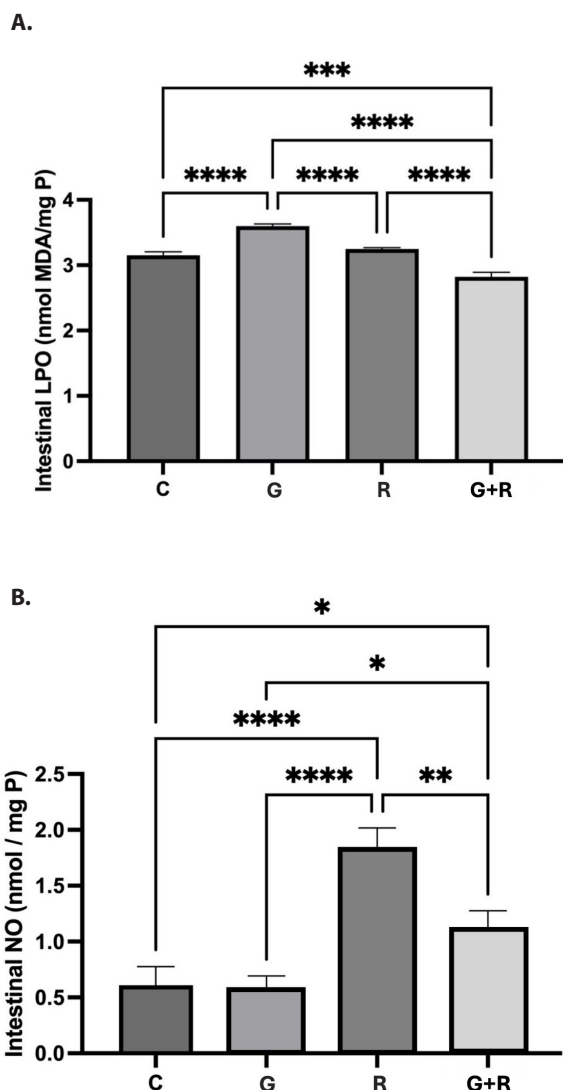


Figure 1. A) Lipid peroxidation (LPO) levels of the groups. B) Nitric oxide (NO) levels of the groups. Data are presented as mean ± SD; **** p<0.0001, *** p<0.001, ** p<0.01, *p<0.05. C: control group, G: gingipain-injected group, R: rotenone-exposed group, G + R: gingipain-injected and rotenone-exposed groups.

The levels of NO in the R and G + R groups were significantly elevated compared with those in the control group. When compared with the G group, the NO levels in the G + R group were significantly higher, and when compared with the R group, the levels were significantly reduced (Figure 1B).

The R group's intestinal GST activity was significantly higher than that of the control, G, and G + R groups. The GST activity of the G and R groups differed significantly (Figure 2B).

SOD activity was significantly reduced in the G group and significantly elevated in the R group compared with that in the C group. In comparison to the G group, SOD activity was significantly increased in the R and G + R groups. The G + R group's SOD activity was much lower than that of the R group (Figure 2A).

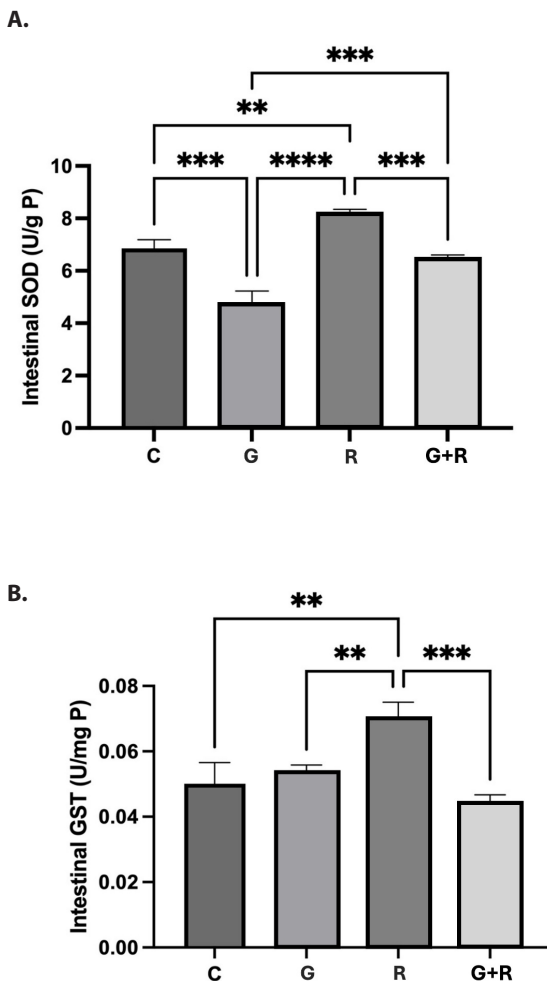


Figure 2. A) Superoxide dismutase (SOD) activity of the groups. B) Glutathione-S-transferase (GST) activity of the groups. Data are presented as mean ± SD; **** p<0.0001, *** p<0.001, ** p<0.01, * p<0.05. C: control group, G: gingipain-injected group, R: rotenone-exposed group, G + R: gingipain-injected and rotenone-exposed groups.

AChE activities were significantly increased in the R and G + R groups compared with the control group. The AChE activity of the G group was significantly decreased compared with the control, R, and G + R groups (Figure 3).

DISCUSSION

Owing to the interconnected nature of the oral cavity and intestinal tract, numerous periodontopathogenic bacteria can migrate to the intestines through swallowing and contribute to dysbiosis in gut microbiota. In the literature, various animal studies have shown that oral *P. gingivalis* administration impairs intestinal permeability, causes dysbiosis, and intensifies inflammation in the intestines (19). The pathogenicity of *P. gingivalis* is significantly organized by gingipain proteases, which have the most attraction among the virulence factors of the bacterium. *P. gingivalis* and gingipain are also linked with the progression of neuroinflammation (20), and inhibition of gingipain decreases the severity of the inflammatory state (3).

Continuous dysbiosis in the gut microbiome leads to alterations in ENS signaling and can affect the CNS, potentially acting as a trigger for neuroinflammation. This interconnected relationship between the oral cavity, intestines, and brain is called the "oral-gut-brain axis" and is a recent growing area of interest (21). In our study, we demonstrated the impact of the endotoxin gingipain on the activity of AChE and the oxidant-antioxidant status in the gut tissues of rotenone-exposed zebrafish.

ACh is a primary neurotransmitter essential for regulating the cholinergic system in the CNS and ENS. In the intestines, ACh is essential for the functioning of digestive processes, including

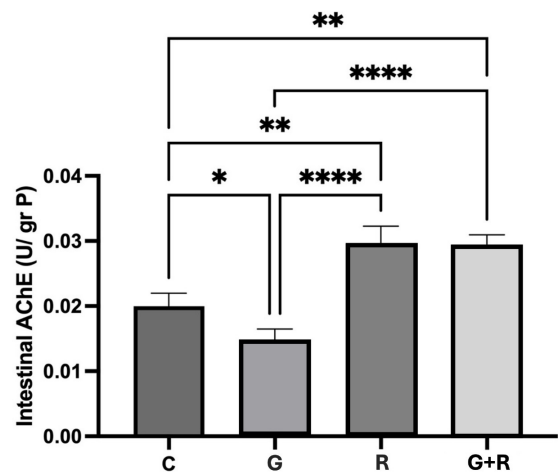


Figure 3. Acetylcholinesterase (AChE) activity in the groups. Data are presented as mean ± SD; **** p<0.0001, *** p<0.001, ** p<0.01, * p<0.05. C: control group, G: gingipain-injected group, R: rotenone-exposed group, G + R: gingipain-injected and rotenone-exposed groups.

the contraction of smooth muscles and secretion of digestive enzymes (8). AChE is an enzyme that regulates the levels of ACh, ensuring that the signaling is properly terminated. The intricate balance between ACh and AChE activity in the gut is important for the proper functioning of the digestive system, and any disruption in this balance can lead to gastrointestinal problems. In our study, gingipain injection significantly decreased AChE activity compared with the control group, proposing a dysregulated increase in ACh levels. Although ACh is an essential regulator of the physiological functions of the gut, excessive elevations in ACh levels could lead to overstimulation of the smooth muscles of the intestines, hypersecretion of digestive enzymes, increased motility, spasms, and disrupted nutrient absorption. In addition, gastrointestinal disorders such as IBS may involve imbalances in neurotransmitter levels, including ACh (9). Our results demonstrated that gingipain can affect the cholinergic system by dysregulating AChE activity, potentially causing improper functioning in the ENS. This impairment may affect the CNS via the gut-brain axis and may potentially cause neuroinflammation.

Rotenone is a strong neurotoxin that can penetrate the blood-brain barrier and accumulate in the mitochondria of dopaminergic neurons. This accumulation inhibits mitochondrial complex I activity, triggering an increased generation of reactive ROS, contributing to dopaminergic neurone degeneration and inducing parkinsonism in zebrafish models (10). The rotenone concentration utilized in our research was based on the study of Unal et al. (22). We detected a substantial increase in AChE activity after 4 weeks of rotenone exposure in both the R and G + R groups compared with the control group. This increase underline a notable decrease in ACh activity associated with reduced intestinal motility and constipation (23). These findings align with research showing a higher incidence of IBS and constipation in individuals with PD than in healthy controls (24). Our results highlight the potential relevance of gastrointestinal dysfunction in PD.

Under conditions of elevated oxidative stress, the excessive generation of ROS interacts with cell membrane lipids, causing their oxidation and disrupting normal cellular function (25). High levels of oxidative stress in intestinal cells can cause damage to intestinal epithelial cells and the gut mucosal barrier. This damage sets off an inflammatory response that releases proinflammatory cytokines and the influx of immune cells to the area. Chronic inflammation in the gut contributes to the pathogenesis of gastrointestinal disorders and neurodegenerative diseases through the gut-brain axis (25). In this study, 4 weeks of gingipain injection remarkably increased LPO levels in the zebrafish intestines compared with the control group, indicating a major disruption in the oxidant-antioxidant balance. In a previous study by our research group, where we injected a single dose of gingipain into zebrafish, and evaluated the LPO levels in gut tissues after 6 h, the antioxidant activity of GST was sufficient to detoxify the LPO levels (26). In the present study, we demonstrated that 4 weeks of chronic gingipain administration intensified intestinal cell damage by

further enhancing the oxidation of cell membrane lipids. This elevated oxidative stress can deteriorate the intestinal barrier, trigger inflammation, and compromise ENS signaling, leading to neuroinflammation/neurodegeneration via the gut-brain axis. In our study, there was no significant difference in LPO levels when comparing the R group with the control group. This result is possibly due to the counterbalancing of LPO levels, facilitated by the significantly elevated antioxidant enzyme levels, SOD, and GST. According to our findings, LPO levels were reduced in the G + R group compared with the G and control groups. This result may indicate that the oxidative response to gingipain in the gut was compromised in rotenone-exposed zebrafish.

SOD and GST both play important roles in distinct detoxification pathways in cell metabolism. SOD is an enzyme that catalyzes the degradation of highly toxic superoxide (O_2^-) molecules into oxygen, water, and hydrogen peroxide, preventing the formation of highly reactive and harmful ROS. GST is an antioxidant enzyme that catalyzes the conjugation of reduced glutathione, xenobiotics, and endogenous compounds with glutathione, facilitating their detoxification and removal from the cell. Dysfunction in antioxidant function in cells has been linked to various diseases associated with oxidative stress, including neurodegenerative diseases (27). In our study, rotenone exposure significantly increased the SOD and GST activities compared with the control for balancing the oxidative stress caused by the neurotoxin. Gingipain injection caused a significant reduction in the SOD activity compared with the control group, which may be due to the consumption of the SOD enzyme to detoxify elevated oxidative stress. Injection of gingipain in the R group also resulted in a significant decrease in both SOD and GST levels. In reaction to increased oxidative stress by rotenone exposure, although the activities of antioxidant enzymes (GST and SOD) were initially upregulated, the cumulative effects of prolonged inflammation generated by gingipain and continuously elevating oxidative stress may overwhelm the cellular defence mechanisms leading to a subsequent decline in the activities of antioxidant enzymes.

NO is involved in various physiological functions within the gastrointestinal system. It serves as a regulator of smooth muscle tone, has antimicrobial properties, contributes to the immune defense in the gut, and controls microbial balance. Although NO is not a direct marker of oxidative stress, under elevated conditions, it can react with ROS and contribute to oxidative damage (28). It is also important in the functioning of ENS, and dysregulation of NO has been observed in individuals with PD (7). In our study, rotenone exposure significantly elevated NO levels compared with the control group since it is a strong neurotoxin that creates high levels of oxidative stress. In the G + R group, there was a significant reduction in NO levels compared with the R group. High levels of ROS can reduce the bioavailability of NO by directly reacting with it, and forming peroxynitrite ($ONOO^-$), and it can impair the function of nitric oxide synthase (NOS), which is involved in NO production (29). In addition, a healthy gut microbiota contributes to the

production of NO, and an imbalance in the microbiome may negatively impact its synthesis (30). Therefore, in our study, the combination of the bacterial endotoxin gingipain and PD-inducing neurotoxin may compromise NO production in the gut, potentially leading to an imbalance in the regulation of ENS.

In our study, we studied the effects of gingipain, the most destructive virulence factor of *P. gingivalis*, on the zebrafish intestine, which may be important because of its potential impact on PD via the gut-brain axis. Gingipain caused significant imbalances in oxidative status and dysregulated AChE activity. The cumulative effect of the endotoxin gingipain and neurotoxin rotenone resulted in pronounced disruptions in oxidant-antioxidant balance, suggesting a potential compromise in cellular defense mechanisms. Moreover, to the best of our knowledge, this is the first study to show the impact of chronic gingipain exposure on AChE activity and oxidative status in the gut tissues of rotenone-exposed zebrafish. Our research highlights the link between an endotoxin produced by pathological periodontal microbiota and gut dysbiosis, which may have an effect on neurodegenerative diseases, particularly PD, underlining the important role of regular periodontal check-ups to keep the periodontal tissues healthy for maintaining a healthy ENS and CNS. Our findings will guide future research on the endotoxins of periodontal pathogenic bacteria and their connexion to neurodegenerative diseases in conjunction with the oral-gut-brain axis.

Ethic Committee Approval: Approval was received for this study from Marmara University Animal Experiments Local Ethics Committee. Protocol code: 17.2022mar.

Peer-review: Externally peer-reviewed.

Author Contributions: Conception/Design of Study- I.I., M.B., D.C., E.E.A., K.N.K.; Consultant: I.I., M.B., I.U., D.C.; Experiments: I.I., E.E.A., K.N.K.; Drafting Manuscript- I.I., M.B., I.U., D.C.; Critical Revision of Manuscript- E.E.A., K.N.K.; Final Approval and Accountability- I.I., M.B., D.C., E.E.A., K.N.K.

Conflicts of Interests: The authors declare that they have no competing interests.

Financial Disclosure: This research was supported by Marmara University Scientific Research and Project Commission, Project no: TDK-2023-10892.

REFERENCES

1. Kassebaum NJ, Smith AGC, Bernabe E, Fleming TD, Reynolds AE, Vos T, et al. Global, regional, and national prevalence, incidence, and disability-adjusted life years for oral conditions for 195 countries, 1990-2015: A systematic analysis for the global burden of diseases, injuries, and risk factors. *J Dent Res* 2017; 96(4): 380-7.
2. How KY, Song KP, Chan KG. *Porphyromonas gingivalis*: An overview of periodontopathic pathogen below the gum line. *Front Microbiol* 2016; 7: 53.
3. Dominy SS, Lynch C, Ermini F, Benedyk M, Marczyk A, Konradi A, et al. *Porphyromonas gingivalis* in Alzheimer's disease brains: Evidence for disease causation and treatment with small-molecule inhibitors. *Sci Adv* 2019; 5(1): eaau3333.
4. Ilievski V, Zuchowska PK, Green SJ, Toth PT, Ragozzino ME, Le K, et al. Chronic oral application of a periodontal pathogen results in brain inflammation, neurodegeneration and amyloid beta production in wild type mice. *PLoS One* 2018; 13(10): e0204941.
5. Adams B, Nunes JM, Page MJ, Roberts T, Carr J, Nell TA, et al. Parkinson's Disease: A systemic inflammatory disease accompanied by bacterial inflammagens. *Front Aging Neurosci* 2019; 11: 210.
6. Klann EM, Dissanayake U, Gurrula A, Farrer M, Shukla AW, Ramirez-Zamora A, et al. The gut-brain axis and its relation to Parkinson's Disease: A review. *Front Aging Neurosci* 2021; 13: 782082.
7. Aquilano K, Baldelli S, Rotilio G, Ciriolo MR. Role of nitric oxide synthases in Parkinson's disease: a review on the antioxidant and anti-inflammatory activity of polyphenols. *Neurochem Res* 2008; 33(12): 2416-26.
8. Harrington AM, Hutson JM, Southwell BR. Cholinergic neurotransmission and muscarinic receptors in the enteric nervous system. *Prog Histochem Cytochem* 2010; 44(4): 173-202.
9. Mishima Y, Ishihara S. Molecular mechanisms of microbiota-mediated pathology in irritable bowel syndrome. *Int J Mol Sci* 2020; 21(22): 8664.
10. Unal I, Emekli-Alturfan E. Fishing for Parkinson's Disease: A review of the literature. *J Clin Neurosci* 2019; 62:1-6.
11. Gunduz G, Beler M, Unal I, Cansiz D, Emekli-Alturfan E, Kose KN. Endotoxin of *Porphyromonas gingivalis* amplifies the inflammatory response in hyperglycemia-induced zebrafish through a mechanism involving chitinase-like protein YKL-40 analogs. *Toxicol Res* 2023; 39(4): 625-36.
12. Cansiz D, Unal I, Ustundag UV, Alturfan AA, Altinoz MA, Elmaci I, et al. Caprylic acid ameliorates rotenone induced inflammation and oxidative stress in the gut-brain axis in Zebrafish. *Mol Biol Rep* 2021; 48(6): 5259-73.
13. Baldwin RR, Lowry JR, Thiessen R, Jr. Some effects of processing on the nutritive properties of proteins. *Food Res* 1951; 16(2): 107-17.
14. Yagi K. Assay for blood plasma or serum. *Methods Enzymol* 1984; 105: 328-31.
15. Miranda KM, Espey MG, Wink DA. A rapid, simple spectrophotometric method for simultaneous detection of nitrate and nitrite. *Nitric Oxide* 2001; 5(1): 62-71.
16. Mylroie AA, Collins H, Umbles C, Kyle J. Erythrocyte superoxide dismutase activity and other parameters of copper status in rats ingesting lead acetate. *Toxicol Appl Pharmacol* 1986; 82(3): 512-20.
17. Habig WH, Pabst MJ, Jakoby WB. Glutathione S-transferases. The first enzymatic step in mercapturic acid formation. *J Biol Chem* 1974; 249(22): 7130-9.
18. Ellman GL, Courtney KD, Andres V, Jr., Feather-Stone RM. A new and rapid colorimetric determination of acetylcholinesterase activity. *Biochem Pharmacol* 1961; 7: 88-95.
19. Feng YK, Wu QL, Peng YW, Liang FY, You HJ, Feng YW, et al. Oral *P. gingivalis* impairs gut permeability and mediates immune responses associated with neurodegeneration in LRRK2 R1441G mice. *J Neuroinflammation* 2020; 17(1): 347.
20. Visentin D, Gobin I, Maglica Z. Periodontal pathogens and their links to neuroinflammation and neurodegeneration. *Microorganisms* 2023; 11(7): 1832.

21. Li D, Ren T, Li H, Liao G, Zhang X. *Porphyromonas gingivalis*: A key role in Parkinson's disease with cognitive impairment? *Front Neurol* 2022; 13: 945523.
22. Unal I, Cansiz D, Surmen MG, Surmen S, Sezer Z, Beler M, et al. Identification of molecular network of gut-brain axis associated with neuroprotective effects of PPARdelta-ligand erucic acid in rotenone-induced Parkinson's disease model in zebrafish. *Eur J Neurosci* 2023; 57(4): 585-606.
23. Gros M, Gros B, Mesonero JE, Latorre E. Neurotransmitter dysfunction in irritable bowel syndrome: Emerging approaches for management. *J Clin Med* 2021; 10(15): 3429.
24. Tai YC, Liao PH, Leta V, Lin CH, Chaudhuri KR. Irritable bowel syndrome based on Rome IV diagnostic criteria associates with non-motor symptoms of Parkinson's disease. *Parkinsonism Relat Disord* 2023; 113: 105496.
25. Li X, Kiprowska M, Kansara T, Kansara P, Li P. Neuroinflammation: A distal consequence of periodontitis. *J Dent Res* 2022; 101(12): 1441-9.
26. Gunduz G BM, Unal I, Cansiz D, Emekli-Alturfan E, Kose KN. Gingipain injection affects intestinal oxidant/antioxidant status and alkaline phosphatase in overfed zebrafish. *Experimed* 2023; 13(2): 80-5.
27. Chang KH, Chen CM. The role of oxidative stress in Parkinson's Disease. *Antioxidants (Basel)* 2020; 9(7): 597.
28. Lubos E, Handy DE, Loscalzo J. Role of oxidative stress and nitric oxide in atherothrombosis. *Front Biosci* 2008; 13: 5323-44.
29. Masha A, Dinatale S, Allasia S, Martina V. Role of the decreased nitric oxide bioavailability in the vascular complications of diabetes mellitus. *Curr Pharm Biotechnol* 2011; 12(9): 1354-63.
30. Wallace JL. Nitric oxide in the gastrointestinal tract: Opportunities for drug development. *Br J Pharmacol* 2019; 176(2): 147-54.

Effects of o-tDCS and tDCS on Maximal Grip Strength

Sercan Seker^{1,2} , Gaye Eskicioglu³ , Zeynep Kucuk⁴ , Sacit Karamursel⁵ 

¹Institute of Graduate Studies in Health Sciences, Istanbul University, Istanbul, Turkiye

²Department of Physiology, Istanbul Faculty of Medicine, Istanbul University, Istanbul, Turkiye

³Department of Neuroscience, Aziz Sancar Institute of Experimental Medicine, Istanbul University, Istanbul, Turkiye

⁴Department of Administrative and Social Sciences, Psychology, Isik University, Faculty of Art and Economics, Istanbul, Turkiye

⁵Department of Physiology, Koc University School of Medicine, Istanbul, Turkiye

ORCID ID: S.S. 0000-0002-6262-7517; G.E. 0000-0001-6562-8008; Z.K. 0000-0003-4729-8556; S.K. 0000-0002-7534-9392

Cite this article as: Seker S, Eskicioglu G, Kucuk Z, Karamursel S. Effects of o-tDCS and tDCS on maximal grip strength. *Experimed* 2024; 14(3): 146-153.

ABSTRACT

Objective: The aim of the current study was to examine and compare the effects of oscillatory transcranial direct current stimulation (o-tDCS) and transcranial direct current stimulation (tDCS) against sham stimulation on maximal intermittent gripping performance.

Materials and Methods: The study included 25 healthy, right-handed male subjects (age range 18-35 years) who were randomly assigned to three separate groups: o-tDCS (n=9), tDCS (n=8) and sham (n=8). The left primary motor cortex was selected as the anodal stimulation region, and a cathode electrode was placed over the right supraorbital area. A hand dynamometer is used to measure the maximum grip values during a maximal intermittent gripping task. Between-group comparisons were made; for each stimulation group, baseline grip values of the participants were compared with those obtained during stimulation.

Results: Although the o-tDCS group showed slightly better improvements in maximal and mean strength, there were no statistically significant differences between stimulation groups ($p>0.05$).

Conclusion: The findings of the study suggest neither o-tDCS nor tDCS has a significant facilitative impact on grip strength values in healthy young males, most likely due to a ceiling effect in this population.

Keywords: Transcranial direct current stimulation, oscillatory transcranial direct current stimulation, grip strength, grip endurance

INTRODUCTION

Grip strength is an important motor function that is frequently used in daily life, sportive activities, and occupations that require repetitive and strenuous manual work. It has been shown to be a reliable, non-invasive marker of overall muscle strength (1).

The literature identified some populations that are disadvantageous in terms of grip strength. Neuroticism, stress, anxiety, and depression have been shown to have a weakening effect on grip strength (2, 3). The increase in right frontal activity was found to be correlated with the stated psychophysiological factors (4). Additionally, grip strength

was found to be lower in dentists and musicians who are engaged in professions requiring fine motor skills (5, 6). Implying that motor control skill develops at the expense of gross motor strength. Indeed, it has been shown that reduced cortical excitability and enhanced intracortical inhibition of the motor cortex alleviate unwanted hand movements (7). However, the mentioned changes in motor cortical activations occur in an opposite manner during the process of strength gain (8).

Both the intrinsic and extrinsic muscles in the forearm and hand need to operate in coordination to produce grip strength. Neural adaptations are essential for effectively coordinated muscle contraction to achieve maximal

Corresponding Author: Sercan Seker **E-mail:** sercanseker1903@gmail.com

Submitted: 13.06.2024 **Revision Requested:** 16.07.2024 **Last Revision Received:** 20.07.2024 **Accepted:** 25.07.2024 **Published Online:** 14.10.2024



Content of this journal is licensed under a Creative Commons Attribution-NonCommercial 4.0 International License.

achievable force. This is corroborated by evidence from strength training participants, which indicated that enhanced synchronization and discharge rate, along with an increase in active motor units, provide the basis for training-induced improvement in maximal force (9–11). Slow motor units are functioning in every voluntary contraction, but it is challenging to activate large motor neurons entirely due to their high threshold. This difficulty in the total recruitment of fast motor units is the reason for untrained individual's inability to exert their potential maximum force. In addition, high-threshold motor neurons are prone to high-force anaerobic work, but in the meantime, they are highly fatigable. For this reason, high force levels cannot be sustained long.

A typical description of fatigue is a progressive decrease in strength. Reduced stimulation of high-threshold motor units and increased inhibitory transmission to the motor cortex represent two mechanisms of centrally developed weariness that diminish neural drive and motor output. Motor fatigue further affects the functioning of frontal regions (such as orbitofrontal areas and middle frontal gyrus) and motor-related areas in conjunction with decreasing force production (12). All of the findings indicated that the primary motor cortex and the right frontal area may conversely influence grip strength.

Transcranial direct current stimulation (tDCS) is a widely used neuromodulation technique that is proven to be effective in facilitating firing rate (13), and might stimulate the motor cortex while mitigating right frontal activity to modulate strength performance and fatigue. tDCS is mainly operated via the polarity-related effects of low-intensity direct current passing through the electrodes. The resting membrane potential is depolarized beneath the anode of the tDCS, facilitating the initiation of an action potential. On the other hand, the cathode reduces the excitability at its target location by hyperpolarization (14). Literature findings appeared to be rather inconclusive regarding the effects of tDCS on maximal strength, especially in the upper limbs (15,16).

Polarity-related effects are also preserved in o-tDCS. In addition, o-tDCS is also capable of entrainment of endogenous brain oscillations via its sinusoidal current (17). Thus, selecting the frequency at which the current is oscillated is of great importance. One of the renowned oscillations that o-tDCS has been shown to affect is alpha brain waves (18). In general, alpha waves are linked to the suppression of task-irrelevant activations in the cortex. A recent study stated that the occurrence of alpha waves in the cortex generally (and in the frontal regions specifically) has a favorable correlation with neural efficiency (19). Additionally, it has been reported that greater pre-stimulus alpha activity in motor-related cortical areas is associated with motor excitability (20).

Considering these findings, the aim of this research was to improve strength performance. For this purpose, a maximal intermittent gripping task that measures dynamic grip performance was employed, which has been adopted in the

literature (21, 22). Through this task, it would be possible to compare the effects of tDCS and o-tDCS on various force parameters. A similar study was recently conducted in the cognitive domain, and the effectiveness of o-tDCS was demonstrated (23).

The study hypothesizes that since traditional tDCS is relatively ineffective for enhancing maximal strength, o-tDCS might be more beneficial due to its potential to not only increase cortical excitability and firing rate, as tDCS mainly does, but also to aid synchrony and neural efficiency through its frequency-related entrainment ability. These effects may lead to better performance in tasks requiring maximal strength and endurance.

In strength studies, the male and female populations are typically examined independently because variations have been found in stimulation-induced increases in muscle strength due to sex differences (24, 25). Hence, the study was conducted in a specific gender (healthy young male population). Although achieving maximal strength improvements in a young healthy population can be challenging due to a possible ceiling effect, a potential increase in grip strength may benefit a wide range of individuals with strength deficits.

MATERIALS AND METHODS

Participants

The study population was consisted of 25 healthy male volunteers between the ages of 18-35 years. A prior sample size calculation for repeated measures analysis of variance (ANOVA) was performed with G*Power software, with an effect size of 0.5, alpha error of 0.05, and statistical power of 0.95 as parameters, and the minimum sample size was calculated as 21. Participants were recruited from right-handed university students in order to standardize the electrode placement based on hand dominance. There were no medical conditions affecting the forearm, shoulder, or hand muscles that might have affected the outcome. All participants were informed in detail about the study procedures and provided written informed consent. The study was approved by the Istanbul University Istanbul Faculty of Medicine Clinical Research Ethics Committee (File no. 2017 / 661). The study was conducted in accordance with the Declaration of Helsinki.

Design

The study was designed as a randomized, single-blind, parallel-group, sham-controlled measurement. Participants were assigned to either the o-tDCS, tDCS, or sham stimulation groups via block randomization method.

Procedure

Participants visited the laboratory twice in total. On the first day, a baseline measurement of handgrip strength was performed for all participants. On another day within that week, participants visited the laboratory again and repeated

the identical task, but this time, during the last 2 min of 20 min of o-tDCS, tDCS, or sham stimulation.

Stimulation Protocol

The TESTi device developed by TeknoFil Limited Company in the MakeLab laboratory of the Department of Physiology of I.U. Istanbul Faculty of Medicine was used for stimulation in this study. TESTi is a single-channel device that can provide direct, sinusoidal, and sham stimulation. The current intensity can be set up between 0 and 4500 µA with this device, and its frequency modulation range is between 0 and 25 Hz.

The current was transmitted to the cortex of the participants through two electrodes moistened with saline solution. The electrode dimensions were 5x7 cm. For o-tDCS, the stimulation frequency was 10 Hz. A sinusoidal current is created by changing the intensity of the direct current as a sinus in a specified range, which is superimposed on a constant offset current. The sine amplitude of the 10-Hz frequency modulation was set to 0.35 mA, and the offset was set to 1.70 mA. For tDCS, the stimulation intensity was 2 mA, and the stimulation duration was 20 min. An identical protocol was followed for sham stimulation, with the exception that the duration of stimulation was limited to 15 s. The aim of this study was to make the participant feel itching and other similar effects that occur in active stimulations (o-tDCS, tDCS); hence, the participants were blind to the stimulation type they were receiving.

All stimulation groups received the exact identical application of the tDCS montage. The anodal electrode was placed above the left primary motor cortex (C3) region according to the international 10-20 electrode system, while the cathode was placed over the supraorbital region in the contralateral hemisphere (Fp2). Electrodes were placed on the scalp using an EEG cap.

Hand Grip Measurement

Grip force measurements were performed using a Camry digital hand dynamometer. The measurement accuracy of the device was 0.1 kg. When participants release their grip at the end of each contraction, the greatest force released during this contraction is displayed on the screen and remains there until the next contraction starts. The maximal force values of the participants were obtained by utilizing this feature of the device.

Before both sessions, the participants performed three trial contractions with their dominant hands to warm up to the task and to become familiar with the use of the hand dynamometer before starting the test.

Measurements of hand grip strength were performed with a maximal intermittent gripping test lasting 1 min in total, with 12 repetitions of a 5 s task cycle, consisting of a 2 s contraction followed by a 3 s rest (21, 26). The synchronization of the participant to the task cycle was achieved through a one-minute video consisting of two visuals representing the “squeeze” and

“release” commands, generated according to contraction and rest periods. While performing this task, the participants were standing with their wrists in the neutral position, their elbows in 180° extension, and their shoulders in adduction with neutral rotation (27). They were asked to follow the video instructions to simultaneously perform the commands. Prior to measurements, all subjects were verbally informed to squeeze with their maximal strength during each contraction.

Parameters

The variables of fatigue index (*FI*), maximal strength, mean strength, and endurance constitute the basic parameters of the study. The percentage of the force readings during the first and last contraction was used to determine the *FI* (22, 28).

$$FI = \frac{\text{First Contraction} - \text{Last Contraction}}{\text{First Contraction}} \times 100$$

Other parameters for both baseline and post-stimulation values were calculated as follows: The percentage of grip strength measurements between the first and final three contractions was used to estimate *endurance* (29).

$$Endurance = \frac{\text{Mean of First Three Contractions}}{\text{Mean of Last Three Contractions}} \times 100$$

The arithmetic mean of the three initial contractions was used to determine *the maximal strength*. *The mean strength* was identified by taking the mean of the force values of all repetitions (29). Furthermore, the percentage change values based on the difference between baseline values and during stimulation values was calculated as follows:

$$\text{Percentage Change of } GV = \frac{\text{During Stimulation Value of } GV - \text{Baseline Value of } GV}{\text{Baseline Value of } GV} \times 100$$

GV: Given Variable

Statistical Analyses

All statistical analyses were performed using SPSS version 22.0 software (SPSS, Chicago, IL, USA). The significance level for all statistical analyses was set as $p < 0.05$. Levene’s test was used to evaluate the homogeneity of variances. The results of this test indicated that the data had a homogeneous distribution of variance between the groups ($p > 0.05$). According to the Shapiro-Wilk test results, all variables had a normal distribution ($p > 0.05$). After analyzing the data for normality with respect to the stimulation type variable, it was observed that all subcategories were normally distributed, leading to the conclusion that parametric tests could be employed.

The study aimed to determine whether any type of stimulation had a significant impact on the participants’ maximal strength, mean strength, and/or endurance scores during stimulation in comparison with baseline. For each parameter, repeated-

measures ANOVA was conducted using a 2x3 design with “time” (baseline values, online stimulation values) as the within-subject factor and the “type of stimulation” (o-tDCS, tDCS, sham) as the between-subject factor.

RESULTS

Age Values

The mean age was 25.7 ± 3.3 (21-28) years in the o-tDCS group, 24.4 ± 2.6 (20-28) years in the tDCS group, and 28.0 ± 5.2 (20-35) years in the sham group, and there were no significant differences between the groups.

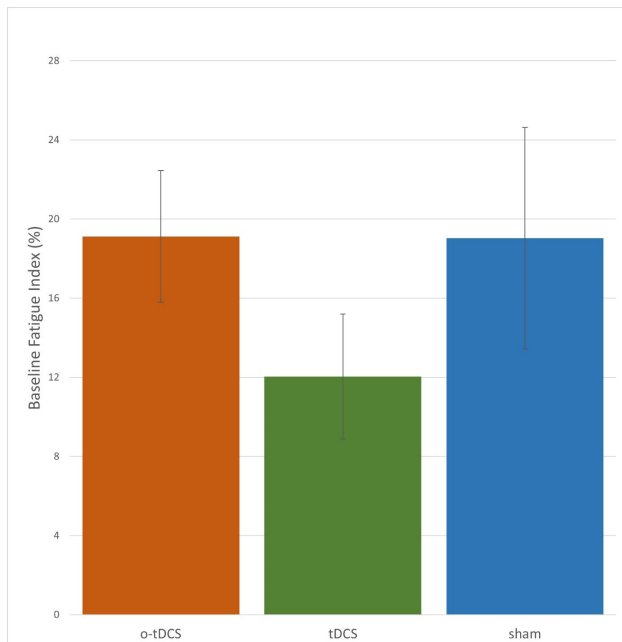


Figure 1. Baseline Fatigue Index (FI) values across stimulation groups (Mean \pm Standard Error).

Baseline Fatigue Index

Initial *FI* values were examined to ensure that the possible effects of different stimulation groups would not stem from baseline differences between the groups in terms of ability to sustain the task and tolerate fatigue. *FI* values reveal that there are no significant differences that could have an impact on outcomes; in particular, the initial *FI* values of the sham and o-tDCS groups were similar (Figure 1). In light of these data, the effects that may occur in the stimulation groups can be comparable.

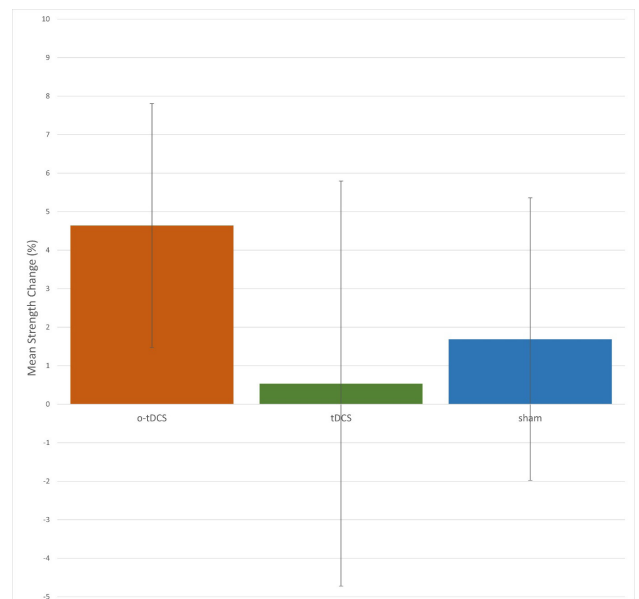


Figure 3. Percentage change in mean strength values according to stimulation type (Mean \pm Standard Error).

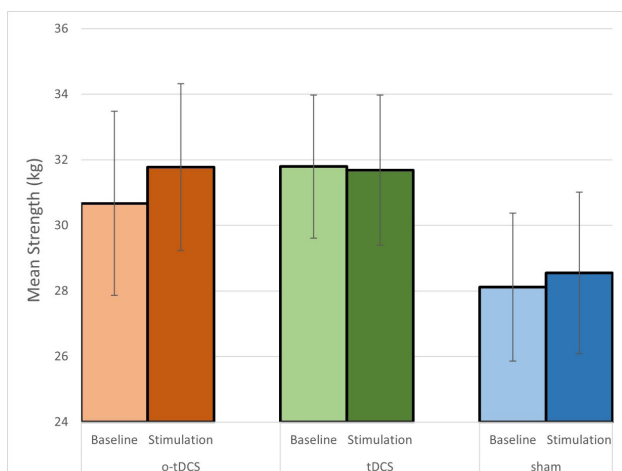


Figure 2. Change in mean strength values (kg) according to stimulation type (Mean \pm Standard Error).

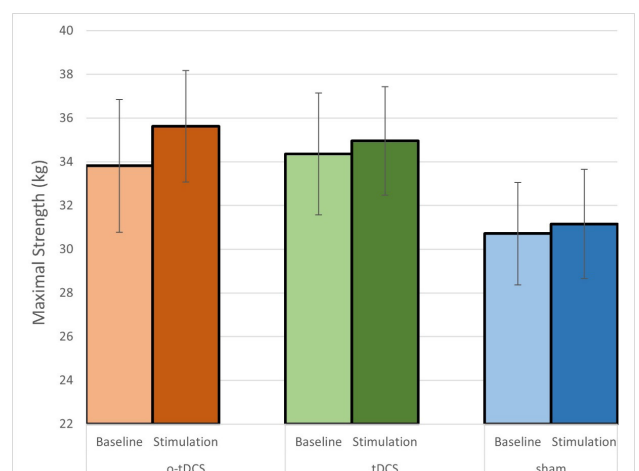


Figure 4. Change in maximal strength values (kg) according to stimulation type (Mean \pm Standard Error).

Table 1. Descriptive statistics of mean and maximum strength and endurance before and after stimulation

Stimulation Types	n	Parameters	Before Stimulation	During Stimulation
			Mean ± SD	Mean ± SD
o-tDCS	9	Mean Strength	30.67 ± 8.42	31.77 ± 7.64
		Maximal Strength	33.81 ± 9.11	35.62 ± 7.66
		Endurance	81.65 ± 11.34	77.62 ± 9.86
tDCS	8	Mean Strength	31.80 ± 6.16	31.68 ± 6.47
		Maximal Strength	34.36 ± 7.89	34.95 ± 7.04
		Endurance	89.13 ± 6.48	80.58 ± 6.10
sham	8	Mean Strength	28.12 ± 6.38	28.54 ± 6.97
		Maximal Strength	30.71 ± 6.64	31.15 ± 7.08
		Endurance	86.04 ± 12.61	80.67 ± 7.85

SD: Standard Deviation; o-tDCS: oscillatory transcranial direct current stimulation; tDCS: transcranial direct current stimulation.

Effect of Stimulation Type on Mean Strength

We investigated whether the subjects’ mean strength before and during the stimulation altered and whether the stimulation type affected their scores. Two-way ANOVA was used for dependent samples. There was no significant interaction effect according to results ($F(2, 22)=0.242, p=0.787, \eta^2=0.001$). There was also no significant main effect of time observed ($F(1, 22)=0.433, p=0.517, \eta^2=0.001$). Lastly, there was no main effect found according to the type of stimulation ($F(2, 22)=0.579, p=0.569, \eta^2=0.047$). The o-tDCS, tDCS, and sham groups did not show a significant difference in their scores (Figure 2, Figure 3).

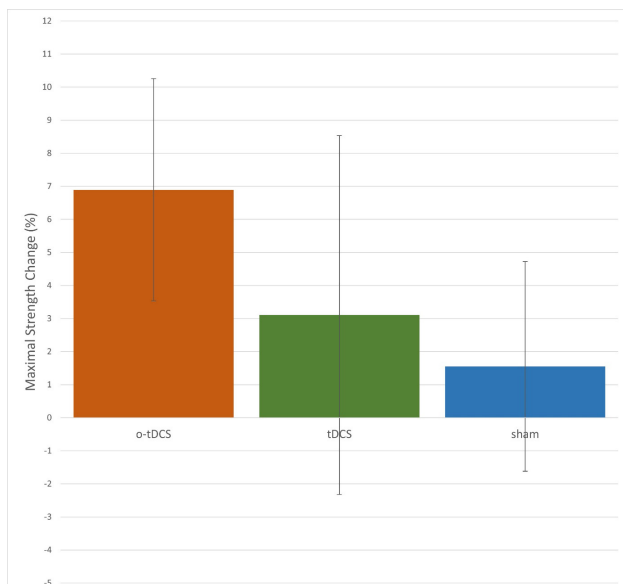


Figure 5. Percentage change in maximal strength values according to stimulation type (Mean ± Standard Error).

Effect of Stimulation Type on Maximal Strength

We investigated whether the subjects’ maximal strength before and during the stimulation altered and whether the stimulation type affected their scores. Two-way ANOVA was used for dependent samples. There was no significant interaction effect according to results ($F(2, 22)=0.356, p=0.704, \eta^2=0.002$). The main effect of time was also insignificant ($F(1, 22)=1.642, p=0.213, \eta^2=0.004$). There was also no main effect of the type of stimulation variable ($F(2, 22)=0.697, p=0.509, \eta^2=0.056$). The o-tDCS, tDCS, and sham groups did not show a significant difference in their scores (Figure 4, Figure 5).

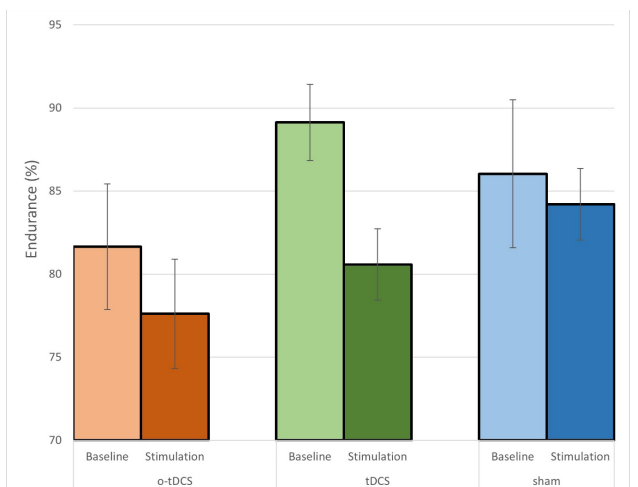


Figure 6. Change in endurance percentage values according to stimulation type (Mean ± Standard Error).

Effects of Stimulation Type on Endurance

We investigated whether the subjects' endurance values before and during the stimulation altered and whether the stimulation type affected their scores. Two-way ANOVA was used for dependent samples. There was no significant interaction effect according to results ($F(2, 22)=0.826, p=0.451, \eta^2=0.021$). There was also no main effect of the type of stimulation variable ($F(2, 24)=1.468, p=0.252, \eta^2=0.074$). Only the main effect of time was significant ($F(1, 22)=5.056, p=0.035, \eta^2=0.065$). It is understood that in all groups, the endurance values decreased during the stimulation compared to their respective baseline values. The o-tDCS, tDCS, and sham groups did not show a significant difference in their scores (Figure 6). Table 1 provides a summary of all findings.

DISCUSSION

The findings of the study indicate that the two types of transcranial electrical stimulation did not have a statistically significant effect on grip strength compared with the control group (sham). Although some improvements were observed in the maximal and mean strength values in the 10 Hz o-tDCS group compared with the tDCS and sham groups, they did not sufficiently vary to reach the level of significance.

The number of participants could be a critical factor affecting the outcome of the study. It is inescapable that a limited sample size reduced the study's statistical capacity to identify minor or modest effects, which could be the main factor in the absence of significance in the results.

A further explanation of the study's lack of strength improvement could be the possible ceiling effect of grip strength in healthy young men. It has been shown in the literature that strength peaks in men between 20 and 30 years of age (30). Given that the age spectrum was mostly identical to the investigated participant population. A task must be sufficiently challenging for a given population to demonstrate a possible facilitative effect of the stimulation. Therefore, the potential ceiling effect may be eliminated in future studies by making the task more difficult by altering task cycle values (such as increasing the contraction time and shortening the rest period) or increasing the duration of the task. It would also be interesting to examine whether similar stimulation would be effective in different cohorts in future studies to avoid a potential age-related ceiling effect.

It should also be noted that there are extremely few reports in the tDCS literature on improving the maximal strength of the upper limbs (especially on young healthy male population). A review published in 2019 identified (31) only three studies that showed effectiveness on strength gains (31-34). Two of these studies were derived from female participants, and the only successful study with male participants investigated the lower limbs (34). Another recent review investigated the impact of tDCS on the upper limbs could not find any significant improvement (16). In light of these findings, the outcome of

the study is not particularly surprising. Although the electrode positioning used in this study has been shown to be the most effective for facilitating motor-evoked potentials, other motor-related regions, such as the premotor area, which has been shown to have a positive effect on dexterity, may also be tried in future studies (35, 36).

A plausible explanation for the statistical insignificance of the results of o-tDCS could be that the participants' brain waves were not entrained to the specified 10 Hz frequency. Spectrum analysis could not be performed because EEG was not utilized in the study, and it is likely that if participants' brain oscillations drift to a frequency that differs from the 10 Hz alpha oscillation, this could have negatively affected the results of the o-tDCS group. Another possibility is that even in the entrainment period, the 10 Hz endogenous brain oscillations did not have the desired facilitative effect. Reaching a clear conclusion on this matter requires studies that implement EEG. Future research utilizing EEG and testing various frequency values for o-tDCS can potentially illuminate areas that this study left unexplored.

It may also be interesting if a similar study would be conducted in a population consisting entirely of women, which would shed light on whether there are differences in the gender-specific effects of stimulation on grip strength.

In addition to the limited number of participants, other study limitations include the lack of anthropometric measurements, such as muscle thickness, which has been suggested to have a possible effect on grip strength (37). In addition, more emphasis could have been placed on acclimating the participants to the task to make them more familiar and efficient while doing it.

In conclusion, the significant effects expected in the study's hypothesis were not achieved even though the o-tDCS stimulation provided a greater increase in both mean and maximal force than the tDCS and sham applications. This study has taken place among the few studies in the literature that investigated the possible differential effects between o-tDCS and tDCS.

Acknowledgement: We thank Adnan Kurt for providing technical support with the stimulation device. We also thank Serkan Aksu for his support in the study conception and data acquisition.

Ethical Committee Approval: The study was approved by the Istanbul University Istanbul Faculty of Medicine Clinical Research Ethics Committee (File no. 2017 / 661).

Informed Consent: Informed written consent was obtained from the participants.

Peer-review: Externally peer-reviewed.

Author Contributions: Conception/Design of Study- S.S., S.K., G.E.; Data Acquisition: S.S., G.E.; Data Analysis/Interpretation: S.K., S.S., Z.K.; Drafting Manuscript- S.K., S.S., G.E., Z.K.; Critical Revision of Manuscript- S.K., S.S.; Final Approval and Accountability- S.K., S.S., G.E., Z.K.

Conflicts of Interests: The authors declare that they have no competing interests.

Financial Disclosure: This study was funded by the Scientific and Technological Research Council of Turkey (TUBITAK 1001 Grant No: 113S302).

REFERENCES

1. Wind AE, Takken T, Helder PJM, Engelbert RHH. Is grip strength a predictor for total muscle strength in healthy children, adolescents, and young adults? *Eur J Pediatr* 2010; 169(3): 281-7.
2. Everhart DE, Harrison DW, Shenal BV, Williamson J, Wuensch KL. Grip-strength, fatigue, and motor perseveration in anxious men without depression. *Neuropsychiatry Neuropsychol Behav Neurol* 2002; 15(2): 133-42.
3. Fink B, Weege B, Pham MN, Shackelford TK. Handgrip strength and the Big Five personality factors in men and women. *Personal Individ Differ* 2016; 88: 175-7.
4. Mathersul D, Williams LM, Hopkinson PJ, Kemp AH. Investigating models of affect: Relationships among EEG alpha asymmetry, depression, and anxiety. *Emotion* 2008; 8(4): 560-72.
5. Ding H, Leino-Arjas P, Murtooma H, Takala EP, Solovieva S. Variation in work tasks in relation to pinch grip strength among middle-aged female dentists. *Appl Ergon* 2013; 44(6): 977-81.
6. Sims SEG, Engel L, Hammert WC, Elfar JC. Hand sensibility, strength, and laxity of high-level musicians compared to nonmusicians. *J Hand Surg* 2015; 40(10): 1996-2002.e5.
7. Stinear CM, Byblow WD. Role of intracortical inhibition in selective hand muscle activation. *J Neurophysiol* 2003; 89(4): 2014-20.
8. Mason J, Frazer AK, Avela J, Pearce AJ, Howatson G, Kidgell DJ. Tracking the corticospinal responses to strength training. *Eur J Appl Physiol* 2020; 120(4): 783-98.
9. Del Vecchio A, Casolo A, Negro F, Scorcelletti M, Bazzucchi I, Enoka R, et al. The increase in muscle force after 4 weeks of strength training is mediated by adaptations in motor unit recruitment and rate coding. *J Physiol* 2019; 597(7): 1873-87.
10. Fling BW, Christie A, Kamen G. Motor unit synchronization in FDI and biceps brachii muscles of strength-trained males. *J Electromyogr Kinesiol* 2009; 19(5): 800-9.
11. Zatsiorsky VM, Kraemer WJ, Fry AC. Science and practice of strength training. Third edition. Champaign, IL: Human Kinetics; 2021.
12. Van Duinen H, Renken R, Maurits N, Zijdwind I. Effects of motor fatigue on human brain activity, an fMRI study. *NeuroImage* 2007; 35(4): 1438-49.
13. Das S, Holland P, Frens MA, Donchin O. Impact of transcranial direct current stimulation (tDCS) on neuronal functions. *Front Neurosci* 2016; 10: 550.
14. Nitsche MA, Paulus W. Excitability changes induced in the human motor cortex by weak transcranial direct current stimulation. *J Physiol* 2000; 527(3): 633-9.
15. Chinzara TT, Buckingham G, Harris DJ. Transcranial direct current stimulation and sporting performance: A systematic review and meta-analysis of transcranial direct current stimulation effects on physical endurance, muscular strength and visuomotor skills. *Eur J Neurosci* 2022; 55(2): 468-86.
16. Hu K, Chen Y, Guo F, Wang X. Effects of transcranial direct current stimulation on upper limb muscle strength and endurance in healthy individuals: a systematic review and meta-analysis. *Front Physiol* 2022; 13: 834397.
17. Neuling T, Rach S, Wagner S, Wolters CH, Herrmann CS. Good vibrations: Oscillatory phase shapes perception. *NeuroImage* 2012; 63(2): 771-8.
18. Merlet I, Birot G, Salvador R, Molaee-Ardekani B, Mekonnen A, Soria-Frith A, et al. From oscillatory transcranial current stimulation to scalp EEG changes: a biophysical and physiological modeling study. *PLoS ONE* 2013; 8(2): e57330.
19. Filho E, Dobersek U, Husselman TA. The role of neural efficiency, transient hypofrontality and neural proficiency in optimal performance in self-paced sports: a meta-analytic review. *Exp Brain Res* 2021; 239(5): 1381-93.
20. Ogata K, Nakazono H, Uehara T, Tobimatsu S. Prestimulus cortical EEG oscillations can predict the excitability of the primary motor cortex. *Brain Stimulat* 2019; 12(6): 1508-16.
21. Bembem MG, Massey BH, Bembem DA, Misner JE, Boileau RA. Isometric intermittent endurance of four muscle groups in men aged 20-74 yr. *Med Sci Sports Exerc* 1996; 28(1): 145-53.
22. White C, Dixon K, Samuel D, Stokes M. Handgrip and quadriceps muscle endurance testing in young adults. *Springer Plus* 2013; 2(1): 451.
23. Vulić K, Bjekić J, Paunović D, Jovanović M, Milanović S, Filipović SR. Theta-modulated oscillatory transcranial direct current stimulation over posterior parietal cortex improves associative memory. *Sci Rep* 2021; 11(1): 3013.
24. Workman C, Fietsam A, Rudroff T. Transcranial direct current stimulation at 4 mA induces greater leg muscle fatigability in women compared to men. *Brain Sci* 2020; 10(4): 244.
25. Rudroff T, Workman CD, Fietsam AC, Kamholz J. Response variability in transcranial direct current stimulation: why sex matters. *Front Psychiatry* 2020; 11: 585.
26. Gerodimos V. Reliability of handgrip strength test in basketball players. *J Hum Kinet* 2012; 31(2012): 25-36.
27. Xu Z yang, Gao D fa, Xu K, Zhou Z qi, Guo Y kun. The Effect of posture on maximum grip strength measurements. *J Clin Densitom* 2021; 24(4): 638-44.
28. Karatrantou K. Dynamic Handgrip Strength Endurance: A reliable measurement in older women. *J Geriatr Phys Ther* 2019; 42(3): E51-6.
29. Nicolay CW, Walker AL. Grip strength and endurance: influences of anthropometric variation, hand dominance, and gender. *Int J Ind Ergon* 2005; 35(7): 605-18.
30. Evans WJ, Hurley BF. Age, gender, and muscular strength. *J Gerontol A Biol Sci Med Sci* 1995; 50A(Special): 41-4.
31. Alix-Fages, Romero-Arenas, Castro-Alonso, Colomer-Poveda, Río-Rodríguez, Jerez-Martínez, et al. Short-term effects of anodal transcranial direct current stimulation on endurance and maximal force production. A systematic review and meta-analysis. *J Clin Med* 2019; 8(4): 536.
32. Hazime FA, da Cunha RA, Solieman RR, Romancini ACB, Pochini A de C, Ejnisman B, et al. Anodal transcranial direct current stimulation (TDCS) increases isometric strength of shoulder rotators muscles in handball players. *Int J Sports Phys Ther* 2017; 12(3): 402-7.
33. Vargas VZ, Baptista AF, Pereira GOC, Pochini AC, Ejnisman B, Santos MB, et al. Modulation of isometric quadriceps strength in soccer players with transcranial direct current stimulation: a crossover study. *J Strength Cond Res* 2018; 32(5): 1336-41.
34. Tanaka S, Hanakawa T, Honda M, Watanabe K. Enhancement of pinch force in the lower leg by anodal transcranial direct current stimulation. *Exp Brain Res* 2009; 196(3): 459-65.
35. DaSilva AF, Volz MS, Bikson M, Fregni F. Electrode positioning and montage in transcranial direct current stimulation. *J Vis Exp JoVE* 2011; (51): 2744.

36. Pavlova E, Kuo MF, Nitsche MA, Borg J. Transcranial direct current stimulation of the premotor cortex: Effects on hand dexterity. *Brain Res* 2014; 1576: 52-62.
37. Trinidad-Fernández M, González-Molina F, Moya-Esteban A, Roldán-Jiménez C, González-Sánchez M, Cuesta-Vargas AI. Muscle activity and architecture as a predictor of hand-grip strength. *Physiol Meas* 2020; 41(7): 075008.

Evaluation of the Molecular Effects of the Anticancer Adjuvant Valproic Acid on HEK293T Cells

Hazal Banu Olgun Celebioglu¹ , Yeliz Ekici¹ , Abdullah Yilmaz² , Feyza Nur Tuncer³ 

¹Graduate School of Health Sciences, Istanbul University, Istanbul, Turkiye

²Department of Immunology, Aziz Sancar Institute of Experimental Medicine, Istanbul University, Istanbul, Turkiye

³Department of Genetics, Aziz Sancar Institute of Experimental Medicine, Istanbul University, Istanbul, Turkiye

ORCID ID: H.B.O.C. 0000-0001-8716-5040; Y.E. 0000-0002-6750-6378; A.Y. 0000-0002-3003-9956; F.N.T. 0000-0001-8233-1839

Cite this article as: Olgun Celebioglu HB, Ekici Y, Yilmaz A, Tuncer FN. Evaluation of the molecular effects of the anticancer adjuvant valproic acid on HEK293T cells. *Experimed* 2024; 14(3): 154-160.

ABSTRACT

Objective: Valproic acid (VPA) can induce apoptosis while inhibiting proliferation in various cancer cells. This study adopted a novel strategy for investigating the molecular effects of VPA on non-cancerous cells. Building upon our previous work, which examined the effects of VPA in PANC-1 cells, we now turn our attention to HEK293T cells to determine the effect of VPA in non-cancerous cells.

Materials and Methods: HEK293T cells were treated with 2.5 and 5-mM VPA. Flow cytometry analyses were performed on the 24, 48, 72, and 96 h. Assays for apoptosis and proliferation were conducted using annexin V/ propidium iodide (PI) staining and carboxyfluorescein-succinimidyl ester (CFSE) dilution, respectively.

Results: No statistical significance was detected between the two different doses of VPA-treated cells and the controls at any time point. While early apoptosis values remained stable until 72 h in all groups, an increase was monitored in cells subjected to VPA for 96 h.

Conclusion: Preliminary results indicated no proliferative effect of VPA treatment. However, it may induce apoptosis in long-term incubations. Nevertheless, additional doses of VPA at increased concentrations should be administered to explore cytotoxic levels and their impact on proliferation and apoptosis.

Keywords: HEK293T, VPA, apoptosis, proliferation

INTRODUCTION

Multicellular organisms maintain a delicate balance between cell proliferation, differentiation, and death, which is crucial for sustainable tissue homeostasis (1). Dysregulation of the cell cycle machinery leads to malignant phenotypes through uncontrolled cell proliferation and suppressed cell death (2). Hence, malfunctions, mutations, or inactivations in these systems frequently lead to cancer development.

Additionally, epigenetic mechanisms have essential roles in maintaining normal growth and development through modulating gene expression machinery, particularly

in the methylation of DNA, modifications of histones, and expression of miRNA, together with the regulation of the cell cycle and apoptosis (3). Several enzymes are responsible for these epigenetic alterations, such as histone acetyltransferases (HATs), histone methyltransferases (HMTs), histone deacetylases (HDACs), and DNA methyltransferases (DNMTs) (4). Cancer is an aggressive malignancy caused by abnormal and uncontrolled cell division, in which gene expression changes, impaired apoptosis, and proliferation dynamics are increased along with cell cycle disruptions (5). DNMT and HDAC inhibitors are widely under investigation for their potential use as epigenetic drugs with significant attention (3).

Corresponding Author: Feyza Nur Tuncer **E-mail:** ftuncer@istanbul.edu.tr

Submitted: 13.06.2024 **Revision Requested:** 12.10.2024 **Last Revision Received:** 21.10.2024 **Accepted:** 25.10.2024 **Published Online:** 29.11.2024



Content of this journal is licensed under a Creative Commons Attribution-NonCommercial 4.0 International License.

Hence, DNMT inhibitors are promising agents for epigenetic drug development. Many genes are mutated or abnormally activated during the development of cancer, and impaired HDAC levels were reported to repress tumor suppressor genes (TSGs) along with the induction of tumorigenesis (4, 6). Eventually, several HDAC inhibitors have been used in the field of cancer treatment with increasing attention. Target-specific inhibitors without substantial side effects are required for effective anticancer treatment (3).

Fatty acid valproic acid (2-propylvaleric acid, VPA) has been frequently used for treating several neuropathies, such as migraine, bipolar disorder, and epilepsy, for decades (7, 8). This anticonvulsant drug functions as an HDAC inhibitor that alters gene expression in many crucial cellular processes (9). VPA inhibition on HDACs influences cell survival by enhancing cellular growth and differentiation, while inhibiting apoptosis and inflammation (10). Hence, the effects of VPA on HDAC inhibition have become widely preferred in cancer therapies because of elevated expression of HDACs in tumor cells and its cost-effective features (11). Combined with conventional treatment methods, molecular-targeted therapies have gained enormous attention as anticancer strategies. Consequently, this synergistic therapeutic approach has been shown to suppress tumor proliferation and metastasis in numerous cancer types (6). Although numerous experimental studies have investigated the effects and benefits of non-toxic VPA on cancer cells, little is known about the molecular response of VPA on healthy human cells compared with cancer cells. With this aim in mind, we used the VPA-treated HEK293T cell line as a

model for healthy cells to observe the effects of VPA treatment on non-cancerous cells.

MATERIALS AND METHODS

Cell Culture

The human embryonic epithelial kidney (HEK293T) cell line was collected from the American Type Culture Collection (ATCC®CRL-3216™; Manassas, VA, USA). Cells were grown in Dulbecco's Modified Eagle's Medium with high glucose (DMEM, Cat. No: 2LM-D1110, Biosera, France) supplemented with 10% heat-inactivated fetal bovine serum (FBS, Cat. No:1027, GIBCO, Thermo Fisher Scientific, USA), and 0.5% streptomycin (Sigma Chemicals, USA) at 37°C under 5% CO₂. Cell detaching was conducted using 0.25% Trypsin-EDTA (Cat. No: LM-T1720, Biosera, France). Optimized cell densities and IC₅₀ values of VPA concentrations for flow cytometry measurements were obtained from a recently published study by Ekici et al. (12) as 1x10⁵ cells/well on 24-well plates treated with 0, 2.5, or 5 mM of VPA. This study aimed to assess the impact of various VPA doses on two distinct cell concentrations to determine the optimal IC₅₀ value of the agent. Two different cell quantities (1x10⁵ and 5x10⁵ cells/well) were cultured in 24-well plates. Consequently, VPA concentrations of 0.25, 0.5, 1, 2.5, and 5 mM/mL were administered. The apoptotic and proliferative dynamics of the cells were evaluated using flow cytometry over the subsequent 4 days. In conclusion, no discrepancies were observed in cell quantities, and the effective IC₅₀ was determined to be 2.5 mM/mL (12). In addition, cells were treated with 1 mL of DMEM containing different concentrations of VPA (P4543, Sigma Chemicals, USA) of 0,

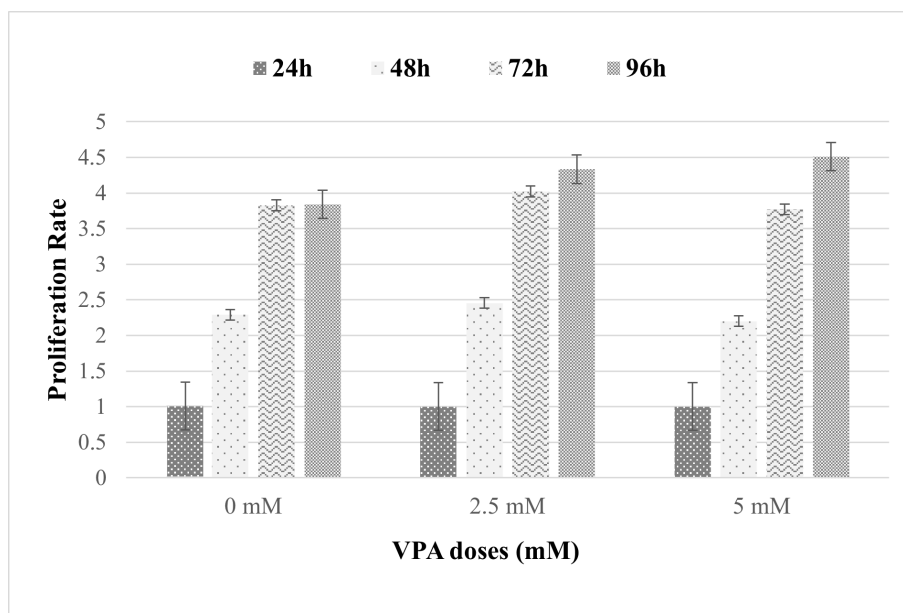


Figure 1. Cell proliferation results.

The average measurements from duplicate experiments are displayed for cells treated with 2.5 or 5 mM of VPA and the control (0 mM) groups at 24, 48, 72, or 96 h. The calculated results indicate the variance in the number of cell doublings, which were normalized to the number of untreated control cells (0 mM VPA). When VPA-treated cells (2.5 and 5 mM) were compared with untreated cells, Tukey's multiple comparison tests did not reveal any significance for both concentrations.

Table 1. The calculations of cell proliferation ascertained by flow cytometry measurements

Time (h)	VPA concentrations		
	0 mM	2.5 mM	5 mM
24	1	1	1
48	2.29 ± 0.08	2.45 ± 0.08	2.20 ± 0.05
72	3.82 ± 0.04	4.02 ± 0.09	3.77 ± 0.03
96	3.84 ± 0.30	4.33 ± 0.25	4.51 ± 0.34

The average data from two independent proliferation experiments are presented as time (hours) versus VPA concentration (millimolar, mM). The calculated results indicate the variance in the number of cell doublings, which were normalized to the number of untreated control cells (0 mM VPA). The variance in cell doublings between VPA-induced and control cells was determined using the $2n = F_{control}/F_{VPA}$; $n = \ln(F_{control}/F_{VPA})/\ln 2$ formula, wherein F represents the detected CFSE fluorescence intensity and n is the deviation in cell division numbers (14, 15). Values are expressed as percentage (means ± SD).

2.5, and 5 mM to perform proliferation and apoptosis experiments. Subsequently, the proliferative and apoptotic activities of cells were measured at the 24, 48, 72, and 96 hours. The untreated cell group was utilized as a negative control for each VPA dose and duration. Carboxyfluorescein-succinimidyl ester (CFSE, 5 μM final concentration) and annexin V/ propidium iodide (PI) stains were applied to all groups of cells prior to flow cytometry measurements. Moreover, 1×10^5 unstained cells/well were cultured in the absence of VPA, which were used as negative controls. Flow cytometric analysis was performed using a NovoCyte flow cytometry (Agilent, USA).

Cell Proliferation

Proliferation measurements followed subsequent staining of cells with CellTrace™ CFSE Cell Proliferation Kit (Thermo Fisher Scientific, USA) according to the manufacturer’s instructions. Cell culturing, monitoring, and calculation protocols were used, as described by Ekici et al. (12). All experiments were performed in duplicates.

Cell Apoptosis

“Dead Cell Apoptosis Kit with Annexin V-fluorescein isothiocyanate (FITC) and PI, for flow cytometry (Thermo Fisher Scientific, USA)” kit was used, which allows the determination of early and late apoptosis and the differentiation of apoptosis from necrosis (13). Apoptosis measurement protocols were followed, as described by Ekici et al. (12). All experiments were performed in duplicates following the manufacturer’s instructions.

Statistical Analyses

All data obtained from proliferation and apoptosis assays were statistically analyzed using two-way analysis of variance (ANOVA), followed by post hoc Tukey multiple comparisons.

The Student’s t-test was used to analyze the variability in the percentage of apoptosis between various time points. When $p \leq 0.05$, the data was deemed significant and presented as means ± standard deviation (SD). All statistical calculations were performed using GraphPad Prism Software.

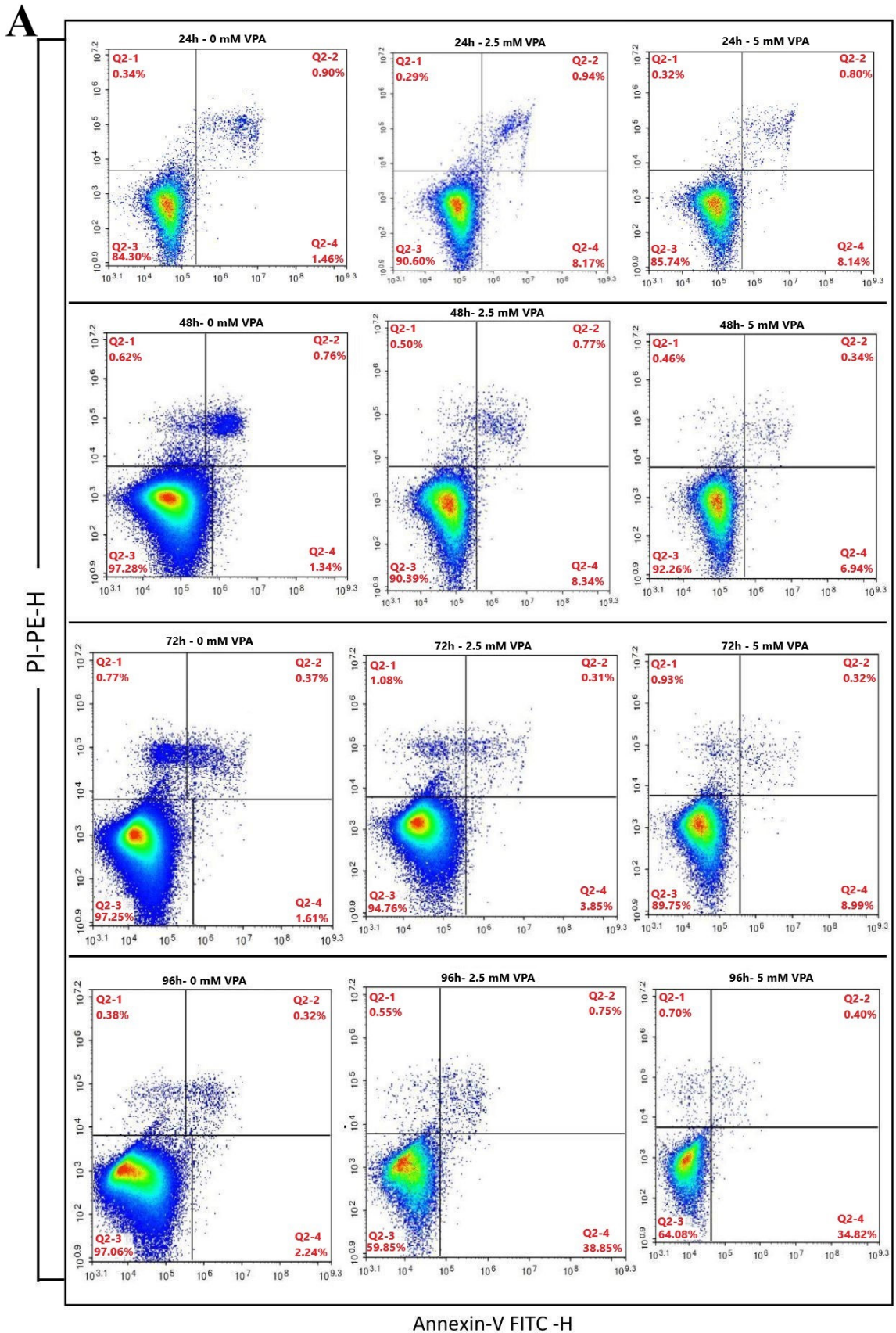
RESULTS

Cell Proliferation Results

The study evaluated the proliferative effects of different VPA doses on cells compared with the untreated control group. When the response of cells was considered in terms of increasing doses of VPA over the same period, the reactions of cells did not differ significantly. When two different VPA concentrations (2.5 and 5 mM) were compared with untreated cells, Tukey’s multiple comparison tests did not reveal any significance for both concentrations ($p = 0.4184$) (Figure 1). The difference in cell doublings between VPA-induced cells and control cells was determined by utilizing the $2n = F_{control}/F_{VPA}$; $n = \ln(F_{control}/F_{VPA})/\ln 2$ formula, wherein F represents the detected CFSE mean fluorescence intensity and n is the number of cell divisions (14, 15). Table 1 presents the proliferation findings of cells from flow cytometry analyses.

Cell Apoptosis Results

In the scope of this study, the effects of different VPA doses at various time intervals on cell apoptosis and necrosis were evaluated. According to the dot plots of the log data obtained from flow cytometry measurements, the percentages of live, early apoptotic, late apoptotic, and necrotic cells at all time intervals are presented in Table 2. Following these results, the early apoptotic features of all groups remained stable for up to 72 h; an increase was observed at the 96th in VPA-treated



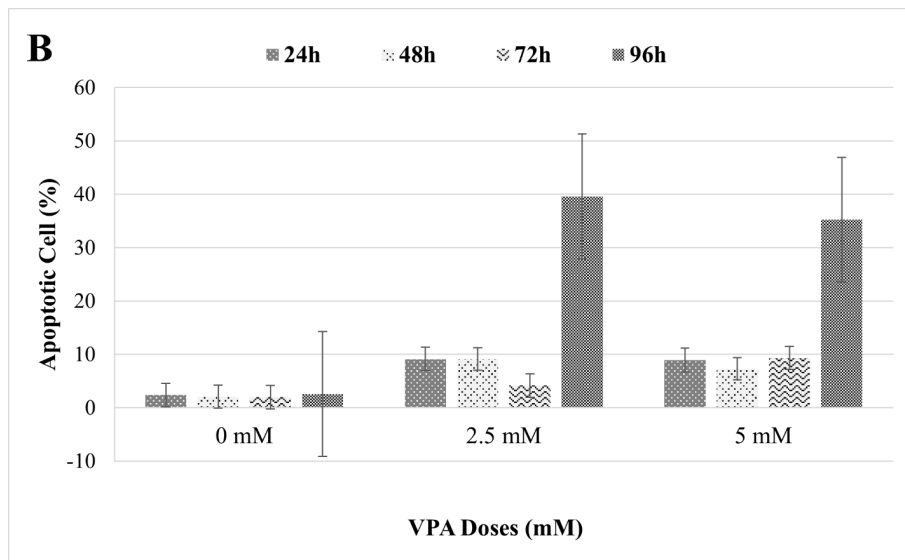


Figure 2. Cell apoptosis results.

The measurements are illustrated from a single experiment for the cells subjected to 2.5 mM and 5 mM VPA and the control (0 mM) groups at the 24, 48, 72, and 96h. A) Representative results of flow cytometric dot plots of cells for Annexin V-PI counterstain. Untreated control cells (on the left panels) and VPA-treated cells (2.5 mM VPA in the middle and 5 mM VPA on the right panels) are exhibited. In the lower left area (Q2-3), live cells are displayed, whereas the lower right (Q2-4) denotes early apoptosis. The upper right (Q2-3) shows late apoptosis, and the upper left (Q2-1) shows necrotic/dead cells. Cells were gated using untreated cells for subsequent analyses. The scatter plot illustrates the apoptosis percentages of cells treated with 2.5 mM and 5 mM VPA and the control groups across three independent experiments. B) The total (early and late) apoptotic cell percentages were compared between the untreated and VPA-treated groups. Over time, the percentage of apoptosis in cells treated with VPA exhibited a significant increase compared to the control groups. The experiments were conducted in independent duplicates. The error bars represent the \pm standard error of the means of replicates.

cells ($p < 0.0001$) (Figure 2). VPA treatment seems to cause a significant increase in the early apoptotic cell numbers compared with the control cells.

DISCUSSION

Cancer is a leading cause of death worldwide (9). Clinical studies have demonstrated that the combination of targeted molecular agents with conventional chemotherapy effectively enhances the inhibition of tumor growth and metastasis in patients with cancer. Hence, VPA is a noteworthy adjuvant drug due to its well-documented adverse effects, which are dose-dependent and reversible in severe toxicity (6, 7).

The utilization of VPA in clinical settings for various malignancies is advancing; however, the specific effects of these HDAC inhibitors in normal non-cancerous cells and the molecular responses elicited by them are limitedly understood (16). Stapnes et al. investigated four different HDAC inhibitors, including VPA on CD34⁺ acute myeloid leukemia (AML) cells, normal bone marrow CD34⁺ cells, and acute lymphoblastic leukemia (ALL) blasts, in terms of proliferation and viability (17). Their results revealed that normal CD34⁺ hematopoietic cells differed from cancerous cells, as they showed growth enhancement at the highest VPA concentrations with no antiproliferative effects. It can be implied that this difference might be caused by the

drug's effects on specific cell populations associated with leukemia but not normal cells (17). In accordance with these findings, our study revealed parallel results; when examining the impact of varying doses of VPA over time, cell proliferation demonstrated a significant linear increase for up to three days following administration. VPA administration did not affect the proliferation kinetics of HEK293T cells, even at varying concentrations. The results indicate that there were consistent outcomes between the experimental and control groups for a period of up to three days. We previously demonstrated that VPA inhibits the proliferation of pancreatic ductal carcinoma, a highly fatal type of cancer. These findings suggest that VPA operates through different mechanisms in healthy cells compared with cancer cells, potentially offering insights into targeted therapeutic strategies (12).

The primary objective of cancer treatment is to prevent cancer cells from replicating by destroying DNA signals or inflammation, both of which lead to apoptosis. However, while achieving this, minimizing damage to healthy cells is as essential as destroying existing cancer cells. Our findings showed that the early apoptotic features remained stable for up to 72 h in the 2.5 and 5 mM VPA and control groups. However, an increase was observed in VPA-treated cells at the 96th hour ($p < 0.001$). A study on epilepsy indicated that a

Table 2. Representative data of flow cytometry analysis of cells stained with Annexin V-FITC and propidium iodide

Time (h)	VPA concentration (mM)	Live Cells (%)	Early Apoptotic Cells (%)	Late Apoptotic Cells (%)	Necrotic Cells (%)
24	0 mM	84.30	1.46	0.90	0.34
	2.5 mM	90.60	8.17	0.94	0.29
	5 mM	85.74	8.14	0.80	0.32
48	0 mM	97.28	1.34	0.76	0.62
	2.5 mM	90.39	8.34	0.77	0.50
	5 mM	92.26	6.94	0.34	0.46
72	0 mM	97.25	1.61	0.37	0.77
	2.5 mM	94.76	3.85	0.31	1.08
	5 mM	89.75	8.99	0.32	0.93
96	0 mM	97.06	2.24	0.32	0.38
	2.5 mM	59.85	38.85	0.75	0.55
	5 mM	64.08	34.82	0.40	0.70

Percentage data from a single experiment for cells subjected to 2.5 mM and 5 mM VPA and control (0 mM) groups at the 24, 48, 72, and 96. The Dead Cell Apoptosis Kit with Annexin V-FITC and PI was used for flow cytometry analysis. Detailed data represent percentage means of live, early apoptotic, late apoptotic, and necrotic cell numbers at all time intervals, obtained from dot plots of cells for Annexin V-PI counterstain, as presented in Figure 2.

clinical dose of 1 mM VPA is considered safe as an antiepileptic medication, whereas 2.7 mM VPA results in low toxicity with benign side effects. Nevertheless, a dosage of 5.1 mM can lead to severe and life-threatening effects (18). When the results of this study are combined with our own findings, VPA increases cell damage over time at doses exceeding 2.5 mM. In our previous study, the IC₅₀ value of VPA in PANC-1 cells was 2.5 mM. At this dose, we observed the onset of early apoptosis at 48 h (12). These results suggest that further research is needed at concentrations between 1 and 2.5 mM to determine the effective dose. This approach may help prevent toxic effects that cause physiological deterioration in healthy cells.

Acknowledgments: The findings of this study were presented as an e-poster at the Medical Biology and Genetics Society Conference 2021.

Ethics Committee Approval: Only cell culture material was used in this study and no living material that would require ethics committee approval was used.

Peer-review: Externally peer-reviewed.

Author Contributions: Conception/Design of Study – H.B.O.C., F.N.T.; Data Acquisition – H.B.O.C., Y.E., A.Y., F.N.T.; Data Analysis/ Interpretation - H.B.O.C., Y.E., F.N.T.; Drafting Manuscript – H.B.O.C., Y.E., F.N.T.; Critical Revision of Manuscript – H.B.O.C., Y.E., F.N.T.; Final Approval and Accountability – H.B.O.C., Y.E., F.N.T.

Conflict of Interest: The authors declare no conflict of interest.

Financial Disclosure: This study is granted by the Scientific Research Projects Coordination Unit of Istanbul University (TDP-2019-32763).

REFERENCES

- Alenzi FQ. Links between apoptosis, proliferation and the cell cycle. *Br J Biomed Sci* 2004; 61(2): 99-102.
- Williams GH, Stoeber K. The cell cycle and cancer. *J Pathol* 2012; 226(2): 352-64.
- Perri F, Longo F, Giuliano M, Sabbatino F, Favia G, Ionna F, et al. Epigenetic control of gene expression: Potential implications for cancer treatment. *Crit Rev Oncol Hematol* 2017; 111: 166-72.
- Chen QW, Zhu XY, Li YY, Meng ZQ. Epigenetic regulation and cancer (review). *Oncol Rep* 2014; 31(2): 523-32.
- Cooper GM. *The Cell: A molecular approach*. 2nd edition. Sunderland (MA): Sinauer Associates; 2000.
- Yagi Y, Fushida S, Harada S, Kinoshita J, Makino I, Oyama K, et al. Effects of valproic acid on the cell cycle and apoptosis through acetylation of histone and tubulin in a scirrhous gastric cancer cell line. *J Exp Clin Cancer Res* 2010; 29(1): 149.
- Bruserud O, Tsykunova G, Hernandez-Valladares M, Reikvam H, Tvedt THA. Therapeutic use of valproic acid and all-trans retinoic acid in Acute Myeloid Leukemia-literature review and discussion of possible use in relapse after allogeneic stem cell transplantation. *Pharmaceuticals (Basel)* 2021; 14(5): 423.
- Janković SM, Janković SV. Lessons learned from the discovery of sodium valproate and what has this meant to future drug discovery efforts? *Expert Opin Drug Discov* 2020; 15(11):1355-64.

9. Xie Z, Ago Y, Okada N, Tachibana M. Valproic acid attenuates immunosuppressive function of myeloid-derived suppressor cells. *J Pharmacol Sci* 2018; 137(4): 359-65.
10. Russo R, Kemp M, Bhatti UF, Pai M, Wakam G, Biesterveld B, et al. Life on the battlefield: Valproic acid for combat applications. *J Trauma Acute Care Surg* 2020; 89(2S Suppl 2): S69-S76.
11. Gotfryd K, Skladchikova G, Lepekhn EA, Berezin V, Bock E, Walmod PS. Cell type-specific anti-cancer properties of valproic acid: independent effects on HDAC activity and Erk1/2 phosphorylation. *BMC Cancer* 2010; 10: 383.
12. Ekici Y, Yilmaz A, Kucuksezer UC, Gazioglu SB, Yamalioglu ZD, Gurok AO, et al. Combined evaluation of proliferation and apoptosis to calculate IC(50) of VPA-induced PANC-1 cells and assessing its effect on the Wnt signaling pathway. *Med Oncol* 2021; 38(9): 109.
13. Vermes I, Haanen C, Steffens-Nakken H, Reutelingsperger C. A novel assay for apoptosis. Flow cytometric detection of phosphatidylserine expression on early apoptotic cells using fluorescein labelled Annexin V. *J Immunol Methods* 1995; 184(1): 39-51.
14. Raz S, Sheban D, Gonen N, Stark M, Berman B, Assaraf YG. Severe hypoxia induces complete antifolate resistance in carcinoma cells due to cell cycle arrest. *Cell Death Dis* 2014; 5(2): e1067.
15. Ahlen MT, Husebekk A, Killie MK, Skogen B, Stuge TB. T-cell responses associated with neonatal alloimmune thrombocytopenia: isolation of HPA-1a-specific, HLA-DRB3*0101-restricted CD4+ T cells. *Blood* 2009; 113(16): 3838-44.
16. Zini R, Norfo R, Ferrari F, Bianchi E, Salati S, Pennucci V, et al. Valproic acid triggers erythro/megakaryocyte lineage decision through induction of GF11B and MLLT3 expression. *Exp Hematol* 2012; 40(12): 1043-54.e6.
17. Stapnes C, Rynningen A, Hatfield K, Øyan AM, Eide GE, Corbascio M, et al. Functional characteristics and gene expression profiles of primary acute myeloid leukaemia cells identify patient subgroups that differ in susceptibility to histone deacetylase inhibitors. *Int J Oncol* 2007; 31(6): 1529-38.
18. Li XN, Shu Q, Su JM, Perlaky L, Blaney SM, Lau CC. Valproic acid induces growth arrest, apoptosis, and senescence in medulloblastomas by increasing histone hyperacetylation and regulating expression of p21Cip1, CDK4, and CMYC. *Mol Cancer Ther* 2005; 4(12): 1912-22.

Epigenetic Signatures in Ovarian Cancer to Determine Potential Diagnostic/Prognostic Biomarkers

Tugce Senturk Kirmizitas^{1,2} , Servet Tunoglu³ , Jean Helmijr² , Samet Topuz⁴ , Maurice Jansen² , Tuba Gunel⁴ 

¹Department of Molecular Biology and Genetics, Faculty of Science, Istanbul University, Istanbul, Turkiye

²Department of Medical Oncology, University Medical Center Rotterdam, Rotterdam, The Netherlands

³Department of Molecular Medicine, Aziz Sancar Institute of Experimental Medicine, Istanbul University, Istanbul, Turkiye

⁴Department of Obstetrics and Gynecology, Istanbul Medical Faculty, Istanbul University, Istanbul, Turkiye

ORCID ID: T.S.K. 0000-0001-6235-251X; S.T. 0000-0001-7625-7425; J.H. 0000-0003-0983-6296; S.Topuz 0000-0002-9069-0185; M.J. 0000-0003-1258-9804; T.G. 0000-0003-3514-5210

Cite this article as: Senturk Kirmizitas T, Tunoglu S, Helmijr J, Topuz S, Jansen M, Gunel T. Epigenetic signatures in ovarian cancer to determine potential diagnostic/prognostic biomarkers. *Experimed* 2024; 14(3): 161-173.

ABSTRACT

Objective: Identification of methylation patterns in cell-free DNA (cfDNA) provides a non-invasive methodology for discovering critical biomarkers that facilitate detection and prognostic evaluation of ovarian cancer (OC). This study explored the epigenetic landscape of OC by examining the DNA methylation patterns of cfDNA.

Materials and Methods: Plasma samples from 5 OC patients and 5 healthy blood donors (HBDs) were processed for cfDNA isolation and methylated DNA immunoprecipitation, followed by next-generation sequencing and bioinformatics analysis to identify differentially methylated regions (DMRs) and genes (DMGs). Integration with The Cancer Genome Atlas (TCGA) data identified differentially expressed genes (DEGs) for functional analysis.

Results: The analysis revealed significant alterations in DNA methylation patterns, with 62 hypermethylated and 2 hypomethylated DMRs in OC compared with HBDs. Hierarchical clustering revealed distinct methylation patterns between OC and HBDs. Integrative analysis identified 18 genes with overlapping methylation and expression changes in OC and a negative correlation between methylation and expression levels ($p < 0.05$). Ten genes exhibited a hypermethylation-downregulation pattern, indicating a suppressive role, whereas eight showed hypermethylation-upregulation. Survival analysis of OC data from TCGA highlighted *B3GNT3* ($p = 0.04$) and *LRP1B* ($p = 0.053$) as promising prognostic markers.

Conclusion: Our study revealed an intricate relationship between DNA methylation alterations and gene expression dysregulation in ovarian cancer. We found that hypermethylation of *B3GNT3* was correlated with its upregulation and poor survival outcomes, whereas hypermethylation of *LRP1B* pointed to its role as a tumor suppressor gene.

Keywords: Epithelial ovarian cancer, methylation, epigenomics, liquid biopsy, cfDNA

INTRODUCTION

Ovarian cancer (OC) is a highly prevalent and deadly cancer that affects female reproductive organs, with an increasing incidence worldwide (1). It is currently the second most common cancer of the female reproductive system. The most

prevalent form, epithelial ovarian cancer (EOC), accounts for 85%–90% of ovarian tumors. OC spreads through direct extension, intra-abdominal seeding, and lymphatic routes, with advanced stages often involving peritoneal metastases, resulting in high mortality and poor prognosis (2). Treatment for advanced OC usually involves surgical tumor removal

Corresponding Author: Tugce Senturk Kirmizitas **E-mail:** tugce.senturk.12@gmail.com

Submitted: 28.05.2024 **Revision Requested:** 16.07.2024 **Last Revision Received:** 06.08.2024 **Accepted:** 06.08.2024



Content of this journal is licensed under a Creative Commons Attribution-NonCommercial 4.0 International License.

and platinum-based chemotherapy (3). Despite treatment advancements, the prognosis remains poor, and OC has the highest mortality rate among gynaecological cancers. OC is typically asymptomatic in the early stages, and the absence of reliable biomarkers for early detection often leads to diagnosis at the late stage, making it more difficult to treat and resulting in worse outcomes. Thus, the development and validation of effective detection and prognostic biomarkers are essential for improving early diagnosis and survival rates for patients (4).

Recent studies have highlighted the crucial role of epigenetic modifications in the development and progression of OC (5-8). Epigenetic changes, particularly DNA methylation, are emerging as promising non-invasive biomarkers for the early detection and monitoring of OC. DNA methylation, which involves addition of methyl groups to DNA promoter regions, regulates gene expression and is mediated by a complex network of enzymes, co-factors, and regulatory proteins (9). Tumor cells often exhibit abnormal DNA methylation at the promoters of tumor-suppressor genes and oncogenes, disrupting key biological processes such as cell proliferation, cell cycle regulation, and apoptosis (9, 10). This disruption is associated with the development and metastasis of OC. In parallel, liquid biopsy has emerged as a promising approach in oncology, enabling non-invasive detection of tumor-derived material from various bodily fluids (11, 12). Cell-free DNA (cfDNA) holds particular significance among the analytes examined, as its aberrant DNA methylation profiles mirror tumorigenesis and cancer progression (13). Despite the challenges associated with low levels of methylated cfDNA, cfDNA methylation analysis shows potential as a biomarker for the diagnose and treatment of ovarian cancer (2, 14).

We investigated the epigenetic landscape of OC by analyzing DNA methylation patterns in cfDNA from plasma samples of OC patients and healthy blood donors (HBDs). We used methylated DNA immunoprecipitation (MeDIP) followed by next-generation sequencing (NGS) to identify differentially methylated regions (DMRs) and genes (DMGs). Additionally, we integrated our findings with differentially expressed genes (DEGs) from The Cancer Genome Atlas (TCGA) dataset to identify genes with concurrent methylation and expression changes, thereby providing a more comprehensive understanding of the epigenetic regulation in OC.

The present study underscores the intricate relationship between DNA methylation alterations and gene expression dysregulation in OC. Our findings contribute to the growing body of knowledge regarding the epigenetic mechanisms driving OC and highlight potential biomarkers and therapeutic targets for improving patient outcomes.

MATERIALS AND METHODS

Sample Collection

To identify DMRs in cfDNA from OC patients compared with healthy individuals, we utilized samples from 5 OC patients and

Table 1. Clinical and demographic characteristics of OC samples

Characteristics	OC (n=5)
Age Mean (Range)	54.4 (35-75)
CA125 Mean (Range)	859 (62-1754)
Types	
Primer Serous	5
FIGO Stage	
Stage 3A	1
Stage 3C	4
Recurrence	
Yes	0
No	3
Unknown	2
Lymphatic Invasion	
Yes	4
No	0
Unknown	1
Family History	
Yes	1
No	3
Unknown	1

5 HBDs. The clinical and demographic characteristics of the patient samples involved in this study are presented in Table 1. Blood samples were obtained from serous adenocarcinoma from OC patients prior to surgery, who had not received any treatment. In the control group called HBDs, individuals with no history of cancer and without other diseases, such as diabetes, endometriosis, or hypertension, were included.

Peripheral blood samples were collected in 10 mL EDTA tubes from individuals meeting the inclusion and exclusion criteria of the study. Using the cold chain method, these samples were transported to the Molecular Biology and Genetics Department of Istanbul University within 4 h. Samples were centrifuged at 600 g for 10 min at 4°C, followed by a second centrifugation at 14.000 g for 10 min at 4°C. Plasma was transferred to 1.5 mL cryotubes and stored at -80°C until cfDNA isolation. This study was approved in 2020 by Istanbul University, Istanbul Faculty of Medicine Clinical Research Ethics Committee under file number 1451. All participants provided voluntary informed consent by completing the consent forms after receiving detailed information.

Table 2. Summary of identified DMRs

DMR ID	Name	Chromosome	Start	End	Log2 Fold Change	p value
DMR1	PDZD7	chr10	1.03E+08	1.03E+08	4.047	0.0485
DMR2	snoU13	chr11	1.23E+08	1.23E+08	4.360	0.0492
DMR3	PRDM11	chr11	45114563	45116563	3.875	0.0405
DMR4	AX747537	chr11	880475	882475	3.495	0.0444
DMR5	NOX4	chr11	89056521	89058521	4.819	0.0156
DMR6	7SK	chr12	1.15E+08	1.15E+08	5.546	0.0062
DMR7	CAPRN2	chr12	30880312	30882312	4.010	0.0493
DMR8	ATN1	chr12	7036479	7038479	4.820	0.0126
DMR9	POU5F1P3	chr12	8285945	8287945	6.275	0.0021
DMR10	ZFH2	chr14	23989063	23991063	3.796	0.0225
DMR11	KIAA0586	chr14	58905398	58907398	5.229	0.0041
DMR12	PPCDC	chr15	75314926	75316926	6.473	0.0018
DMR13	ZNF774	chr15	90894476	90896476	3.443	0.0487
DMR14	MCTP2	chr15	94840429	94842429	4.333	0.0191
DMR15	NR2F2	chr15	96873110	96875110	4.493	0.0234
DMR16	DQ585716	chr15	97323965	97325965	4.530	0.0141
DMR17	TEKT5	chr16	10720360	10722360	4.247	0.0236
DMR18	TMCS	chr16	19428017	19430017	4.174	0.0127
DMR19	DYNC1LI2	chr16	66753798	66755798	4.443	0.0279
DMR20	BX537921	chr16	8739037	8741037	8.220	0.0001
DMR21	RP11-744K17.9	chr17	21903061	21905061	2.733	0.0359
DMR22	LYRM9	chr17	26204339	26206339	4.942	0.0234
DMR23	RP11-647F2.2	chr17	72298777	72300777	5.677	0.0101
DMR24	SECTM1	chr17	80277899	80279899	3.640	0.0359
DMR25	MC5R	chr18	13824542	13826542	-5.334	0.0160
DMR26	PRDX2	chr19	12906633	12908633	4.601	0.0229
DMR27	NOTCH3	chr19	15287335	15289335	3.812	0.0473
DMR28	B3GNT3	chr19	17904918	17906918	4.022	0.0389
DMR29	LINC01224	chr19	23581035	23583035	4.373	0.0292
DMR30	PRODH2	chr19	36289891	36291891	4.090	0.0339
DMR31	CCER2	chr19	39398619	39400619	4.632	0.0209
DMR32	ZNF574	chr19	42571628	42573628	4.469	0.0262
DMR33	PTGIR	chr19	47122724	47124724	3.825	0.0445

DMR34	ZNF358	chr19	7583128	7585128	3.674	0.0349
DMR35	FMO5	chr1	1.47E+08	1.47E+08	4.349	0.0320
DMR36	S100A16	chr1	1.54E+08	1.54E+08	3.405	0.0481
DMR37	RP11-144L1.4	chr1	1.58E+08	1.58E+08	3.953	0.0374
DMR38	TRNA_Gly	chr1	17052779	17054779	3.877	0.0118
DMR39	TAS1R2	chr1	19165092	19167092	4.081	0.0454
DMR40	FCAMR	chr1	2.07E+08	2.07E+08	4.695	0.0187
DMR41	TRNA_Glu	chr1	2.49E+08	2.49E+08	4.613	0.0366
DMR42	LRP8	chr1	53715361	53717361	4.423	0.0149
DMR43	ZBTB46-AS1	chr20	62438441	62440441	4.134	0.0291
DMR44	LINC01548	chr21	34536775	34538775	5.074	0.0047
DMR45	CCDC74B-AS1	chr2	1.31E+08	1.31E+08	3.800	0.0286
DMR46	LRP1B	chr2	1.42E+08	1.42E+08	4.373	0.0292
DMR47	CD28	chr2	2.05E+08	2.05E+08	3.848	0.0443
DMR48	CXCR2P1	chr2	2.19E+08	2.19E+08	4.560	0.0391
DMR49	CCDC88A	chr2	55560229	55562229	4.529	0.0260
DMR50	LINC02049	chr3	1.21E+08	1.21E+08	4.815	0.0075
DMR51	FBXL21	chr5	1.35E+08	1.35E+08	4.745	0.0147
DMR52	RN7SL295P	chr5	1.6E+08	1.6E+08	5.323	0.0079
DMR53	WWC1	chr5	1.68E+08	1.68E+08	3.975	0.0385
DMR54	UIMC1	chr5	1.76E+08	1.76E+08	4.694	0.0191
DMR55	AX747985	chr5	1.79E+08	1.79E+08	4.473	0.0109
DMR56	MIR340	chr5	1.79E+08	1.79E+08	4.629	0.0077
DMR57	TRNA_Ser	chr6	27508553	27510553	4.376	0.0236
DMR58	MIR4641	chr6	41565460	41567460	4.838	0.0074
DMR59	EXOC4	chr7	1.34E+08	1.34E+08	5.972	0.0066
DMR60	SPDYE1	chr7	44039488	44041488	4.853	0.0076
DMR61	RNU6-229P	chr7	68865187	68867187	4.499	0.0413
DMR62	TG	chr8	1.34E+08	1.34E+08	4.594	0.0110
DMR63	RP11-115J16.1	chr8	9181560	9183560	4.215	0.0318
DMR64	MIR3134	chr9	1.15E+08	1.15E+08	-5.190	0.0205

Summary of 64 statistically significant DMRs identified using the h19 reference genome. Each DMR was assigned a unique DMR ID ranging from 1 to 64. DMRs were identified based on their chromosomal locations, represented by the "Chromosome", "Start", and "End" columns. The statistical significance of each DMR is indicated by the calculated p value and log2 fold change, which were computed using the DESeq2 methodology. DMR: Differentially methylated region.

Table 3. Genes with overlapping methylation and expression patterns in OC

Overlapped DMG-DEG			CfMEDIP DMG		TCGA DEG	
Symbol	Name	Called	Fold Change	p value	Fold Change	p value
PRDM11	PR/SET domain 11	Hyper-Down	3.874	0.0493	-1.081	8.04E-31
CAPRIN2	C family member 2	Hyper-Down	4.009	0.0126	-2.246	8.97E-96
ATN1	Atropine 1	Hyper-Down	4.820	0.0020	-1.111	5.79E-24
POU5F1P3	POU class 5 homeobox 1 pseudogene 3	Hyper-Down	6.275	0.0234	-1.438	1.25E-179
NR2F2	Nuclear receptor subfamily 2 group F member 2	Hyper-Down	4.492	0.0126	-3.255	2.59E-106
TMC5	Transmembrane channel like 5	Hyper-Up	4.174	0.0278	1.38	2.33E-31
DYNC1LI2	Dynein cytoplasmic 1 light intermediate chain 2	Hyper-Down	4.442	0.0233	-1.598	9.79E-46
LYRM9	YR motif containing 9	Hyper-Down	4.941	0.0358	-2.219	1.39E-98
SECTM1	Secreted and transmembrane protein 1	Hyper-Up	3.639	0.0472	1.837	2.44E-19
NOTCH3	Notch receptor 3	Hyper-Up	3.812	0.0389	1.407	1.51E-13
B3GNT3	Beta-1,3-N-acetylglucosaminyltransferase 3	Hyper-Up	4.021	0.02912	3.373	6.70E-66
LINC01224	Long intergenic non-protein-coding RNA 1224	Hyper-Up	4.373	0.03203	2.348	6.18E-72
FMOS	Flavin containing monooxygenase 5	Hyper-Down	4.349	0.04812	-1.071	3.61E-59
S100A16	S100 calcium binding protein A16	Hyper-Up	3.404	0.01485	1.236	3.16E-17
LRP8	LDL receptor-related protein 8	Hyper-Up	4.423	0.02604	1.594	4.91E-34
CCDC88A	Coiled-coil domain containing 88A	Hyper-Down	4.528	0.03853	-1.23	3.43E-35
WWC1	WW and C2 domain containing 1	Hyper-Up	3.974	0.01912	4.036	7.61E-154
UIMC1	Ubiquitin interaction motif containing 1	Hyper-Down	4.693	0.02923	-1.982	3.34E-134

Log2 Fold Change (Log2FC) values represent differences in DNA methylation (cfMEDIP) and gene expression (TCGA mRNA) between OC and HBD. Positive Log2FC values denote hypermethylation in cfMEDIP and upregulation in gene expression. Conversely, negative Log2FC values indicate hypomethylation in cfMEDIP and downregulation in gene expression. Hyper-up genes refer to those exhibiting a positive correlation between hypermethylation and upregulation, whereas hyper-down genes denote a distinct pattern in which hypermethylation is linked with downregulation. DMG: Differentially methylated gene; DEG: Differentially expressed gene; OC: Ovarian cancer; HBD: Healthy blood donor.

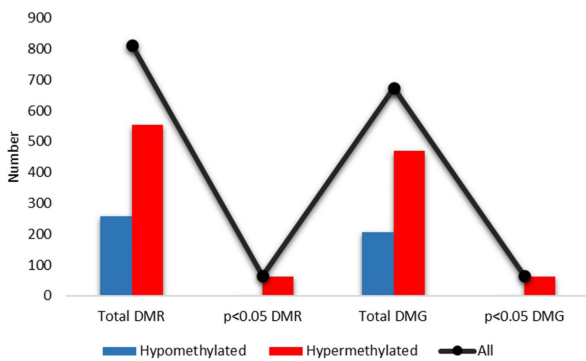


Figure 1. Categorization of DMRs and DMGs. This figure presents a bar plot illustrating the categorization of DMRs and DMGs based on methylation status. The bars are color-coded, with hypermethylated regions in red and hypomethylated regions in blue. In addition, a black line represents the total number of DMRs and DMGs. DMR: Differentially methylated region; DMG: Differentially methylated gene.

Isolation of cfDNA

For cfDNA isolation, frozen plasma samples were thawed at room temperature, which can cause the presence of cryoprecipitates. To eliminate these substances, plasma samples were centrifuged at 16,000 g for 5 min at 4°C, and the supernatant was carefully transferred to a new tube, avoiding the pellet. This supernatant was then used for cfDNA isolation following the recommended protocol for 4 mL of plasma outlined in the QIAamp® Circulating Nucleic Acid Kit (Qiagen, Catalogue No: 55114, Hilden, Germany). The concentration of isolated cfDNA was measured using a Qubit dsDNA HS Assay Kit (Thermo Fisher Scientific, Catalogue No: Q32851, Waltham, MA, USA) and a Qubit fluorometer (Thermo Fisher Scientific, Waltham, MA, USA). The quality and fragment size distribution of cfDNA were assessed using an Agilent High Sensitivity DNA Reagent Kit (Agilent Technologies, Catalogue No: 5067-4626, Santa Clara, CA, USA) and an Agilent Bioanalyzer (Agilent Technologies, Santa Clara, CA, USA). Specifically, to ensure the integrity of our cfDNA samples, we performed quality control using an Agilent Bioanalyzer after the final library amplification. This assessment confirmed that the final libraries contained only cfDNA fragments with no detectable genomic DNA contamination, thereby validating the effectiveness of our purification process and the high purity of the cfDNA used in our study.

Circulating Cell-Free Methylated DNA Immunoprecipitation

Filler DNA was prepared according to established procedures. A pool of six PCR amplicons, each differ in size and CpG density (1CpG, 5CpG, 10CpG, 15CpG, 20LCpG, and 20SCpG), as originally described by Taiwo et al., were generated (15).

Among these, fragments of 1CpG, 5CpGs, 10CpGs, 15CpGs, and 20LCpGs were methylated *in vitro*, whereas the 20SCpG fragment remained unmethylated. A 50:50 ratio of methylated to unmethylated DNA was utilized in the filler DNA mixture, consistent with previous studies. The library preparation protocol using the Kapa Hyper Prep Kit (Roche, Catalogue No: KK8504, Basel, Switzerland) was followed. Briefly, library preparation involves three primary stages: end repair and adenylation, adaptor ligation and purification, and final library amplification. The initial phase of end repair and adenylation was performed according to the protocol. To ensure consistency, the initial cfDNA input for the library preparation was standardized at 10 ng per sample. The NEBNext Multiplex Oligos (New England Biolabs, Catalogue No: E7335S, Ipswich, MA, USA) adaptors were customized according to the initial cfDNA concentration and the recommended minimum 100:1 adaptor/insert ratio using the Kapa Hyper Prep Kit. After adaptor ligation, purification was conducted employing AMPure XP beads (Beckman Coulter, Catalogue No: A63881, Brea, CA, USA) by the protocol. Before the immunoprecipitation method, the pool DNA amount (comprising adaptor-ligated cfDNA and filler DNA) was adjusted to 100 ng for all samples, with the initial amount of adaptor-ligated cfDNA set at 10 ng for each sample and the remaining 90 ng supplemented with previously prepared and quantified filler DNA fragments. The 5-mC monoclonal antibody was diluted 1:15 and added to the samples. The immunoprecipitation was carried out following the MagMeDIP Kit (Diagenode, Catalogue No: C02010021, Seraing, Belgium) protocol with pooled cell-free DNA (cfDNA) with lambda DNA and spike-in DNA. Magnetic bead-based washing procedure was executed to expunge non-specifically bound DNA fragments, followed by incubation at 17°C for 4 h. The final libraries were indexed using the NEB index primer set 1 (New England Biolabs, Catalogue No: E7335L, Ipswich, MA, USA) to label individual samples.

Next-Generation Sequencing

The final libraries from all samples were combined in equimolar concentrations to create a pooled library, which was diluted to 4 nM and sequenced using paired-end reads of 150 bp. Library quantification, dilution, and loading were performed according to the manufacturer’s instructions. NGS was performed using the Illumina NovaSeq 6000 platform (Illumina, San Diego, CA, USA).

Bioinformatics Analysis

Raw sequencing data from cfMeDIP-seq underwent adapter trimming, low-quality base removal, and filtering using Trimmomatic. Raw sequencing data were normalized using DESeq2 normalization and Methylation Z-score normalization. DESeq2 normalizes raw read counts based on gene length and calculates size factors, which are the median ratios of observed read counts to geometric mean counts across all genes. Normalized read counts were obtained by dividing raw counts by these size factors, adjusting for sequencing



Figure 2. Genomic distribution of DMRs.

This figure presents a chromosome ideogram plot showing the genomic positions of all 64 identified DMRs across the chromosomes. Each DMR is indicated by a red marker along the chromosome, providing insight into the genomic distribution of DNA methylation alterations associated with OC. DMR: Differentially methylated region; OC: Ovarian cancer; chr: Chromosome.

depth, and enabling fair comparisons between samples. Normalized data were aligned to the human reference genome (hg19) using Burrows-Wheeler alignment. DMRs and methylation levels in DMRs relative to the HBDs were determined using DESeq2. Z-score normalization was applied to DESeq2 normalized data. The method transforms data to have a mean of zero and a standard deviation of one by comparing relative methylation patterns across samples. For each gene, the mean and standard deviation of normalized counts across all samples were calculated, and each count

was adjusted by subtracting the mean and dividing by the standard deviation. The analysis focused on 2-kilobase regions around transcription start sites and considered only autosomal chromosomes. The regions without raw data in more than 75% of the samples were excluded. Statistical evaluation of the results involved calculating p values and adjusted p values (q values) using the Benjamini-Hochberg correction in DESeq2. DMRs with a calculated $p < 0.05$ were considered significant. The GEPIA2 website (<http://gepia2.cancer-pku.cn/#index>) was used to obtain a list of differentially expressed genes. Analysis

was performed using the LIMMA method, similar to DESeq2, but was designed for low-density data sets like microarray data. Only genes with a $p < 0.05$ were considered significant. To determine the correlation between DMG and DEG levels, Spearman's correlation analysis was performed.

To conduct the survival analysis, we used GEPIA2, which evaluates the relationship between gene expression levels and patient survival based on TCGA data (<https://portal.gdc.cancer.gov/>). GEPIA2 employs log-rank tests and Cox proportional hazard models to analyze survival outcomes and create survival curves. We analyzed gene expression data from 424 ovarian cancer samples provided by TCGA. The data cover sample collection periods from 1992 to 2014, with survival times ranging from 0 to 180 months, as shown in the survival plots.

Moreover, we assessed the diagnostic potential of 64 DMGs and 18 specific DMG-DEGs by performing Principal Component Analysis (PCA) using GEPIA2. PCA is a statistical technique that simplifies complex datasets by reducing their dimensionality while emphasizing significant patterns. It identifies principal components, which are the directions of greatest variance in the data. By representing the dataset as a linear combination of these components, PCA facilitates the visualization and interpretation of the distinctions between OC tumor and normal ovarian tissues. This analysis utilized transcriptomic data from TCGA ovarian cancer samples to evaluate the efficacy of these DMGs can differentiate between tumor and normal ovary tissue.

Statistical Analyses and Visualization

Visualization of methylation and gene expression profiles was conducted using online tools (<https://www.bioinformatics.com.cn/en>, <http://www.heatmapper.ca/> and <http://cancer-pku.cn/>). The relationship between methylation level changes in DMRs and expression levels of genes in these regions was analyzed using the nonparametric Spearman correlation test.

RESULTS

In this study, we identified and analyzed DMRs in cfDNA from OC patients compared with HBDs, focusing on elucidating the epigenetic alterations associated with OC. Furthermore, we assessed the effects of DMRs on methylated gene expression using data from TCGA.

Epigenetic Shifts in Ovarian Cancer: Revealing Methylation Dynamics

The cfMeDIP-seq bioinformatics analysis demonstrated that the total number of unique reads for all samples ranged from 5 million to 15 million. This coverage depth is considered sufficient for robust differential analysis using DESeq2. Analysis of cfDNA from OC patients revealed substantial alterations in DNA methylation patterns. A total of 811 DMRs between OC and HBDs were identified, indicating epigenetic dysregulation associated with OC. Among these DMRs, 554 regions

exhibited hypermethylation, whereas 257 regions showed hypomethylation in the OC group compared with the controls. Further refinement of the analysis at a significance threshold of $p < 0.05$ yielded 64 DMRs (Table 2), with 62 hypermethylated and 2 hypomethylated regions meeting this criterion (Figure 1). We observed that all statistically significant DMRs ($p < 0.05$) are in distinct genes across the genome (Figure 2). Only 3% of the DMRs were identified as hypomethylated, whereas 97% of the significant DMRs were hypermethylated (Figure 3).

Characterizing Epigenetic Patterns of Ovarian Cancer

In our exploration of the epigenetic signature in ovarian cancer, we calculated the methylation Z-score for each DMR ($p < 0.05$) across all samples. This allowed us to quantitatively assess the methylation status of each DMR relative to the overall methylation pattern in the dataset. Subsequently, visualization of these methylation patterns using a heatmap provided a comprehensive overview of the methylation profiles across samples and DMRs. Hierarchical cluster analysis employing the average linkage method and Spearman rank correlation metrics revealed distinct patterns of methylation similarity or dissimilarity between samples and DMRs (Figure 4). These

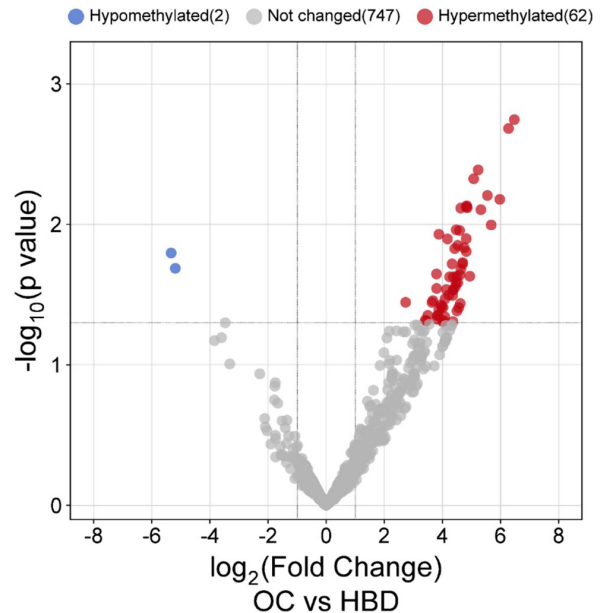


Figure 3. Volcano plot analysis of the DMRs. This figure displays a volcano plot depicting the statistical significance (p value) and fold change (\log_2 foldchange) of DMRs. DMRs meeting the significance criterion ($p < 0.05$) and exhibiting a fold change greater than -1 or less than 1 are highlighted. Hypermethylated and hypomethylated DMRs are represented by red and blue dots, respectively. DMR: Differentially methylated region; OC: Ovarian cancer; HBD: Healthy blood donor.

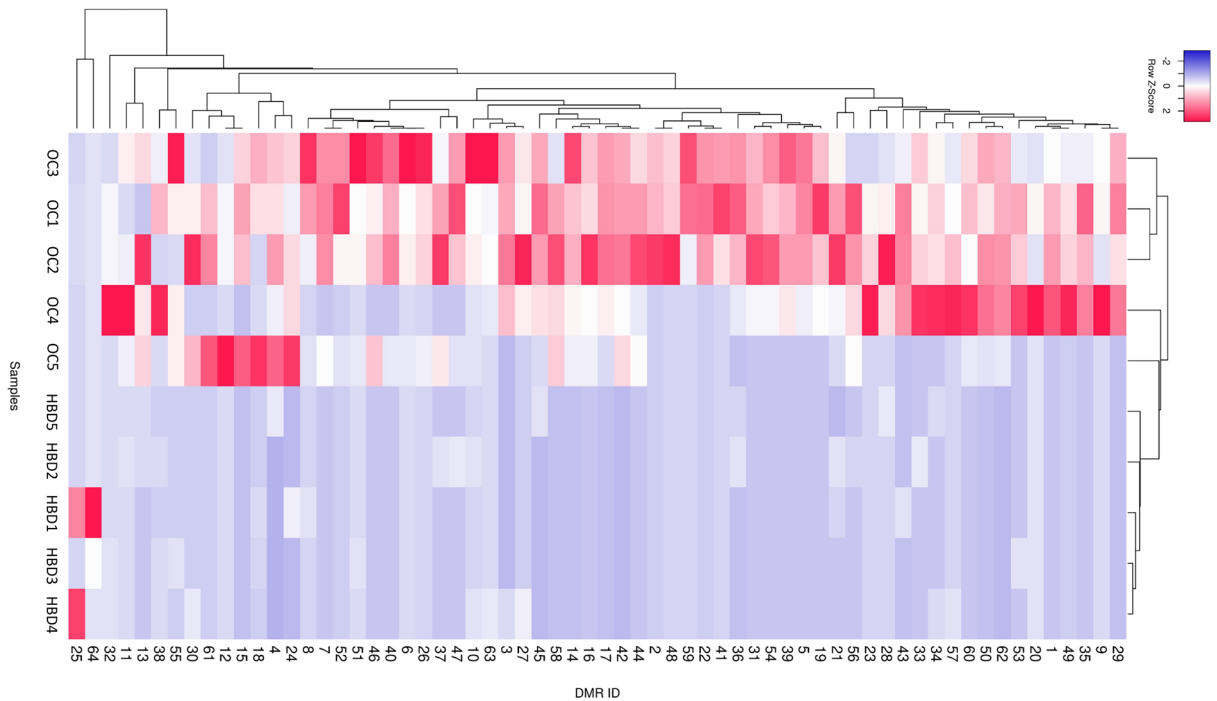


Figure 4. Heatmap of DNA methylation signatures.

Heatmap showing the methylation status of DMRs in OC samples relative to HBDs. Methylation levels are represented on a scale from -2 to 2, with hypermethylation displayed in red and hypomethylation displayed in blue. Using hierarchical cluster analysis with the average linkage method and Spearman rank correlation metrics, the heatmap highlights distinct patterns of methylation alterations in OC and HBDs. OC: Ovarian cancer; HBD: Healthy blood donor; DMR ID: Differentially methylated region identifier.

results provided insights into sample clustering based on epigenetic signatures. As a result, a detailed examination of the clusters in the heatmap revealed a clear and strong correlation within the HBD group, as evidenced by the very short vertical cluster arms on the right side. Additionally, the OC samples were distinctly separated, with a strong correlation among the three OC samples observed on the left side.

Integrative Analysis of DMGs and DEGs in OC

To explore the functional implications of the identified DMRs, we investigated the differentially expressed genes in OC from TCGA data using the GEPIA2 database. We identified 7641 DEGs in TCGA OC tissue samples compared to normal ovarian tissue from genotype-tissue expression (GTEx). We compared our DMGs from cfMEDIP with these DEGs from GEPIA2. This analysis identified 18 genes with overlapping differential methylation and expression patterns in ovarian cancer (Table 3).

Our correlation analysis, employing Spearman's rank correlation, assessed the relationship between methylation status of DMGs and expression level of DEGs in OC samples. A $p < 0.05$ was applied to determine statistical significance. The analysis revealed two distinct correlation patterns. Ten genes exhibited a negative correlation between hypermethylation

and gene downregulation, indicating a hypermethylation-downregulation relationship. These genes include *PRDM11*, *CAPRN2*, *ATN1*, *POU5F1P3*, *NR2F2*, *DYNC1LI2*, *LYRM9*, *FMO5*, *CCDC88A*, and *UIMC1*. In contrast, eight genes exhibited a positive correlation between hypermethylation and gene upregulation, representing a hypermethylation-upregulation relationship. These genes were *TMC5*, *SECTM1*, *NOTCH3*, *B3GNT3*, *LINC01224*, *S100A16*, *LRP8*, and *WWC1* (Figure 5).

Survival analysis was performed to evaluate the prognostic significance of these 18 overlapping genes. Among them, *B3GNT3*, a hyper-up gene, demonstrated a significant association with overall survival. Additionally, we explored the role of two DMGs identified as cancer driver genes in the COSMIC database. Although the expression of one of these genes, *LRP1B*, was not statistically significant when compared with normal tissues in the OC TCGA dataset, it approached statistical significance for overall survival ($p = 0.053$) and was associated with decreased gene expression (Figure 6).

Principal Component Analysis Reveals Distinct Clusters

To further investigate all DMGs and overlapped DMG-DEG, we performed a PCA using GEPIA2. For the first PCA, we used 64

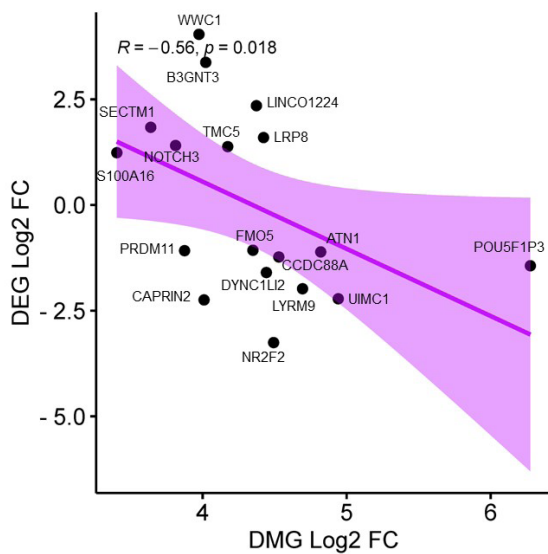


Figure 5. Correlation analysis between DNA methylation and gene expression.

The results of Spearman correlation analysis examining the relationship between levels of DNA methylation and gene expression in OC samples versus HBD. Each data point in the scatter plot represents a gene, with the x-axis indicating the DMG and the y-axis representing the DEG expression level. The negative correlation between DMG and DEG levels is indicated by a downward trend in the scatter plot. The statistical significance of the correlation was assessed using the p value, with values below 0.05 considered significant. DMG: Differentially methylated gene; DEG: Differentially expressed gene; OC: Ovarian cancer; HBD: Healthy blood donor.

DMGs identified in our cfMEDIP analysis. However, only 51 of the DMGs were recognized in the GEPIA2 database. We refined our analysis by focusing on 18 DMGs that overlapped with DEGs identified in GEPIA2, and included 2 additional DMGs from the COSMIC database (*LRP1B* and *CD28*), resulting in a total of 20 DMGs for the second PCA (Figure 7). In the first PCA analysis, PC1, PC2, and PC3 explained 54%, 9%, and 4% of the variance, respectively. In the second PCA analysis, similar patterns were observed for PC1 (42%), PC2 (18%), and PC3 (8%).

DISCUSSION

Our study provides a comprehensive analysis of DNA methylation alterations in OC by examining cfDNA in plasma samples. By comparing the methylation patterns between OC patients and HBDs, we identified significant epigenetic changes that highlight the potential role of DNA methylation in OC pathogenesis. Using cfDNA isolated from 5 OC patients and 5 HBDs for cfMEDIP-Seq, bioinformatics analysis identified differentially methylated regions (DMRs), revealing significant methylation alterations predominantly in OC samples. Hierarchical clustering and heatmap visualization highlighted distinct methylation patterns in OC and HBDs. Integration with

TCGA data identified 18 genes with overlapping methylation and expression changes, with *B3GNT3* emerging as a potential prognostic marker. Additionally, *LRP1B* and *CD28* were identified as cancer driver genes in the COSMIC database. These findings underscore the importance of DNA methylation in OC and suggest novel diagnostic and therapeutic strategies.

Our results revealed significant alterations in DNA methylation patterns between OC patients and HBDs, with 62 hypermethylated and 2 hypomethylated DMRs identified. The predominance of hypermethylation events aligns with the established notion that tumor suppressor genes are often silenced by promoter hypermethylation in cancer (16). This silencing can disrupt normal cellular functions, such as cell cycle regulation, apoptosis, and DNA repair, contributing to tumorigenesis (17, 18). The notable predominance of hypermethylated DMRs suggests the potential concerted efforts of cancer cells to silence tumor suppressor genes and activate oncogenes; however, caution is advised in interpreting this bias due to technical constraints. These findings underscore the complexity of DNA methylation alterations in ovarian cancer and provide a foundation for further exploration of their functional implications in disease progression and diagnosis. The distinguish ability of the identified 64 DMGs between OC patients and the HBDs was assessed using Methylation Z-scores obtained from methylation datasets. Heatmap analysis provides valuable insights into how OC and HBDs are clustered based on their epigenetic patterns. Further investigation into the biological implications of these methylation patterns and their association with clinical outcomes in ovarian cancer is warranted.

Our integrative analysis using TCGA dataset revealed 18 genes exhibiting both differential methylation and expression in OC. The majority of these genes demonstrated a negative correlation between methylation and expression levels, consistent with the epigenetic regulation model in which promoter hypermethylation leads to gene silencing. Notably, we identified a subset of ten “hyper-down genes” where hypermethylation correlated with downregulation, supporting their potential role as tumor suppressor genes. Conversely, the remaining eight genes exhibited hypermethylation upregulation patterns, which may indicate complex regulatory mechanisms or context-dependent roles in OC (19).

PCA analysis, which was conducted using both the 64 DMGs and the 20 DMGs overlapping with DEGs or driver gene lists, demonstrated a clear separation between OC samples and normal samples. The OC samples formed distinct clusters in the PCA plots, highlighting significant differences in the DMG-DEG expression profiles. The observed separation underscores the robustness of the identified DMRs and their potential role in differentiating between ovarian cancer and normal ovarian tissue.

Among the DMGs analyzed, *B3GNT3* and *LRP1B* emerged as particularly notable. *B3GNT3* was identified as significant in

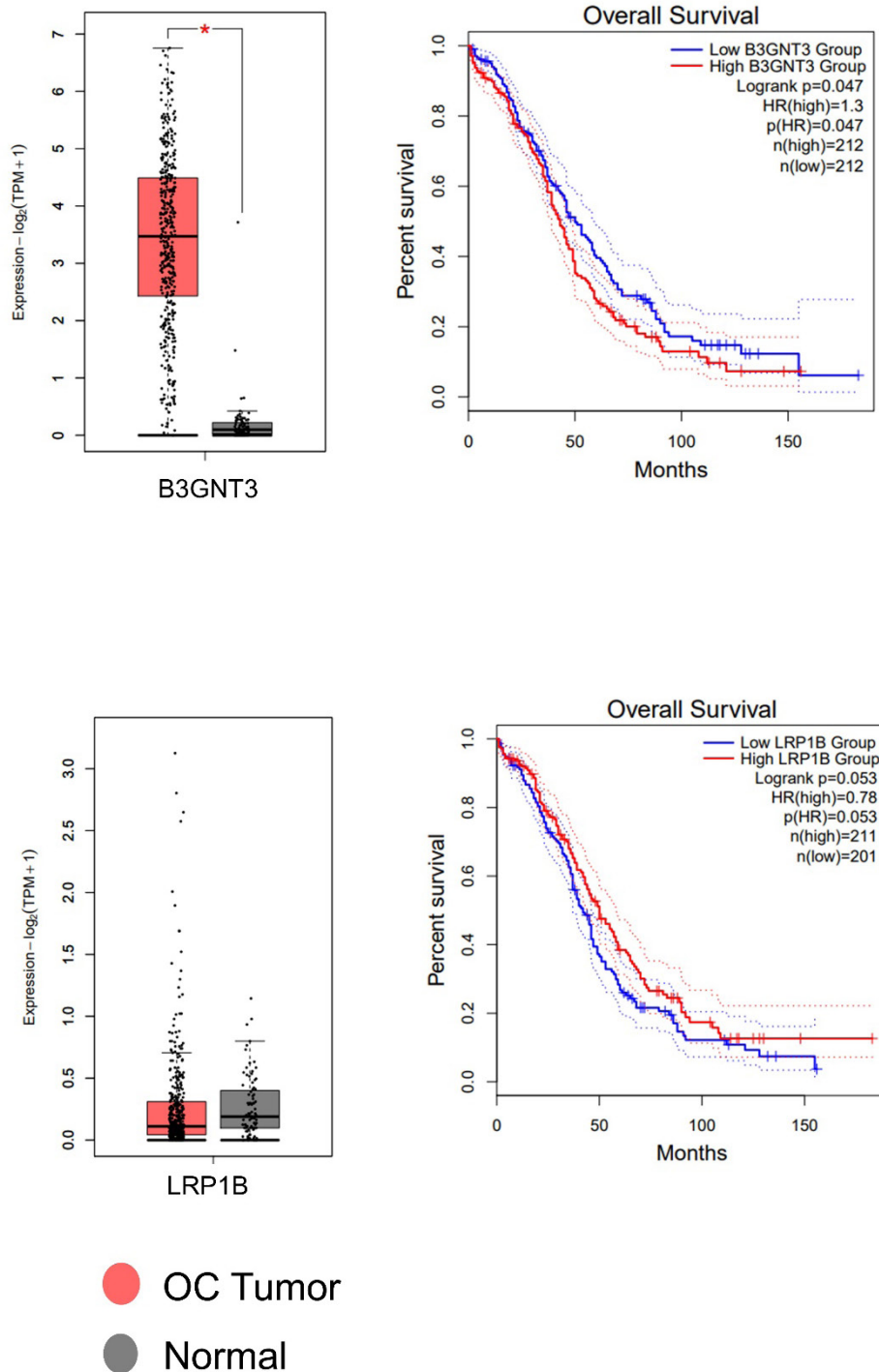


Figure 6. Expression and survival analyses of the B3GNT3 and LRP1B Genes in TCGA.

This figure presents the results of gene expression analysis (left) and survival analysis (right) conducted to assess the expression levels and prognostic significance of two genes, B3GNT3 (top) and LRP1B (bottom), in OC. The left panel displays the gene expression levels of B3GNT3 and LRP1B in OC samples compared with the normal ovarian tissue samples. Expression levels are depicted on the y-axis, with compared groups (legend indicates) on the x-axis. The right panel illustrates the survival analysis results for B3GNT3 and LRP1B in ovarian cancer patients. Kaplan-Meier survival curves depict the overall survival probability over time for patients with high and low expression levels of B3GNT3 and LRP1B. TCGA: The Cancer Genome Atlas; OC: Ovarian cancer.

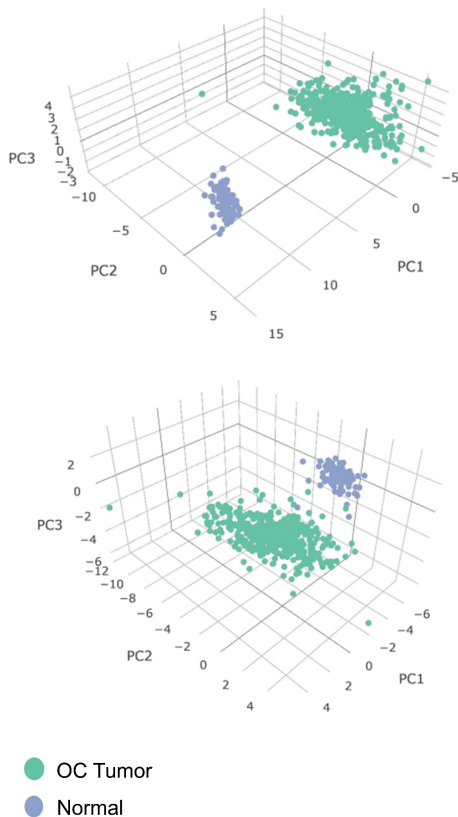


Figure 7. PCA of DMR Signature in TCGA data.

3D PCA plot of the distribution of OC and normal ovarian tissue samples based on DMR signature. The axes of the plot represent the three principal components (PC1, PC2, and PC3), with PCA-1 depicted at the top and PCA-2 at the bottom, capturing the highest variance in the data. In the first PCA, 64 DMGs identified in the cfMEDIP analysis were utilized, while in the second PCA, a refined set of 20 DMGs, including 18 overlapping DEGs identified in GEPIA2 and 2 additional DMGs from the COSMIC database (*LRP1B* and *CD28*), were included. The color legend indicates OC and normal ovarian tissue.

PCA: Principal component analysis; DMR: Differentially methylated region; DMG: Differentially methylated gene; DEG: Differentially expressed gene; OC: Ovarian cancer; TCGA: The Cancer Genome Atlas; COSMIC: Catalogue of somatic mutations in cancer.

survival analysis, highlighting its potential as a prognostic marker. *LRP1B*, while nearly significant with a p value close to the threshold, is recognized for its role as a cancer driver gene. We focused on these two genes because of their relevance to survival outcomes, as they exhibited more pronounced associations than other DMGs. However, we acknowledge that other identified genes may have diagnostic value and warrant further investigation.

B3GNT3 is a glycosyltransferase enzyme involved in the glycosylation of proteins, including programmed death-ligand 1 (PD-L1), which plays a role in tumor immune evasion. In certain cancers, the upregulation of *B3GNT3* can enhance the glycosylation and stability of PD-L1, contributing to tumor progression by helping tumor cells evade the immune response (20, 21). Moreover, upregulated *B3GNT3* in gynecologic cancers correlates with diagnosis, poor prognosis, immune infiltration, and NF- κ B signaling activation, suggesting its role as a carcinogenic factor in these cancers (22). In this study, *B3GNT3* was identified as a hyper-upregulated gene. Its hypermethylation was paradoxically associated with its upregulation and poor survival outcomes, suggesting a potential oncogenic role. This finding is particularly intriguing because it contradicts the typical model in which hypermethylation leads to gene silencing. Instead, it indicates that *B3GNT3* may be activated through alternative regulatory mechanisms in OC.

In contrast, *LRP1B* was identified as a tumor suppressor gene with hypermethylation correlated with its downregulation. Previous studies have implicated *LRP1B* in various cancers, where its loss of function is associated with increased tumorigenicity and metastasis (23, 24). Our results corroborate these findings and highlight the potential of *LRP1B* as a therapeutic target. Restoring *LRP1B* function through demethylating agents or other epigenetic therapies could offer a novel approach for OC treatment.

It is important to acknowledge the limitations of our study, including its relatively small sample size and the need for validation in independent cohorts. Additionally, translating epigenetic findings into clinical practice poses challenges related to standardization of methodologies and integration into existing diagnostic and prognostic frameworks. Addressing these challenges is crucial for realizing the full potential of epigenetic markers in the management of ovarian cancer. Despite these challenges, our findings provide valuable insights into the epigenetic landscape of ovarian cancer and pave the way for further research into personalized therapeutic interventions targeting aberrant DNA methylation.

Ethics Committee Approval: This study was approved in 2020 by Istanbul University, Istanbul Faculty of Medicine Clinical Research Ethics Committee under file number 1451.

Informed Consent: All participants provided voluntary informed consent by completing the consent forms after receiving detailed information.

Peer-review: Externally peer-reviewed.

Author Contributions: Conception/Design of Study – T.S.K., S.T., M.J., T.G.; Data Acquisition – T.S.K., J.H., S.T., M.J.; Data Analysis/Interpretation – T.S.K., J.H., M.J.; Drafting Manuscript – T.S.K., M.J., T.G., J.H., S.T.; Critical Revision of Manuscript – T.S.K., M.J., T.G., S.Topuz.; Final Approval and Accountability – T.S.K., M.J., T.G., J.H., S.T., S.Topuz.

Conflict of Interest: The authors declare no conflict of interest.

Financial Disclosure: This study was supported by the Scientific Research Projects Coordination Unit of Istanbul University, project number 36308.

REFERENCES

1. Feng J, Xu L, Chen Y, Lin R, Li H, He H. Trends in incidence and mortality for ovarian cancer in China from 1990 to 2019 and its forecasted levels in 30 years. *J Ovarian Res* 2023; 16(1): 139.
2. Balla A, Bhak J, Biró O. The application of circulating tumor cell and cell-free DNA liquid biopsies in ovarian cancer. *Mol Cell Probes* 2022; 66: 101871.
3. Hinchcliff E, Westin SN, Herzog TJ. State of the science: contemporary front-line treatment of advanced ovarian cancer. *Gynecol Oncol* 2022; 166(1): 18-24.
4. Roque R, Ribeiro IP, Figueiredo-Dias M, Gourley C, Carreira IM. Current applications and challenges of next-generation sequencing in plasma circulating tumor DNA of ovarian cancer. *Biology* 2024; 13(2): 88.
5. Giannopoulou L, Mastoraki S, Buderath P, Strati A, Pavlakis K, Kasimir-Bauer S, et al. ESR1 methylation in primary tumors and paired circulating tumor DNA of patients with high-grade serous ovarian cancer. *Gynecol Oncol* 2018; 150(2): 355-60.
6. Lu H, Liu Y, Wang J, Fu S, Wang L, Huang C, et al. Detection of ovarian cancer using plasma cell-free DNA methylomes. *Clin Epigenetics* 2022; 14(1): 74.
7. Margolin G, Petrykowska HM, Athamanolap P, Goncarenco A, Osei-Tutu A, Annunziata CM, et al. Leveraging locus-specific epigenetic heterogeneity to improve the performance of blood-based DNA methylation biomarkers. *Clin Epigenetics* 2020; 12: 154.
8. Marinelli LM, Kisiel JB, Slettedahl SW, Mahoney DW, Lemens MA, Shridhar V, et al. Methylated DNA markers for plasma detection of ovarian cancer: discovery, validation, and clinical feasibility. *Gynecol Oncol* 2022; 165(3): 568-76.
9. Peng S, Zhang X, Wu Y. Potential applications of DNA methylation testing technology in female tumors and screening methods. *Biochim Biophys Acta Rev Cancer* 2023; 1878(5): 188941.
10. Papanicolau-Sengos A, Aldape K. DNA methylation profiling: an emerging paradigm for cancer diagnosis. *Annu Rev Pathol* 2022; 17: 295-321.
11. Asante D-B, Calapre L, Ziman M, Meniawy TM, Gray ES. Liquid biopsy in ovarian cancer using circulating tumor DNA and cells: ready for prime time? *Cancer Lett* 2020; 468: 59-71.
12. Govindarajan M, Wohlmuth C, Waas M, Bernardini MQ, Kislinger T. High-throughput approaches for precision medicine in high-grade serous ovarian cancer. *J Hematol Oncol* 2020; 13: 1-20.
13. Sánchez-Herrero E, Serna-Blasco R, Robado de Lope L, González-Rumayor V, Romero A, Provencio M. Circulating tumor DNA as a cancer biomarker: an overview of biological features and factors that may impact on ctDNA analysis. *Front Oncol* 2022; 12: 943253.
14. Li Y, Fan Z, Meng Y, Liu S, Zhan H. Blood-based DNA methylation signatures in cancer: a systematic review. *Biochim Biophys Acta Mol Basis Dis* 2023; 1869(1): 166583.
15. Taiwo O, Wilson GA, Morris T, Seisenberger S, Reik W, Pearce D, et al. Methylome analysis using MeDIP-seq with low DNA concentrations. *Nat Protoc* 2012; 7(4): 617-36.
16. Geissler F, Nesic K, Kondrashova O, Dobrovic A, Swisher EM, Scott CL, et al. The role of aberrant DNA methylation in cancer initiation and clinical impacts. *Ther Adv Med Oncol* 2024; 16: 17588359231220511.
17. Chen YC, Elnitski L. Aberrant DNA methylation defines isoform usage in cancer, with functional implications. *PLoS Comput Biol* 2019; 15(7): e1007095.
18. Rini BI, Zhang J, Hall O, Bergener J, Wang Y, Brown B, et al. 1910P evaluation of a genome-wide methylome enrichment platform for circulating tumor DNA quantification and prognostic performance in renal cell carcinoma (RCC). *Ann Oncol* 2023; 34: S1028.
19. Rauluseviciute I, Drabløs F, Rye MB. DNA hypermethylation associated with upregulated gene expression in prostate cancer demonstrates the diversity of epigenetic regulation. *BMC Med Genomics* 2020; 13(1): 6.
20. Ren X, Lin S, Guan F, Kang H. Glycosylation targeting: a paradigm shift in cancer immunotherapy. *Int J Biol Sci* 2024; 20(7): 2607-21.
21. Leng X, Wei S, Mei J, Deng S, Yang Z, Liu Z, et al. Identifying the prognostic significance of *B3GNT3* with PD-L1 expression in lung adenocarcinoma. *Transl Lung Cancer Res* 2021; 10(2): 965.
22. Xu J, Guo Z, Yuan S, Li H, Luo S. Upregulation of *B3GNT3* is associated with immune infiltration and activation of NF- κ B pathway in gynecologic cancers. *J Reprod Immunol* 2022; 152: 103658.
23. Príncipe C, Dionísio de Sousa IJ, Prazeres H, Soares P, Lima RT. LRP1B: a giant lost in cancer translation. *Pharmaceutics* 2021; 14(9): 836.
24. Cowin PA, George J, Fereday S, Loehrer E, Van Loo P, Cullinane C, et al. *LRP1B* deletion in high-grade serous ovarian cancers is associated with acquired chemotherapy resistance to liposomal doxorubicin. *Cancer Res* 2012; 72(16): 4060-73.

Identification of Peptides Binding Specifically to Colon Cancer Cells through Phage Display Peptide Library Screening

Deniz Sahin¹ , Zeynep Kanlidere² , Bariscan Ekal¹ , Berkehur Abayli¹ ,
Yordan Hayat³ , Ece Selcuk⁴ 

¹Department of Molecular Biology and Genetics, Faculty of Science and Letters, Istanbul Technical University, Istanbul, Turkiye

²Department of Basic Pharmaceutical Sciences, Faculty of Pharmacy, Acibadem Mehmet Ali Aydinlar University, Istanbul, Turkiye

³Department of Medical Biotechnology, Institute of Health Sciences, Acibadem Mehmet Ali Aydinlar University, Istanbul, Turkiye

⁴Department of Molecular Biology and Genetics, Faculty of Engineering and Natural Sciences, Istanbul Medeniyet University, Istanbul, Turkiye

ORCID ID: D.S. 0000-0003-3822-0319; Z.K. 0000-0003-1363-9105; B.E. 0009-0002-2994-9810, B.A. 0000-0002-8530-4227;
Y.H. 0000-0002-9123-5424; E.S. 0000-0002-2207-433X

Cite this article as: Sahin D, Kanlidere Z, Ekal B, Abayli B, Hayat Y, Selçuk E. Identification of peptides binding specifically to colon cancer cells through phage display peptide library screening. *Experimed* 2024; 14(3): 174-182.

ABSTRACT

Objective: Colorectal cancer ranks among the most frequently occurring cancers. Addressing the diagnosis and treatment challenges requires the advancement of alternative approaches that can more precisely differentiate between cancerous and healthy cells.

Materials and Methods: We identified colon cancer cell surface specific 12-mer peptides using subtractive phage display technique. Four rounds of biopanning were conducted using the M13 bacteriophage PhD-12 peptide library with the human colon cancer cell line HCT-116. Subtractive selection involved the use of the human rectal cancer cell line SW837 and the healthy CCD112-CoN cell line. Binding levels of selected phage clones were tested by ELISA-HRP binding assays. Experimentally identified peptide sequences were synthesized by solid-phase chemistry. Peptides were labelled at the N-terminus with a fluorescent dye for visualization of cells by confocal microscopy.

Results: Peptide COL419 (Serine-Valine-Alanine-Histidine-Leucine-Serine-Proline-Histidine-Serine-Threonine-Threonine-Alanine; SVAHLSPHSTTA) can differentiate colon and rectal cancers from healthy cells. In addition, the COL-AA peptide (Histidine-Tyrosine-Proline-Threonine-Asparagine-Leucine-Histidine-Tyrosine-Proline-Threonine-Asparagine-Leucine; HYPTNLHYPTNL), which was designed from the amino acid composition analysis of the experimentally selected peptide sequences bound to colon cancer cells and neither rectal cancer cells nor healthy colorectal cells.

Conclusion: The peptides determined specifically target colon cancer cells. These findings enhance our understanding of the differences between these cancer types. The selected peptides have the potential for clinical application in targeted diagnosis and treatment of colon cancer.

Keywords: Colon cancer, peptides, phage display, rectal cancer, targeted approaches

INTRODUCTION

Globally, colorectal cancer (CRC) ranks as the third most prevalent type of cancer in terms of diagnosis and is the second major contributor to cancer-related mortality (1). CRC can have its beginnings in either the colon or rectum, and the terminology used to describe it varies depending on its point of origin, either as colon cancer or rectal

cancer. Although colon and rectal cancers arise at similar anatomical sites, they are two different types of cancer with significant differences in pathogenesis. Rectal cancer has characteristics that should be treated separately because of its anatomical and biological differences. Therefore, in our study, rectal cancer cells as well as normal colon cells were used to identify colon cancer-specific peptides. This strategy provided a critical step in distinguishing results

Corresponding Author: Deniz Sahin **E-mail:** sahinden@itu.edu.tr

Submitted: 27.06.2024 **Revision Requested:** 02.09.2024 **Last Revision Received:** 07.09.2024 **Accepted:** 04.10.2024 **Published Online:** 02.12.2024



Content of this journal is licensed under a Creative Commons Attribution-NonCommercial 4.0 International License.

specific to colon cancer cells. Each cancer type has different risk factors, symptoms, and treatment options and needs to be treated as a separate type of cancer (2).

Conventional methods for diagnosing and treating CRC have proven inefficient, necessitating the development of novel techniques. Small peptides targeting tumors can improve treatment efficacy and reduce the side effects of traditional approaches. Compared to monoclonal antibodies and large protein ligands, peptides have several advantages, including smaller size, easier synthesis, and superior biocompatibility (3-5). Additionally, their affinity, charge, hydrophobicity, and stability can be chemically modified for optimal *in vivo* applications.

Phage display can be used for various targets, including cancer cells (6, 7). It has been used in numerous studies to select peptides/antibody fragments for various targets, thereby aiding in the assessment of molecular interactions. These include identifying cellular receptors (8), screening epitopes or mimotopes (9), and confirming peptides that target specific cells or tissues (10, 11). During selection, an array of peptide sequences is displayed on the tips of M13 phages, allowing attachment to the target. Non-specific peptides are eliminated, leaving M13 phages with high-affinity peptides that can be amplified. This method offers an alternative to conventional approaches, enabling the discovery of targeting molecules for diagnostic and therapeutic purposes (12, 13).

This study aimed to identify small peptides with the ability to effectively discriminate between colorectal cancer cells and healthy cells, as well as differentiate between colon and rectal cancer cells. To achieve this, HCT-116 (ATCC[®] CCL-247[™]) colon cancer cells, SW837 (ATCC[®] CCL-235[™]) rectal cancer cells, and CCD-112CoN (ATCC[®] CRL-1541[™]) normal human colon cells were employed. These cells were used in the subtraction biopanning process alongside a phage display peptide library to identify peptides that specifically bind to colon cancer cells. Although this study aimed to target colon and rectum cancers, the results obtained will also contribute to understanding the reasons for the difference between the two types of cancer. The outcomes have the potential to facilitate applications in the fields of diagnosis and treatment.

MATERIALS AND METHODS

Cell Lines and Cell Culture

Human colon cancer cells HCT-116 (ATCC[®] CCL-247[™]), human rectal cancer cells SW837 (ATCC[®] CCL-235[™]) and healthy colon cells CCD-112CoN (ATCC[®] CRL-1541[™]) were purchased from the American Type Culture Collection (ATCC). HCT-116 and CCD-112CoN cells were cultivated in Dulbecco's Modified Eagle Medium (DMEM; 10% fetal bovine serum, 2mM L-glutamine, 100 µg/mL penicillin and 100 µg/mL streptomycin). SW837 cells were initially cultured in Leibovitz's L-15 (ATCC[®] 30-2008[™]) medium before being transferred to DMEM medium. The cells were subcultured in plastic culture flasks (25 cm²) and placed

in an incubator (37°C and 5% CO₂ atmosphere). When the cells reached a subconfluent state, they were collected, and their total number was determined using a hemocytometer.

In vitro Panning

Subtractive biopanning was performed using HCT-116 colon cancer cells as targets, with SW837 rectum cancer cells and CCD-112CoN colon cells as absorbers. Cell cultures were maintained in DMEM containing 10% fetal bovine serum (FBS) at 37°C and 5% CO₂. *In vitro* screening followed kit manual guidelines with minor adaptations. At 70% confluence, cells were washed with phosphate-buffered saline (PBS), blocked with 2% bovine serum albumin (BSA) at 37°C for 1 h, and incubated with 1 x 10¹¹ pfu phages. Unbound phages from CCD-112CoN cells were transferred to SW837 cells for a second subtraction step. The supernatant was then transferred to HCT-116 cells and incubated for 2 h. After washing with PBS with Tween 20, bound phages were eluted with glycine-HCl and neutralized with Tris-HCl. Some samples were used for microtitration, while the rest were amplified in *Escherichia coli* (*E. coli*) strain ER2738. Subsequent rounds increased the detergent and salt concentrations to 0.5%.

Phage Titering

The selective enrichment of phages bound to HCT-116 cells was achieved after four biopanning rounds. Phage titers from each round were assessed using a blue-white plaque assay on tetracycline-enriched agar plates. The number of phages entering and obtained from each biopanning cycle was determined by blue-white colony screening. The initial biopanning cycle began with 1 x 10¹¹ pfu/mL, and the same pfu count was obtained by amplifying the elution sample. This ensured a consistent number of phage clones in each cycle. Subsequent cycles started with 5 x 10¹⁰ pfu/mL for titer calculations. At the end of each cycle, the entering and recovered phages were counted, demonstrating decreasing phage diversity.

Cell-based Enzyme-Linked Immunosorbent Assay (ELISA)

For the cell-based ELISA, cells were cultured in 96-well plates until reaching 80-90% confluence and then blocked for 1 h with 2% BSA in PBS. Following three PBS washes, cells were fixed with 4% paraformaldehyde at room temperature for 15 min. After another three PBS washes, cells were blocked again with 2% BSA in PBS for 1 h at 37°C. Next, 1 x 10¹¹ pfu of phages were added to each cell type and incubated at room temperature for 1 h. Thirty selected phage clones were assessed. Wells were washed four times with 0.2% Tween 20 in PBS. HRP-conjugated anti-M13 monoclonal antibody (1:3000 dilution) was added to each well, and plates were incubated at 37°C for 2 h. After three washes with PBS, tetramethylbenzidine (TMB) solution was added and incubated at room temperature for 30 min. The reaction was stopped by adding 2M H₂SO₄. Absorbance at 450 nm was measured using a microplate reader. Negative controls

included PBS and cells without phage clones. All experiments were conducted in triplicate.

Amplification and Sequencing of Selected Phages

5 phage clones selected in cell-based ELISA analysis were amplified and purified for DNA sequencing. ssDNA of the selected clones was isolated and used for sequencing (Medsantek, Istanbul, Turkiye) using the -96gIII primer (5'-CCCTCATAGTTAGCGTAACG-3').

Synthesis and Characterization of Peptides

Experimentally selected and theoretically designed peptides were synthesized by solid-phase peptide synthesis using the standard Fmoc/tBu strategy. The synthesis were carried out in a microwave-assisted fully automated peptide synthesizer at 0.1 mmol synthesis scale using Rink Amide resin (0.70 mmol/g). For the labeled peptides, the N-terminal amino group was linked with 5(6)-carboxyfluorescein in the presence of DIC/HOBt reagents. Subsequently, a mixture of trifluoroacetic acid (TFA)/H₂O/triisopropylsilane (TIS) (95:2.5:2.5 v/v) was used to detach the peptides from the resin for 30 min at 37°C. The peptides were then precipitated in cold diethyl ether, centrifuged at 4000 rpm for 5 min, and freeze-dried from water. The crude peptides were purified by reversed-phase high performance liquid chromatography (RP-HPLC, Agilent Technologies, 1260 Infinity) on a semipreparative Agilent VariTide RPC C18 column using gradient elution (A: 0.1% TFA in water; B: 0.1% TFA in acetonitrile/water, 80:20, v/v). Peptides were analyzed by liquid chromatography-mass spectrometry (LC-MS)/MS system (Agilent Technologies, 6420 Triple Quad). The mass spectra were recorded in positive ion mode in the 200–2000 m/z range.

Peptide-based Immunofluorescence Assay

Candidate peptides labeled with 5-(6)-carboxyfluorescein were used in a peptide-based immunofluorescence assay to validate their specific binding to HCT-116 colon cancer cells. HCT-116, SW837, and CCD-112CoN cells were cultured in DMEM at 37°C and seeded onto 4-well chamber slides at 1 x 10⁴ cells per well until 70% confluence. The cells were washed with PBS, fixed with 4% paraformaldehyde for 15 min at room temperature, washed again, and blocked with 2% BSA in PBS for 30 min at 37°C. Labeled peptides (1 μM) were incubated with each cell type on a rocker platform for 90 min at room temperature. Samples were washed with PBS (0.1% Tween 20) and incubated with 4', 6-diamidino-2-phenylindole (DAPI) staining solution for 5 min. After two PBS rinses, confocal fluorescence microscopy was used for examination. The experiments were performed simultaneously with uniform microscope settings for all samples.

RESULTS

Subtraction Biopanning and Subsequent Analysis of Peptide Enrichment From a 12-peptide Phage Display Library

In this study, a subtraction biopanning strategy was used to enrich positive phage clones from a 12-peptide phage display library. HCT-116 human colon cancer cells served as target cells, whereas SW837 human rectum cancer cells and CCD-112CoN human healthy colon cells served as absorber cells. The aim was to eliminate phages that bound non-specifically to absorber cells and enhance the selectivity of target cells (14).

The peptide library was initially applied to CCD-112CoN cells, and unbound phages were then incubated with SW837 cells. Unbound phage clones were subjected to conventional biopanning with HCT-116 cells. Successive rounds intensified washing conditions. Bound phages were recovered and amplified in *E. coli* ER2738 for subsequent rounds. In the fourth round, an additional subtraction phase with BSA was conducted to further reduce non-specific binding.

Enrichment analysis after four biopanning rounds showed a 140-fold increase in the number of phages recovered from HCT-116 cells (Table 1), indicating successful selective amplification of target-binding phages (15).

Table 1. Enrichment analysis of positive phage clones from 12-peptide phage library

Round of Screening	Input Phage (pfu/mL)	Output Phage (pfu/mL)	Recovery (%)
1	1x10 ¹¹	1x10 ⁵	1x10 ⁻⁶
2	5x10 ¹⁰	1.8x10 ⁵	3.6x10 ⁻⁶
3	5x10 ¹⁰	4.5x10 ⁵	9x10 ⁻⁶
4	5x10 ¹⁰	7x10 ⁶	14x10 ⁻⁵

Table 2. Amino acid sequences of the 5 chosen phage clones for subsequent examination

Phage Clones	Peptide Sequence	MW	pI
COL401	VHMQLIPDNVR	1477.75	9.58
COL409	TYPNTQTHLLNA	1372.5	6.4
COL411	YELPPYPPTKAH	1412.61	6.75
COL414	WPLRGHSNPTLY	1440.62	8.75
COL419	SVAHLSPHSTTA	1207.31	6.66

MW: Molecular weight ; pI: Isoelectric point

Primary Identification of Positive Phage Clones with Cell-based ELISA

After the fourth round of biopanning, 30 phage clones were randomly selected and assessed for binding selectivity using cell-based ELISA. Horseradish peroxidase (HRP)-conjugated anti-M13 phage antibody identified phage clones with affinity for HCT-116 colon cancer cells. Five clones (COL401, COL409, COL411, COL414, and COL419) were chosen for further analysis due to their high binding affinity (Table 2). Clones that exhibited at least 1.25-fold higher binding to colon cancer cells compared to healthy colon cells were selected as the threshold. The specificity of these clones was tested on CCD-112CoN normal colon and SW837 rectum cancer cells. Figure 1 shows the binding levels of each clone to both target and

control cells. DNA sequencing identified the 12-mer peptide sequences responsible for binding. Among the five clones, those with minimal binding to CCD-112CoN cells were prioritized for further experiments. The M13KE phage control indicated non-specific binding to cancer and healthy cells. Notably, the COL419 clone exhibited higher binding levels on HCT-116 cells and lower binding on SW837 cells.

Amino Acid Composition Analysis of Selected Peptide Sequences

To identify favored and disfavored amino acids in the selection process, we compared the frequency of each amino acid in the top 5 binding peptides from the cell-based ELISA experiments with the initial frequencies in the PhD-12 peptide library (Table 3). Amino acids that were more prevalent in the top binding peptides exhibited an affinity for target cell-specific binding (16). Table 3 shows that the positively expressed amino acids in the selected peptides for the HCT116 surface were histidine (H), tyrosine (Y), proline (P), threonine (T), asparagine (N), and leucine (L). Most of these amino acids have polar side groups; histidine is weakly basic at neutral pH, whereas Y, P, and L are hydrophobic, and N and L are hydrophilic.

Based on the amino acid composition analysis of the 5 selected peptides for colon cancer cells, the peptide sequences to be synthesized were determined. The COL419 peptide sequence exhibited the highest binding level among the sequences selected after the fourth biopanning cycle. The COL-AA peptide was designed to contain positively selected amino acids compared to the initial expression rate. The COL-AA sequence included two repeats of H, Y, P, T, N, and L. Both the COL419 (SVAHLSPHSTTA) and COL-AA (HYPTNLHYPTNL) peptides were synthesized, purified, and conjugated with 5(6)-carboxyfluorescein.

Peptide Synthesis

5-(6)-carboxyfluorescein labelled peptides were synthesized and then purified by HPLC. Peptide bond can be detected at 214 nm and 5-(6)-carboxyfluorescein can be detected at 517 nm. Thus, we monitored HPLC with these two wavelengths. Chromatographic peaks that gave a signal at both wavelengths simultaneously were collected for further verification by mass spectrometry. The HPLC profiles of peptides COL-AA and COL419 are given in Figure 2 a, b, c and Figure 3 a, b, respectively.

Assessing the Targeting Affinity by Peptide-Based Immunofluorescence Assay

The peptide-based immunofluorescence assays provided valuable insights into the binding specificities of the synthesized COL419 and COL-AA peptides. The COL419 peptide exhibited strong binding to both HCT-116 colon cancer and SW837 rectal cancer cell lines (Figure 4). However, COL419 exhibited negligible binding to healthy CCD112-CoN colorectal cells. This suggests that COL419 can differentiate between cancerous (HCT-116 and SW837) and non-cancerous colorectal cells

Table 3: Amino acid composition analysis of experimentally selected 5 best binders on the HCT-116 cell surface

Amino acid	PhD-12%	EO#	EO%	D%
Histidine, H	4.6	6	10	117.4
Tyrosine, Y	3.6	4	6.7	85.2
Proline, P	8.1	9	15	85.2
Threonine, T	7.8	7	11.7	49.6
Asparagine, N	4.5	4	6.7	48.1
Leucine, L	8.9	7	11.7	31.1
Alanine, A	7.4	4	6.7	-9.9
Arginine, R	5.7	3	5	-12.3
Glutamine, Q	3.9	2	3.3	-14.5
Valine, V	6.1	3	5	-18
Tryptophan, W	2.3	1	1.7	-27.5
Lysine, K	2.3	1	1.7	-27.5
Serine, S	11.2	4	6.7	-40.5
Methionine, M	3.1	1	1.7	-46.2
Glutamic acid, E	3.1	1	1.7	-46.2
Aspartic acid, D	4.6	1	1.7	-63.8
Glycine, G	5.8	1	1.7	-71.3
Phenylalanine, F	2.7	0	0	-100
Cysteine, C	1.5	0	0	-100

PhD-12%: PhD-12 peptide library amino acid composition percentages; EO#: experimentally observed/selected amino acid number in 5 selected binders; EO%: percentage of experimentally observed/selected amino acids; D%: percentage difference of experimentally expressed amino acid to library expression ratio.

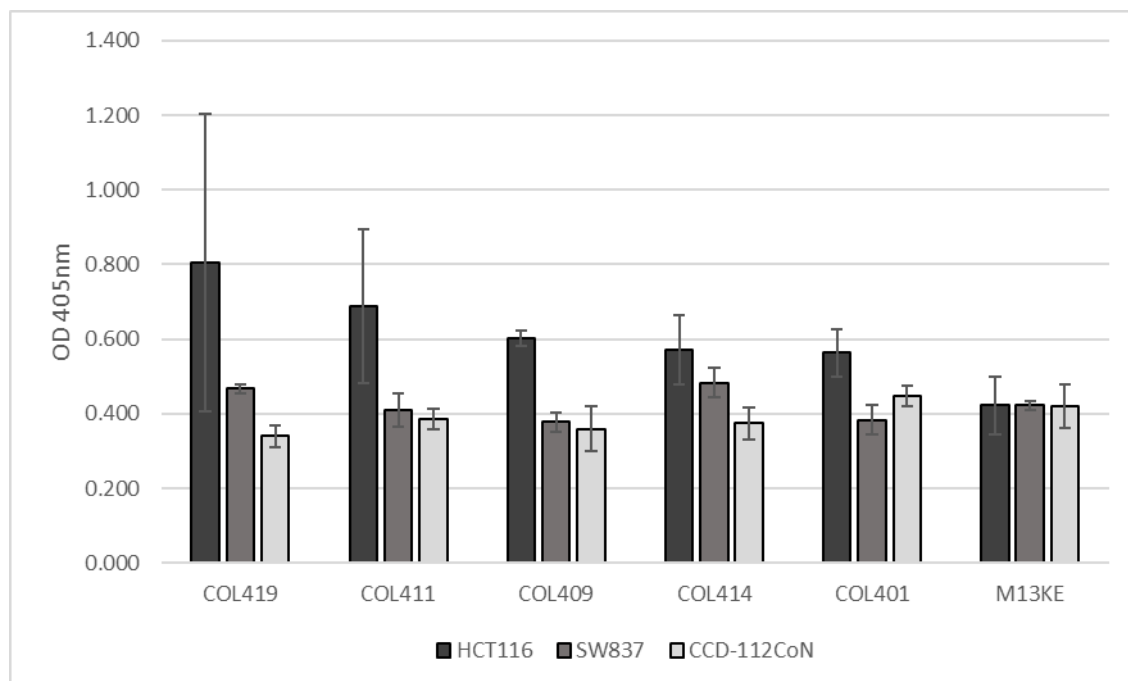


Figure 1. Cell-based ELISA results for 5 best phage clones on HCT-116, SW837 and CCD-112CoN cells. Binding levels of selected phage clones were tested on both target and absorber cells; COL419 had the best binding level among the clones. The M13KE phage was used as the control phage clone.

(CCD112-CoN), but does not distinguish between colon and rectal cancers. In contrast, the designed COL-AA peptide, comprised of two repeating units of histidine, tyrosine, proline, threonine, asparagine, and leucine amino acids (HYPTNL), bound specifically to colon cancer cells. Conversely, no binding was observed on the rectal cancer or healthy colorectal cells.

DISCUSSION

The subtraction biopanning strategy applied in this study enables the isolation of peptide ligands that interact exclusively with a given target cell by eliminating ligands that bind to non-target cells present in a sample (14). The progressive increase in the number of recovered phages over four rounds of biopanning demonstrated the successful enrichment of target-binding phages. This outcome underscores the utility of subtraction biopanning in enhancing the selectivity of phage clones, which is crucial for their application in targeted therapies and diagnostics.

The selection of 5 phage clones (COL401, COL409, COL411, COL414, and COL419) based on their strong binding affinity to HCT-116 colon cancer cells is a significant step in this research. These clones can serve as promising candidates for further development and applications in cancer diagnosis and treatment. Their ability to distinguish between cancer and normal cells highlights their potential for targeted therapies.

In a phage display biopanning experiment, the end-enriched pool contains clones with peptides that bind strongly to the

target. Comparing the amino acid frequencies in this enriched pool with those in the original naive library can reveal key residues that are overrepresented and thus important for binding. Specifically, if certain amino acids are found with much higher frequency in the enriched pool, it indicates that these residues likely make critical contacts and contribute significantly to the interaction with the target (16).

The analysis of amino acid composition within the selected clones provided further insight into the binding specificity of the peptides. The abundance of serine and threonine residues may enhance binding through potential hydrogen bonding and hydrophilic interactions.

Aromatic sequences like histidine and tyrosine and repeating sequences may contribute to the specificity of the peptide. The COL-AA peptide is a sequence designed using experimentally selected peptide amino acid composition information, and the differential binding shown in the peptide-based immunofluorescence assay indicates that the amino acid composition information of experimentally selected peptides can be followed as a promising approach for the determination of target-specific peptides.

In the literature, several peptides have been reported as colorectal cancer-specific peptides identified by phage display, such as the CBP-DWS peptide (Aspartic acid-Tryptophan-Serine-Serine-Tryptophan-Valine-Tyrosine-Arginine-Aspartic-acid-Proline-Glutamine-Threonine; DWSSWVYRDPQT) (17), L20 peptide (Alanine-Asparagine-Leucine-Asparagine-Leucine-Tryptophan-

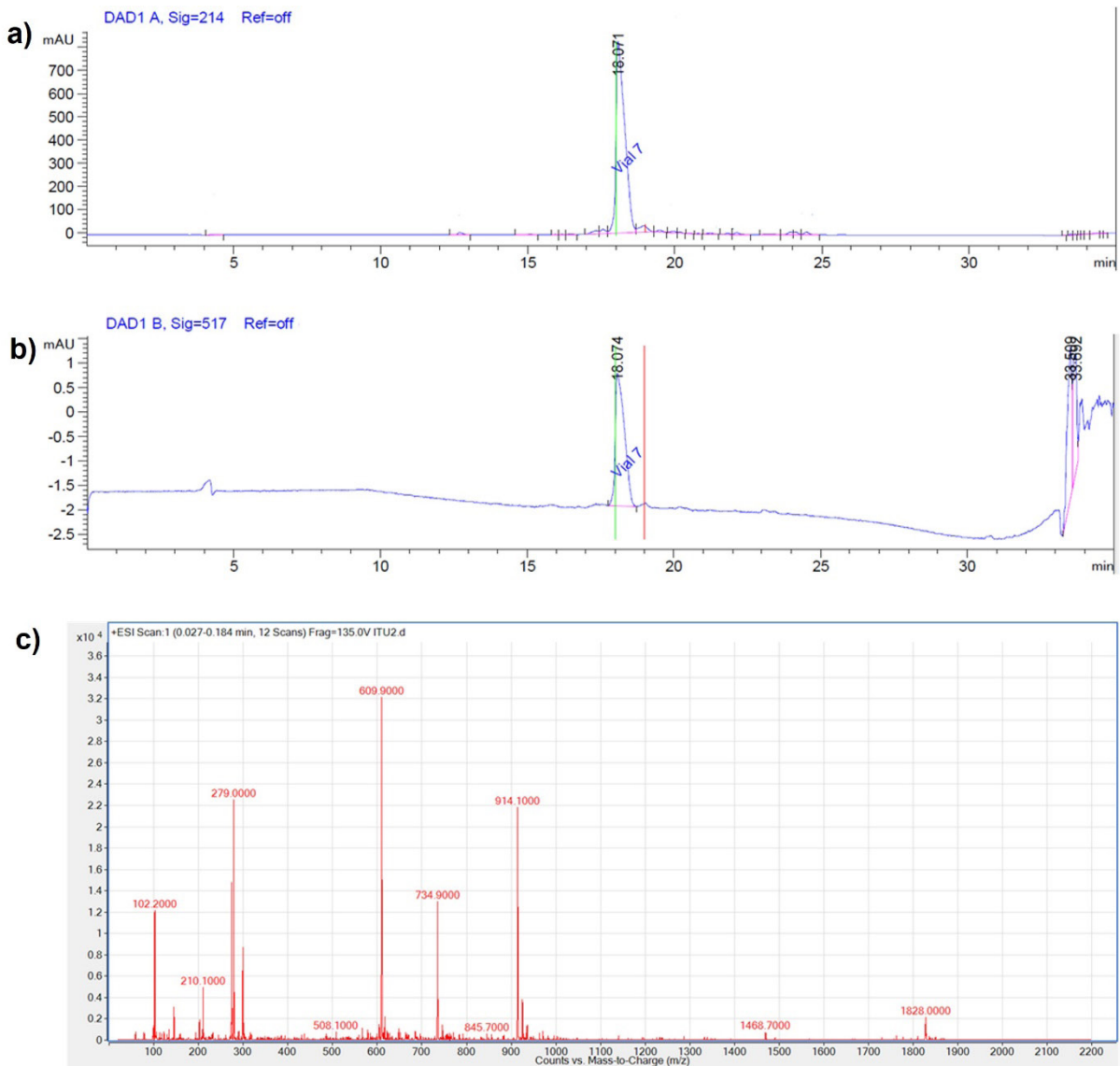


Figure 2. Reverse phase-HPLC profiles of 5-(6)-carboxyfluorescein labelled COL-AA at wavelengths of 214 and 517 nm. Solvent system; a) 0.1% TFA in water; b) 0.1% TFA in acetonitrile/water, 80:20, v/v; c) gradient 5-80%. LC-MS/MS analysis of 5-(6)-carboxyfluorescein labelled COL-AA peptide with molecular formula of (C₈₉H₁₀₇N₁₉O₂₄); m/z calculated for (M+H)⁺: 1826.777, found: 1828.0000; calculated for (M+2H)⁺: 913.892, found: 914.1000; calculated for (M+3H)⁺: 609.597, found: 609.9000.

Threonine-Aspartic acid-Tyrosine-Isoleucine-Arginine-Tryptophan; ANLNLWTDYIRW (18), disulfide-constrained RPMrel peptide (Cysteine-Proline-Isoleucine-Glutamic acid-Aspartic acid-Arginine-Proline-Methionine-Cysteine; CPIEDRPMC) (19), cyclic peptide TCP-1 (Cysteine-Threonine-Proline-Serine-Proline-Phenylalanine-Serine-Histidine-Cysteine; CTPSPFSHC) (5), RKOpep peptide (Cysteine-Proline-Lysine-Serine-Asparagine-Asparagine-Glycine-Valine-Cysteine; CPKSNNQVC) (20), CCBP1 peptide (Histidine-Alanine-Methionine-Arginine-Alanine-Glutamine-Proline; HAMRAQP) (21) and CP15 peptide (Valine-Histidine-Leucine-Glycine-Tyrosine-Alanine-Threonine; VHLGYAT) (22). Although the specificity of the peptides

identified in these studies has been demonstrated for different colorectal cancer cell lines and tissue samples, the specificity of the peptides to differentiate colon and rectal cancer cells has not been studied. Among these peptides, the CBP-DWS, L20, CCBP1, and CP15 peptides are enriched in aromatic residues like tryptophan and tyrosine, which likely facilitate binding through pi-pi stacking and hydrophobic interactions. RPMrel and TCP-1 peptides contain high proportions of charged residues glutamate, aspartate and histidine that promote electrostatic interactions with cancer cell receptors. The asparagine content of the RKOpep peptide may confer affinity through its hydrophilic and hydrogen bonding nature.

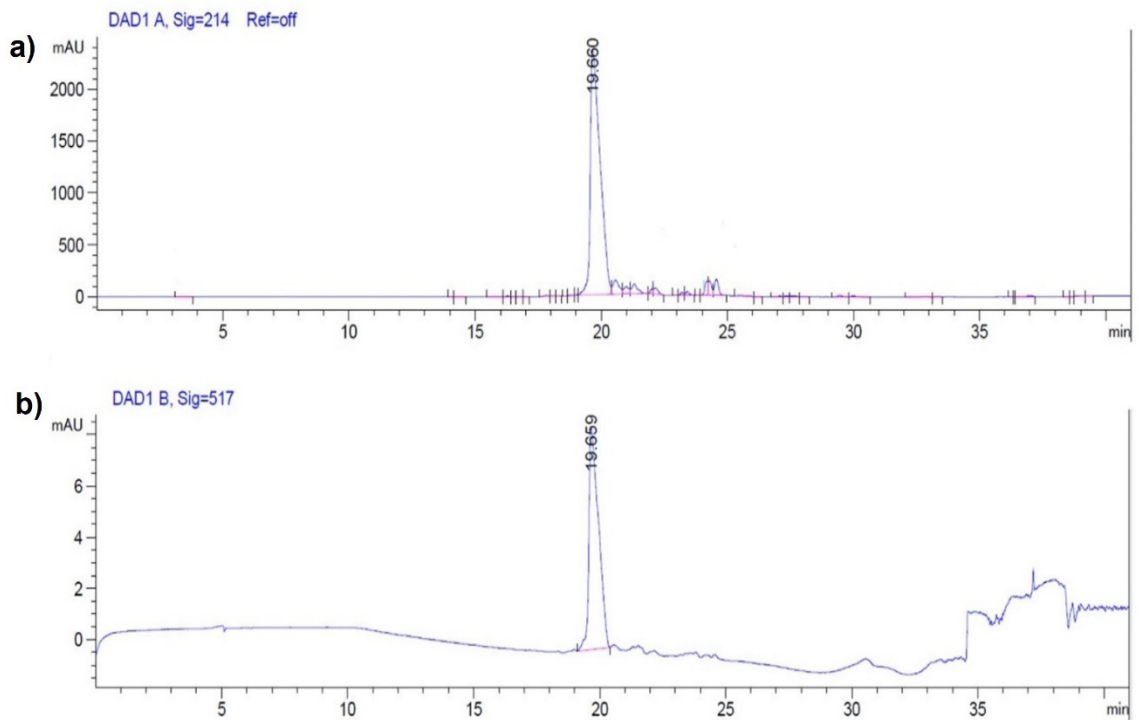


Figure 3. Reverse phase HPLC profiles of 5-(6)-carboxyfluorescein labelled COL419. Solvent system; a) 0.1% TFA in water; b) 0.1% TFA in acetonitrile/water (80:20, v/v; gradient 5-80%).

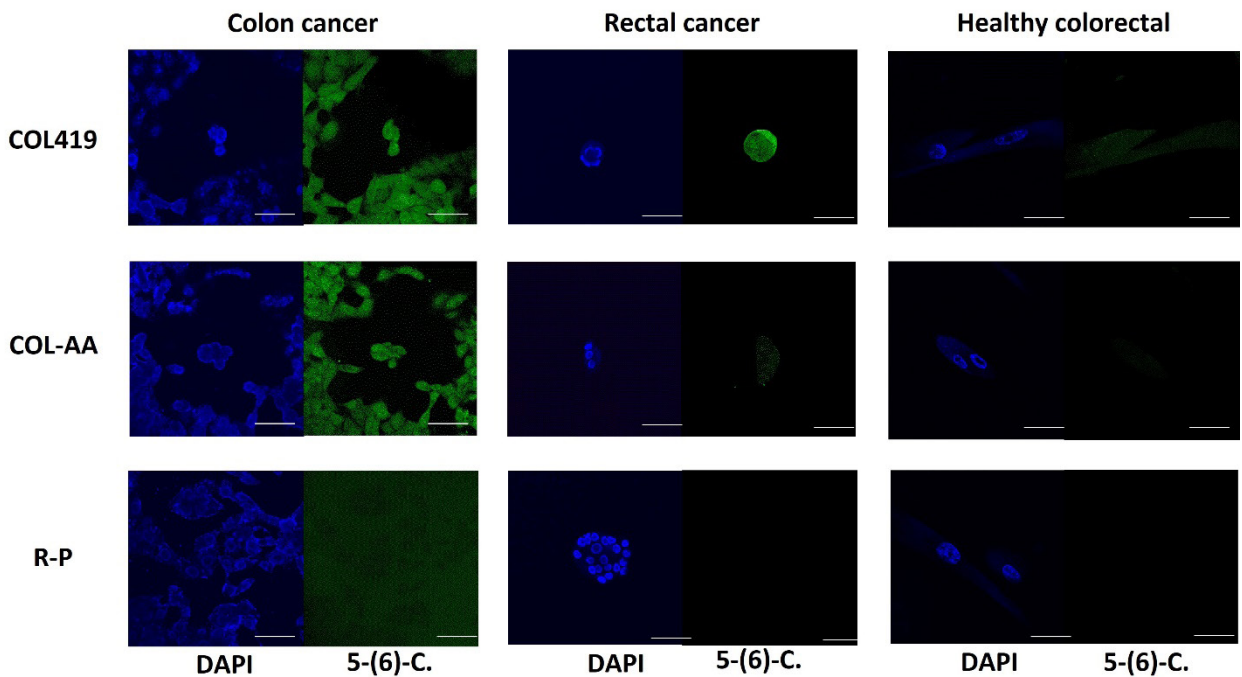


Figure 4. Confocal fluorescence binding assays for COL419 and COL-AA peptides. The degree of binding of colon-specific COL419 and COL-AA peptides to HCT-116 colon cancer, SW837 rectal cancer, and CCD-112 healthy colorectal cells was demonstrated using DAPI and 5-(6)-carboxyfluorescein stain. (R-P: Random peptide selected from phage library.) Scale bars: 50 μ m.

On the other hand, COL419 peptide is enriched in serine, threonine, and alanine residues. Their hydroxyl groups can form hydrogen bonds, whereas alanine provides hydrophobic contacts. COL-AA possesses a repetitive sequence with proline, asparagine, leucine, and tyrosine. Proline induces rigidity, whereas the others enable hydrophobic and hydrogen bonding. The COL419 and COL-AA peptides identified in this study exhibited significant binding specificity toward colon cancer cells. This further corroborates the efficacy of phage display technology as a means of isolating tumor-specific peptides. Related studies have demonstrated the isolation of peptides directed against different cancer antigens through phage display libraries (23, 24). These findings underscore the potential of small peptides in cancer targeting and drug delivery applications.

Overall, both experimentally selected and theoretically designed peptides successfully differentiated colorectal cancer cells from healthy cells. Further optimization of the peptide sequences could potentially achieve subtype-specific recognition between colon and rectal cancers.

CONCLUSION

The subtraction biopanning strategy employed in this study successfully enriched positive phage clones that specifically bind to HCT-116 cells. Through a series of rounds of biopanning and selective amplification, five phage clones were identified as best binders. Further analysis of their amino acid composition and binding specificity revealed the presence of specific amino acids and their selective expression in binding peptides called experimentally selected COL419 and theoretically designed COL-AA peptides. The synthesized peptides exhibited targeted binding to HCT-116 cells in immunofluorescence assays. Both the COL419 and COL-AA peptides can differentiate colon and rectal cancer cells from healthy cells. The COL-AA peptide can differentiate colon cancer cells from both rectal cancer cells and normal healthy colorectal cells. These findings contribute to our understanding of peptide-target interactions and provide potential avenues for developing targeted approaches for colon cancer research and therapy. The COL419 and COL-AA peptides identified in this study have considerable potential for future applications in cancer targeting and drug delivery systems. These peptides can be employed to facilitate targeted delivery of therapeutic agents to tumor sites owing to their cancer cell-specific binding ability. The identified peptide sequences can be further optimized and used as targeting ligands in drug delivery systems or diagnostic agents specifically designed for HCT-116 colon cancer cells. By targeting these specific cells, it may be possible to enhance the efficacy and reduce the off-target effects of therapeutic interventions.

Ethics Committee Approval: Ethics committee approval is not required due to the use of commercial cell lines.

Peer-review: Externally peer-reviewed.

Author Contributions: Conception/Design of Study – D.S., Z.K., B.E., B.A., Y.H.; Data Acquisition – D.S., Z.K., B.E., B.A., Y.H., E.S.; Data Analysis/Interpretation - D.S., Z.K., B.E., B.A., Y.H.; Drafting Manuscript – D.S., Z.K., B.E., B.A., Y.H., E.S.; Critical Revision of Manuscript – D.S., Z.K.; Final Approval and Accountability – D.S., Z.K., B.E., B.A., Y.H., E.S.

Conflict of Interest: The authors declare no conflict of interest.

Financial Disclosure: This work was supported by Scientific Research Projects (BAP) Coordination Unit of Istanbul Technical University (Project number, TGA-2017-40974).

REFERENCES

1. Sung H, Ferlay J, Siegel RL, Laversanne M, Soerjomataram I, Jemal A, et al. Global cancer statistics 2020: GLOBOCAN estimates of incidence and mortality worldwide for 36 cancers in 185 countries. *CA Cancer J Clin* 2021; 71: 209-49.
2. Paschke S, Jafarov S, Staib L, Kreuser ED, Maulbecker-Armstrong C, Roitman M, et al. Are colon and rectal cancer two different tumor entities? A proposal to abandon the term colorectal cancer. *Int J Mol Sci* 2018; 19(9): 2577.
3. Dmitrieva MD, Voitova AA, Dymova MA, Richter VA, Kuligina EV. Tumor-targeting peptides search strategy for the delivery of therapeutic and diagnostic molecules to tumor cells. *Int J Mol Sci* 2020; 22(1): 314.
4. Raucher D. Tumor targeting peptides: novel therapeutic strategies in glioblastoma. *Curr Opin Pharmacol* 2019; 47: 14-19.
5. Liu R, Li X, Xiao W, Lam KS. Tumor-targeting peptides from combinatorial libraries. *Adv Drug Deliv Rev* 2017; 110: 13-37.
6. Kehoe JW, Kay BK. Filamentous phage display in the new millennium. *Chem rev* 2005; 105(11): 4056-72.
7. Zhang ZF, Shan X, Wang YX, Wang W, Feng SY, Cui YB. Screening and selection of peptides specific for esophageal cancer cells from a phage display peptide library. *J Cardiothorac Surg* 2014; 9: 1-7.
8. Lü X, Yao M, Zhang JM, Yang J, Lei YF, Huang XJ, Yin W. Identification of peptides that bind hepatitis C virus envelope protein E2 and inhibit viral cellular entry from a phage-display peptide library. *Int J Mol Med* 2014; 33(5): 1312-8.
9. Pérez-Martínez D, Infante YC, Ramírez BS, Rojas G. Domain-level epitope mapping of polyclonal antibodies against HER-1 and HER-2 receptors using phage display technology. *Sci Rep* 2022; 12(1): 12268.
10. Sahin D, Taflan SO, Yartas G, Ashktorab H, Smoot DT. Screening and identification of peptides specifically targeted to gastric cancer cells from a phage display peptide library. *APJCP* 2018; 19(4): 927.
11. Rojas G, Tundidor Y, Infante YC. High throughput functional epitope mapping: revisiting phage display platform to scan target antigen surface. *MAbs* 2014; 6(6): 1368-76.
12. Sun J, Zhang C, Liu G, Liu H, Zhou C, Lu Y, Li X. A novel mouse CD133 binding-peptide screened by phage display inhibits cancer cell motility in vitro. *Clin Exp Met* 2012; 29: 185-96.
13. Thundimadathil J. Cancer treatment using peptides: current therapies and future prospects. *J Amino Acids* 2012; 2012: 967347.

14. Zhang D, Huang J, Li W, Zhang Z, Zhu M, Feng Y, He S. Screening and identification of a CD44v6 specific peptide using improved phage display for gastric cancer targeting. *Ann Transl Med* 2020; 8: 21.
15. Panagides N, Zacchi LF, De Souza MJ, Morales RAV, Karnowski A, Liddament MT, et al. Evaluation of phage display biopanning strategies for the selection of anti-cell surface receptor antibodies. *Int J Mol Sci* 2022; 23(15): 8470.
16. Freund NT, Enshell-Seijffers D, Gershoni JM. Phage display selection, analysis, and prediction of B cell epitopes. *Curr Protoc Immunol* 2009; 86(1): 9-8.
17. Hou L, Zhu D, Liang Y, Tian X, Li L, Wang P, Meng X. Identification of a specific peptide binding to colon cancer cells from a phage-displayed peptide library. *Br J Cancer* 2018; 118(1): 79-87.
18. Kwak MH, Yi G, Yang SM, Choe Y, Choi S, Lee HS, Park JM. A dodecapeptide selected by phage display as a potential theranostic probe for colon cancers. *Transl Oncol* 2020; 13(9): 100798.
19. Kelly KA, Jones DA. Isolation of a colon tumor specific binding peptide using phage display selection. *Neoplasia* 2003; 5(5): 437-44.
20. Ferreira D, Silva AP, Nobrega FL, Martins IM, Barbosa-Matos C, Granja S, et al. Rational identification of a colorectal cancer targeting peptide through phage display. *Sci Rep* 2019; 9(1): 3958.
21. Bakhshinejad B, Sadeghizadeh M. Identification of a novel colon adenocarcinoma cell targeting peptide using phage display library biopanning. *Biotechnol Appl Biochem* 2022; 69(6): 2753-65.
22. Zhang Y, Chen J, Zhang Y, Pan Y, Zhao J, Ren L, et al. A novel PEGylation of chitosan nanoparticles for gene delivery. *Biotechnol Appl Bioc* 2007; 46(4): 197-204.
23. Yu X, Yan J, Chen X, Wei J, Yu L, Liu F, et al. Identification of a peptide binding to cancer antigen Kita Kyushu lung cancer antigen 1 from a phage-display library. *Cancer Science* 2021; 112(10): 4335-45.
24. Bakhshinejad B, Sadeghizadeh M. Identification of a novel colon adenocarcinoma cell targeting peptide using phage display library biopanning. *Biotechnol Appl Biochem* 2022; 69(6): 2753-65.

Metabolomic Profiling and Biological Activities of Cell-Free Supernatants of *Bacillus* sp. Isolates: Antibacterial, Antibiofilm, and Anti-quorum Sensing Activities

Gamze Benli Yardimci^{1,2} , Ekrem Murat Gonulalan³ , Nurnehir Baltaci Bozkurt¹ , Emirhan Nemutlu⁴ , Engin Kocak⁵ , Mujde Eryilmaz^{2,6} 

¹Department of Pharmaceutical Microbiology, Faculty of Pharmacy, Afyonkarahisar Health Sciences University, Afyonkarahisar, Turkiye

²Department of Pharmaceutical Microbiology, Faculty of Pharmacy, Ankara University, Ankara, Turkiye

³Department of Pharmacognosy, Faculty of Pharmacy, Afyonkarahisar Health Sciences University, Afyonkarahisar, Turkiye

⁴Department of Analytical Chemistry, Faculty of Pharmacy, Hacettepe University, Ankara, Turkiye

⁵Department of Analytical Chemistry, Gulhane Faculty of Pharmacy, University of Health Sciences, Ankara, Turkiye

⁶Department of Pharmaceutical Microbiology, Faculty of Pharmacy, Acibadem Mehmet Ali Aydinlar University, Istanbul, Turkiye

ORCID ID: G.B.Y. 0000-0002-6469-8116; E.M.G. 0000-0002-8171-3824; N.B.B. 0000-0001-7054-8889; E.N. 0000-0002-7337-6215; E.K. 0000-0002-1076-1300; M.E. 0000-0003-3760-1996

Cite this article as: Benli Yardimci G, Gonulalan EM, Baltaci Bozkurt N, Nemutlu E, Kocak E, Eryilmaz M. Metabolomic profiling and biological activities of cell-free supernatants of *Bacillus* sp. Isolates: antibacterial, antibiofilm, and anti-quorum sensing activities. *Experimed* 2024; 14(3): 183-193.

ABSTRACT

Objective: The objective of this research was to explore the antibacterial, antibiofilm, and anti-quorum sensing (anti-QS) activities of cell-free supernatants (CFSs) of *Bacillus* sp. and correlate these activities with their metabolite profiles.

Materials and Methods: We used 55 *Bacillus* sp. isolates from soil samples. The antibacterial activities of the CFSs were investigated using disk diffusion and agar well diffusion methods. Antibiofilm activities were assessed using the crystal violet microplate method and anti-QS activities were evaluated using the disc diffusion method. The identification of biologically active isolates was performed using matrix-assisted laser desorption ionization–time of flight mass spectrometry (MALDI-TOF-MS). The metabolite profiles of active CFSs were analyzed using gas chromatography-mass spectrometry (GC-MS).

Results: Only S-45 exhibited antibacterial activity against *Staphylococcus aureus* ATCC 25923. Biofilm inhibition percentages of the CFSs against *Staphylococcus epidermidis* ATCC 35984 and *Pseudomonas aeruginosa* PAO1 varied between 92.58% - 3.96% and 78.96% - 0.64%, respectively. Only S-37 exhibited anti-QS activity. The most biologically active isolates belonged to the *Bacillus cereus* group. Based on the GC-MS results, 102 metabolites were identified. According to correlation analyses between the results of antibiofilm activity and metabolite profiles, we determined that compounds belonging to the amino acid and peptide groups, hydroxy acids and derivatives, and fatty acyls exhibited a highly positive correlation. The metabolite profiles of S-45 and S-37 were not significantly different from the negative control (S-46). Therefore, these activities could not be associated with the metabolite content.

Conclusion: The correlation between specific metabolite profiles and bioactivities indicates the potential of these bioactivities for innovative pharmaceutical applications. Future research should focus on isolating and testing these individual metabolites to confirm their specific roles and mechanisms.

Keywords: Antibacterial activity, antibiofilm activity, anti-quorum sensing activity, *Bacillus* sp., GC-MS, metabolomics

Corresponding Author: Mujde Eryilmaz **E-mail:** mujdeyuce@gmail.com

Submitted: 08.07.2024 **Revision Requested:** 26.09.2024 **Last Revision Received:** 23.10.2024 **Accepted:** 25.10.2024 **Published Online:** 04.12.2024



Content of this journal is licensed under a Creative Commons Attribution-NonCommercial 4.0 International License.

INTRODUCTION

Antibiotic resistance is considered one of the most critical threats to humanity's future (1). Bacterial infections caused by resistant strains lead to prolonged hospitalization, increased healthcare costs, treatment failures, and mortality (2, 3). Safe and effective novel compounds that can act through different mechanisms are needed to fight antibiotic resistance (4).

The inadequacy of existing antibacterials for treating resistant bacterial infections and the inability to discover new antibacterials have directed researchers to investigate molecules that can inhibit the mechanisms associated with pathogenicity (5). Bacteria communicate with each other to synthesize virulence factors that contribute to their pathogenicity. This communication mechanism, achieved through extracellular chemical signaling molecules, is referred to as quorum sensing (QS). Bacterial processes such as bioluminescence, conjugation, biofilm production, and sporulation are known to be regulated by the QS mechanism (6). A biofilm is a collection of microbial cells attached to a surface and surrounded by extracellular polymeric substances. Biofilm formation is a mechanism by which bacteria maintain their viability (7).

Plants, bacteria, marine organisms, terrestrial vertebrates, and invertebrates are sources of active natural compounds that can be used in medicine (8). Metabolites produced by many microorganisms in different natural habitats are widely used in fields such as medicine, pharmacy, agriculture, and biotechnology (9). Soil is an environment that exhibits a diversity of organic and inorganic matter. Soil properties and environmental conditions influence the composition of microorganisms and their metabolite content (10,11). The genus *Bacillus* is a predominant group of bacteria in soil microflora (12). The members of the genus *Bacillus* are industrially important due to their easy production, resistance to adverse environmental conditions, and metabolic properties such as antibiotic, enzyme, organic acid, pigment, and toxin production. Bacitracin, subtilin, ricin, mersacidin, amicoumacin, subtilosin produced by *Bacillus subtilis* (*B. subtilis*), polymyxin produced by *paenibacillus polymyxa*, pumilio pumilin produced by *B. pumilus*, and iturins produced by *B. subtilis* and *B. amyloliquefaciens* can be given as examples of antibiotics. However, subtilisin produced by *B. subtilis* and amylase produced by *B. amyloliquefaciens* are examples of enzymes. Surfactin, fengycin, and iturin from *B. subtilis* are examples of surfactants, antifungals, and antivirals, respectively (10,13-15). Metabolites produced by *Bacillus* species, such as surfactants, alpha-amylase, and bacteriocin, have been shown to exhibit antibiofilm effects by disrupting and inhibiting the formation of bacterial biofilms (16). Metabolites from *Bacillus* species, such as lactonase enzyme and fengycin, have been shown to exhibit anti-QS effects by interfering with bacterial QS systems (17-19).

The purpose of this study was to investigate the antibacterial, antibiofilm, and anti-QS activities of *Bacillus* sp. cell-free supernatants (CFSs) and correlated these activities with their metabolite profiles. The findings of this study are significant because the antibacterial, antibiofilm, and anti-QS activities exhibited by the metabolites produced by *Bacillus* sp. suggest promising alternatives for combating antibiotic-resistant bacterial infections. Furthermore, the correlation between specific metabolite profiles and their bioactivities indicates considerable potential for innovative pharmaceutical applications.

MATERIALS AND METHODS

Isolation and Cultivation of Bacterial Strains

In this study, 74 soil samples were collected from various regions of Ankara, Afyonkarahisar, and Istanbul. In order to characterize the soil samples used in this study, detailed information regarding the regions from which the samples were collected, including their specific properties, is provided in Table 1. Each soil sample (approximately 10 gr in weight) was collected using clean, dry, and sterile amber-colored glass bottles, along with a sterile spatula. To prepare the samples for isolation, 1 gr of each soil sample was mixed with 10 mL of sterile distilled water. The suspension was then heated to 100°C and maintained at 100°C for 5 min to eliminate vegetative cells. Serial dilutions (10^{-1} to 10^{-4}) were prepared from the samples, and 0.1 mL of each dilution was spread onto Nutrient Agar (NA) (Merck, Germany) plates. The plates were incubated at 37°C for 18-24 h. Following incubation, the selected colonies were stained using Gram staining. Gram-positive and rod-shaped bacilli were selected for further identification tests, which included assessments of spore-forming capability, motility, and catalase activity (20).

Identification of Bacterial Species

The identification of biologically active isolates was performed using matrix-assisted laser desorption ionization–time of flight mass spectrometry (MALDI-TOF-MS) (Bio Mérieux, France). Bacterial cultures were incubated on blood agar plates at 37°C for 24 h. A single bacterial colony was picked using a 1 µL sterile loop and applied to a metal target plate. Subsequently, 1 µL of matrix solution (α -cyano-4-hydroxycinnamic acid; CHCA) was added to the sample on the target plate. The prepared target plate was then loaded into the device for analysis. The spectral data obtained from the MALDI-TOF-MS were compared against the reference library to identify the bacterial isolates (21).

Obtaining Cell-Free Supernatants

To obtain the CFSs from the *Bacillus* sp. isolates, cultures from 24 h NA plates were inoculated into Luria Bertani Broth (LBB) (Merck, Germany) and incubated at 37°C for 72 h. To eliminate the bacterial cells from the medium, the incubated samples were centrifuged at 12.000 g for 10 min at 4°C. Next, the supernatants were filtered through a 0.45-µm pore filter (20).

Table 1. Regions where soil samples were collected and their properties

Soil Sample	Region	Collection Date	Soil Sample	Region	Collection Date	Soil Sample	Region	Collection Date
S-1	<i>Platanus orientalis</i> tree, Ankara	March 2021	S-20	Rocky ground, Ankara	May 2021	S-39	<i>Pinus sp.</i> tree, Ankara	August 2021
S-2	Next to the manhole cover, Ankara	March 2021	S-21	İmrahor Valley, Ankara	May 2021	S-40	<i>Pinus sp.</i> tree, Ankara	August 2021
S-3	Next to the pool drain, Ankara	March 2021	S-22	İmrahor Valley, Ankara	May 2021	S-41	<i>Pinus sp.</i> tree, Ankara	August 2021
S-4	<i>Aesculus hippocastanum</i> tree, Ankara	March 2021	S-23	<i>Salix alba</i> L. Ankara	May 2021	S-42	Potted, Ankara	September 2021
S-5	Next to the manhole cover, Ankara	March 2021	S-24	<i>Salix alba</i> L. Ankara	May 2021	S-43	Potted, Ankara	September 2021
S-6	Thermal water, Afyonkarahisar	April 2021	S-25	<i>Pinus pinea</i> tree, Ankara	July 2021	S-44	Shrub soil, Ankara	September 2021
S-7	Garden soil, Afyonkarahisar	April 2021	S-26	<i>Eymir Lake</i> , Ankara	July 2021	S-45	Near the water canal, İstanbul	August 2021
S-8	Cemetery garden, Afyonkarahisar	April 2021	S-27	<i>Eymir Lake</i> , Ankara	July 2021	S-46	Garden soil, Ankara	September 2021
S-9	Garden soil, Afyonkarahisar	April 2021	S-28	<i>Eymir Lake</i> , Ankara	July 2021	S-47	<i>Pinus sp.</i> tree, Ankara	September 2021
S-10	<i>Fraxinus excelsior</i> tree, Afyonkarahisar	April 2021	S-29	<i>Eymir Lake</i> , Ankara	July 2021	S-48	Shrub soil, Ankara	September 2021
S-11	<i>Rose sp.</i> , Ankara	April 2021	S-30	<i>Eymir Lake</i> , Ankara	July 2021	S-49	Potted plant, Ankara	September 2021
S-12	<i>Rose sp.</i> , Ankara	April 2021	S-31	<i>Eymir Lake</i> , Ankara	July 2021	S-50	Garden soil, Ankara	September 2021
S-13	<i>Pinus pinea</i> tree, Ankara	April 2021	S-32	Shrub soil, Ankara	July 2021	S-51	Riverbed, Ankara	September 2021
S-14	<i>Pinus pinea</i> tree, Ankara	April 2021	S-33	Shrub soil, Ankara	July 2021	S-52	Riverbed, Ankara	September 2021
S-15	<i>Pinus pinea</i> tree, Ankara	April 2021	S-34	Shrub soil, Ankara	August 2021	S-53	Riverbed, Ankara	September 2021
S-16	<i>Pinus pinea</i> tree, Ankara	April 2021	S-35	Landscape plants, Ankara	August 2021	S-54	Riverbed, Ankara	September 2021
S-17	Potted Ankara	April 2021	S-36	<i>Pinus pinea</i> tree, Ankara	August 2021	S-55	Landscape plants, Ankara	September 2021
S-18	Potted Ankara	April 2021	S-37	Garden soil, Ankara	August 2021			
S-19	Potted Ankara	April 2021	S-38	<i>Prunus cerasifera</i> tree, Ankara	August 2021			

Table 2. The bacteria identified by MALDI-TOF-MS

Observed Activity	Isolate	MALDI-TOF-MS
Antibacterial activity	45	<i>B. cereus</i>
	37	<i>B. cereus</i>
Antibiofilm activity	21	<i>B. cereus</i>
	14	<i>B. cereus</i>
	16	<i>B. cereus</i>
	17	<i>B. altitudinis/pumilus</i>
	23	<i>B. subtilis/amyloliquefaciens/vallismortis</i>
	22	<i>B. altitudinis/pumilus</i>
	15	<i>Priestia megaterium (B. megaterium)</i>
	18	<i>Peribacillus simplex (B. simplex)</i>
	19	<i>B. cereus</i>
	24	<i>B. cereus</i>
	12	<i>B. cereus</i>
	20	<i>Peribacillus simplex (B. simplex)</i>
	25	<i>B. cereus</i>
	43	<i>Peribacillus simplex (B. simplex)</i>
	36	<i>B. subtilis/amyloliquefaciens/vallismortis</i>
34	<i>B. cereus</i>	

Antibacterial Activity Tests

To assess the antibacterial activities of the CFSs, agar well diffusion and disk diffusion methods were used. The two techniques were used together to evaluate the antibacterial activity more comprehensively. The tested bacterial strains were *Klebsiella pneumoniae* ATCC 13883, *Acinetobacter baumannii* ATCC 1709, *Escherichia coli (E. coli)* ATCC 25922, *Pseudomonas aeruginosa (P. aeruginosa)* ATCC 27853, and *Staphylococcus aureus (S. aureus)* ATCC 25923.

Bacterial cultures grown for 18-24 h were adjusted to McFarland 0.5 and then spread onto Mueller-Hinton Agar (MHA) (Merck, Germany) plates. In the disk diffusion method, the CFSs were impregnated into sterile blank discs with a diameter of 6 mm (20 µL). After placing the impregnated disks on the inoculated media, the plates were incubated at 35 ± 1°C for 18-20 hours. Ciprofloxacin (5 µg) was used as the positive control, and Mueller-Hinton Broth (MHB) (Merck, Germany) was used as the

negative control (19, 22, 23). For the agar well diffusion method, four wells (6 mm diameter) were made in plates containing the media inoculated standard test bacteria. Subsequently, 20 µL of sterile MHA, cooled to 45°C, was added to the bottom of each well. Next, 50 µL of CFS was added to each well. Incubation of the plates was carried out at 35 ± 1°C for 18-20 h. After this period, the diameters of the inhibition zones were measured (23).

Antibiofilm Activity Test

The antibiofilm activities of the CFSs were investigated using the crystal violet microplate method with *P. aeruginosa* PAO1 and *S. epidermidis* ATCC 35984 as test bacteria (24, 25).

The test bacteria were cultivated in Brain Heart Infusion (BHI) broth (Merck, Germany). Following incubation, the inoculum was adjusted to 10⁶ cfu/mL with BHI broth supplemented with 2% sucrose. Subsequently, 100 µL of the bacterial suspension was added to each well of 96-well plates. The plates were incubated at 37°C for 24 h to allow biofilm formation. After the incubation period, the medium was removed, and non-adherent bacterial cells were washed away with sterile phosphate-buffered saline (PBS, pH 7.2).

Next, 100 µL of CFSs were added to the wells containing biofilms and incubated again at 37°C for 24 h. After incubation, the well contents were discarded, and the wells were rinsed with PBS. The plates were then allowed to dry at room temperature for an hour. Subsequently, 100 µL of a 0.5% crystal violet solution was transferred to each well to stain the biofilm cells. Following 30 min, the wells were washed using PBS. Next, the wells were treated with an acetone-alcohol (30:70, v/v) solution to dissolve the dye within the biofilm matrix. For the negative control, BHI broth containing 2% sucrose was used.

The optical density of the dissolved crystal violet at 620 nm (OD 620 nm) was measured using a microplate reader (Thermo Scientific Multiskan GO Microplate Spectrophotometer, Vantaa, Finland). The percentage of biofilm inhibition values was calculated using the following formula:

$$\text{Biofilm inhibition (\%)} = \frac{[(\text{OD (control)} - \text{OD (sample)}) / \text{OD (control)}] \times 100}$$

Anti-Quorum Sensing Activity

The anti-QS activities of the CFSs were assessed using the disc diffusion method with the reporter bacteria *Chromobacterium violaceum* ATCC 12472 (25, 26).

The test bacterium was cultured in LBB, and the density of the overnight bacterial suspension was adjusted to 1.5 × 10⁸ CFU/mL. After spreading the bacterial suspension onto Luria Bertani Agar (LBA) (Merck, Germany), sterile blank discs (Bioanalyse®, Ankara, Turkiye) (6 mm diameter) impregnated with 20 µL of the CFSs were placed. Following a 24-h incubation period at 30°C, the plates were examined for the presence of a violacein inhibition zone. The formation of an inhibition zone around the disks indicates potential anti-QS activity.

Table 3. GC/MS based metabolomic profiling (Major metabolites)

Super Class	Class /Subclass/ Parent	Number of Metabolites
Organic acids and derivatives	Amino acids, peptides, and analogs	32
	Hydroxy acids and derivatives	5
	Dicarboxylic acids and derivatives	4
Organic oxygen compounds	Carbohydrates and carbohydrate conjugates	22
Lipids and lipid-like molecules	Fatty acyls	4
	Glycerolipids	3
Benzeneoids	Benzene and substituted derivatives	1
	Phenols	1
Organoheterocyclic compounds	Indoles, and derivatives, diazines, dihydrofurans, lactones, pyridines and derivatives	10
Phenylpropanoids and polyketides	Cinnamic acids and derivatives, phenylpropanoic acids, coumarins and derivatives	4

GC-MS Metabolomics Analysis of CFSs

The metabolite profiles of the CFSs were analyzed using GC-MS-based metabolomics, as previously described (27). A GC-MS (Shimadzu GCMS-QP2010 Ultra) with a DB-5MS stationary phase column (30 m + 10 m DuraGuard × 0.25 mm i.d. and 0.25-µm film thickness) was used for metabolite analysis. The oven temperature program was set to 60°C for 1 min, increased to 325°C, at a 10 minute ramp and maintained for 10 min at 325°C. This resulted in a total separation time of 37.5 min. The MS detector was used in electron ionization mode (EI). Data acquisition was performed in full-scan mode. MS-DIAL software version 3.96 was used for peak detection, alignment, and deconvolution. In the pre-data process, a minimum peak height of 1000 amplitude was selected, and the other parameters were set to their default values. The identification cutoff value was set at 70%, and the retention time tolerance was 1 min. The Fiehn retention index database was used for metabolite identification.

Principal Component Analysis (PCA)

Principal component analysis (PCA) was used to condense multidimensional data into fewer dimensions while keeping the majority of the original data. In this study, PCA was used to visualize the distribution of the isolates based on metabolite variations. MetaboAnalyst was used to create the PCA score plots (28).

Correlation Analysis

Microsoft Excel was used for the correlation analysis. The correlation function was used to determine the relationship between two properties (amounts of metabolites and

activity results). The correlation coefficient reflects the level of correlation. As the correlation coefficient approaches +1 or -1, it indicates a positive (+1) or negative (-1) correlation between the properties. A positive correlation suggests that activity increases with increasing concentration. A coefficient closer to 0 denotes no or weak correlation.

RESULTS

Isolated/Identified *Bacillus* sp.

As a result of the identification tests, 55 *Bacillus* sp. were isolated from 74 diverse soil samples. The biological activity studies were conducted using the CFSs of these isolates. The identification of biologically active isolates was performed using MALDI-TOF-MS. The identified bacteria are listed in Table 2.

Antibacterial Activity of Cell-Free Supernatants

Based on the test results of 55 *Bacillus* sp. isolates, using the agar disk diffusion and agar well diffusion methods, only S-45 exhibited an inhibitory effect against *S. aureus* ATCC 25923 (Figure 1). None of the other CFSs used in this study demonstrated antibacterial activity against the test bacteria using either of the methods.

Antibiofilm Activity Test

The percentage of biofilm inhibition by CFSs against *S. epidermidis* ATCC 35984 varied between 92.58% and 3.96%. However, S-5, S-7, S-10, S-26, S-29, S-32, S-33, S-35, S-36, S-38, S-39, S-41, and S-46 did not exhibit any activity (Figure 2). For *P. aeruginosa* PAO1, the biofilm inhibition percentages of the CFSs varied between 78.96% and 0.64%. However, S-1, S-28, S-31, S-46, S-47, S-48, S-49, S-50, S-51, S-53, and S-54 showed no activity (Figure 3).

Table 4. Correlation analysis between the antibiofilm activity of *P. aeruginosa* PA01 and metabolite profiles ($r^2 \geq 0.70$ / $r^2 \leq -0.70$)

Correlation coefficient (r^2)	Metabolite name	Ontology
0.97	D-(+)-Malic acid	Beta hydroxy acids and derivatives
0.93	Homocystine	Alpha amino acids
0.87	Hexadecylglycerol	Monoalkylglycerols
0.84	N-Acetyl-L-Leucine	Leucine and derivatives
0.82	DOPA	Tyrosine and derivatives
0.79	Alanylalanine	Dipeptides
0.77	2-Deoxyguanosine	Purine 2'-deoxyribonucleosides
0.76	Glycolic acid	Alpha-hydroxy acids and derivatives
0.76	Putrescine	Monoalkylamines
0.76	Alanine-alanine	Dipeptides
0.76	n-Butylamine	Monoalkylamines
0.75	L-Ascorbic acid	Butenolides
0.75	Malonic acid	Dicarboxylic acids and derivatives
0.73	Saccharopine	Glutamic acid and derivatives
0.72	Thymine	Hydroxypyrimidines
0.70	N-Acetyl-L-aspartic acid	Aspartic acid and derivatives
-0.70	Nicotianamine	L-alpha-amino acids
-0.71	Spermidine	Dialkylamines
-0.72	Panose	Oligosaccharides
-0.77	Octacosanoic acid	Very long-chain fatty acids
-0.80	Lactitol	Fatty acyl glycosides of mono- and disaccharides
-0.81	Oxalic acid	Dicarboxylic acids and derivatives

Anti-Quorum Sensing Activity Test

A transparent inhibition zone around the disk indicates potential QS inhibitory activity. Among the samples, only S-37 showed a weak inhibition zone (Figure 4). In addition, none of the tested CFSs showed anti-QS activity.

GC-MS Metabolomics Analysis of CFSs

GC-MS metabolite profiling was performed to elucidate the compounds responsible for the observed activities of CFS numbers S-45 with antibacterial activity, S-37 with anti-QS activity, and S-16 and S-43 with high biofilm inhibition percentages. S-46, which showed no activity, was selected as the negative control in the study. In total, 102 primary and secondary metabolites were identified, and the class of the metabolites were summarized in Table 3.

The metabolite profiles of S-45 and S-37 did not differ significantly from the negative control. Therefore, these activities could not be associated with the metabolite contents of the samples.

Correlation Analysis

Correlation analyses were performed between CFSs with activity and metabolite profiles, and correlation coefficients (r^2) for each metabolite were calculated. As a result of the correlation analysis between the results of antibiofilm activity on *P. aeruginosa* PA01 and metabolite profiles, 16 metabolites exhibited a positive correlation ($r^2 \geq 0.70$), while 6 metabolites exhibited a negative correlation ($r^2 \leq -0.70$) (Table 4).

The correlation analysis between the results of antibiofilm activity on *S. epidermidis* ATCC 35984 and metabolite profiles showed that 9 metabolites have a positive correlation ($r^2 \geq$

Table 5. Correlation analysis between the antibiofilm activity of *S. epidermidis* ATCC 35984 and metabolite profiles ($r^2 \geq 0.70$ / $r^2 \leq -0.70$)

Correlation coefficient (r^2)	Metabolite name	Ontology
0.95	L-Asparagine	Asparagine and derivatives
0.85	L-Iditol	Sugar alcohols
0.85	N-Acetyl-DL-serine	N-acyl-L-alpha-amino acids
0.85	Urea	Non-metal pyrophosphates
0.83	L-Prolinamide	5-piperazinylimidazo[1,2-a]pyridines
0.78	N-Acetyl-L-Leucine	Leucine and derivatives
0.74	Glucose	Hexoses
0.74	Homocystine	Alpha amino acids
0.70	L-Norleucine	L-alpha-amino acids
-0.72	D-(+)-Mannose	Hexoses
-0.74	N-carbamoyl-L-aspartic acid	Aspartic acid and derivatives
-0.76	Hexose	Hexoses
-0.78	Oxalic acid	Dicarboxylic acids and derivatives
-0.90	Maltose	O-glycosyl compounds
-1.00	Spermine	Dialkylamines

0.70), while 6 metabolites have a negative correlation ($r^2 \leq -0.70$) (Table 5).

PCA

A 3D PCA graph showing the similarity of the metabolite contents of the CFSs to each other is given below (Figure 5).

As seen in the PCA graphs, S-46's metabolite content was significantly different from the others. S-46 did not show any effect in the activity assays performed within the scope of our study. The other CFSs had similar metabolite profiles and gave positive results in activity assays.

DISCUSSION

Chemical compounds derived from various bacterial groups can have biological effects on pathogenic microorganisms. The metabolite content of soil bacteria may vary depending on factors such as the content of organic and inorganic matter,

water ratio, and physical environmental conditions of soil samples (29).

Boottanun et al. reported that CFSs of *B. amyloliquefaciens* isolated from soil exhibited antibacterial effects against *S. aureus*, *Clostridium difficile*, *Enterococcus faecium*, *Burkholderia pseudomallei*, and *Acinetobacter baumannii* (20). Similarly, Thapa et al. investigated the antibacterial activity of secondary metabolites from various soil-derived *Bacillus* spp. using the agar well diffusion method against clinically significant pathogens, including *S. aureus*, *E. coli*, *Pseudomonas* spp., and *Salmonella* spp. (30). Their findings indicated that three out of the 24 isolates showed antibacterial properties against *S. aureus*, and three isolates (including one effective against *S. aureus*) were effective against *Salmonella* spp. Consistent with these findings, our study determined that the CFS from one isolate (S-45) exhibited a significant antibacterial effect against the Gram-positive bacterium *S. aureus* ATCC 25923.

QS is involved in the formation of various virulence factors of bacteria, including biofilm. It is considered a different strategy for the management of bacterial infections. El Aichar et al. investigated various biological activities of *Bacillus* strains isolated from soil and other ecological niches. The isolated *B. subtilis* DZ17 and *B. thuringiensis* DZ16 strains showed anti-QS and antibiofilm activities against *Streptococcus mutans* ATCC 25175 and *P. aeruginosa* PAO1 strains by inhibiting AI-2 and AHL signaling molecules (19). In a study conducted with the *C. violaceum* ATCC 12472 biosensor strain against *Serratia marcescens*, a causative agent of urinary tract infections, it was reported that *B. subtilis* R-18 extract showed anti-QS effect and inhibited bacterial adhesion in the early stages of biofilm formation (18). In our study, S-37 was found to inhibit the AHL bacterial communication molecule.

Nalini et al. investigated the antibiofilm activity of lipopeptide-producing *B. cereus* against the *E. coli* MTCC 2939 and *P. aeruginosa* MTCC 2453 strains. They reported biofilm inhibition rates of 56% and 62% for the lipopeptide-containing filtrates, respectively. In our study, using *P. aeruginosa* PAO1 as the test bacterium, the highest biofilm inhibition rate was observed for isolate S-43, achieving a value of 78.96% (31).

In our study, GC-MS analysis revealed that CFSs contain compounds from amino acid and peptides, cinnamic acids, alpha hydroxy acids, and dicarboxylic acids. Previous studies have shown that these compounds have antibacterial activity (32-35). In our study, we did not associate the observed antibacterial activity with the S-45 metabolite content. The obtained CFSs contain numerous primary and secondary metabolites. This difference in metabolite content suggests that the observed activities may not be attributed to a single compound alone. The combined effects of these synergistic or antagonistic metabolites may explain the observed activities (36, 37).

In a study conducted by Kachhadia et al., *B. cereus* RC1 extract was found to produce cyclic dipeptides such as cyclo (L-Leu-

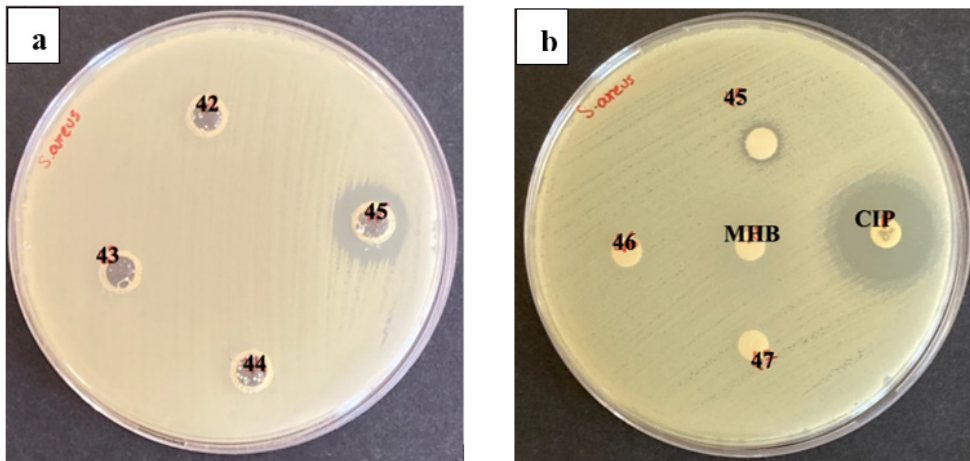


Figure 1. The test results of the S-45 using the (a) agar well diffusion method and (b) agar disk diffusion method (MHB: negative control, CIP: Ciprofloxacin-positive control).

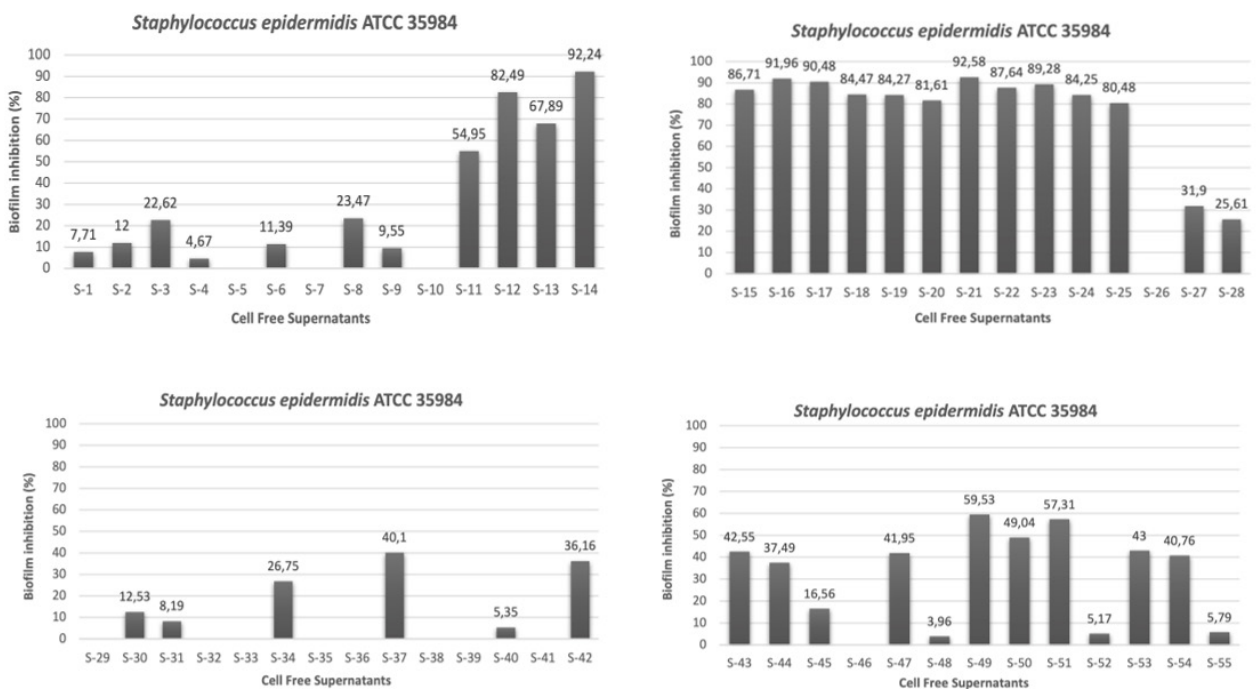


Figure 2. The biofilm inhibition percentages of the CFSs against *S. epidermidis* ATCC 35984.

L-Pro) and diketopiperazines, which are key metabolites responsible for anti-QS activity. These metabolites significantly inhibited quorum sensing and biofilm formation (38). In our study, only sample S-37 exhibited anti-QS activity. However, we could not associate the observed antibacterial activity with the metabolite content of S-37. The presence of similar metabolites in our samples further supports the potential of *Bacillus* sp. extracts to disrupt quorum sensing pathways and reduce bacterial virulence.

In another study, an antimicrobial peptide obtained from the *Bacillus* CBSMS07 strain was found to inhibit biofilm formation by reducing microbial cell density on the surface of *P. aeruginosa* and *E. coli* (39). Additionally, Moryl et al. reported that a filtrate from *B. subtilis* l'1a containing surfactin, iturin, and fengycin lipopeptides exhibited strong antibiofilm activity against urinary tract pathogens, possibly due to the synergistic effect of these compounds (40). In our study, we found that compounds belonging to amino acids and peptides, hydroxy acids and derivatives, and fatty acyls exhibited a high positive correlation with antibiofilm activity against *P. aeruginosa* PAO1

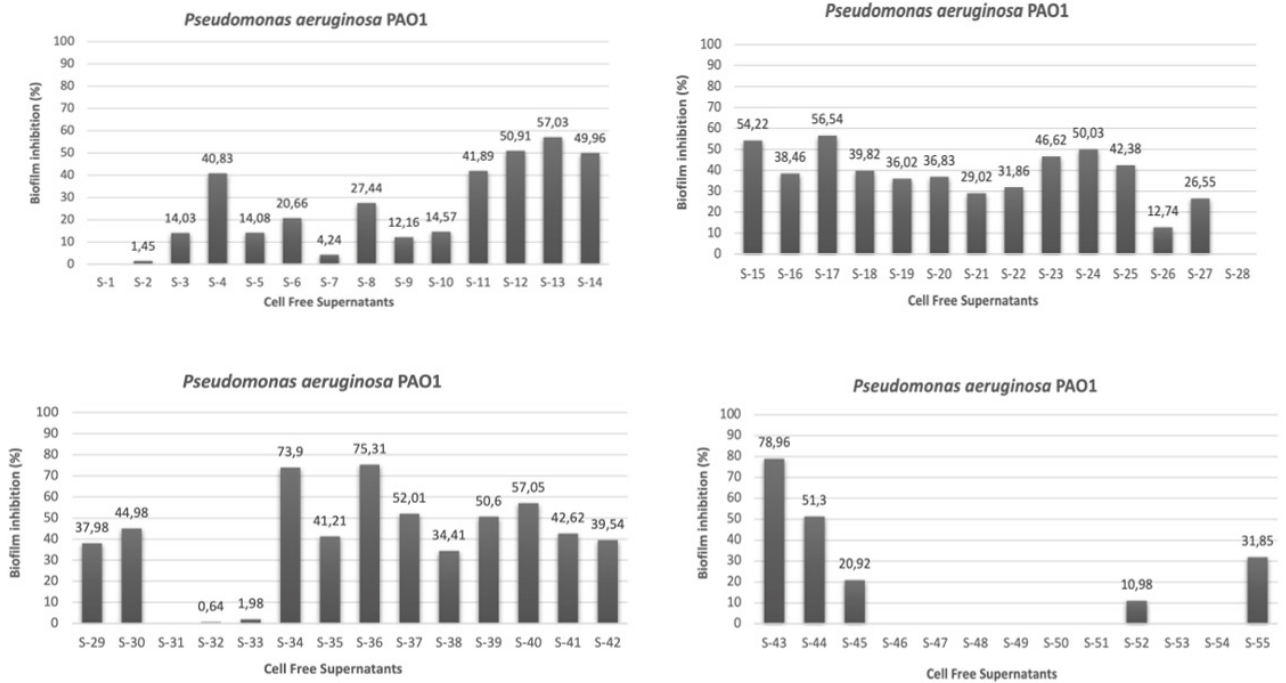


Figure 3. The biofilm inhibition percentages of the CFSs against *P. aeruginosa* PAO1.

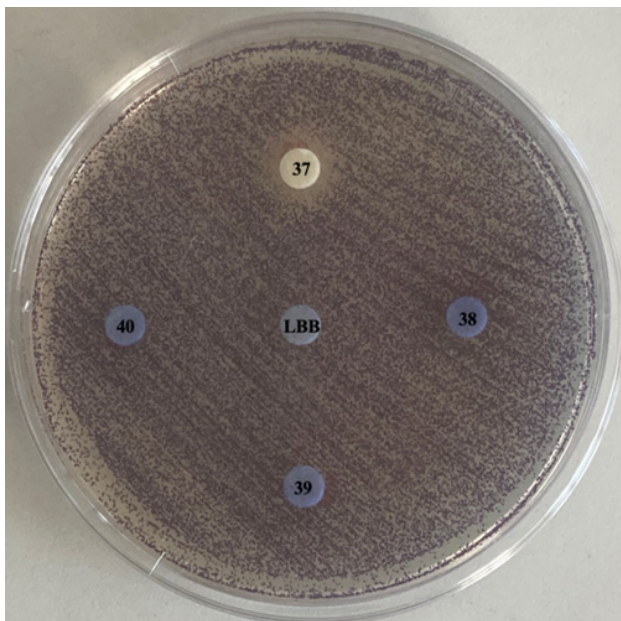


Figure 4. The anti-QS activity of S-37.

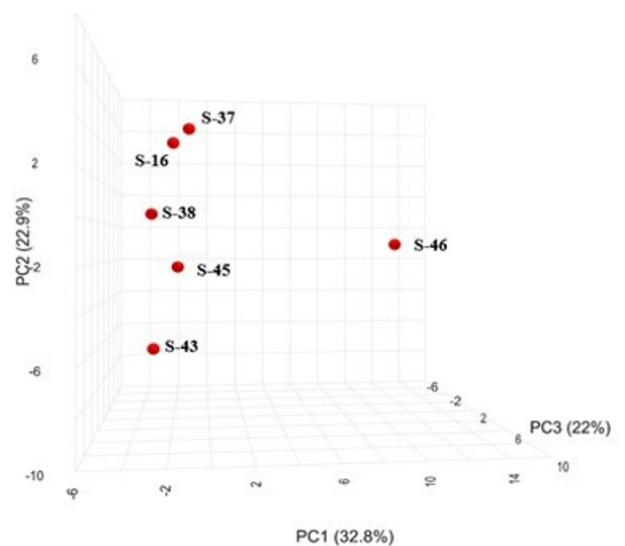


Figure 5. 3-D PCA graphs of S-16, S-37, S-38, S-43, S-45, S-46.

and *S. epidermidis* ATCC 35984. Malic acid, previously shown to have antibiofilm activity, also displayed a high positive correlation with antibiofilm activity in our study (41, 42). Additionally, amino acid-peptide group compounds with high positive correlation were identified in our correlation studies on *S. epidermidis* ATCC 35984, which is consistent with findings from other studies (43, 44).

In recent years, numerous peptides that exert strong inhibitory effects against microbial biofilms have been identified. This is significant because infections associated with biofilms are often not effectively eliminated by antibiotics alone (45). Cyclo (L-leucyl-L-propyl), a cyclic dipeptide, has been reported to dose-dependently inhibit the biofilm of *S. epidermidis* and *L. monocytogenes*, with an inhibition rate of more than 80% (46). Gowrishankar et al. showed that the same compound inhibited

the production of virulence factors such as exopolymer, biofilm, lipase, and protease at different levels against *S. marcescens* (46). Yu et al. showed that the active compound Cyclo (L-Tyr-L-Pro) reduced biofilm formation of *P. aeruginosa* PAO1 by 48% at 0.5 mg/mL and inhibited the QS system of *P. aeruginosa* (47).

Dostert et al. investigated the antibiofilm activity of amino acid-containing compounds and their combination with ciprofloxacin for synergistic activity. It was reported that amino acids can disperse mature biofilms and inhibit the biofilm formation of *S. aureus* (48). According to our findings, L-asparagine ($r^2=0.95$), N-acetyl-DL-serine ($r^2=0.85$), L-prolinamide ($r^2=0.83$), and N-acetyl-L-leucine ($r^2=0.78$) compounds in the amino acid group showed high correlation with *S. epidermidis* ATCC 35984. We also found that homocystine, a derivative of alpha amino acids, had a high positive correlation with *P. aeruginosa* PAO1 ($r^2=0.93$) and *S. epidermidis* ATCC 35984 ($r^2=0.74$).

In the study, which demonstrated the presence of various fatty acyl compounds through GC-MS analysis and their effects on the QS system (LasI), it was found that the extract obtained from *Streptomyces griseoincarnatus* HK 12 showed antibiofilm activity against *P. aeruginosa* and *S. aureus* with approximately 80% inhibition at 100 µg/mL (49). According to our correlation results, lactitol, a fatty acid group compound, showed a more negative correlation with antibiofilm activity. However, palmitic acid, as determined by GC-MS analysis showed positive correlation ($r^2=0.66$) against *S. epidermidis* ATCC 35984 strain.

The similarities between the isolates were based on metabolite variations determined using PCA graphs. Subsequently, we performed correlation analyses between the metabolite profiles of chosen CFSs, selected based on their activities, and the percentage of biofilm inhibition results obtained against *P. aeruginosa* PAO1 and *S. epidermidis* ATCC 35984. As a result of this correlation analysis, we identified metabolites that exhibited a strong positive correlation. These results underscore the potential of specific metabolites in *Bacillus* sp. extracts for combating biofilm-related infections and highlight the need for further research to isolate and test individual compounds.

CONCLUSION

Antibacterials are essential therapeutic agents for treating bacterial infections. The rising incidence of antibiotic resistance has accelerated the search for new agents with different mechanisms of action that can be safely and effectively used in treatment. *Bacillus* species are known to produce various compounds with biological activities. In our study, we investigated the antibacterial, antibiofilm, and anti-QS activities of CFSs obtained from soil bacteria and identified metabolites potentially responsible for these activities. Our correlation studies revealed *Bacillus* sp. metabolites that were positively correlated with antibiofilm activity. The results of this study are expected to lead to the discovery of promising new therapeutics.

Ethics Committee Approval: Only cell culture material was used in this study and no living material that would require ethics committee approval was used.

Peer-review: Externally peer-reviewed.

Author Contributions: Conception/Design of Study – G.B.Y., E.M.G., N.B.B., E.N., E.K., M.E.; Data Acquisition – G.B.Y., M.E., N.B.B.; Data Analysis/Interpretation – G.B.Y., E.M.G., E.N., E.K., M.E.; Drafting Manuscript – G.B.Y., E.M.G., E.N., E.K., M.E.; Critical Revision of Manuscript – G.B.Y., E.M.G., N.B.B., E.N., E.K., M.E.; Final Approval and Accountability – G.B.Y., E.M.G., N.B.B., E.N., E.K., M.E.

Conflict of Interest: The authors declare no conflict of interest.

Financial Disclosure: No funding was received to conduct this study.

REFERENCES

1. Peschel A, Sahl HG. The co-evolution of host cationic antimicrobial peptides and microbial resistance. *Nat Rev Microbiol* 2006; 4(7): 529-36.
2. Dadgostar P. Antimicrobial resistance: implications and costs. *Infect Drug Resist* 2019; 12: 3903-10.
3. Varela MF, Stephen J, Lekshmi M, Ojha M, Wenzel N, Sanford LM, et al. Bacterial resistance to antimicrobial agents. *Antibiotics* 2021; 10(5): 593.
4. Cheng G, Dai M, Ahmed S, Hao H, Wang X, Yuan Z. Antimicrobial drugs in fighting against antimicrobial resistance. *Front Microbiol* 2016; 7: 470.
5. Cicek Polat D, Gümüşok S, Rızvanoglu SS, Eryılmaz M. Bioactivities of *Cotinus coggygria* and its HPLC-DAD phenolic profiles. *Plant Biosyst* 2023; 157(5): 1061-66.
6. Tobias NJ, Brehm J, Kresovic D, Brameyer S, Bode HB, Heermann R. New vocabulary for bacterial communication. *ChemBioChem* 2020; 21(6): 759-68.
7. Sauer K, Stoodley P, Goeres DM, Hall-Stoodley L, Burmølle M, Stewart PS, et al. The biofilm life cycle: Expanding the conceptual model of biofilm formation. *Nat Rev Microbiol* 2022; 20(10): 608-20.
8. Amedei A, M D'Elios M. New therapeutic approaches by using microorganism-derived compounds. *Curr Med Chem* 2012; 19(22): 3822-40.
9. Chevrette MG, Handelsman J. Needles in haystacks: reevaluating old paradigms for the discovery of bacterial secondary metabolites. *Nat Prod Rep* 2021; 38(11): 2083-99.
10. Sansinenea E, Ortiz A. Secondary metabolites of soil *Bacillus* spp. *Biotechnol Lett* 2011; 33(8): 1523-38.
11. Wagg C, Bender SF, Widmer F, Van Der Heijden MG. Soil biodiversity and soil community composition determine ecosystem multifunctionality. *P Natl A Sci* 2014; 111(14): 5266-70.
12. Singh P, Sharma R, Shukla A K, Singh R. Isolation of *Bacillus* spp. from soil for antimicrobial production and antibiotic resistance. *Adv Biotech & Micro* 2018; 8(4): 1-5.
13. Johnvesly B, Manjunath BR, Naik GR. Pigeon pea waste as a novel, inexpensive, substrate for production of a thermostable alkaline protease from thermoalkalophilic *Bacillus* sp. JB-99. *Bioresource Technol* 2002; 82(1): 61-4.

14. Baruzzi F, Quintieri L, Morea M, Caputo L. Antimicrobial compounds produced by *Bacillus* spp. and applications in food. *Formatex* 2011; 2(1): 1102-11.
15. Wang T, Liang Y, Wu M, Chen Z, Lin J, Yang L. Natural products from *Bacillus subtilis* with antimicrobial properties. *Chinese J Chem Eng* 2015; 23(4): 744-54.
16. Ali SAM, Sayyed RZ, Mir MI, Khan MY, Hameeda B, Alkhanani MF, et al. Induction of systemic resistance in maize and antibiofilm activity of surfactin from *Bacillus velezensis* MS20. *Front Microbiol* 2022; 13: 879739.
17. Dong YH, Gusti AR, Zhang Q, Xu JL, Zhang LH. Identification of quorum-quenching N-acyl homoserine lactonases from *Bacillus* species. *Appl Environ Microb* 2002; 68(4): 1754-9.
18. Devi KR, Srinivasan S, Ravi AV. Inhibition of quorum sensing-mediated virulence in *Serratia marcescens* by *Bacillus subtilis* R-18. *Microb Pathogenesis* 2018; 120: 166-75.
19. El Aichar F, Muras A, Parga A, Otero A, Nateche F. Quorum quenching and anti-biofilm activities of halotolerant *Bacillus* strains isolated in different environments in Algeria. *J Appl Microbiol* 2022; 132(3): 1825-39.
20. Boottanun P, Potisap C, Hurdle JG, Sermswan RW. Secondary metabolites from *Bacillus amyloliquefaciens* isolated from soil can kill *Burkholderia pseudomallei*. *AMB Express* 2017; 7(1): 1-11.
21. Lay Jr JO. MALDI-TOF mass spectrometry of bacteria. *Mass Spectrom Rev* 2001; 20(4): 172-94.
22. Matuschek E, Brown DF, Kahlmeter G. Development of the EUCAST disk diffusion antimicrobial susceptibility testing method and its implementation in routine microbiology laboratories. *Clin Microbiol Infect* 2014; 20(4): O255-66.
23. Eryilmaz M, Gurpinar SS, Palabiyik IM, Guriz H, Gerceker D. Molecular identification and antimicrobial activity of vaginal *Lactobacillus* sp.. *Curr Pharm Biotechnol* 2018; 19(15): 1241-7.
24. Eryilmaz M, Kart D, Gurpinar SS. Investigation of antibiofilm activities of *Lactobacillus* sp. metabolites isolated from vaginal flora. *Turk Mikrobiol Cem Derg* 2019; 49(3): 169-74.
25. Junejo B, Eryilmaz M, Rizvanoglu SS, Palabiyik IM, Ghumro T, Mallah A, et al. Pharmacological assessment of Co₃O₄, CuO, NiO and ZnO nanoparticles via antibacterial, anti-biofilm and anti-quorum sensing activities. *Water Sci Technol* 2023; 87(11): 2840-51.
26. Gajdacs M, Spengler G. Standard operating procedure (SOP) for disk diffusion-based quorum sensing inhibition assays. *APH* 2019; 89(4): 117-125.
27. Nemutlu E, Zhang S, Xu YZ, Terzic A, Zhong L, Dzeja PD, et al. Cardiac resynchronization therapy induces adaptive metabolic transitions in the metabolomic profile of heart failure. *J Card Fail* 2015; 21(6): 460-9.
28. Pang Z, Zhou G, Ewald J, Chang L, Hacariz O, Basu N, et al. Using MetaboAnalyst 5.0 for LC-HRMS spectra processing, multi-omics integration and covariate adjustment of global metabolomics data. *Nature Protocols* 2022; 17: 1735-61.
29. Nithya C, Begum MF, Pandian SK. Marine bacterial isolates inhibit biofilm formation and disrupt mature biofilms of *Pseudomonas aeruginosa* PAO1. *Appl Microbiol Biot* 2010; 88(1): 341-58.
30. Thapa A, Budhathoki A, Sapkota A, Sainju M, Shrestha P, Pant SP. Isolation, identification and screening of *Bacillus* species with antimicrobial activity from different soil samples of Kathmandu Valley. *Nepal J Biotechnol* 2021; 9(2): 1-6.
31. Nalini S, Parthasarathi R, Prabudoss V. Production and characterization of lipopeptide from *Bacillus cereus* SNAU01 under solid state fermentation and its potential application as anti-biofilm agent. *Biocatal Agric Biotechnol* 2016; 5:123-32.
32. Hilpert K, Volkmer-Engert R, Walter T, Hancock RE. High-throughput generation of small antibacterial peptides with improved activity. *Nat Biotechnol* 2005; 23(8):1008-12.
33. Sova M. Antioxidant and antimicrobial activities of cinnamic acid derivatives. *Mini Rev Med Chem* 2012; 12(8): 749-67.
34. Falardeau J, Wise C, Novitsky L, Avis TJ. Ecological and mechanistic insights into the direct and indirect antimicrobial properties of *Bacillus subtilis* lipopeptides on plant pathogens. *J Chem Ecol* 2013; 39(7): 869-78.
35. Siebert A, Wysocka M, Krawczyk B, Cholewiński G, Rachoń J. Synthesis and antimicrobial activity of amino acid and peptide derivatives of mycophenolic acid. *Eur J Med Chem* 2018; 143: 646-55.
36. Demirezer LO, Gonulalan EM, Nemutlu E. Fitoterapide metabolomiks (fitomiks) çalışmaları ve önemi. Ankara: Türkiye Klinikleri Yayınevi. 2022. p. 68-74.
37. Waris M, Kocak E, Gonulalan EM, Demirezer LÖ, Kır S, Nemutlu E. Metabolomics analysis insight into medicinal plant science. *Trac-Trend Anal Chem* 2022; 157: 116795.
38. Kachhadia R, Kapadia C, Singh S, Gandhi K, Jajda H, Alfarraj S, et al. Quorum Sensing Inhibitory and Quenching Activity of *Bacillus cereus* RC1 Extracts on Soft Rot-Causing Bacteria *Lelliottia amnigena*. *ACS Omega* 2022; 7(29): 25291-308.
39. Khan MM, Kim YK, Cho SS, Jin YY, Suh JW, Lee DY, et al. Response surface optimization of culture conditions for cyclic lipopeptide MS07 from *Bacillus siamensis* reveals diverse insights targeting antimicrobial and antibiofilm activity. *Processes* 2020; 8(6): 744.
40. Moryl M, Spętana M, Dziubek K, Paraszkiwicz K, Różalska S, Plaza G, et al. Antimicrobial, antiadhesive and antibiofilm potential of lipopeptides synthesised by *Bacillus subtilis*, on uropathogenic bacteria. *ABP* 2015; 62(4): 725-32.
41. Singh N, Goel G, Raghav M. Prevalence and characterization of *Cronobacter* spp. from various foods, medicinal plants, and environmental samples. *Curr Microbiol* 2015; 71:31-8.
42. Akbas MY, Cag S. Use of organic acids for prevention and removal of *Bacillus subtilis* biofilms on food contact surfaces. *Food Sci Technol Int* 2016; 22(7): 587-97.
43. Laverty G, McCloskey AP, Gorman SP, Gilmore BF. Anti-biofilm activity of ultrashort cinnamic acid peptide derivatives against medical device-related pathogens. *J Pept Sci* 2015; 21(10): 770-8.
44. Pletzer D, Hancock RE. Antibiofilm peptides: potential as broad-spectrum agents. *J Bacteriol* 2016; 198(19): 2572-8.
45. Wu H, Moser C, Wang HZ, Høiby N, Song ZJ. Strategies for combating bacterial biofilm infections. *Int J Oral Sci* 2015; 7(1): 1-7.
46. Gowrishankar S, Sivaranjani M, Kamaladevi A, Ravi AV, Balamurugan K, Karutha Pandian S. Cyclic dipeptide cyclo (l-leucyl-l-prolyl) from marine *Bacillus amyloliquefaciens* mitigates biofilm formation and virulence in *Listeria monocytogenes*. *FEMS Pathog Dis* 2016; 74(4): ftw017.
47. Yu X, Li L, Sun S, Chang A, Dai X, Li H, et al. A cyclic dipeptide from marine fungus *Penicillium chrysogenum* DXY-1 exhibits anti-quorum sensing activity. *ACS Omega* 2021; 6(11): 7693-700.
48. Dostert M, Belanger CR, Hancock RE. Design and assessment of anti-biofilm peptides: steps toward clinical application. *J Innate Immun* 2019; 11(3): 193-204.
49. Kamarudheen N, Rao KB. Fatty acyl compounds from marine *Streptomyces griseoincarnatus* strain HK12 against two major biofilm forming nosocomial pathogens; an in vitro and in silico approach. *Microb Pathog* 2019; 127: 121-30.

Development of Natural Castile Soaps from Vegetable Oils

Gokhan Ozokan¹, Abdulkerim Bilginer¹

¹BioArge Laboratories, Yıldız Technical University Technocity, İkitelli, İstanbul, Türkiye

ORCID ID: G.O. 0000-0003-1140-1996; A.B. 0000-0002-7129-2149

Cite this article as: Ozokan G, Bilginer A. Development of natural castile soaps from vegetable oils. *Experimed* 2024; 14(3): 194-202.

ABSTRACT

Objective: Castile soaps are believed to be natural, 100% biodegradable, non-toxic surfactants and in some cases, they have antimicrobial properties. As raw materials, they are used extensively in the cosmetic industry for personal and home care products. Natural castile soap bases are generally produced in super fat stoichiometry to protect skin from caustic damage. The super fat method optimizes the total amount of caustic required for the saponification of natural vegetable oils and keeps these oils at the maximum level in the final product. The aim of this study was to develop natural soap based raw materials and castile soaps from various vegetable oils such as olive oil, coconut oil, castor oil, almond oil and jojoba oil.

Materials and Methods: Castile soaps were produced using the super fat method by measuring the saponification values of the vegetable oils. Viscosity, pH, appearance, and microbiological tests were performed to determine their shelf life.

Results: The castile formulations did not contain any preservatives, no microbiological risk was observed during their shelf life. All soap based raw materials and castil formulations have a two-year shelf life. These castile soaps are 100% soluble in water.

Conclusion: This article documents the laboratory-scale production of six soap based raw materials and the development of five castile formulations for personal and household cleaning. Super fat method optimized the total amount of caustic required for the saponification of natural vegetable oils such as olive oil, coconut oil, castor oil and maintains the oils in the product at the maximum level without allowing the presence of free caustic in the final product. Super fat castile soaps are the safest personal and household cleaning products because they don't contain caustic residue, have their long shelf life and feature high solubility in water minimizing the risk of residue on skin and surface.

Keywords: Castile soap, super fat, vegetable oil, cosmetic products, preservative

INTRODUCTION

Traditional soap bases are obtained by reacting natural vegetable oils or fatty acids with caustic (sodium hydroxide or potassium hydroxide) in an aqueous environment. Although they are alkaline in aqueous solutions, they are the least damaging surfactants to the skin compared with classic petrochemical surfactants. Moreover, they do not change the pH of the skin (1-3).

The most important factor affecting soap formulation is high pH value. The basic pH value (pH: 10-11) has an antimicrobial effect in the final formulations, providing protection against harmful pathogens and viruses.

This eliminates the need to add preservatives to the formulations (1).

Potassium salts of natural soap bases are widely used in personal care products, such as hand soap, shampoo and toothpaste as well as in household cleaning products, especially laundry and dishwashing soaps and surface cleaners (4, 5).

Castile soap is a traditional natural soap that can only be obtained by soaping vegetable oils, predominantly olive oil. The natural glycerine formed in the saponification reaction remains in the soap. Apart from olive oil, the most commonly used vegetable oils are coconut oil, palm kernel oil, hemp seed oil, castor oil and jojoba oil. Castile soap

Corresponding Author: Gokhan Ozokan **E-mail:** gozokan@gmail.com

Submitted: 03.07.2024 **Revision Requested:** 28.07.2024 **Last Revision Received:** 25.10.2024 **Accepted:** 06.11.2024 **Published Online:** 26.11.2024



Content of this journal is licensed under a Creative Commons Attribution-NonCommercial 4.0 International License.

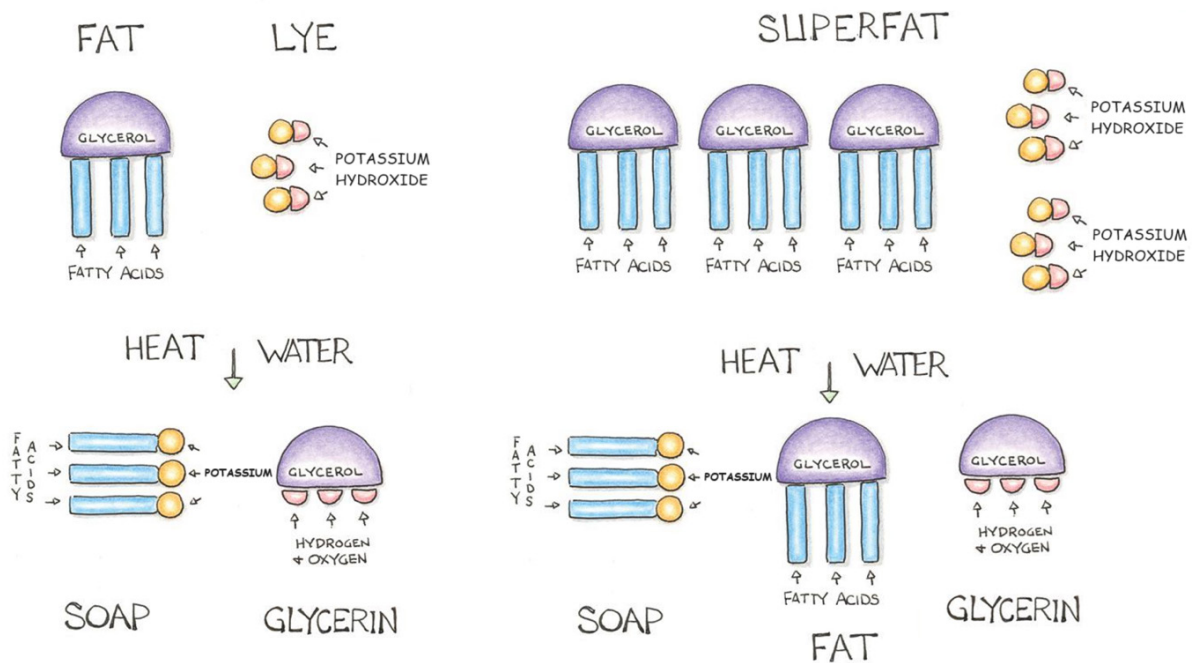


Figure 1. Super fat saponification (<https://infinalab.com/product-testing-service/laboratory-tests-to-determine-ingredients-in-soap/>).

does not contain animal fats or synthetic ingredients. It is a concentrated soap and does not contain thickeners. It is 100% biodegradable (environmentally friendly) and can be used for hand and body cleaning; house, baby and pet washing. The natural pH of castile soap is alkaline (pH: 10), thus it provides an environment in which bacteria and viruses cannot live (4- 6).

The super fat method optimizes the total amount of caustic required for the saponification of natural vegetable oils and maintains the oils in the product at the maximum level without allowing the presence of free caustic in the final product (Figure 1). There are several reasons why soaps may become slightly oilier. Human skin contains a certain amount of sebum (oil), which varies depending on the region. Soaps are made to be oilier to maintain the necessary sebum balance after washing hands with natural liquid soap. Super fat liquid soap maintains the sebum balance after washing hands, while the film formed by the sebum (oil) layer formed in the hand area makes it difficult for water to evaporate from the skin, allowing the skin to remain moist for a long time (7, 8).

Coconut oil and coconut fatty acid are frequently used in soaps. The benefit of coconut oil is that it contains high levels of mono-unsaturated fatty acids, such as palmitic, capric, caprylic, oleic, stearic, and linoleic acids. The lauric acid content of approximately 44-52% ensures that it is oxidation resistant. The main reason for using coconut oil in soap is that it is an extraordinary cleaner with a very high foam quality. Coconut oil is one of the best cleaning substances to be used in soaps. In addition, it has antibacterial and anti-inflammatory properties. It works well with skins that have reddish infections, such as

eczema-prone dry skins and acne-prone oily skins. Coconut oil is also a strong antioxidant. It is a natural moisturizer and has great benefits for the skin (9-14).

Olive oil has been used since Ancient Egypt and Greece and is primarily rich in oleic acid and other monounsaturated fatty acids. In addition to fatty acids, it contains strong antioxidant substances such as polyphenols, squalene and flavonoids. The phenolic substance complex combined with vitamin E synergistically strengthens its preservative effect. Olive oil also has a high antioxidant capacity. Soaps manufactured using olive oil clean skin without irritation. Their rich components provide day-long care for the skin and ensure it stays moisturized throughout the day. Natural soaps based on olive oil help the skin to renew its natural oils to ensure lasting protection, and they do not contain any of the hard chemicals and synthetic odors found in many soaps (15-18).

Castor oil obtained from the seeds of the *Ricinus communis* plant, castor oil is a multipurpose herbal product used by people for thousands of years. Castor oil has several medical, industrial, and pharmaceutical applications. It is generally used as an additive in foods, medications, and skin care products. Castor oil is rich in ricinoleic acid, a mono-unsaturated fatty acid. These types of oils play the role of moisturizers and are used to hydrate the skin. Humectants prevent the loss of water from the external layer of the skin, thus maintaining moisture inside. Castor oil is commonly used in cosmetics to support hydration and is generally added to cosmetic products, such as lotions, make up products and cleaners. Castor oil increases foam in soap and gives it a creamy texture, resulting in an

Table 1. Starting materials for castile soap bases

Starting Material	Trade Name/Supplier	Saponification Number (Calculated)
Coconut Fatty Acid	Distilled Coconut Fatty Acid DNF 300/Evyap	263
Olive Fatty Acid	Greenfac 7986/GreenOleo	196
Pure Olive Oil	Verde N6362/4K Kimya	189
Castor Oil	Pressed Castor Oil/Interfat	167
Gum Rosin	Gum Rosin WW Grade/Hatkim	180
Sweet Almond Oil	Almond oil/Interfat	196
Nettle Seed Oil	Nettle Seed Oil/Mecitefendi	186
Avocado Oil	Organic Avocado Oil/Interfat	186
Jjoba Oil	Jjoba Organic Golden Oil/Jjoba Desert	97

abundant foamy sensation. A ratio of approximately 10% castor oil in soaps has been shown to have beneficial effects (19-21).

Gum rosin also known as colophony or Greek pitch (Latin: *pix græca*), Gum rosin is a solid resin produced by heating fresh liquid resins to vaporize volatile liquid terpene compounds. Gum rosin is obtained from pine trees and other coniferous plants. It is semi-translucent and its color changes from yellow to black. The term 'Colophony' comes from colophonia resina, the name of an ancient Ionian city. It has a mild pine scent. Gum resin is made from residues obtained by distillation of oleoresin from pine trees. Rosin and its chemical derivatives are usually used to make pitch for soaps, lacquer, seal wax, printing ink, dryers, paper dyes, glues, binding agents, solder flux, shiny grease for dyes, and barrels. Furthermore, rosin can be turned into triethylamine acetate to kill algae, bacteria, mold, mollusca and other pests (22-26).

The present study aimed to develop natural soap based raw materials and castile soaps from various vegetable oils such as olive oil, coconut oil, castor oil, almond oil and jjoba oil.

Materials and Methods

Castile soaps were produced using the super fat method by measuring the saponification values of the vegetable oils. Viscosity, pH, appearance, and microbiological tests were performed to determine their shelf life.

pH measurement: The pH electrode was immersed in the solution (2% soap-water dilution) to be measured.

Equipment: Mettler Toledo Seven Excellence; pH Electrode: InLab Expert Pro-ISM

Viscosity measurement: A 100 g sample was poured into a 150ml beaker and a suitable viscometer spindle was dipped into the beaker. Readings were taken at the selected rotation speed (rpm) to measure the unchanging viscosity value for 5 minutes.

Equipment: Brookfield DV3T viscometer; Spindles: RV03, T-Bar C93, T-Bar D94

Calculation of Saponification Number:

Five g oil sample for analysis was weighed and placed into a 250 ml glass conical flask (the exact amount is noted), and 50 ml (approximately 42.43 g) of 0.5 N KOH-EtOH solution was added. The solution was boiled under reflux for 60-90 minutes. After boiling, the solution was allowed to cool to room temperature. 2-3 drops of 1% phenolphthalein solution were added to the solution and titrated with 0.5 N HCl solution (the colour changes from pink to light yellow). The same process was repeated using a blank test.

Preparation of 0.5 N KOH-EtOH: 33 g potassium hydroxide was dissolved in 100ml of pure water. Approximately 900mL of ethyl alcohol is added and the volume is completed in a 1 L volumetric flask.

Saponification value = $28.05 \times (a-b)/c$

a: 0.5 N HCl mL in blank test (50mL KOH-EtOH)

b: 0.5 N HCl mL during saponification

c: amount of oil (grams)

Synthesis of Soap Bases

All syntheses were carried out by heating natural vegetable oils (triglycerides) or fatty acids with a caustic in an aqueous solution. When oil is used, glycerin is formed as a by-product of the saponification reaction. When fatty acids are used, only a soap base is formed (Table 1).

General Synthesis Procedure

Addition of caustic solution: 500 g of fatty acid or vegetable oil was taken into the reaction vessel. 30% potassium hydroxide

Table 2. Reaction conditions

Soap Base	Weight of the Starting Material	Superfat Ratio	Reaction Time (hour)	Reaction Temperature	pH	Total Weight of Soap Base
Potassium Cocoate	500g Coconut Fatty Acid	1.0	1.5	80°C	11.2	1600 g
Potassium Oliviate	500g Olive Fatty Acid	0.88	1.5	80°C	10.7	800 g
Potassium Oliviate	500g Pure Olive Oil	0.88	5	90°C	10.7	800 g
Potassium Castorate	500g Castor Oil	0.92	5	80°C	9.2	750 g
Potassium Rosinate	500g Gum Rosin	1.0	4	90°C	10.4	1500 g
Natural Soap Base for Hair Products	A mixture of 430g Sweet Almond Oil, 40g Nettle seed Oil, 15g Avocado oil and 15g Jojoba Oil	0.90	5	90°C	10.7	750 g

solution was added according to the saponification number and the super fat ratio.

Reaction Monitoring

Heat was applied for one and half hours, and the solution was slowly stirred at approximately 80°C. The pH of the solid soap base in aqueous solution (2%) was measured to determine whether the reaction was complete (Table 2).

Dilution of the Soap Base

The hot solid soap base is then dissolved in hot water and allowed to cool to room temperature. The total weight of the soap is adjusted by adding cool water.

Caustic Formulation

Weight of potassium hydroxide solution = (Weight of Starting Material) x (Saponification Number) x (Super fat ratio) / (% concentration of potassium hydroxide x 10)

Castile Soap Based Formulations

Various amounts of the soap base (potassium cocoate, potassium olivate, etc.) mixtures were created depending on

the intended use of the formulation. The potassium cocoate content is kept high when the intention is to increase its cleaning properties. The rate of potassium olivate, which has a high moisturizing function, is high in viscous products that have a lot of contact with the skin. Natural essential oils (lavender, tea tree lemongrass, orange and eucalyptus) were used in the formulations to increase the antimicrobial effect and for odour-related reasons (Table 3). In addition, various inorganic salts (sodium bicarbonate, sodium carbonate, and sodium citrate), white vinegar and citric acid were used to increase the cleaning properties of the formulations and to adjust their viscosity.

Hand Soap

Potassium olivate, potassium cocoate and potassium castorate were used in this gel formulation. A certain amount of orange oil or lavender oil was added to enhance the antibacterial effect. In addition, white vinegar and baking soda were used to enhance the cleaning properties (Table 4).

Laundry Soap

Only potassium cocoate was used in this liquid formulation. Sodium carbonate and sodium citrate were added to reduce

Table 3. Natural essential oils

Natural Essential oils	INCI/Supplier	Use Level (Product)
Lavender Oil	Lavandula Angustifolia Herb Oil/Sensient	0.2% (Laundry Soap)
Orange Oil	Citrus Sinensis Peel Oil/Ventos	0.4% (Hand Soap)
Lemongrass Oil	Cymbopogon Flexuosus Oil/Sensient	0.25% (Dishwashing Soap)
Tea Tree Oil	Melaleuca Alternifolia Leaf Oil/Sensient	0.05% (Hair Soap)
Eucalyptus Oil	Eucalyptus Globulus Leaf Oil/Nuka	0.05% (Surface Cleaner)

Table 4. Hand soap formulation

Ingredients	% (w/w)
Potassium Oliviate	23.00
Potassium Cocoate	7.00
Potassium Castorate	1.00
Fragrance (Natural Essential Oils)	0.1-0.50
Sodium Bicarbonate	0.25-0.50
Citric Acid or White Vinegar	0.1-0.50
Pure Water	67.5-68.5

the effect of lime in water. In addition, essential oils such as lavender oil or orange oil were used to enhance the antibacterial effect (Table 5).

Surface Cleaner

Potassium rosinate, potassium cocoate, potassium olivate and potassium castorate were used in this liquid formulation. The amount of potassium rosinate was optimized to effectively clean the surfaces and form an anti-pollution layer. In addition, eucalyptus oil was added to enhance the antibacterial effect (Table 6).

Table 5. Laundry soap formulation

Ingredients	% (w/w)
Potassium Cocoate	80.00
Fragrance (Natural Essential Oils)	0.1-0.5
Sodium Carbonate	0.01-0.10
Sodium Citrate	0.01-0.10
Pure Water	19.30-19.88

Table 6. Surface cleaner formulation

Ingredients	% (w/w)
Potassium Oliviate	2.50
Potassium Cocoate	4.00
Potassium Castorate	0.25
Potassium Rosinate	0.25
Fragrance (Natural Essential Oils)	0.05-0.10
Sodium Citrate	0.01-0.05
Pure Water	92.85-92.94

Dishwashing Soap

Potassium cocoate, potassium olivate and potassium castorate were used in this gel formulation. The proportion of potassium cocoate is kept high to maintain the high cleaning properties of dishwashing soap. In addition, sodium carbonate, sodium bicarbonate, white vinegar and lemongrass oil were added to increase the viscosity, rheology and cleaning properties of the product (Table 7).

Hair Soap

A natural soap base consisting of sweet almond oil, nettle seed oil, avocado oil and jojoba oil, potassium cocoate, potassium

Table 7. Dishwashing soap formulation

Ingredients	% (w/w)
Potassium Oliviate	18.50
Potassium Cocoate	25.00
Potassium Castorate	1.00
Fragrance (Natural Essential Oils)	0.1-0.50
Citric acid or White Vinegar	0.1-0.50
Sodium Carbonate	0.75
Sodium Bicarbonate	1.50
Pure Water	52.25-53.05

olivate and potassium castorate was used to provide care for hair. Tea tree oil was used to prevent dandruff (Table 8).

RESULTS

Table 8. Hair soap formulation

Ingredients	% (w/w)
Potassium Oliviate	20.0-25.0
Potassium Cocoate	5.0-10.0
Potassium Castorate	1.0-2.0
Mixture of Sweet Almond Oil, Nettle Seed Oil, Avocado Seed Oil and Jojoba Seed Oil Potassium Soap	2.0-4.0
Fragrance (Natural essential oils)	0.05-0.50
Sodium Bicarbonate	0.25-0.50
Citric Acid or White Vinegar	0.10-0.50
Pure Water	57.5-71.5

Table 9. Physical properties of soap bases

Soap Base	Density at 20°C	Total solid (calculated)	Water solubility at 20°C (w/w, soap/water)
Potassium Cocoate	1.0 ± 0.1 g/cm ³	33%	1.28
Potassium Oliviate (from Fatty Acid)	0.9 ± 0.1 g/cm ³	72%	0.31
Potassium Oliviate (from Oil)	0.9 ± 0.1 g/cm ³	70%	0.33
Potassium Castorate	0.9 ± 0.1 g/cm ³	70%	0.5
Potassium Rosinate	1.0 ± 0.1 g/cm ³	40%	1.0
Natural Soap Base for Hair Products	0.9 ± 0.1 g/cm ³	70%	0.33

Table 10. Stability results of soap bases

Soap Base	Stability (25°C, 60% humidity) 2 years			Stability (40°C, 75% humidity) 6 months		
	pH	Viscosity	Appearance	pH	Viscosity	Appearance
Potassium Cocoate	11.2-11.0	50-55 cP	light yellow liquid	11.2-11.0	50-55 cP	yellow liquid
Potassium Oliviate (from fatty acid)	10.7-10.5	50000-55000 cP	yellow-orange semi-solid	10.7-10.4	50000-60000 cP	orange semi-solid
Potassium Oliviate (from oil)	10.7-10.5	50000-53000 cP	yellow-orange semi-solid	10.7-10.4	50000-55000 cP	orange semi-solid
Potassium Castorate	9.2-9.3	150000-170000 cP	orange-yellow semi-solid	9.2-9.3	150000 -180000 cP	dark orange semi-solid
Potassium Rosinate	10.4-10.5	50-65 cP	dark orange-red liquid	10.4-10.5	50-80 cP	dark red liquid
Natural Soap Base for Hair Products	10.7-10.4	75000-80000 cP	orange semi-solid	10.7-10.4	75000 -85000 cP	dark-orange semi-solid

Six natural soap based raw materials were created in liquid or semi-solid physical form.

When fatty acid forms of vegetable oils are used in saponification reactions, the reactions take one and half hours to complete (using coconut fatty acid or olive fatty acid). For vegetable oils, the reaction time was approximately five hours.

The physical properties of the soap based raw materials are summarized in Table 9. Total solid content is calculated using the following equation. The water solubility of the natural soap based raw materials was observed to be higher than 0.3.

$$\text{Total solid percentage} = (\text{weight of the starting materials}) / (\text{total weight of the soap base}) \times 100$$

The stability results of the soap bases are summarized in Table 10. Only a slight change was observed in the color and viscosity of the soap bases during the two-year period.

Viscosity Measurement: Potassium cocoate (RV03 Spindle, 35 rpm), potassium olivate (T-Bar C93 Spindle, 5 rpm), potassium castorate (T-Bar D94 Spindle, 5 rpm), potassium rosinate (RV03 Spindle, 35 rpm), natural soap base for hair products (T-Bar C93 Spindle, 5 rpm).

Five liquid or gel soap-based formulations were developed using these soap based raw materials.

Pure water (deionized water: <5 µS/cm) must be used in all reactions and formulations to prevent inconsistency in the appearance of the formulations.

One hour of mixing (1000rpm, IKA RW20) is sufficient for the formulations. Transparent appearances were obtained by allowing them to rest for approximately one hour.

The shelf life of natural soap bases and castile soaps is approximately 2 years under room conditions. Viscosity, pH, appearance and microbiological tests were performed to

Table 11. Stability results of formulations

Formulation	Stability (25°C, 60% humidity) 2 years			Stability (40°C, 75% humidity) 6 months		
	pH	Viscosity	Appearance	pH	Viscosity	Appearance
Hand Soap	10.2-10.3	700-800 cP	yellow gel	10.2-10.3	700-850 cP	yellow-orange gel
Laundry Soap	11.2-11.0	10 cP	light yellow liquid	11.2-10.8	10 cP	yellow liquid
Surface Cleaner	10.5-10.2	<10 cP	orange-red liquid	10.5-10.0	<10 cP	orange-red liquid
Dishwashing Soap	10.5-10.2	1500-2000 cP	yellow gel	10.5-10.0	1500-2200 cP	orange gel
Hair Soap	9.9-9.8	1200-1300 cP	orange gel	9.9-9.7	1200-1350 cP	dark orange gel

Table 12. Microbiological test results

Formulation	Water Content (%)	Preservative	Bacteria/mL for 2 years (ISO 21149)	Yeasts and Mould/mL for 2 years (ISO 16212)
Hand Soap	~68	No	< 1	< 1
Laundry Soap	~19	No	< 1	< 1
Surface Cleaner	~92	No	< 1	< 1
Dishwashing Soap	~52	No	< 1	< 1
Hair Soap	~60	No	< 1	< 1

determine the shelf life. The stability results of the formulations are summarized in Table 11. Only slight changes were observed in the color and the viscosity of the formulations during the two-year period.

Viscosity Measurement: Hand soap (RV03 Spindle, 65 rpm), laundry soap (RV03 Spindle, 35 rpm), surface cleaner (RV03 Spindle, 35 rpm), dishwashing soap (RV03 Spindle, 30 rpm), hair soap (RV03 Spindle, 55 rpm).

Microbiological test results of formulations are summarized in Table 12. Generally, microbiological risk is very high in personal and home care formulations with high water content. Although these formulations contained high water content, no microbiological growth was observed during the shelf life. Microbiological tests were performed according to iso standards (27, 28).

DISCUSSION

While there are many publications on industrial surfactants (sls, sles etc.), there are very few studies in the literature on natural soaps. There is also no literature study comparing industrial surfactants with castil soaps. The word soap is used very incorrectly in the cosmetic industry. Every product with surfactants is named soap, but natural soaps are castile (traditional) soaps obtained by the saponification reaction of natural vegetable oils.

This study demonstrates the viability of producing natural soap based raw materials from vegetable oils and fatty acids to reduce costs and increase efficiency when manufacturing personal and household cleaning products.

Castile soap surfactants obtained as a result of natural vegetable oils or fatty acids reacting with a caustic are widely used in cosmetic products and the chemical industry. The trend towards natural and non-toxic raw materials recently has increased the importance of this soap based raw materials. In line with the updates in the Natural Cosmetics Standards (COSMOS, ISO 16128), these soap based raw materials can be called 100% natural (29-31). Although the saponification of vegetable oils using a caustic is a chemical reaction, in Figure 2, the value in the NNI and SyMo columns specified by the standard is 0, and these soap based raw materials are considered 100% natural (or Natural origin index:1).

Natural castile soap formulations have a basic pH (10-11) due to their chemical structure. High pH values have antimicrobial effects and are effective against harmful pathogens and viruses, thus eliminating the need to add preservatives, which often have toxic effects, to the final products. Although the castile formulations did not contain preservatives, no microbiological growth was observed during their 2-year shelf life.

CERTIFICATION LEVEL: COSMOS APPROVED RAW MATERIAL (SCOPE 2)								
Commercial name	INCI	Function	%PPAI	%CPAI	%NNI	%SyMo	Restriction	Approved since
S-Base Hair	Potassium Oleate, Potassium Linoleate, Potassium Palmitate, Potassium Stearate	Surfactant	0	100	0	0		04.04.2024
S-Base PO-FA	Potassium Oliviate	Surfactant	0	100	0	0		04.04.2024
S-Base PC	Potassium Cocoate	Surfactant	0	100	0	0		04.04.2024
S-Base PO-HP	Potassium Oliviate	Surfactant	0	100	0	0		04.04.2024
S-Base PCS	Potassium Castorate	Surfactant	0	100	0	0		04.04.2024
S-BASE PR	Potassium Rosinate	Surfactant	0	100	0	0		04.04.2024
S-BASE MIX	Aqua, Potassium Oliviate, Potassium Cocoate, Potassium Castorate, Vinegar, Sodium Bicarbonate	Surfactant	0	31,5	0	0		04.04.2024

Figure 2. ETKO Cosmos Certificate for soap bases.

CONCLUSION

Synthetic surfactants are generally poorly soluble in water. They remain on dishes, clothes and surfaces after washing, and build up over time. When they come into contact with our bodies, they can cause irritation and allergic effects on the skin surface. In contrast, natural castile soaps are 100% soluble in water, minimizing the risk of residue. This makes it easier to develop personal and household cleaning products that are safer for consumer health.

This article documents the laboratory-scale production of six soap based raw materials and the development of five castile formulations for personal and household cleaning. Super fat method optimized the total amount of caustic required for the saponification of natural vegetable oils maintains the oils in the product at the maximum level without allowing the presence of free caustic in the final product. Super fat castile soaps are believed to be the safest personal and household cleaning products and they have been used safely for centuries.

Ethics Committee Approval: Ethics committee approval was not required because the study used no material or experimental animals that would require approval.

Peer-review: Externally peer-reviewed.

Author Contributions: Conception/Design of Study - G.O.; Data Acquisition - G.O., A.B.; Data Analysis/Interpretation - G.O., A.B.; Drafting Manuscript - G.O.; Critical Revision of Manuscript - G.O.; Final Approval and Accountability - G.O.

Conflict of Interest: The authors declare no conflict of interest.

Financial Disclosure: The authors declare that they received no financial support for this study.

REFERENCES

1. Takagi Y, Kaneda K, Miyaki M, Matsuo K, Kawada H, Hosokawa H. The long-term use of soap does not affect the pH-maintenance mechanism of human skin. *Skin Res Technol* 2015; 21(2): 144-8.
2. Mehling A, Kleber M, Hensen H. Comparative studies on the ocular and dermal irritation potential of surfactants. *Food Chem Toxicol* 2007; 45(5): 747-58.
3. Löffler H, Happle R. Profile of irritant patch testing with detergents: sodium lauryl sulfate, sodium laureth sulfate and alkyl polyglucoside. *Contact Dermatitis* 2003; 48(1): 26-32.
4. Failor C. Making natural liquid soaps: herbal shower gels, conditioning shampoos, moisturizing hand soaps, luxurious bubble baths, and more. USA: Storey Books; 2000.
5. Panda H. Herbal soaps & detergent hand book. India: National Institute of Industrial Research Delhi; 2011.
6. Girgis AY. Production of high quality castile soap from high rancid olive oil. *Grasas y Aceites* 2003; 54(3): 226-33.
7. Thompson J. Liquid soapmaking: tips, techniques and recipes for creating all manner of liquid and soft soap naturally. USA: Jackie Thompson; 2014.
8. Cavitch SM. The natural soap book. USA: Storey Books; 1995.
9. Intahphuak S, Khonsung P, Panthong A. Anti-inflammatory, analgesic, and antipyretic activities of virgin coconut oil. *Pharm Biol* 2010; 48(2): 151-7.
10. Nevin KG, Rajamohan T. Virgin coconut oil supplemented diet increases the antioxidant status in rats. *Food Chem* 2006; 9(2): 260-6.
11. Sari M. The utilization of vco (virgin coconut oil) in manufacturing of solid soap with red betel leaf extract addition. *IOP Conf Ser: Mater Sci Eng* 2018; 335(1): 012038.
12. Peedikayil FC, Remy V, John S, Chandru TP, Sreenivasan P, Bijapur GA. Comparison of antibacterial efficacy of coconut oil and chlorhexidine on streptococcus mutans: an in vivo study. *J Int Soc Prev Community Dent* 2016; 6(5): 447-52.
13. Shahdan IA, Abllah Z, Jalaludin AA, Nasir NAMM. Virgin coconut oil and its antimicrobial properties against pathogenic microorganisms: a review. *Adv Health Sci Res* 2018; 8: 192-9.

14. Varma SR, Sivaprakasam TO, Arumugam I, Dilip N, Raghuraman M, Pavan KB, et al. In vitro anti-inflammatory and skin protective properties of virgin coconut oil. *J Tradit Complement Med* 2018; 9(1): 5-14.
15. Lin TK, Zhong L, Santiago JS. Anti-inflammatory and skin barrier repair effects of topical application of some plant oils. *Int J Mol Sci* 2017; 19(1): 70.
16. Debicka MG, Przychodzen P, Cappello F, Jankowska AK, Gammazza AM, Knap N, et al. Potential health benefits of olive oil and plant polyphenols. *Int J Mol Sci* 2018; 19(3): 686.
17. Cui Z, Xin M, Yin H, Zhang J, Han F. Topical use of olive oil preparation to prevent radiodermatitis: results of a prospective study in nasopharyngeal carcinoma patients. *Int J Clin Exp Med* 2015; 8(7): 11000-6.
18. Waterman E, Lockwood B. Active components and clinical applications of olive oil. *Altern Med Rev* 2007; 12(4): 331-42.
19. Widyasanti A, Ayuningtyas B, Rosalinda S. Characterization of liquid soap from castor oil (*ricinus communis*) with the addition of white tea extracts. *IOP Conf Ser: Earth Environ Sci* 2020; 443: 012061.
20. Patel VR, Dumancas GG, Viswanath LCK, Maples R, Subong BJJ. Castor oil: properties, uses, and optimization of processing parameters in commercial production. *Lipid Insights* 2016; 9: 1-12.
21. Abdulrasheed A, Aroke UO, Muazu MT. Characterization and utilization of castor bean seed oil extract for production of medicated soap. *Am J Eng Res* 2015; 4(12): 67-72.
22. Kugler S, Ossowicz P, Matusiak KM, Wierzbicka E. Advances in rosin-based chemicals: the latest recipes, applications and future trends. *Molecules* 2019; 24(9): 1651.
23. Pohle WD, Speh CF. Detergent action of rosin soaps and fatty acid - rosin soaps. *Oil Soap* 1940; 17: 214-6.
24. Pohle WD. Solubility of calcium soaps of gum rosin, rosin acids and fatty acids. *Oil Soap* 1941; 18: 244-5.
25. Kesler CC. Process of making rosin soap, 1928, US1663764A. Available from: <https://patents.google.com/patent/US1663764A/en>
26. Karlberg AT, Hagvall L. Colophony: rosin in unmodified and modified form, *Kanerva's Occupational Dermatology* 2020; 467-79.
27. ISO 21149-2017 Cosmetics - microbiology - enumeration and detection of aerobic mesophilic bacteria. Available from: <https://www.iso.org/standard/72240.html>
28. ISO 16212-2017 Cosmetics - microbiology - enumeration of yeast and mould. Available from: <https://www.iso.org/standard/72241>.
29. Cosmos Standard Technical Guide, Version 4.0, 1 January 2023. Available from: https://media.cosmos-standard.org/filer_public/a9/35/a935e9a9-6623-4d5d-b0dd-0c56c81417c3/cosmos-standard_v40.pdf
30. ISO 16128-1-2016 Guidelines on technical definitions and criteria for natural and organic cosmetic ingredients and products. Available from: <https://www.iso.org/standard/62503.html>
31. ISO 16128-2-2017 Cosmetics - guidelines on technical definitions and criteria for natural and organic cosmetic ingredients. Available from: <https://www.iso.org/standard/65197.html>

Impact of the COVID-19 Pandemic on the Distribution of Viral Pathogens Involved in Febrile Seizures

Emel Eksi-Alp¹ , Gizem Dikencik-Cuceloglu² , Aytac Goktug¹ , Mahmut Firat Halici³ , Gulser Esen Besli¹ , Eda Kepenekli⁴ 

¹Division of Pediatric Emergency, Department of Pediatrics, Faculty of Medicine, Marmara University, Istanbul, Turkiye

²Department of Pediatrics, Faculty of Medicine, Marmara University, Istanbul, Turkiye

³Department of Pediatrics, Faculty of Medicine, Medeniyet University, Istanbul, Turkiye

⁴Division of Pediatric Infectious Diseases, Department of Pediatrics, Faculty of Medicine, Bahcesehir University, Istanbul, Turkiye

ORCID ID: E.E.A. 0000-0002-6531-6466; G.D.C. 0000-0002-5935-4853; A.G. 0000-0002-0242-2368; M.F.H. 0009-0002-8362-9404; G.E.B. 0000-0001-6837-5384; E.K. 0000-0003-1886-5224

Cite this article as: Eksi-Alp E, Dikencik-Cuceloglu G, Goktug A, Halici MF, Besli GS, Kepenekli E. Impact of the COVID-19 pandemic on the distribution of viral pathogens involved in febrile seizures. *Experimed* 2024; 14(3): 203-209.

ABSTRACT

Objective: To evaluate the impact of the COVID-19 pandemic on the distribution of viral pathogens responsible for febrile seizures (FS) in children.

Materials and Methods: This multicenter study reviewed cases diagnosed as compatible with FS between March 2018 and March 2022. Patients who underwent viral testing were included. Demographic and clinical data were reviewed from the system files.

Results: Laboratory tests targeting viral etiology were performed in 114 of 1683 patients with FS. The viral etiology of FS was consistent before and during the pandemic. The findings demonstrated a statistically significant increase in the number of patients who reported their first FS during the pandemic (81.3%) as opposed to before (63.6%) ($p=0.041$). There were no significant differences in viral test positivity rates before and during the pandemic ($p=0.817$). While influenza virus was mostly isolated in the pre-pandemic period, influenza and SARS-CoV-2 were almost equally isolated in the post-pandemic period.

Conclusion: Febrile seizures are usually benign, with no adverse events. However, this situation may be stressful for families, but identifying the cause can provide relief. The development of rapid diagnostic tests that simultaneously screen for both SARS-CoV-2 and influenza viruses could be valuable for efficient patient follow-up and treatment.

Keywords: Febrile seizure, pandemic, SARS-CoV-2

INTRODUCTION

Severe acute respiratory syndrome coronavirus 2 (SARS-CoV-2), which is responsible for the Coronavirus Disease 2019 (COVID-19) pandemic, emerged in December 2019. After being recognized as a worldwide pandemic, the virus quickly spread to children, and the clinical course, with multiple system involvement, began to be defined for the pediatric population. Patients infected with SARS-CoV-2 initially presented to the pediatric emergency departments (ED) with fever, respiratory and gastrointestinal signs and

symptoms. Soon after, pediatric cases presenting to EDs with central nervous system (CNS) signs and symptoms, such as acute altered mental status, febrile/afebrile seizures, encephalitis and meningitis were identified (1, 2).

The most prevalent seizure type during childhood is febrile seizure (FS). FS is characterized by fever-induced seizure in children aged 6–60 months. To be diagnosed with FS, the patient should not be diagnosed with CNS infection, should not have a history of afebrile seizures, and should not have an acute metabolic abnormality. This condition

Corresponding Author: Emel Eksi-Alp **E-mail:** emel.eksi@gmail.com

Submitted: 19.02.2024 **Revision Requested:** 25.04.2024 **Last Revision Received:** 28.10.2024 **Accepted:** 20.11.2024 **Published Online:** 04.12.2024



Content of this journal is licensed under a Creative Commons Attribution-NonCommercial 4.0 International License.

affects 2-5% of children in Western countries, with a slightly higher incidence in Asian children. If FS occurs only once within 24 hours, lasts less than 15 minutes, and is generalized, it is termed as simple FS. However, if it is focal, persists for more than 15 minutes, or recurs within 24 hours, it is classified as complex FS (3, 4). Viral infections are the most common cause of FS. Influenza virus and human herpes virus-6 (HHV-6) are the most frequently isolated viral pathogens in FS cases because of their potentially high febrile clinical course compared with other infectious agents (5-7). Although FS is most commonly encountered in the infant stage, some cases during the COVID-19 pandemic were diagnosed at an atypical age (8). Since some standardized information did not fully apply in the course of this infectious disease, protective measures have been taken, such as the obligation to wear surgical masks in closed areas, encouraging society to be more careful about hand hygiene, and activating remote working and online education options to reduce crowded environments as much as possible. These measures have decreased the incidence of COVID-19 and other infectious diseases (9).

Currently, information regarding FS in children with COVID-19 is limited, and studies addressing the actual prevalence, frequency, and characteristics of COVID-19-induced FS are scarce. Therefore, significant information gaps exist in this context. The primary aim of our study was to determine the influence of the COVID-19 pandemic on the prevalence of viral agents that contribute to the etiology of FSs. Our secondary objectives included examining the extent to which specific viral agents can be identified in children experiencing FS and delineating the clinical characteristics associated with particular pathogens.

MATERIALS AND METHODS

Study Group

The current multicenter study was conducted at the Pediatric Emergency Departments (EDs) of Marmara University and Medeniyet University, both of which are distinguished by their large tertiary care hospitals in Istanbul, Türkiye. These institutions recorded approximately 120,000 pediatric ED admissions annually. The study included patients with FS who underwent viral testing for respiratory or gastrointestinal infections between March 2018 and March 2022. Patients were grouped into those admitted before and during the pandemic according to the date of 11.03.2020 when the COVID-19 pandemic was declared in Türkiye.

We followed the definition of FS provided by the International League Against Epilepsy and the American Academy of Pediatrics (3, 4). In certain circumstances, FS may occur when body temperature starts to increase, but fever is not detected (10, 11). Therefore, during the admission of patients presenting with seizures, if their body temperature measurements are below 38°C, but they exhibit a fever pattern consistent with the FS definition during pediatric ED follow-ups, they are included in the FS category. Patients diagnosed with FS

(ICD-10 codes R56, R56.0, and R56.8) were reviewed. Eligible records from children aged 6–60 months who presented with FSs and underwent investigations for viral etiology were included. Demographic features, signs and symptoms, vital parameters, nasopharyngeal swab antigen / polymerase chain reaction (PCR) tests, and SARS-CoV-2 PCR results, detailed medical history, presence of FS or epilepsy in the family, fecal rotavirus and adenovirus antigen tests, length of stay (LOS) in the pediatric ED and pediatric ward, and emergency discharge status (discharge, ward admission, pediatric intensive care unit admission or exitus) were recorded for each patient. Patients with progressive chronic neurometabolic diseases or acute metabolic disorders and those aged <6 months or >60 months were excluded. Patients were divided into two groups as 6-24 months (group 1) and 25-60 months (group 2). We investigated whether there was a difference between these groups in terms of SARS-CoV-2 positivity in patients presenting with FS during the pandemic.

Viral Testing

The etiological agents were detected in the central laboratories of the hospitals using routine diagnostic protocols. This study was approved by the Marmara University, Clinical Research Ethics Committee, on July 22, 2022, with number 09.2022.949. In this study, 18 respiratory viruses (SARS-CoV-2, enterovirus, human parainfluenza virus, rhinovirus, bocavirus, adenovirus, human coronavirus [HKU1, NL63, 229E, OC43], human metapneumovirus, Influenza virus A and B, parainfluenza virus 1-2-3-4, respiratory syncytial virus [RSV]) and 2 gastrointestinal viruses (rotavirus, adenovirus) were studied. For the detection of respiratory viruses, CiTest® (Combo Rapid Test), Bio-Speedy® (Bioexen), TUSEB DiaKIT® SARS-COV-2, Coronex® (DS Bio and Nano Technology), and Microcult® (Tıpkımsan), rotavirus and adenovirus combo rapid test cassette (CiTest Diagnostics Inc.) kits for rotavirus and adenovirus antigens in stool were used. There were no restrictions in the continuity of viral testing for SARS-CoV-2 as well as other agents in our centers during the pandemic period.

Statistical Analyses

Statistical analyses were conducted using Jamovi (version 2.3.21.0). Categorical data are presented as numbers and percentages. To evaluate the impact of SARS-CoV-2 on patient distribution, patient data obtained before and during the pandemic periods were analyzed within their respective time frames, and percentages of patients were proportioned according to the number of patients in their period. Means and standard deviations were used for continuous data, whereas abnormally distributed data were depicted as medians (interquartile range [IQR] 25-75%). Nonparametric categorical data were compared using the chi-square test or Fisher's exact test, as required. Intergroup comparisons of non-normally distributed parameters were performed using the Mann-Whitney-U (MWU) test. A $p < 0.05$ was considered significant.

RESULTS

The records of 1683 patients who presented to our pediatric ED with FS were examined. Viral testing was performed in 114 of the patients. The remaining 1,569 patients did not undergo any virologic study. Table 1 presents the demographic and clinical traits of 114 patients. 66 (57.9%) patients were observed before the pandemic and 48 patients (42.1%) were observed during the pandemic. During the pandemic, 30 (62.5%) of the study participants were admitted before the emergence of the SARS-CoV-2 omicron variant. No statistically significant difference was observed in terms of age in the patient groups admitted to the pediatric EDs with FS before and during the pandemic ($p=0.55$, MWU test). In addition to the median age in Table 1, SARS-CoV-2-positive patients had a median age of 26 months (IQR: 15.5-28.5). No noteworthy difference was observed in the distribution of SARS-CoV-2 PCR positivity across age

groups among patients monitored for FS ($p=0.225$). Before the pandemic, the median body temperature of patients was 37.8°C (IQR: 36.8-38.2°C), whereas during the pandemic, it was 38°C (IQR: 37.0-38.5°C). There were no significant differences in body temperature between the two periods ($p=0.329$).

Before the pandemic period, 42 patients (63.6%) presented to the ED with their first FS. During the pandemic, 39 patients (81.3%) presented with their first FS. The proportion of patients with first FS during the pandemic was significantly higher than that before the pandemic ($p=0.041$). Additionally, there was a marked increase in the prevalence of FSs with a familial history among patients before the pandemic ($p=0.009$). The present study investigated additional symptoms reported by patients upon admission to the ED. Notably, cough was the predominant symptom ($n=43$, 37.7%), followed closely by a runny/stuffy nose ($n=41$, 36%). Upon further analysis, we observed a shift in symptom prevalence during the pandemic:

Table 1. Demographic and clinical characteristics of the study population

	Total number of participants n (%)	Before the pandemic n (%)	During the pandemic n (%)	p value
Gender (girls/boys)	41/73 (36/64)	22/44 (33/66)	19/29 (39.5/48)	0.492
Median age, year (IQR)	19 (14–26)	18 (14–26)	21 (14.8–26.3)	0.55
FS type				0.362
Simple	72 (63.7)	44 (66.7)	28 (58.3)	
Complex	42 (36.8)	22 (33.3)	20 (41.7)	
FS, first time	81 (71.1)	42 (63.6)	39 (81.3)	0.041
Family history of FS	42 (36.8)	31 (47)	11 (22.9)	0.009
Family history of epilepsy	12 (10.5)	8 (12.1)	4 (8.3)	0.759
Chronic disease	4 (3.5)	2 (3)	2 (4.2)	1
Neurologic disease	2 (50)	1 (50)	1 (50)	
Cardiac disease	1 (25)	1 (50)		
Gastroenterologic disease	1 (25)		1 (50)	
Additional symptoms				
Cough	43 (37.7)	21 (31.8)	22 (45.8)	0.127
Sneezing	18 (15.8)	9 (13.6)	9 (18.8)	0.460
Runny/stuffy nose	41 (36)	22 (33.3)	19 (39.6)	0.492
Diarrhea	23 (20.5)	17 (25.8)	6 (13)	0.101
Vomiting	12 (10.5)	6 (9.1)	6 (12.5)	0.558
Rash	3 (2.7)	2 (3.1)	1 (2.1)	1
Fever etiology				
Acute upper/lower airway infections	79 (69.3)	46 (69.7)	35 (72.9)	0.695
Acute gastroenteritis	28 (24.6)	16 (24.2)	12 (25)	
Other	7 (6.3)	4 (6.1)	1 (2.1)	

IQR: Interquartile range

while a runny/stuffy nose was the most common additional symptom before the pandemic (n=22, 33.3%), cough took precedence during the pandemic (n=22, 45.8%). However, no statistically significant difference was observed when comparing additional symptoms between different time periods.

Of the 68 tests to determine viral etiology before the pandemic, 44 (64.7%) were positive. During the pandemic, 31 (64.5%) of 48 tests were positive (Figure 1). There was no significant difference in the overall positivity rates between the two periods (p=0.817). Both respiratory tract viruses that could be tested in the laboratory and viral antigen (rotavirus and adenovirus) positivity in stool samples from patients with diarrhea were included in this group. Due to acute gastroenteritis, stool samples of 24 (36.3%) patients before the pandemic and 18 (37.5%) patients during the pandemic were

studied in the laboratory. The positivity rates of the stool test were 7/24 (29.1%) and 5/18 (27.7%), respectively. Research on viral respiratory tract infections was conducted for all samples, except those associated with fecal samples. SARS-CoV-2 PCR was performed on 28 (58.3%) patients admitted during the pandemic, and 10 (35.7%) of them were positive. During the pandemic, 22 (34.4%) of the tests other than SARS-CoV-2 PCR were positive. When comparing the positivity rates between the pre-pandemic and during-pandemic periods, the observed difference approached statistical significance (p=0.059).

The distribution of viruses detected in patients is shown in Figure 2. The influenza virus was the most frequently isolated virus in pre-pandemic tests (n=28, 24.6%). Of the 28 influenza-positive cases, 20 were Influenza A (71.4%), and 8 were Influenza B (28.6%). The most frequently isolated pre-pandemic viruses were enterovirus/rhinovirus (n=5) and rotavirus (n=4), followed by influenza. During the pandemic, Influenza and SARS-CoV-2 viruses were detected almost equally (n=12, 10.5% [Influenza A n=10, 83.3% and Influenza B n=2, 16.6%] and n=11, 9.6%, respectively). There were no statistically significant differences between the distribution of influenza subgroups before and during the pandemic (p=0.693). Rotavirus (n=4) was detected during the pandemic after influenza and SARS-CoV-2.

The median LOS in the ED was 7 h (IQR: 6–8) before and 6 h (IQR: 6–8) during the pandemic. There was no statistical difference between before and during the pandemic in terms of LOS in the ED (p=0.467). Before the pandemic, 17 (25.8%) patients required admission to a pediatric ward, whereas during the pandemic, 21 (41.8%) patients required admission from the ED to a pediatric ward. Accordingly, the hospitalization rate of children included in the study was significantly higher during the pandemic (p=0.044). When the LOS in pediatric EDs was compared, it was 6 h (IQR: 6) in SARS-CoV-2-positive patients and 7 h (IQR: 6–8) in other viral infections that could be detected. Patients with a viral infection other than SARS-CoV-2 positivity had a significantly higher ED LOS (p=0.03). None of

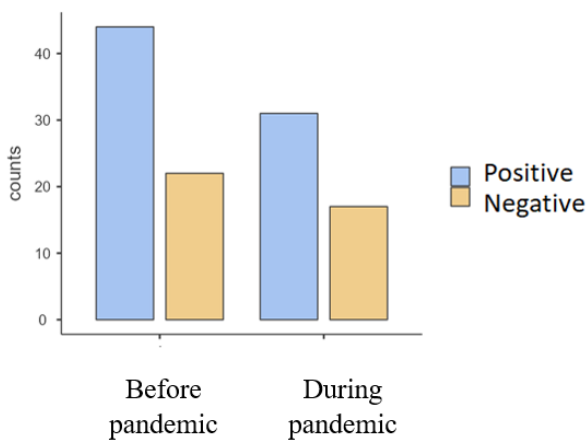


Figure 1. Viral test positivity rates before and during the pandemic.

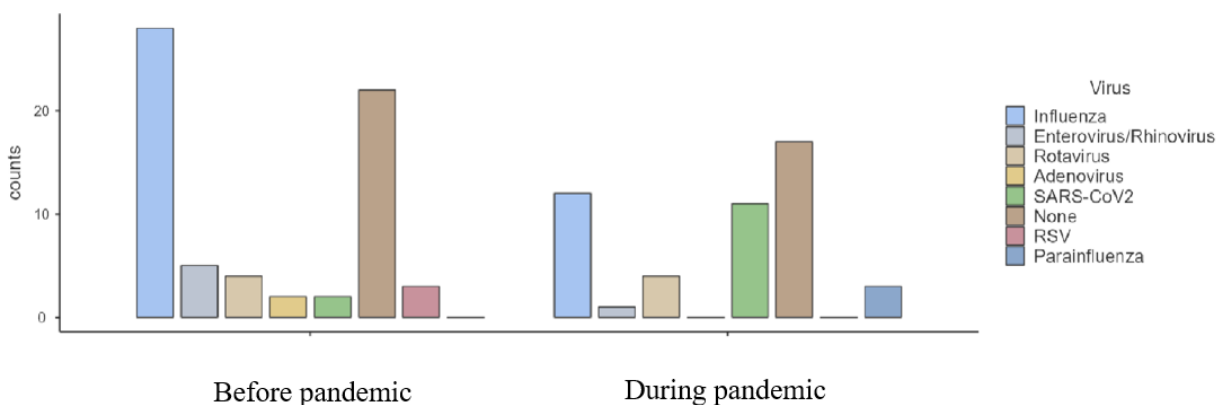


Figure 2. Distribution of viruses detected in patients with febrile convulsions before and during the pandemic (Note: SARS-CoV-2, detected before the pandemic, represents the old type of coronavirus.)

the patients followed up during the study were hospitalized in the intensive care unit, and exitus was not observed.

DISCUSSION

When the demographic data of our study were analyzed, we observed that the median ages of patients with FS were similar before and during the pandemic. Similarly, the mean age of patients admitted with FS during the COVID-19 pandemic was close to the average age before the pandemic (12). However, some studies have shown that FS is also encountered in patients aged >60 months, defined as late-onset FS, especially in the SARS-CoV-2 omicron variant period (13). In our study, we did not encounter any patients with late-onset FS. Certain seizures classified as FS might not actually be FSs because the infection might have migrated to the central nervous system. This could explain how these seizures vary from typical FSs. Further research is needed to determine whether epileptic seizures caused by SARS-CoV-2 infection are truly FS or whether the central nervous system is involved.

In our investigation, in line with the study by Park et al. which explored the impact of the COVID-19 pandemic on respiratory viruses, the frequencies of individuals presenting with first-time FS during the pandemic exhibited a marked increase (14). The higher incidence of first-time FS during the pandemic may be due to strict isolation measures during the pandemic, which resulted in fewer human contacts and reduced the transmission of many infectious agents. Thus, SARS-CoV-2 may have been detected at a relatively higher rate among patients experiencing their first FS episode admitted to pediatric EDs with fever.

It has been reported that FS was more common during the SARS-CoV-2 omicron variant period (11, 15, 16). When we examined the FS admissions in our centers during the pandemic, we determined that there was an intensity of admissions in the time interval before the omicron variant period. For instance, a study by Han et al. in Korea found that 64 out of 33,457 patients diagnosed with COVID-19 had FS, all occurring during the omicron period (17). The discrepancy between our study and other studies during the admission period may be due to the prolonged home isolation practice in our country. Additionally, the extended closure of schools and preschools that provide care for children has contributed to a reduction in viral transmission.

It has been observed that most patients presenting to the pediatric ED with FS have simple FS. In our study, although the rate of patients admitted to the ED with complex FS during the pandemic was higher than that before the pandemic, this difference was not significant. In 2016, a prospective EFES study conducted in Turkiye indicated that a higher percentage of complex FSs were linked to the coronaviruses OC43 and 229 (18). This was also supported by the findings of a study conducted in China, in which complex FS affected 33% of patients, a larger percentage than previously documented. This could be connected to COVID-19's particular neurologic

effects. The fundamental process by which COVID-19 induces seizures may be associated with inflammation and direct viral damage to nerve cells. COVID-19 has a clinical course involving many systems. Being neurotoxic and neuroinvasive, it increases angiotensin-converting enzyme 2 (ACE2) and neuronal infection in cerebral vascular endothelial cells. Therefore, it initiates an inflammation cascade. Cytokines such as Interleukin (IL)-1 β , IL-6, tumor necrosis factor- α , and IL-17 also play a role in inflammation. Children are more prone to FSs because of the hyperinflammatory response caused by the activation of glial cells by these cytokines, which raises nervous system excitability (19, 20).

When the signs and symptoms of the patients enrolled in the study were examined, the most frequent respiratory symptoms, such as cough, runny nose, and stuffy nose, occurred regardless of the time of admission. Most patients continued their follow-up and treatment with a diagnosis of upper or lower respiratory tract infection. Diagnosing patients with fever and FS in the pediatric ED is challenging. In a Korean study by Kim et al., 54.3% of patients reported no symptoms associated with fever. Therefore, to the extent necessary, it is important for patients to be monitored and treated by conducting viral screening according to their symptoms and findings to identify the infection that triggered FS (13).

Viral infections and FS are strongly related (21). A study conducted in Iran by Khiabani et al. revealed that approximately 3% of patients who presented with FS tested positive for SARS-CoV-2 (22). In contrast to this study, we found that during the pandemic, children with FS who were followed up in our pediatric ED had a high SARS-CoV-2 PCR positivity rate in appropriate cases. This high rate can be explained by prioritizing laboratory tests for other possible factors as a result of detailed anamnesis and physical examination before taking a test directly for COVID-19 in patients presenting with FS despite the pandemic period and applying the SARS-CoV-2 PCR test after ruling out other diagnoses for etiology.

Infectious gastroenteritis and influenza virus infections are two separate risk factors for FS in Japan (23, 24). Similar to this study, adenovirus was the most commonly found virus in the EFES study, followed by influenza virus (47.2%) (including influenza A and B, which were identified at 24.3% and 22.9%, respectively), and human RSV (16%) (18). Our study shows that in addition to these data, SARS-CoV-2 should be recognized as a leading infectious agent causing FS.

When the LOS in the pediatric ED was compared before and during the pandemic and according to the type of viral infection, it was found that patients who were SARS-CoV-2-positive and presented to the pediatric ED with FS had a shorter LOS. This may be because COVID-19 infections in children tend to cause milder clinical symptoms compared to adults (25). However, if the admission periods of the cases were considered rather than the viruses detected, the rate of hospitalization of patients in pediatric wards during the pandemic was significantly higher.

This situation can be explained by the fact that, as a result of the measures taken during the pandemic period, there were more vacant beds in the wards of the hospitals as a result of the decrease in intra-community contact; thus, the number of infectious diseases and admission rates to EDs decreased. We can conclude that if there were more beds in the pediatric wards, the LOS in the EDs decreased, and more patients were transferred to the wards.

The current study has several limitations. Due to the retrospective nature of our study, patients lacking an ICD code corresponding to their diagnosis were excluded, potentially introducing selection bias. We did not have the results of the subgroup analysis in patients who were admitted with FS and were SARS-CoV-2-positive, so it was not possible to identify which variant of the virus was more likely to cause FS. Although publications in the literature support that the omicron variant is more associated with FS, we found that the patients in our study during the pandemic period were mostly referred to the pre-omicron.

CONCLUSION

In conclusion, most FS episodes are self-limiting and do not cause any problems. However, families may find them extremely upsetting. Parents tend to ask their children's physicians about the cause of FS, which is also a stressful event for them. When we encounter such a situation in pediatric ED, it is important that we perform etiological tests so that we can both know the disease course and provide the necessary detailed explanation to the family. During the pre-pandemic period, influenza virus was the most commonly detected pathogen in viral tests conducted on patients followed-up in pediatric EDs with a diagnosis of FS. However, during the pandemic, both influenza virus and SARS-CoV-2 played comparable roles in the etiology of FS. Given the urgency of diagnosing febrile illnesses in children, we propose developing rapid diagnostic tests that can simultaneously screen for both SARS-CoV-2 and influenza. Such tests could be valuable for efficient patient follow-up and treatment.

Acknowledgements: The authors thank the microbiology laboratory team who always supported clinicians in emergency departments and all the healthcare workers we lost due to COVID-19 during the pandemic.

Ethics Committee Approval: This study was approved by the Marmara University Clinical Research Ethics Committee on July 22, 2022, with number 09.2022.949.

Peer-review: Externally peer-reviewed.

Authors' Contributions: Conception/Design of Study – E.E.A, E.K.; Data Acquisition, Performing experiments, Data Analysis/ Interpretation and Statistical Analyses – E.E.A., O.G.D., A.G., M.F.H., G.E.B.; Drafting Manuscript – E.E.A., E.K.; Critical Revision of Manuscript – G.E.B., E.K.

Conflicts of Interests: The authors declare that they have no competing interests.

Financial Disclosure: The authors declare that this study has received no financial support.

Clinical Trial Registration: The authors report that this study is not a clinical trial.

REFERENCES

1. Fink EL, Robertson CL, Wainwright MS, Roa JD, Lovett ME, Stulce C, et al. Prevalence and risk factors of neurologic manifestations in hospitalized children diagnosed with acute SARS-CoV-2 or MIS-C. *Pediatr Neurol* 2022; 128: 33-44.
2. Kim Y, Walser SA, Asghar SJ, Jain R, Mainali G, Kumar A. A comprehensive review of neurologic manifestations of COVID-19 and management of pre-existing neurologic disorders in children. *J Child Neurol* 2021; 36: 324-30.
3. Capovilla G, Mastrangelo M, Romeo A, Vigeveno F. Recommendations for the management of "febrile seizures": Ad Hoc Task Force of LICE Guidelines Commission. *Epilepsia* 2009; 50 (Suppl 1): 2-6.
4. Steering Committee on Quality Improvement and Management, Subcommittee on Febrile Seizures American Academy of Pediatrics. Febrile seizures: clinical practice guideline for the long-term management of the child with simple febrile seizures. *Pediatrics*. 2008; 121(6): 1281-6.
5. Pavlidou E, Hagel C, Panteliadis C. Febrile seizures: recent developments and unanswered questions. *Childs Nerv Syst* 2013; 29(11): 2011-7.
6. Çiftçi E, Tuygun N, Özdemir H, Tezer H, Şensoy G, Devrim İ, et al. Clinical and epidemiological features of Turkish children with 2009 pandemic influenza A (H1N1) infection: experience from multiple tertiary paediatric centres in Turkey. *Scand J Infect Dis* 2011; 43 (11-12): 923-9.
7. Britton PN, Blyth CC, Macartney K, Dale RC, Li-Kim-Moy J, Khandaker G, et al. The spectrum and burden of influenza-associated neurological disease in children: combined encephalitis and influenza sentinel site surveillance from Australia, 2013-2015. *Clin Infect Dis* 2017; 65(4): 653-60.
8. Iijima H, Kubota M, Ogimi C. Change in seizure incidence in febrile children with COVID-19 in the era of Omicron variant of concern. *J Pediatr Infect Dis Soc* 2022; 11: 514-57.
9. Sakamoto H, Ishikane M, Ueda P. Seasonal influenza activity during the SARS-CoV-2 outbreak in Japan. *JAMA* 2020; 323(19): 1969-71.
10. Chung S. Febrile seizures. *Korean J Pediatr* 2014; 57(9): 384-95.
11. Houshmandi MM, Moayedi A, Rahmati MB, Nazemi A, Fakhrai D, Zare S. Human herpes virus type 6 and febrile convulsion. *Iran J Child Neurol* 2015; 9(4): 10-4.
12. Salleh H, Soon IS, Chong VH. Frequency and risk factors for febrile seizures during COVID-19 pandemic waves: an observational study. *Eur J Pediatr* 2023; 182(7): 3337-45.
13. Kim JM, Park EG, Lee JY, Kim YH, Kim HS, et al. Characteristics of febrile seizures with SARS-CoV-2 infection in the Omicron era. *Transl Pediatr* 2023; 12(5): 807-15.
14. Park EG, Kim JM, Suh W, Han JY, Han SB. Impact of COVID-19 on the incidence of respiratory viral infections and clinical characteristics of associated febrile seizures. *Transl Pediatr* 2023; 12(4): 528-37.
15. Ludvigsson JF. Convulsions in children with COVID-19 during the Omicron wave. *Acta Paediatr* 2022; 111: 1023-6.

16. Joung J, Yang H, Choi YJ, Lee J, Ko Y. The impact of Omicron wave on pediatric febrile seizure. *J Korean Med Sci* 2023; 38(3): 18.
17. Han MJ, Heo JH, Hwang JS, Jang YT, Lee M, Kim SJ. Incidence of febrile seizures in children with COVID-19. *J Clin Med* 2023; 12(3): 1076.
18. Carman KB, Calik M, Karal Y, Isikay S, Kocak O, Ozcelik A, et al. Viral etiological causes of febrile seizures for respiratory pathogens (EFES study). *Hum Vaccin Immunother* 2019(15): 496-502.
19. Fang C, Zhou Y, Fan W, Zhang C, Yang Y. Clinical features of febrile seizures in children with COVID-19: an observational study from a tertiary care hospital in China. *Front Pediatr* 2023; 11: 1290806.
20. Sawires R, Buttery J, Fahey M. A review of febrile seizures: Recent advances in understanding of febrile seizure pathophysiology and commonly implicated viral triggers. *Front Pediatr* 2021; 9: 801321.
21. Dantzer R. Neuroimmune interactions: from the brain to the immune system and vice versa. *Physiol Rev* 2018; 98(1): 477-504.
22. Soti Khiabani M, Mohammadi MS, Ashrafi MR, Haider SB, Haider SI, Mahmoudi S, et al. Evaluation of patients presenting with febrile seizures in an Iranian referral hospital: emphasis on the frequency of meningitis and co-infections. *BMC Pediatr* 2023; 23(1): 316.
23. Kawakami I, Inoue M, Adachi S, Koga H. The weather condition and epidemics as triggers for febrile seizure: A single-center retrospective observational study. *Epilepsy Behav* 2020; 111: 107306.
24. Keum HR, Lee SJ, Kim JM, Kim SW, Baek HS, Byun JC, et al. Seasonal trend of viral prevalence and incidence of febrile convulsion: A Korea public health data analysis. *Children (Basel)* 2023; 10(3): 529.
25. Ludvigsson JF. Systematic review of COVID-19 in children shows milder cases and a better prognosis than adults. *Acta Paediatr* 2020; 109(6): 1088-95.

Could Increased *Glp1r* Expression via Sitagliptin in the GLP-1/GLP-1 Receptor Axis in the Diet-Induced Obesity Rat Model be Important in Liver Metabolism?

Neslihan Cevik¹ , Gulper Nacarkahya² , Serkan Gurgul³ , Cem Horozoglu⁴ 

¹Institute of Health Sciences, Gaziantep University, Gaziantep, Turkiye

²Department of Medical Biology, Faculty of Medicine, Gaziantep University, Gaziantep, Turkiye

³Department of Biophysics, Faculty of Medicine, Gaziantep University, Gaziantep, Turkiye

⁴Department of Medical Biochemistry, Faculty of Medicine, Halic University, Istanbul, Turkiye

ORCID ID: N.C. 0000-0001-9631-8221; G.N. 0000-0002-8512-8833; S.G. 0000-0002-1450-490X; C.H. 0000-0001-8998-2028

Cite this article as: Cevik N, Nacarkahya G, Gurgul S, Horozoglu C. Could increased *Glp1r* expression via sitagliptin in the GLP-1/GLP-1 receptor axis in the diet-induced obesity rat model be important in liver metabolism? *Experimed* 2024; 14(3): 210-214.

ABSTRACT

Objective: The aim of this study was to evaluate the contribution of sitagliptin, which is used in the treatment of type 2 diabetes mellitus due to its insulinotropic effects, to the levels of glucagon-like peptide-1 (GLP-1) expressed in many systemic tissues in obesity, in liver, skeletal muscle, and fat tissue.

Materials and Methods: Adult Wistar albino rats (n=32) were randomly divided into four groups for 16 weeks of intervention. These groups were control (C) (n=8), obese (Ob) (n=8), sitagliptin (C+Stg) (n=8), and obese (Ob+Stg) given sitagliptin (n=8). *Glp1r* expression in rat liver, muscle, and adipose tissue was confirmed by quantitative real-time PCR.

Results: No significant change was detected in *Glp1r* expression levels in muscle and fat tissue in 4 groups. A 10.64-fold increase in *Glp1r* gene expression was observed in Ob compared to C (p=0.008). Additionally, a 4.03-fold increase in expression level was found in Ob+Stg compared to Ob (p=0.02) and a 12.52-fold increase in expression level was found in Ob+Stg compared to C (p=0.01).

Conclusion: The increased *Glp1r* expression intensity in obese individuals using sitagliptin compared with controls and obese individuals not using sitagliptin may play a role in the reorganization of liver metabolism that is impaired due to obesity, such as the gluconeogenesis process.

Keywords: Sitagliptin, GLP-1, obesity, liver metabolism, Glp1r, GLP1R

INTRODUCTION

Obesity is a risk factor for metabolic and cardiovascular complications and is a health problem with an increasing prevalence worldwide. Type 2 diabetes mellitus (T2DM), a major component of obesity, is associated with impaired glucose tolerance due to insulin resistance. Pancreatic beta cell damage affects insulin secretion and disrupts carbohydrate catabolism in the liver, adipose tissue, muscle, and many other tissues. Glucagon-like peptide-1 (GLP-1)

regulation can be a therapeutic target for the correction of these metabolic problems (1).

GLP-1 and glucose-related insulinotropic peptide (GIP) are the main hormones involved in glucose regulation (2). Both the GIP receptor (GIPR) and the GLP-1 receptor (GLP1R) bind to the G protein-coupled receptor family, activate adenylate cyclase, and cause the activation of cAMP and protein kinase A. K⁺ ions pass out of the cell and Na⁺ ions pass into the cell, causing membrane depolarization, increasing insulin secretion together with the increase in intracellular

Corresponding Author: Cem Horozoglu **E-mail:** cem_horozoglu@hotmail.com

Submitted: 13.10.2024 **Revision Requested:** 12.11.2024 **Last Revision Received:** 15.11.2024 **Accepted:** 02.12.2024 **Published Online:** 10.12.2024



Content of this journal is licensed under a Creative Commons Attribution-NonCommercial 4.0 International License.

Ca²⁺ (3). GLP-1 receptors are expressed in many systems, especially the nervous, circulatory, and respiratory systems. GLP-1 secretion of glucagon results in indirect stimulation of insulin and/or somatostatin secretion. The cellular mechanisms and effects of GLP-1 in preventing glucagon secretion may be better characterized (4).

In healthy individuals, after food intake, the previously released storage insulin (phase 1 insulin) is normally released from the pancreatic beta cells. Then, the insulin produced in the β cells (phase 2 insulin) is released and used. The intestinal hormones GLP-1 and GIP play important roles in glucose homeostasis by stimulating insulin release from the pancreas in the physiological axis and inhibiting glucagon secretion after food intake (5). In patients with T2DM and obesity, the insulin response that should increase after carbohydrate intake is reduced or delayed, glucagon secretion increases, resulting in postprandial hyperglycemia. In other words, pancreatic insulin secretion cannot occur at an adequate level due to the effect of GLP-1, and the insulinotropic effect of incretin hormones in the peptide structure is reduced in obese and T2DM patients (6). Dipeptidyl peptidase-4 (DPP-4) inhibitors are in the group of oral antidiabetic drugs and are currently used in the treatment of T2DM. DPP-4 inhibitors used to treat T2DM prevent the degradation of GLP-1, causing incretin such as GLP-1 to secrete insulin in response to increased blood glucose levels and lower blood glucose levels. This provides lower HbA1c levels (7, 8, 9). GLP-1 improves glucose tolerance and pancreatic α - and β -cell function by suppressing glucose-dependent insulin stimulation and glucagon secretion. It also has extrapancreatic effects, such as slowing gastric emptying and suppressing appetite. Inhibition of DPP-4 activity prolongs the half-life of intact biologically active GLP-1 (10).

Clinical investigations in the literature have focused on the correlation of GLP-1 levels with serum levels, and the reflections of sitagliptin on tissue biochemistry are quite limited. We aimed to evaluate the role of sitagliptin in increasing *Glp1r* (also known as GLP-1; GLP-R1) expression in muscle, liver, and fat tissue of Wistar albino rats.

MATERIALS AND METHODS

Animals

In this study, 32 Wistar albino adult male rats were provided by Gaziantep University Experimental Animal Research Center. For the study, Animal ethics committee approvals were obtained from Gaziantep University Animal Experiments Local Ethics Committee (HADYEK) dated 10.02.2020, numbered 133 protocol 2020/5 and dated 07/06/2020, numbered 32 Protocol 2020/16.

Animal Feeding Protocol and Tissue Procurement

The animals were cared for and fed at the Gaziantep University Experimental Animal Research Center in a room maintained at 20-24°C and 45-65% humidity during a 12-hour day and night cycle.

The control (C) and sitagliptin-control (C+Stg) groups were fed with normal rat chow for 16 weeks, while the obese (Ob) and sitagliptin-obese (Ob+Stg) groups were fed with a high-fat diet (60%). The high fat diet content was 200 g of casein, 3 g of L-cystine, 7.8 g of corn starch, 100 g of maltodextrin10, 172.8 g of sucrose, 50 g of cellulose, 25 g of soybean oil, 177.5 g of animal fat, mineral mixture S10026, 13 g of dicalcium phosphate, 13 g of potassium citrate, 10 g of vitamin mixture W10001 10 g, Choline bitartrate 2 g, Yellow food coloring 0.05 g) (Arden AS, Ankara, Turkiye).

In sitagliptin dose selection, the dose with the lowest liver toxicity and highest bioavailability was selected according to the results of a previous study (11). Sitagliptin (Merck Pharmaceuticals) containing groups were created by gavage at a dosage of 10 mg/kg/day once daily for the second 8 weeks. As a sitagliptin source, sitagliptin hydrochloride monohydrate was prepared by dissolving it in 750 μ L of distilled water with the help of a vortex. At the end of the sixteenth week, general anesthesia (Xylazine-10 mg/kg + Ketamine- 90-100 mg/kg, intraperitoneal) was applied to obtain liver, muscle, and fat tissue samples from all groups, and the tissues were collected. Collected tissues were stored at -80°C.

RNA Isolation and Quantitative Real-Time Polymerase Chain Reaction

A tissue homogenate was created using ceramic bead tubes (Lysing Matrix D 2 mL MP BIO) for 50 mg tissue according to the manufacturer's instructions. RNA was obtained after alcohol-based washing and elution via spin column filter according to the kit instructions (GeneAll Cat No./ID: 305101). Measurements were performed using a spectrophotometer (NanoDrop 8000, DE 19810, Thermo Fisher, USA). cDNA synthesis was performed by following the instructions of the kit containing the Reverse Transcription enzyme (A.B.T.[™] GenEx SYBR Assay, South Korea). Expression of the detected *Glp1r* gene was performed using quantitative real-time PCR (qRT-PCR) with Sybr Green PCR Master mix (A.B.T.[™]) with qRT-PCR Rotor Gene Q (Qiagen). According to the assay protocol, the primer annealing temperature was set to 60°C, and 45 qRT-PCR cycles were performed. Ct values were evaluated according to the formula $2^{-\Delta\Delta Ct}$ to calculate the relative fold change. In this calculation, glyceraldehyde-3-phosphate dehydrogenase (GAPDH) was used as an internal control in all tissues.

Statistical Analyses

The Ct values of *Glp1r* and the Ct values of *GAPDH* as the reference gene were determined for 4 groups in triplicates. The data normalized with *GAPDH* were used to determine fold changes between groups using the $2^{-\Delta\Delta Ct}$ formula. When the distribution of data from the samples was examined, it was observed that they did not show a normal distribution. Accordingly, due to the small number of tissues, the evaluation was performed using the Mann-Whitney U test. p values less than 0.05 were accepted as the significance limit.

RESULTS

Liver *Glp1r* Expression

The changes in the C+Stg, Ob, and Ob+Stg groups and other changes compared with group C are shown in Table 1 and Figure 1. Although a 1.17-fold (0.85 fold change) decrease in *Glp1r* expression was observed in C compared with C+Stg ($p=0.84$), and a 42.18-fold increase in *Glp1r* expression was observed in Ob+Stg compared with C ($p=0.08$), no statistical significance was found. On the other hand, a 10.64-fold increase in *Glp1r* gene expression was observed in Ob compared with C ($p=0.008$). In addition, a 4.03-fold increase in expression level was found in Ob+Stg compared with Ob ($p=0.02$), and a 12.52-fold increase in expression level was found in Ob+Stg compared with C ($p=0.01$).

Glp1r Expression in Skeletal Muscle and Lipid Tissue

The distribution of other groups according to C and fold change are shown in Table 2 and Figure 2. Compared with C, there was a 12.35-fold increase in *Glp1r* gene expression in C+Stg ($p=0.14$), a 2.95-fold increase in Ob ($p=0.22$), and a 4.75-fold decrease in Ob+Stg (fold change 0.21, $p=0.039$). Compared with the C+Stg group, there was a 41.47-fold decrease in the Ob+Stg group ($p=0.57$), and a 5.22-fold decrease in the Ob group ($p=0.37$). In addition, although mild, there was a 0.08-fold decrease in Ob+Stg compared with Ob ($p=0.9$).

DISCUSSION

DPP-4 inhibitors are agents that regulate glucose in an insulinotropic manner via GLP-1 (12). In a sitagliptin-treated T2DM rat model study, showed no change in blood glucose levels but decreased body weight (13). In a study conducted on obese individuals with T2DM, an increase in CB-1R level was detected in diabetic liver after treatment with sitagliptin. It was also reported that weight decreased in both the control and diabetic groups (14). In a study conducted on obese insulin-resistant subjects, an increase in the expression of GIP was detected. It was determined that the receptor status and GLP-1 signaling in adipose tissue increased in obese and insulin-resistant patients (15). In contrast to this study, no significant results were found for *Glp1r* expression in adipose tissue compared to our study when compared with the control. In

a study conducted by Prakash et al. in 2020, they found that sitagliptin regulated adiponectin and activating protein kinase (AMPK) levels in the liver of obese mice (16). They reported that it reduced the amount of adipose tissue that is caused by obesity and that the increase in GLP-1 levels in metabolic syndrome and fatty liver had an effect that is independent of insulin (16). In a study conducted by Nahon et al. in 2018 on patients with prediabetes, they reported that they detected an increase in the expression of the PPAR- γ coactivator- β (*PGC1 β*) gene, which encodes the mitochondrial biogenesis inducer in skeletal muscle, after 12 weeks of sitagliptin administration in males with prediabetes (17). In another study, the increase in genes responsible for the oxidation of fatty acids was evaluated through insulin sensitivity, and it was found that this process was supported by the use of sitagliptin (18, 19). In another study that detected a critical decrease in plasma glucose levels due to 5 weeks of sitagliptin use, the *GIP* expression level increased during this period, but there was no major change in adipose tissue (20). Similarly, significant decreases in VLDL and triacylglycerol levels were detected in overweight men after 6 weeks of sitagliptin use (21, 22). In a study conducted by Li et al. in 2017, sitagliptin and metformin were compared in a study conducted for the treatment of T2DM with an observation period of 12-24 weeks. In this study, they showed that the use of sitagliptin alone reduced weight gain and hypoglycemia. In obese patients, insulin treatment reduced body mass index, hypoglycemia, and cholesterol levels. In this regard, it was reported to be more effective than metformin (23). Supporting this, it has been reported that sitagliptin plays a role in reducing the adiponectin/leptin ratio (24). Although this ratio, which shows the dysfunction of the adipose tissue, suggests that sitagliptin may be an important mediator in lipid biochemistry, no significant result was obtained from the *Glp1r* level in our study. This may be due to the longer-term effect of sitagliptin on the adipose tissue or, as in the previous study, the pathophysiological process in the adipose tissue may be due to adiponectin/leptin and may be secondary to other factors.

In recent years, the roles of sitagliptin in regulating some pathophysiological processes that play a role in obesity and obesity-related disease patterns have been investigated. Results have been obtained indicating that sitagliptin may be effective in suppressing the increased inflammatory response in obesity via cytokines and in eliminating the oxidative

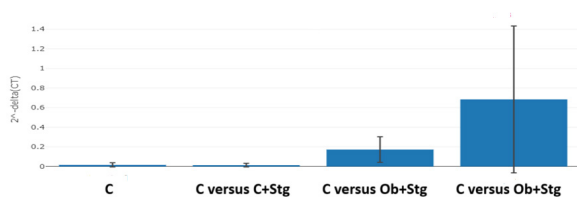


Figure 1. Distribution of *Glp1r* gene expression in liver according to groups.

Table 1. Comparison of *Glp1r* expression in the liver between groups and according to sitagliptin

Group	Fold Change	p value
C versus C+Stg	0.85	0.84
C versus Ob	10.64	0.008
C+Stg versus Ob+Stg	42.90	0.09
C versus Ob+Stg	12.52	0.01
Ob versus Ob+Stg	4.03	0.02
Ob versus C+Stg	42.18	0.08

Table 2. Comparison of *Glp1r* expression in lipid and muscle tissue between groups and according to sitagliptin

GROUPS	Fold Change	p value
Muscle Tissue		
C versus C+Stg	12.35	0.14
C versus Ob	2.95	0.22
C versus Ob+Stg	0.21	0.39
C+Stg versus Ob+Stg	-41.47	0.57
C+Stg versus Ob	-5.22	0.37
Ob versus Ob+Stg	0.08	0.91
Lipid Tissue		
C versus C+Stg	4.55	0.11
C versus Ob	395.03	0.33
C versus Ob+Stg	0.10	0.14
C+Stg versus Ob+Stg	-28.23	0.20
C+Stg versus Ob	86.77	0.33
Ob versus Ob+Stg	0.01	0.24

load brought about by inflammation via malondialdehyde (MDA) (25). As part of this process, because its atherogenic activity can be suppressed via lncRNAs targeting *GLP-1*, and thus endothelial nitric oxide synthase (eNOS) activity can be restored, results obtained can be interpreted as protective of the vascular system (26).

The limited sample size, lack of blood glucose and lipid levels, and single-dose sitagliptin administration are among the limitations of this study. Despite this, some important findings

were identified in our study. Increasing the expression of *Glp1r*, which is known to reduce gluconeogenesis in the liver and reduce liver steatosis and thus have a blood sugar-regulating effect, is an important therapeutic target in obesity, which is a multifactorial condition. The increase in *Glp1r* expression between the control and obese groups in our study shows that we have created an experimentally accurate obesity model. This suggests that sitagliptin can be used to regulate liver metabolism to reverse obesity. In obese patients, muscle atrophy in muscle tissue, high fat retention in muscle, and impaired amino acid metabolism are also factors that increase progression. Increased muscle perfusion induced by GLP-1 receptor-mediated signals and the transport of oxygen and insulin to myocytes are among the factors that contribute to progression. In our study, *Glp1r* levels did not significantly increase in the sitagliptin-treated groups. This suggests that sitagliptin does not play an extensive role in the correction of muscle-based pathophysiological processes in obesity. Similarly, although a decrease in *Glp1r* was observed in Ob+Stg compared with C in fat tissue, no statistical relationship was found. This suggests that sitagliptin is limited in regulating processes such as fatty acid oxidation, intracellular cholesterol transport, and white adipocyte differentiation, which are associated with adipose tissue-based pathophysiology in obesity.

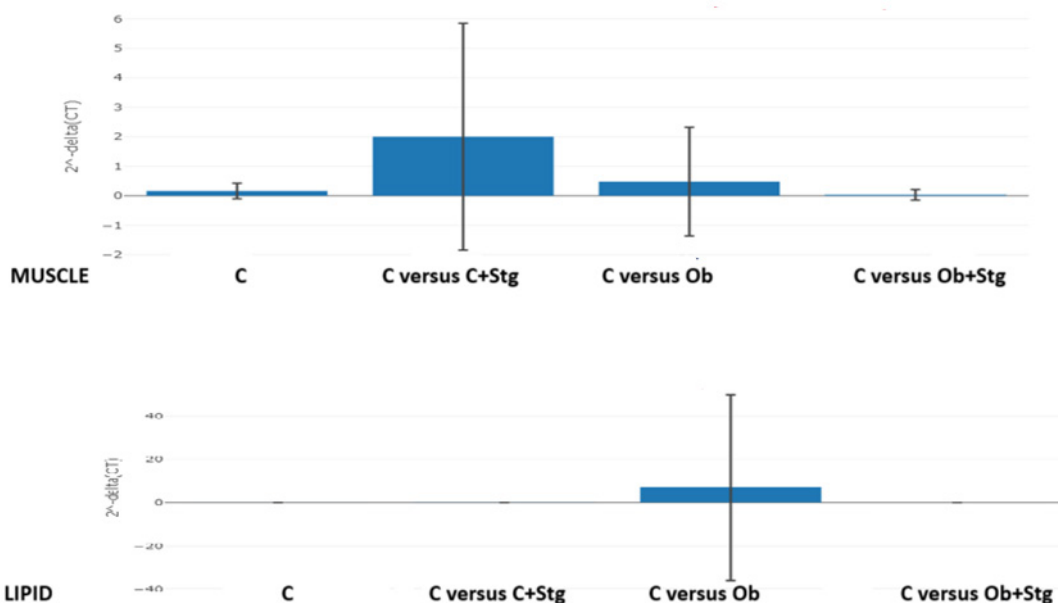


Figure 2. Distribution of *Glp1r* expression in lipid and muscle tissues according to groups.

Ethics Committee Approval: For the study, Animal ethics committee approvals were obtained from Gaziantep University Animal Experiments Local Ethics Committee (HADYEK) dated 10.02.2020, numbered 133 protocol 2020/5 and dated 07/06/2020, numbered 32 Protocol 2020/16.

Peer-review: Externally peer-reviewed.

Author Contributions: Conception/Design of Study – N.C., G.N., S.G., C.H.; Data Acquisition – N.C., G.N., S.G., C.H.; Data Analysis/ Interpretation - N.C., G.N., S.G., C.H.; Drafting Manuscript – N.C., G.N., S.G., C.H.; Critical Revision of Manuscript – N.C., G.N., S.G., C.H.; Final Approval and Accountability – N.C., G.N., S.G., C.H.

Conflict of Interest: The authors declare no conflict of interest.

Financial Disclosure: The authors declare that they received no financial support for this study.

REFERENCES

- Burcelin R, Gourdy P. Harnessing glucagon-like peptide-1 receptor agonists for the pharmacological treatment of overweight and obesity. *Obes Rev* 2017; 18(1): 86-98.
- Scott LJ. Sitagliptin: A review in type 2 diabetes. *Drugs* 2017; 77(2): 209-24.
- Sheikh A. Direct cardiovascular effects of glucagon like peptide-1. *Diabetol Metab Syndr* 2013; 5(1): 47.
- Nauck MA, Heimesaat MM, Behle K, Holst JJ, Nauck MS, Ritzel R, et al. Effects of glucagon-like peptide 1 on counterregulatory hormone responses, cognitive functions, and insulin secretion during hyperinsulinemic, stepped hypoglycemic clamp experiments in healthy volunteers. *J Clin Endocrinol Metab* 2002; 87: 1239-46.
- McIntosh CH, Demuth HU, Pospisilik JA, Pederson R. Dipeptidyl peptidase IV inhibitors: how do they work as new antidiabetic agents? *Regul Pept* 2005; 128(2): 159-65.
- Mannucci E, Pala L, Ciani S, Bardini G, Pezzatini A, Sposato I, et al. Hyperglycaemia increases dipeptidyl peptidase IV activity in diabetes mellitus. *Diabetologia* 2005; 48(6): 1168-72.
- Kosat E. Sitagliptin'in rat karaciğer ve böbrek dokusunda oksidatif stres metabolizması üzerine etkisi. Adnan Menderes Üniversitesi, Sağlık Bilimleri Enstitüsü, Yüksek Lisans Tezi. 2011.
- Dupre J, Behme MT, Hramiak IM, McFarlane P, Williamson MP, Zabel P, et al. Glucagon-like peptide I reduces postprandial glycemic excursions in IDDM. *Diabetes*. 1995; 44(6): 626-30.
- Ahrén B. DPP-4 inhibitors. *Best Pract Res Clin Endocrinol Metab* 2007; 21(4): 517-33.
- Roberge JN, Brubaker PL. Secretion of proglucagon-derived peptides in response to intestinal luminal nutrients. *Endocrinology* 1991; 128(6): 3169-74.
- Hewedy WA. Effects of treatment with sitagliptin on hepatotoxicity induced by acetaminophen in mice. *Brazilian J Pharma Sci* 2020; 56: e18482.
- Karasiç A, Aschner P, Katzeff H, Davies MJ, Stein PP. Sitagliptin, a DPP-4 inhibitor for the treatment of patients with type 2 diabetes: a review of recent clinical trials. *Curr Med Res Opin* 2008; 24(2): 489-96.
- Coskun ZM, Koyuturk M, Karabulut S, Bolkent S. CB-1R and GLP-1R gene expressions and oxidative stress in the liver of diabetic rats treated with sitagliptin. *Pharmacol Rep* 2017; 69(4): 822-9.
- O'Harte FP, Gray AM, Abdel-Wahab YH, Flatt PR. Effects of non-glycated and glycated glucagon-like peptide-1(7-36) amide on glucose metabolism in isolated mouse abdominal muscle. *Peptides* 1997; 18(9): 1327-33.
- Kato H, Nagai Y, Ohta A, Tenjin A, Nakamura Y, Tsukiyama H, et al. Effect of sitagliptin on intrahepatic lipid content and body fat in patients with type 2 diabetes. *Diabetes Res Clin Pract* 2015; 109(1): 199-205.
- Prakash S, Rai U, Kosuru R, Tiwari V, Singh S. Amelioration of diet-induced metabolic syndrome and fatty liver with sitagliptin via regulation of adipose tissue inflammation and hepatic Adiponectin/AMPK levels in mice. *Biochimie* 2020; 168: 198-209.
- Nahon KJ, Doornink F, Straat ME, Botani K, Martinez-Tellez B, Abreu-Vieira G, et al. Effect of sitagliptin on energy metabolism and brown adipose tissue in overweight individuals with prediabetes: a randomised placebo-controlled trial. *Diabetologia*. 2018; 61(11): 2386-97.
- Akaslan SB, Degertekin CK, Yılmaz G, Cakir N, Arslan M, Toruner FB. Effects of sitagliptin on nonalcoholic fatty liver disease in diet-induced obese rats. *Metab Syndr Relat Disord* 2013; 11(4): 243-50.
- Tahara A, Matsuyama-Yokono A, Shibasaki M. Effects of antidiabetic drugs in high-fat diet and streptozotocin-nicotinamide-induced type 2 diabetic mice. *Eur J Pharmacol* 2011; 655(1-3): 108-16.
- Yang F, Dang S, Lv H, Shi B. Combined treatment with a gastric inhibitory polypeptide receptor antagonist and a peptidyl peptidase-4 inhibitor improves metabolic abnormalities in diabetic mice. *J Int Med Res* 2021; 49(1): 300060520985664.
- Tremblay AJ, Lamarche B, Kelly I, Charest A, Lépine MC, Droit A, et al. Effect of sitagliptin therapy on triglyceride-rich lipoprotein kinetics in patients with type 2 diabetes. *Diabetes Obes Metab* 2014; 16(12): 1223-9.
- Hematyar J, Rashidi H, Zakerkish M, Payami SP, Ghaderian SB. Effect of sitagliptin versus glibenclamide on glycemic markers, lipid profile inflammatory and oxidative stress factors in type 2 diabetes patients: a double-blinded randomized controlled trial. *Maedica (Bucur)* 2022; 17(4): 762-70.
- Li S, Li H, Wang R, Zhang JP. The effect of sitagliptin on obese patients with insulin treatment-induced diabetes mellitus. *Eur Rev Med Pharmacol Sci* 2017; 21(15): 3490-5.
- Shams HA, Aziz HM, Al-Kuraishy HM. The potential effects of metformin and/or sitagliptin on leptin/adiponectin ratio in diabetic obese patients: a new therapeutic effect. *J Pak Med Assoc* 2024; 74(10 (Supple-8)): 241-5.
- Wang X, Weng W, Cui Y, Zou C. Sitagliptin alleviates obesity in immature mice by inhibiting oxidative stress and inflammation. *Reprod Sci* 2024; 31(11): 3549-59.
- Zong Y, Wang X, Zhang Y, Tan N, Zhang Y, Li L, Liu L. Sitagliptin ameliorates Creb5/IncRNA ENSMUST00000213271-mediated vascular endothelial dysfunction in obese mice. *Cardiovasc Drugs Ther* 2024; 38(4): 679-91.

Determining Prostate Cancer-Related Pathways and the Role of the *RPH3AL* Gene

Didem Seven¹ , Omer Faruk Bayrak¹ 

¹Department of Medical Genetics, Yeditepe University School of Medicine, Istanbul, Turkiye

ORCID ID: D.S. 0000-0003-3406-5905; O.F.B. 0000-0001-7562-6604

Cite this article as: Seven D, Bayrak OF. Determining prostate cancer-related pathways and the role of the *RPH3AL* gene. Experimed 2024; 14(3): 215-220.

ABSTRACT

Objective: Prostate cancer is the fifth leading cause of death worldwide. Treatment modalities for advanced prostate cancer include androgen deprivation therapy (ADT), chemotherapy, radiotherapy, and targeted therapy. Transcriptomic profiling in prostate cancer enhances our understanding of the disease at the molecular level, facilitating more accurate diagnosis and personalized treatment choices, and ultimately improving patient outcomes. Identifying new therapeutic biomarkers for prostate cancer is important for developing targeted therapy options. This study aimed to elucidate the pathways associated with prostate cancer and identify differentially expressed genes.

Materials and Methods: An RNA-seq dataset, GSE210205, was used to reveal transcriptomic differences between prostate cancer and benign prostate cell lines. GEO2R analysis, GSEA analysis, WebGestalt analysis, and GEPIA analyses were performed to generate differentially expressed genes, identify enriched pathways, and investigate gene expression in prostate cancer.

Results: Pathways such as Wnt/ β -catenin signaling, DNA IR-induced double-strand breaks, cellular response via ATM, Type II interferon signaling, and TGF- β signaling were enriched in the prostate cancer transcriptome. Among the five most over-expressed genes, *RPH3AL* was the most prominent.

Conclusion: *RPH3AL* is a potential biomarker for prostate cancer based on transcriptomic profiling. Further investigation is required to validate the role and potential of this agent as a therapeutic target.

Keywords: Prostate cancer, transcriptomic profiling, *RPH3AL*, TGF- β

INTRODUCTION

Prostate cancer is the second most frequently diagnosed cancer in men and the fifth leading cause of death globally, with 1.6 million new diagnoses and 366,000 deaths annually attributed to this condition. Risk factors for prostate cancer include age, African American ethnicity, and a family history of the disease, with potential influences from diet and other factors (1). The introduction of widespread screening for prostate-specific antigen (PSA) led to a high increase in the incidence of prostate cancer. In cases of localized prostate cancer, in which the tumor remains confined within the prostate gland and has not metastasized to adjacent tissues or distant organs, primary treatment modalities typically

include radical prostatectomy (RP) and whole-prostate radiation therapy. As the disease progresses to more severe stages, involving local invasion into nearby tissues and metastasis to distant sites, systemic medical therapies become predominant. Common sites of metastasis in prostate cancer include the bones, lymph nodes, liver, and lungs. The presence of metastasis significantly affects the prognosis and treatment strategy of prostate cancer patients (2). In advanced stages, androgen deprivation therapy (ADT) serves as the cornerstone treatment, often followed by radiotherapy, chemotherapy, immunotherapy, and targeted therapy. The widespread adoption of these interventions underscores the importance of effectively managing and addressing the potential complications associated with each

Corresponding Author: Didem Seven **E-mail:** didem.seven@yeditepe.edu.tr

Submitted: 27.06.2024 **Revision Requested:** 16.08.2024 **Last Revision Received:** 23.10.2024 **Accepted:** 06.12.2024 **Published Online:** 11.12.2024



Content of this journal is licensed under a Creative Commons Attribution-NonCommercial 4.0 International License.

treatment modality (3). Unraveling the molecular pathogenesis of cancer requires a better understanding of the genetic and molecular mechanisms responsible for its onset, progression, and dissemination. This knowledge is essential for developing targeted therapies, predicting outcomes, and improving personalized treatment strategies. Transcriptomic profiling in prostate cancer enhances our understanding of the disease at the molecular level, facilitating more accurate diagnosis and personalized treatment choices, and ultimately improving patient outcomes (4). Prostate cancer initiation and progression are driven by a complex interplay of genetic, epigenetic, and environmental factors. Identifying the pathways involved in prostate cancer progression is crucial for understanding disease progression and developing targeted therapies.

To better understand cancer predisposition, many researchers have focused on Genome-Wide Association Studies (GWAS). These studies on genetic susceptibility identified the rs7212943 variant, located within the *RPH3AL* gene, as a potential regulatory variant involved in the regulation of exocytosis in endocrine and exocrine cells (5). Additionally, the single nucleotide polymorphisms (SNPs) rs461251 and rs684232, which contain cis-regulatory elements, are associated with promoters that interact with the *RPH3AL* gene through H3K27Ac modifications in prostate cancer (6). Downregulation of the *RPH3AL* gene has been observed in bladder cancer and is associated with the development of muscle-invasive tumors. To the best of our knowledge, the expression of this gene has not been reported in prostate cancer.

In this study, we identified pathways associated with prostate cancer pathogenesis using an RNA-seq dataset, focusing on the expression of *RPH3AL*.

Materials and Methods

Prostate Cancer Dataset

To elucidate the molecular dynamics underlying the aggressive phenotype of prostate cancer compared with benign

prostate tissue, the following cell lines were utilized: BPH-1, an immortalized cell line derived from benign prostatic hyperplasia, is frequently used as a human model for studying prostate growth and physiology (7). DU 145, an epithelial cell line, was isolated from the brain of a 69-year-old Caucasian male with prostate cancer, whereas PC-3 was derived from a bone metastasis of prostate cancer (8, 9). The Gene Expression Omnibus (GEO) database provided RNA-seq data for the aforementioned cell lines (accession number GSE210205). This dataset includes 4 replicates of each BPH-1, DU145, and PC3 cell lines. We employed both Differential Expression (via GEO2R) and Gene Set Enrichment Analysis (GSEA) analysis techniques to evaluate the GEO data.

GEO2R analysis

GEO2R is an analytical tool designed to examine gene expression data retrieved from the GEO database. It is particularly valuable for conducting comparative analyses of gene expression across different experimental conditions or groups. Using GEO2R, we performed differential expression analysis to identify differentially expressed genes in tumor cells compared with benign control cells, with a false discovery rate of 0.001. Following the tool's guidelines, raw counts were used to assess gene expression using DeSeq2, with normalization of median ratios to normalize sequencing depth and RNA composition. As the samples were from a specific study, normalization for sequence depth had a minimal impact (10). The analysis included volcano plots. The volcano plot, in turn, visualizes differentially expressed genes by plotting statistical significance ($-\log_{10}(p \text{ value})$) against the magnitude of change ($\log_2(\text{fold change})$), allowing an intuitive display of genes that are both statistically significant and have substantial gene expression changes. Differentially expressed genes were identified by filtering the expression data, with a p value threshold of <0.001 and a \log_2 fold change value of ≥ 0.5 based on default settings, previous studies, and upon inspecting the size of the resulting gene set that were differentially expressed between tumor and benign cells.

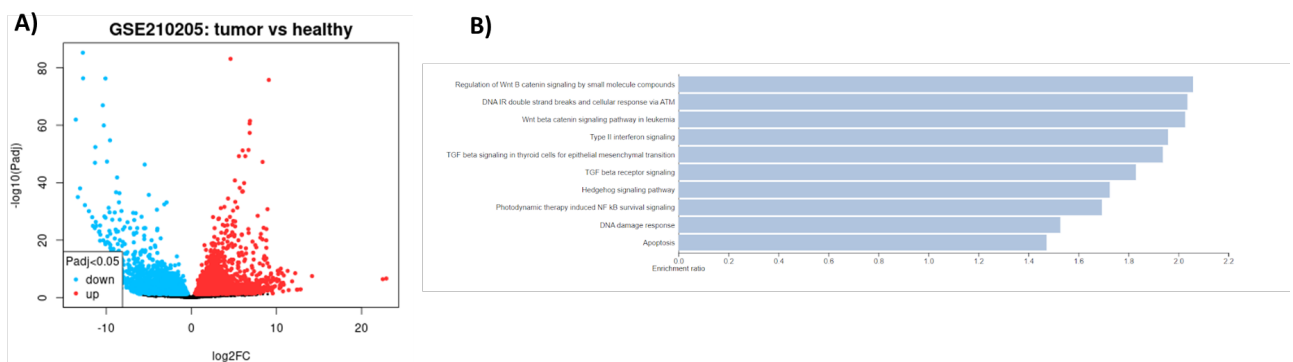


Figure 1. The volcano plot illustrates differentially expressed genes, with upregulated genes represented by red dots and downregulated genes represented by blue dots. B) The bar graph presents the results of the Over-Representation Analysis (ORA), highlighting the top 10 enriched pathways. The x-axis displays the enrichment ratio, whereas the y-axis lists the pathways in descending order of enrichment.

Gene Set Enrichment Analysis of RNA-seq Data

GSEA is a computational technique used to assess whether predefined sets of genes are over-represented in a large set of genes, with possible associations with different phenotypes. The data analysis was performed using the GSEA tool (version 4.1.0). The gene sets used for GSEA were obtained from Database C4 of MSigDB (<http://www.broad.mit.edu/cancer/software/gsea>). C4 refers to a set of gene sets that are computationally defined by mining large collections of cancer-oriented microarray data (11). The specific parameters employed in the GSEA were as follows: the number of permutations was set to 100, and the type of permutation was configured to the gene set to address any potential issues arising from a limited sample size.

WebGestalt Analysis

The WEB-based Gene Set Analysis Toolkit (WebGestalt) is a robust and versatile platform for GSEA and various other forms of gene set enrichment analysis. This approach empowers researchers to input a list of genes and evaluate their enrichment across biological contexts, including signaling pathways, disease associations, and gene ontology categories. In WebGestalt, it was performed over-representation analysis (ORA) using wikipathways cancer with the following parameters: the organism of interest was *Homo sapiens*, and only gene symbols from the gene list were used ($p=0.001$).

GEPIA

Gene Expression Profiling Interactive Analysis (GEPIA) is a web-based platform that integrates RNA sequencing data from the Cancer Genome Atlas (TCGA) and the Genotype-Tissue Expression (GTEx) project. It allows users to explore and analyze gene expression patterns in tumor and normal tissues, offering insights into the functional relationships, prognostic significance, and potential molecular interactions across various cancer types and healthy tissue counterparts. The mRNA expression of *RPH3AL* was determined for prostate cancer. GEPIA also facilitates survival analysis based on gene expression levels, employing the log-rank test, also known as the Mantel-Cox test, to evaluate hypotheses. This analysis allows users to assess the correlation between gene expression and patient survival outcomes (12).

RESULTS

The dataset has 2566 differentially expressed genes with a $p<0.001$. 1128 of the genes were downregulated while 1438 were upregulated. A volcano plot generated from the Geo2R analysis illustrates the statistical significance ($-\log_{10}$ p value) against the magnitude of the expression difference (\log_2 fold change) (Figure 1A). Regulation of Wnt Beta catenin signaling, DNA IR double-strand breaks, cellular response via ATM, Type II interferon, and TGF beta signaling were the most enriched pathways according to the Webgestalt analysis (Figure 1B).

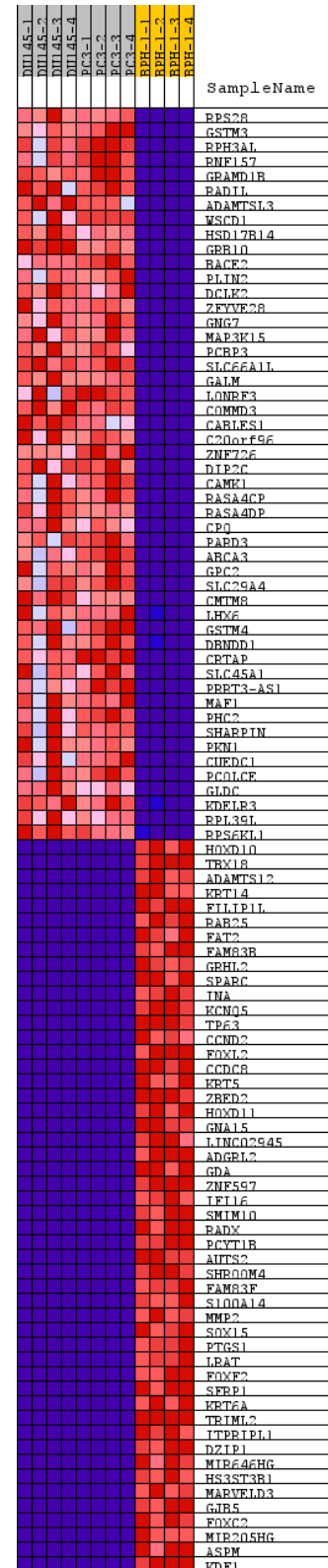


Figure 2. Heatmap of differentially expressed genes (DEGs) derived from GSE210205. Red indicates high gene expression and purple represents downregulated expression.

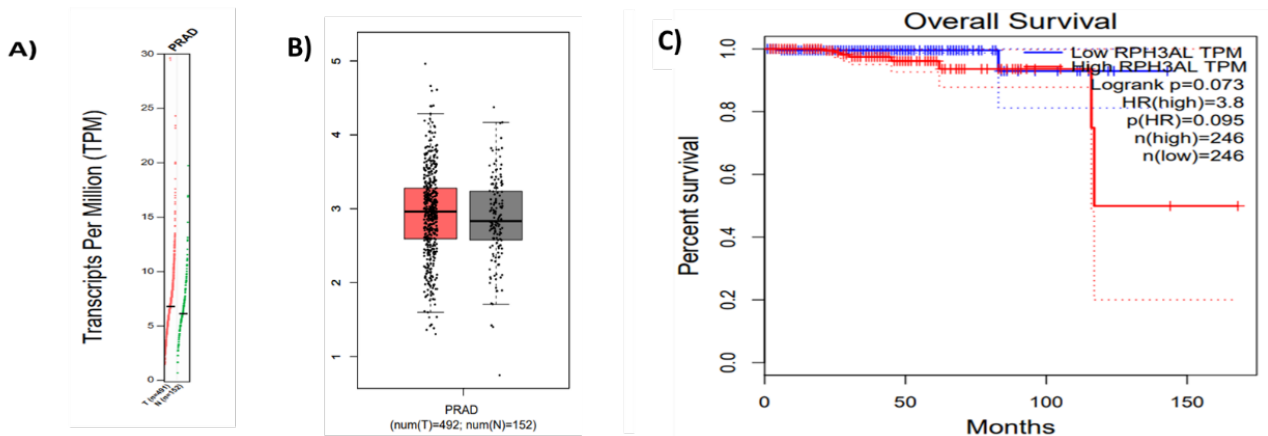


Figure 3. A) *RPH3AL* gene read count in healthy and prostate cancer samples. Green dots represent healthy prostate tissue, while red dots indicate cancerous tissue, showing increased levels of the *RPH3AL* transcript in cancer samples. B) Expression levels of *RPH3AL* in tumor and healthy tissue. Boxplot showing the increased level of *RPH3AL* mRNA levels compared with healthy tissue. C) Overall survival graph for prostate cancer patients in relation to *RPH3AL* gene expression, demonstrating that higher levels of *RPH3AL* are associated with decreased survival rates.

The heatmap generated by GSEA is shown in Figure 2. Among the five most over-expressed genes, *RPH3AL* was identified. The association between *RPH3AL* and prostate cancer has not been previously investigated. Previously, this gene was considered a biomarker of colorectal cancer. Therefore, we decided to conduct an in-depth analysis of this gene in patients with prostate cancer.

GEPIA analysis revealed that tumor samples exhibited higher expression of the *RPH3AL* gene compared with benign prostate tissue (Figure 3A). The mRNA expression levels in tumor and normal tissues were analyzed using the GEPIA database (<http://gepia.cancer-pku.cn>), which incorporates data from 492 tumor samples and 152 normal samples derived from the TCGA and GTEx datasets. The expression levels of *RPH3AL* in patients with prostate cancer were specifically evaluated. Boxplots were used to visualize the expression levels in both tumor and normal tissues, and differential expression analysis was conducted using one-way ANOVA (Figure 3B). Additionally, higher expression of the *RPH3AL* gene was associated with a lower survival rate in prostate cancer (Figure 3C).

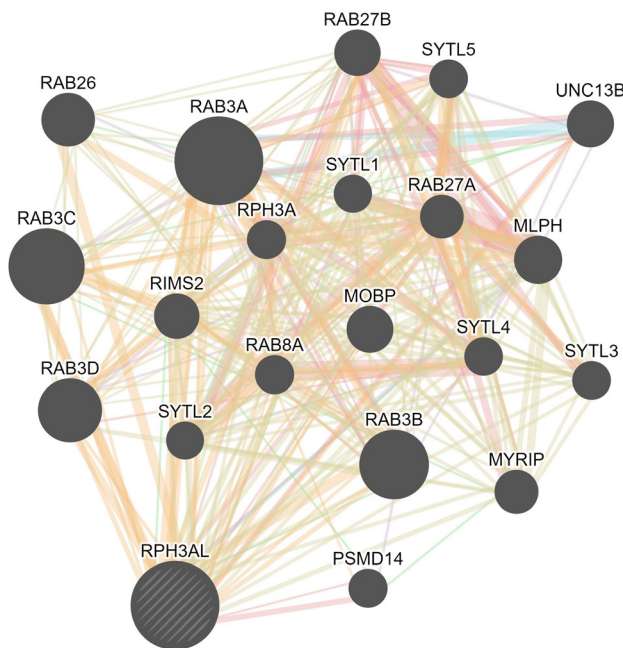


Figure 4. *RPH3AL* gene interaction network generated using GeneMANIA analysis. The network illustrates various types of interactions associated with the *RPH3AL* gene: pink lines represent physical interactions, purple lines indicate co-expression, green lines show genetic interactions, and yellow lines denote predicted interactions.

We analyzed *RPH3AL* gene interactions using GeneMANIA (Figure 4). The database prediction revealed that *RPH3AL* exhibited physical interactions with members of the RAB family, which are small GTPases involved in regulating intracellular membrane trafficking.

DISCUSSION

The management of prostate cancer has evolved significantly over the past decade because of substantial advances in understanding the genomic landscape and underlying biology of prostate cancer. However, the heterogeneity, particularly in advanced prostate cancer, presents a challenge in combating diverse cancer cell populations. Identifying appropriate therapeutic targets is vital for effectively treating prostate cancer and improving patient outcomes. This study aimed to identify the responsible pathways and potential biomarkers associated with prostate cancer by analyzing the GSE210205 dataset. By comparing benign and metastatic prostate cancer cell lines, we sought to identify significant differences that may inform therapeutic targets and diagnostic markers. Our specific objectives include elucidating the molecular mechanisms

driving prostate cancer progression and identifying critical genes and pathways that could function as biomarkers or therapeutic targets.

The expression of Wnt ligands and secreted Wnt antagonists is frequently dysregulated in prostate cancer, leading to outcomes that often do not correlate with the anticipated effects of these proteins on the stability of β -catenin. Prostate cancer commonly exhibits aberrant expression and mislocalization of β -catenin (13,14). Consistent with these observations, the most significantly enriched pathway identified was the regulation of Wnt/ β -catenin signaling. In mammalian cells, the occurrence of double-strand breaks (DSBs) triggers a robust cellular response, including checkpoint signaling and repair mechanisms, or cell death through apoptosis. Central to this process is the MRN (MRE11/RAD50/NBS1) complex, which binds to DSBs and facilitates the activation of the Ataxia Telangiectasia Mutated (ATM) protein. ATM, a critical kinase related to phosphatidylinositol 3-kinase (PI3K), plays a pivotal role in orchestrating the DNA damage response (DDR) (15). In prostate cancer cell lines, an increase in DNA ionizing radiation (IR)-induced double-strand breaks and subsequent cellular response through the ATM pathway was noted. Previous studies have implicated members of this pathway, such as BRCA1 and BRCA2 genes (16), although a direct connection to this specific pathway has not been established. This study is the first to demonstrate an association between prostate cancer, IR-induced double-strand breaks, and cellular response via the ATM pathway. Type II interferon has been identified as an enriched pathway in prostate cancer. This pathway begins with binding of IFN-gamma to its receptor, initiating a phosphorylation cascade involving members of the JAK and STAT protein families (17). Previous studies have suggested interferons as a promising therapeutic approach for advanced prostate cancer (18). Recently, Hagiwara et al. provided evidence that MUC1 may functionally contribute to the activation of the type II interferon pathway in prostate cancer (19).

Finally, enrichment of TGF- β signaling was identified in the prostate cancer dataset. Recently, there has been significant interest in inhibiting TGF- β activity, blocking its receptor binding, and disrupting signaling pathways using small molecule inhibitors. These approaches represent burgeoning research areas with the aim of targeting the tumor microenvironment as a novel therapeutic strategy for prostate cancer (20). Our study highlights TGF- β as a promising therapeutic target for advanced prostate cancer, in line with prior research.

We also identified the most significantly differentially expressed genes. Among the top five highlighted over-expressed genes, *RPH3AL* (Rabphilin 3A Like (without C2 domains)) also called NOC2, was over-expressed in tumor cell lines and exhibited minimal expression in benign prostate cell lines. The existing literature provides limited information about this gene. *RPH3AL* encodes a protein that regulates calcium-ion-dependent

exocytosis in both endocrine and exocrine cells (21). It was initially identified in medulloblastoma tumors by cloning a tumor suppressor region (22). Recently, Lv et al. identified differentially methylated probes (DMP) for Alzheimer's disease, and *RPH3AL* was found to be glia-specific DMPs (23). In a genetic investigation of kidney function, a relationship was found between the glomerular filtration rate and the *RPH3AL* gene variant (24). In clinical practice, predicted TP53 gene mutations enhance clinical-genomic risk stratification by identifying more aggressive tumors. A study based on gene expression assessment found that TP53 mutation is associated with low expression of *RPH3AL*, whereas high expression indicates the wild-type TP53 (25). *RPH3AL* exhibited decreased levels of RNA and protein expression in breast cancer tissues compared with normal tissues, suggesting as a biomarker (26). Conversely, the detection of autoantibodies against Rabphilin-3A-like protein has been identified as a potential biomarker in the sera of colorectal cancer patients (27). Genemania analysis of the *RPH3AL* gene demonstrated that the RAB family closely interacts with it. Shibasaki et al. revealed the physical and functional interaction between Noc2 and Rab3 during exocytosis (28).

In addition to the analysis results of the GSE210205 dataset, which contains metastatic DU-145 and PC3 and benign prostate cell lines, GEPIA analysis also showed higher expression of *RPH3AL* in the tumor compared with the normal samples. The patients that exhibit higher expression of *RPH3AL* have a lower percentage of survival. Overall, these data suggest that *RPH3AL* gene acts as an oncogene in prostate cancer.

The results of this initial study indicate that the *RPH3AL* gene serves as a biomarker of prostate cancer progression. However, expression levels in patients and cell lines should also be analyzed using quantitative real-time reverse transcription-polymerase chain reaction (qRT-PCR) to validate these findings. The functional properties of this gene should also be investigated to better understand its impact on prostate cancer. This is the first study to address *RPH3AL* expression in patients with prostate cancer. Further studies are required to elucidate the functional properties of *RPH3AL* in prostate cancer.

Acknowledgment: Extend my deepest gratitude to Dr. Emrah Nikerel for his expert guidance and support in conducting the GSEA analysis.

Ethics Committee Approval: Ethics committee approval was excluded in this study because online bioinformatics tools are open sources and freely used in all research.

Peer-review: Externally peer-reviewed.

Author Contributions: Conception/Design of Study – D.S.; Data Acquisition – D.S.; Data Analysis/Interpretation- D.S.; Drafting Manuscript – D.S.; Critical Revision of Manuscript – D.S., O.F.B.; Final Approval and Accountability – D.S., O.F.B.

Conflict of Interest: The authors declare no conflict of interest.

Financial Disclosure: The authors declare that they received no financial support for this study.

REFERENCES

1. Pernar CH, Ebot EM, Wilson KM, Mucci LA. The epidemiology of prostate cancer. *Cold Spring Harb Perspect Med* 2018; 8(12): a030361.
2. Kulasegaran T, Oliveira N. Metastatic castration-resistant prostate cancer: Advances in treatment and symptom management. *Curr Treat Options Oncol* 2024; 25(7): 914-31.
3. Michaelson MD, Cotter SE, Gargollo PC, Zietman AL, Dahl DM, Smith MR. Management of complications of prostate cancer treatment. *CA Cancer J Clin* 2008; 58(4): 196-213.
4. Fraser M, Berlin A, Bristow RG, van der Kwast T. Genomic, pathological, and clinical heterogeneity as drivers of personalized medicine in prostate cancer. *Urol Oncol-Semin Ori* 2015; 33(2): 85-94.
5. Matsumoto M, Miki T, Shibasaki T, Kawaguchi M, Shinozaki H, Nio J, et al. Noc2 is essential in normal regulation of exocytosis in endocrine and exocrine cells. *Proc Natl Acad Sci U S A* 2004; 101(22): 8313-8.
6. Guo YP. Understanding prostate cancer genetic susceptibility and chromatin regulation: University of Southern California, Doctoral Thesis. 2019.
7. Wu Q, Zhou Y, Chen L, Shi J, Wang CY, Miao L, et al. Benign prostatic hyperplasia (BPH) epithelial cell line BPH-1 induces aromatase expression in prostatic stromal cells via prostaglandin E2. *J Endocrinol* 2007; 195(1): 89-94.
8. Kaighn ME, Narayan KS, Ohnuki Y, Lechner JF, Jones LW. Establishment and characterization of a human prostatic carcinoma cell line (PC-3). *Invest Urol* 1979; 17(1):16-23.
9. Stone KR, Mickey DD, Wunderli H, Mickey GH, Paulson DF. Isolation of a human prostate carcinoma cell line (DU 145). *Int J Cancer* 1978; 21(3): 274-81.
10. Love MI, Huber W, Anders S. Moderated estimation of fold change and dispersion for RNA-seq data with DESeq2. *Genome Biol* 2014; 15(12): 550.
11. Alhamdoosh M, Law CW, Tian L, Sheridan JM, Ng M, Ritchie ME. Easy and efficient ensemble gene set testing with EGSEA. *F1000Res* 2017; 6: 2010.
12. Tang Z, Li C, Kang B, Gao G, Li C, Zhang Z. GEPIA: a web server for cancer and normal gene expression profiling and interactive analyses. *Nucleic Acids Res* 2017; 45(W1): W98-W102.
13. Kypta RM, Waxman J. Wnt/beta-catenin signalling in prostate cancer. *Nat Rev Urol* 2012; 9(8): 418-28.
14. Wang C, Chen Q, Xu H. Wnt/beta-catenin signal transduction pathway in prostate cancer and associated drug resistance. *Discov Oncol* 2021; 12(1): 40.
15. Shibata A, Jeggo PA. ATM's role in the repair of dna double-strand breaks. *Genes (Basel)* 2021; 12(9): 1370.
16. Castro E, Eeles R. The role of BRCA1 and BRCA2 in prostate cancer. *Asian J Androl* 2012; 14(3): 409-14.
17. Fenton SE, Saleiro D, Platanias LC. Type I and II interferons in the anti-tumor immune response. *Cancers (Basel)* 2021; 13(5): 1037.
18. Hastie C. Interferon gamma, a possible therapeutic approach for late-stage prostate cancer? *Anticancer Res* 2008; 28(5B): 2843-9.
19. Hagiwara M, Fushimi A, Bhattacharya A, Yamashita N, Morimoto Y, Oya M, et al. MUC1-C integrates type II interferon and chromatin remodeling pathways in immunosuppression of prostate cancer. *Oncoimmunology* 2022; 11(1): 2029298.
20. Guo W, Liu H, Yan Y, Wu D, Yao H, Lin K, et al. Targeting the TGF-beta signaling pathway: an updated patent review (2021-present). *Expert Opin Ther Pat* 2024; 34(3): 99-126.
21. Eisenhofer G, Huynh TT, Elkahloun A, Morris JC, Bratslavsky G, Linehan WM, et al. Differential expression of the regulated catecholamine secretory pathway in different hereditary forms of pheochromocytoma. *Am J Physiol Endocrinol Metab* 2008; 295(5): E1223-33.
22. Smith JS, Tachibana I, Allen C, Chiappa SA, Lee HK, Mclver B, et al. Cloning of a human ortholog (RPH3AL) of (RNO)Rph3al from a candidate 17p13.3 medulloblastoma tumor suppressor locus. *Genomics* 1999; 59(1): 97-101.
23. Lv L, Zhang D, Hua P, Yang S. The glial-specific hypermethylated 3 untranslated region of histone deacetylase 1 may modulates several signal pathways in Alzheimer's disease. *Life Sciences* 2021; 265: 118760.
24. Martínez Arroyo O. Insights into the role of the RAB3A-RAB27A system on the development of kidney injury associated with type II diabetes mellitus. University of Valencia, Doctoral Thesis. 2024.
25. Chipidza FE, Alshalalfa M, Mahal BA, Karnes RJ, Liu Y, Davicioni E, et al. Development and validation of a novel TP53 mutation signature that predicts risk of metastasis in primary prostate cancer. *Clin Genitourin Cancer* 2021; 19(3): 246-54.e5.
26. Putcha BD, Jia X, Katkooi VR, Salih C, Shanmugam C, Jadhav T, et al. Clinical implications of Rabphilin-3A-Like gene alterations in breast cancer. *PLoS One* 2015; 10(6): e0129216.
27. Chen JS, Kuo YB, Chou YP, Chan CC, Fan CW, Chen KT, et al. Detection of autoantibodies against Rabphilin-3A-like protein as a potential biomarker in patient's sera of colorectal cancer. *Clin Chim Acta* 2011; 412(15-16): 1417-22.
28. Shibasaki T, Seino S. Physical and functional interaction of noc2/rab3 in exocytosis. *Methods Enzymol* 2005; 403: 408-19.

EXPERIMED

AIMS AND SCOPE

Experimed is a scientific, open access periodical published in accordance with independent, unbiased, and double-blinded peer-review principles. It is the official online-only publication of İstanbul University Aziz Sancar Institute of Experimental Medicine and published three times a year in April, August, and December.

The journal targets national and international audiences, has both national and international members in the editorial board, and aims to enhance international author contributions.

As of 2022 the publication language of the journal is only English. The manuscripts submitted for publication in the journal must be scientific work in English.

Experimed aims to contribute to the literature by publishing manuscripts at the highest scientific level on all fields of basic and clinical medical sciences. The journal publishes original articles, case reports, reviews, and letters to the editor that are prepared in accordance with ethical guidelines.

The scope of the journal includes but not limited to; experimental studies in all fields of medical sciences.

The target audience of the journal includes specialists and professionals working and interested in all disciplines of basic and clinical medical sciences.

There are no article processing charges or submission fees for any submitted or accepted articles. All expenses of the journal are covered by the İstanbul University.

Statements or opinions expressed in the manuscripts published in the journal reflect the views of the author(s) and not the opinions of the İstanbul University Aziz Sancar Institute of Experimental Medicine, editors, editorial board, and/or publisher; the editors, editorial board, and publisher disclaim any responsibility or liability for such materials.

Editor in Chief: Prof. Dr. Bedia Cakmakoglu

Address: İstanbul University, Aziz Sancar Institute of Experimental Medicine, Vakıf Gureba Avenue, 34093, Çapa, Fatih, İstanbul, Türkiye

Phone: +90 212 414 2000-33305

Fax: +90 212 532 4171

E-mail: bedia@istanbul.edu.tr

Publisher: İstanbul University Press

Address: İstanbul University Central Campus, 34452 Beyazıt, Fatih / İstanbul - Türkiye

Phone: +90 212 440 0000

EXPERIMED

INSTRUCTIONS TO AUTHORS

Context

Experimed is an international, scientific, open access periodical published in accordance with independent, unbiased, and double-blinded peer-review principles. The journal is the official on-line-only publication of Istanbul University Aziz Sancar Institute of Experimental Medicine and it is published triannually on April, August, and December. The publication language of the journal is English.

Experimed aims to contribute to the literature by publishing manuscripts at the highest scientific level on all fields of basic and clinical medical sciences. The journal publishes original articles, case reports, reviews, and letters to the editor that are prepared in accordance with ethical guidelines.

Editorial Policy

The editorial and publication processes of the journal are shaped in accordance with the guidelines of the International Council of Medical Journal Editors (ICMJE), the World Association of Medical Editors (WAME), the Council of Science Editors (CSE), the Committee on Publication Ethics (COPE), the European Association of Science Editors (EASE), and National Information Standards Organization (NISO). The journal conforms to the Principles of Transparency and Best Practice in Scholarly Publishing (doaj.org/bestpractice).

Originality, high scientific quality, and citation potential are the most important criteria for a manuscript to be accepted for publication. Manuscripts submitted for evaluation should not have been previously presented or already published in an electronic or printed medium. The journal should be informed of manuscripts that have been submitted to another journal for evaluation and rejected for publication. The submission of previous reviewer reports will expedite the evaluation process. Manuscripts that have been presented in a meeting should be submitted with detailed information on the organization, including the name, date, and location of the organization.

Peer-Review Policy

Only those manuscripts approved by its every individual author and that were not published before in or sent to another journal, are accepted for evaluation. Submitted manuscripts that pass preliminary control are scanned for plagiarism using iThenticate software. After plagiarism check, the eligible ones are evaluated by editor-in-chief for their originality, methodology, the importance of the subject covered and compliance with the journal scope. The selected manuscripts are sent to at least three national/international external referees for evaluation and publication decision is given by editor-in-chief upon modification by the authors in accordance with the referees' claims. Editor-in-chief evaluates manuscripts for their scientific content without regard to ethnic origin, gender, sexual orientation, citizenship, religious belief or political philosophy of the authors and ensures a fair double-blind peer review of the selected manuscripts.

Editor in chief does not allow any conflicts of interest between the authors, editors and reviewers and is responsible for final decision for publication of the manuscripts in the Journal.

Reviewers' judgments must be objective. Reviewers' comments on the following aspects are expected while conducting the review.

- Does the manuscript contain new and significant information?
- Does the abstract clearly and accurately describe the content of the manuscript?
- Is the problem significant and concisely stated?
- Are the methods described comprehensively?
- Are the interpretations and conclusions justified by the results?
- Is adequate references made to other Works in the field?
- Is the language acceptable?

Reviewers must ensure that all the information related to submitted manuscripts is kept as confidential and must report to the editor if they are aware of copyright infringement and plagiarism on the author's side.

A reviewer who feels unqualified to review the topic of a manuscript or knows that its prompt review will be impossible should notify the editor and excuse himself from the review process.

The editor informs the reviewers that the manuscripts are confidential information and that this is a privileged interaction. The reviewers and editorial board cannot discuss the manuscripts with other persons. The anonymity of the referees is important.

Ethical Principles

The Journal takes as principle to comply with the ethical standards of World Medical Association (WMA) Declaration of Helsinki – Ethical Principles for Medical Research Involving Human Subjects and WMA Statement on Animal Use in Biomedical Research.

An approval of research protocols by the Ethics Committee in accordance with international standards mentioned above is required for experimental, clinical, and drug studies and for some case reports. If required, ethics committee reports or an equivalent official document will be requested from the authors. For manuscripts concerning experimental research on humans, a statement should be included that shows that written informed consent of patients and volunteers was obtained following a detailed explanation of the procedures that they may undergo. For studies carried out on animals, the measures taken to prevent pain and suffering of the animals should be stated clearly. Information on patient consent, the name of the ethics committee, and the ethics committee approval number should also be stated in the Materials and Methods section of the manuscript. It is the authors' responsibility to carefully protect the patients' anonymity. For photographs that may reveal the identity of the patients, signed releases of the patient or of their legal representative should be enclosed.

For studies involving animals, it is required to obtain approval of research protocols from an ethics committee. The committee reviews protocols to ensure compliance with applicable regulations and guidelines, including the Guide for the Care and Use of Laboratory Animals (8th Edition, 2011) and the International Guiding Principles for Biomedical Research Involving Animals (2012). These guidelines offer comprehensive instructions on how to carry out animal research ethically and humanely and are widely acknowledged as the benchmark for such research.

EXPERIMED

Authors should provide detailed explanation of the ethical treatment of animals in their manuscripts, including measures taken to avoid pain and distress. This is crucial to ensure the humane conduct of the study and enable verification that it conforms to the relevant ethical criteria. The ARRIVE checklist is a useful tool authors can use to present this information clearly and thoroughly.

Registration of Clinical Trials

Any research study (clinical trial) that prospectively assigns human participants or groups of humans to one or more health-related interventions to evaluate the effects on health outcomes' registration should be done following the guidelines at International Clinical Trials Registry Platform (ICTRP). The journal supports the development of registries following the related policy as explained at WAME's Registration of Clinical Trials page.

The data of the studies that received ethics committee approval in Turkey are provided to the International Clinical Trials Registry Platform by the Ministry of Health. Information regarding ethics committee approvals are given in the articles of the journal.

Plagiarism

Experimed is extremely sensitive about plagiarism. All submissions are screened by a similarity detection software (iThenticate by CrossCheck) at any point during the peer-review or production process. Even if you are the author of the phrases or sentences, the text should not have unacceptable similarity with the previously published data.

When you are discussing others' (or your own) previous work, please make sure that you cite the material correctly in every instance.

In the event of alleged or suspected research misconduct, e.g., plagiarism, citation manipulation, and data falsification/fabrication, the Editorial Board will follow and act in accordance with COPE guidelines.

Authorship

Each individual listed as an author should fulfill the authorship criteria recommended by the International Committee of Medical Journal Editors

(ICMJE - www.icmje.org). The ICMJE recommends that authorship be based on the following 4 criteria:

1. Substantial contributions to the conception or design of the work; or the acquisition, analysis, or interpretation of data for the work; AND
2. Drafting the work or revising it critically for important intellectual content; AND
3. Final approval of the version to be published; AND
4. Agreement to be accountable for all aspects of the work in ensuring that questions related to the accuracy or integrity of any part of the work are appropriately investigated and resolved.

In addition to being accountable for the parts of the work he/she has done, an author should be able to identify which co-authors are responsible for specific other parts of the work. In addition, authors should have confidence in the integrity of the contributions of their co-authors.

All those designated as authors should meet all four criterias for authorship, and all who meet the four criteria should be identified as authors. Those who do not meet all four criterias should be acknowledged in the title page of the manuscript.

Experimed requires corresponding authors to submit a signed and scanned version of the authorship contribution form (available for download through <http://experimed.istanbul.edu.tr/en/>) during the initial submission process in order to act appropriately on authorship rights and to prevent ghost or honorary authorship. If the editorial board suspects a case of "gift authorship," the submission will be rejected without further review. As part of the submission of the manuscript, the corresponding author should also send a short statement declaring that he/she accepts to undertake all the responsibility for authorship during the submission and review stages of the manuscript.

Conflict of Interest

The journal requires the authors and all individuals taking part in the evaluation process to disclose any existing or potential conflict of interest (such as financial ties, academic commitments, personal relationships, institutional affiliations) that could unduly influence one's responsibilities. To disclose potential conflicts of interest, the ICMJE Potential Conflict of Interest Disclosure Form should be filled in and submitted by authors as explained in the Author Form of the journal. Cases of a potential conflict of interest are resolved within the scope of COPE Conflict of Interest Flowcharts and ICMJE Conflict of Interest guidelines.

Besides conflict of interest, all financial support received to carry out research must be declared while submitting the paper.

The Editorial Board of the journal handles all appeal and complaint cases within the scope of COPE guidelines. In such cases, authors should get in direct contact with the editorial office regarding their appeals and complaints. When needed, an ombudsperson may be assigned to resolve cases that cannot be resolved internally. The Editor in Chief is the final authority in the decision-making process for all appeals and complaints.

Copyright and Licensing

Authors publishing with the journal retain the copyright to their work licensed under the Creative Commons Attribution-NonCommercial 4.0 International license ("<https://creativecommons.org/licenses/by-nc/4.0/>" CC BY-NC 4.0) which permits unrestricted, non-commercial use, distribution, and reproduction in any medium, provided the original work is properly cited.

Open Access Statement

The journal is an open access journal and all content is freely available without charge to the user or his/her institution. Except for commercial purposes, users are allowed to read, download, copy, print, search, or link to the full texts of the articles in this journal without asking prior permission from the publisher or the author. This is in accordance with the HYPERLINK "<https://www.budapestopenaccessinitiative.org/read>" BOAI definition of open access.

The open access articles in the journal are licensed under the terms of the Creative Commons Attribution-NonCommercial 4.0 International ("<https://creativecommons.org/licenses/by-nc/4.0/deed.en>" CC BY-NC 4.0) license.

EXPERIMED

Disclaimer

Statements or opinions expressed in the manuscripts published in *Experimed* reflect the views of the author(s) and not the opinions of the editors, the editorial board, or the publisher; the editors, the editorial board, and the publisher disclaim any responsibility or liability for such materials. The final responsibility in regard to the published content rests with the authors.

MANUSCRIPT PREPARATION

The manuscripts should be prepared in accordance with ICMJE-Recommendations for the Conduct, Reporting, Editing, and Publication of Scholarly Work in Medical Journals (updated in December 2015 - <http://www.icmje.org/icmje-recommendations.pdf>). Authors are required to prepare manuscripts in accordance with the CONSORT guidelines for randomized research studies, STROBE guidelines for observational original research studies, STARD guidelines for studies on diagnostic accuracy, PRISMA guidelines for systematic reviews and meta-analysis, ARRIVE guidelines for experimental animal studies, and TREND guidelines for non-randomized public behavior.

Manuscripts can only be submitted through the journal's online manuscript submission and evaluation system, available at <http://experimed.istanbul.edu.tr/en/>. Manuscripts submitted via any other medium will not be evaluated.

Manuscripts submitted to the journal will first go through a technical evaluation process where the editorial office staff will ensure that the manuscript has been prepared and submitted in accordance with the journal's guidelines. Submissions that do not conform to the journal's guidelines will be returned to the submitting author with technical correction requests.

Authors are required to submit the following:

- Copyright Agreement Form,
- ICMJE Potential Conflict of Interest Disclosure Form (should be filled in by all contributing authors)

during the initial submission. These forms are available for download at <http://experimed.istanbul.edu.tr/en/>.

Preparation of the Manuscript

Title page: A separate title page should be submitted with all submissions and this page should include:

- The full title of the manuscript as well as a short title (running head) of no more than 50 characters,
- Name(s), affiliations, ORCID IDs and highest academic degree(s) of the author(s),
- Grant information and detailed information on the other sources of support,
- Name, address, telephone (including the mobile phone number) and fax numbers, and email address of the corresponding author,
- Acknowledgment of the individuals who contributed to the preparation of the manuscript but who do not fulfill the authorship criteria.

Abstract: An English abstract should be submitted with all submissions except for Letters to the Editor. The abstract of Original Articles should be structured with subheadings (Objective, Material

and Method, Results, and Conclusion). Please check Table 1 below for word count specifications.

Keywords: Each submission must be accompanied by a minimum of three to a maximum of six keywords for subject indexing at the end of the abstract. The keywords should be listed in full without abbreviations. The keywords should be selected from the National Library of Medicine, Medical Subject Headings database (<https://www.nlm.nih.gov/mesh/MBrowser.html>).

Manuscript Types

Original Articles: This is the most important type of article since it provides new information based on original research. The main text of original articles should be structured with Introduction, Material and Method, Results, and Discussion subheadings. Please check Table 1 for the limitations for Original Articles.

Statistical analysis to support conclusions is usually necessary. Statistical analyses must be conducted in accordance with international statistical reporting standards (Altman DG, Gore SM, Gardner MJ, Pocock SJ. Statistical guidelines for contributors to medical journals. *Br Med J* 1983; 7; 1489-93). Information on statistical analyses should be provided with a separate subheading under the Materials and Methods section and the statistical software that was used during the process must be specified.

Units should be prepared in accordance with the International System of Units (SI).

Editorial Comments: Editorial comments aim to provide a brief critical commentary by reviewers with expertise or with high reputation in the topic of the research article published in the journal. Authors are selected and invited by the journal to provide such comments. Abstract, Keywords, and Tables, Figures, Images, and other media are not included.

Review Articles: Reviews prepared by authors who have extensive knowledge on a particular field and whose scientific background has been translated into a high volume of publications with a high citation potential are welcomed. These authors may even be invited by the journal. Reviews should describe, discuss, and evaluate the current level of knowledge of a topic in clinical practice and should guide future studies. The main text should contain Introduction, Clinical and Research Consequences, and Conclusion sections. Please check Table 1 for the limitations for Review Articles.

Case Reports: There is limited space for case reports in the journal and reports on rare cases or conditions that constitute challenges in diagnosis and treatment, those offering new therapies or revealing knowledge not included in the literature, and interesting and educative case reports are accepted for publication. The text should include Introduction, Case Presentation, Discussion, and Conclusion subheadings. Please check Table 1 for the limitations for Case Reports.

Letters to the Editor: This type of manuscript discusses important parts, overlooked aspects, or lacking parts of a previously published article. Articles on subjects within the scope of the journal that might attract the readers' attention, particularly educative cas-

EXPERIMED

Table 1. Limitations for each manuscript type

Type of manuscript	Word limit	Abstract word limit	Reference limit	Table limit	Figure limit
Original Article	3500	200 (Structured)	30	6	7 or total of 15 images
Review Article	5000	200	50	6	10 or total of 20 images
Case Report	1000	200	15	No tables	10 or total of 20 images
Letter to the Editor	500	No abstract	5	No tables	No media

es, may also be submitted in the form of a "Letter to the Editor." Readers can also present their comments on the published manuscripts in the form of a "Letter to the Editor." Abstract, Keywords, and Tables, Figures, Images, and other media should not be included. The text should be unstructured. The manuscript that is being commented on must be properly cited within this manuscript.

Tables

Tables should be included in the main document, presented after the reference list, and they should be numbered consecutively in the order they are referred to within the main text. A descriptive title must be placed above the tables. Abbreviations used in the tables should be defined below the tables by footnotes (even if they are defined within the main text). Tables should be created using the "insert table" command of the word processing software and they should be arranged clearly to provide easy reading. Data presented in the tables should not be a repetition of the data presented within the main text but should be supporting the main text.

Figures and Figure Legends

Figures, graphics, and photographs should be submitted as separate files (in TIFF or JPEG format) through the submission system. The files should not be embedded in a Word document or the main document. When there are figure subunits, the subunits should not be merged to form a single image. Each subunit should be submitted separately through the submission system. Images should not be labeled (a, b, c, etc.) to indicate figure subunits. Thick and thin arrows, arrowheads, stars, asterisks, and similar marks can be used on the images to support figure legends. Like the rest of the submission, the figures too should be blind. Any information within the images that may indicate an individual or institution should be blinded. The minimum resolution of each submitted figure should be 300 DPI. To prevent delays in the evaluation process, all submitted figures should be clear in resolution and large in size (minimum dimensions: 100 × 100 mm). Figure legends should be listed at the end of the main document.

All acronyms and abbreviations used in the manuscript should be defined at first use, both in the abstract and in the main text. The abbreviation should be provided in parentheses following the definition.

When a drug, product, hardware, or software program is mentioned within the main text, product information, including the name of the product, the producer of the product, and city and the country of the company (including the state if in USA), should

be provided in parentheses in the following format: "Discovery St PET/CT scanner (General Electric, Milwaukee, WI, USA)"

All references, tables, and figures should be referred to within the main text, and they should be numbered consecutively in the order they are referred to within the main text.

Limitations, drawbacks, and the shortcomings of original articles should be mentioned in the Discussion section before the conclusion paragraph.

References

While citing publications, preference should be given to the latest, most up-to-date publications. Authors are responsible for the accuracy of references. References should be prepared according to Vancouver reference style. If an ahead-of-print publication is cited, the DOI number should be provided. Journal titles should be abbreviated in accordance with the journal abbreviations in Index Medicus/ MEDLINE/PubMed. When there are six or fewer authors, all authors should be listed. If there are seven or more authors, the first six authors should be listed followed by "et al." In the main text of the manuscript, references should be cited using Arabic numbers in parentheses. The reference styles for different types of publications are presented in the following examples.

Journal Article: Rankovic A, Rancic N, Jovanovic M, Ivanović M, Gajović O, Lazić Z, et al. Impact of imaging diagnostics on the budget – Are we spending too much? *Vojnosanit Pregl* 2013; 70: 709-11.

Book Section: Suh KN, Keystone JS. Malaria and babesiosis. Gorbach SL, Barlett JG, Blacklow NR, editors. *Infectious Diseases*. Philadelphia: Lippincott Williams; 2004.p.2290-308.

Books with a Single Author: Sweetman SC. *Martindale the Complete Drug Reference*. 34th ed. London: Pharmaceutical Press; 2005.

Editor(s) as Author: Huizing EH, de Groot JAM, editors. *Functional reconstructive nasal surgery*. Stuttgart-New York: Thieme; 2003.

Conference Proceedings: Bengtsson S, Sothemin BG. Enforcement of data protection, privacy and security in medical informatics. In: Lun KC, Degoulet P, Piemme TE, Rienhoff O, editors. *MEDINFO 92. Proceedings of the 7th World Congress on Medical Informatics*; 1992 Sept 6-10; Geneva, Switzerland. Amsterdam: North-Holland; 1992. pp.1561-5.

EXPERIMED

Scientific or Technical Report: Cusick M, Chew EY, Hoogwerf B, Agrón E, Wu L, Lindley A, et al. Early Treatment Diabetic Retinopathy Study Research Group. Risk factors for renal replacement therapy in the Early Treatment Diabetic Retinopathy Study (ETDRS), Early Treatment Diabetic Retinopathy Study Kidney Int: 2004. Report No: 26.

Thesis: Yılmaz B. Ankara Üniversitesindeki Öğrencilerin Beslenme Durumları, Fiziksel Aktiviteleri ve Beden Kitle İndeksleri Kan Lipidleri Arasındaki İlişkiler. H.Ü. Sağlık Bilimleri Enstitüsü, Doktora Tezi. 2007.

Manuscripts Accepted for Publication, Not Published Yet: Slots J. The microflora of black stain on human primary teeth. Scand J Dent Res. 1974.

Epub Ahead of Print Articles: Cai L, Yeh BM, Westphalen AC, Roberts JP, Wang ZJ. Adult living donor liver imaging. Diagn Interv Radiol. 2016 Feb 24. doi: 10.5152/dir.2016.15323. [Epub ahead of print].

Manuscripts Published in Electronic Format: Morse SS. Factors in the emergence of infectious diseases. Emerg Infect Dis (serial online) 1995 Jan-Mar (cited 1996 June 5): 1(1): (24 screens). Available from: URL: [http:// www.cdc.gov/ncidod/EID/cid.htm](http://www.cdc.gov/ncidod/EID/cid.htm).

REVISIONS

When submitting a revised version of a paper, the author must submit a detailed "Response to the reviewers" that states point by point how each issue raised by the reviewers has been covered and where it can be found (each reviewer's comment, followed by the author's reply and line numbers where the changes have been made) as well as an annotated copy of the main document. Revised manuscripts must be submitted within 30 days from the date of the decision letter. If the revised version of the manuscript is not submitted within the allocated time, the revision option may be canceled. If the submitting author(s) believe that additional time is required, they should request this extension before the initial 30-day period is over.

Accepted manuscripts are copy-edited for grammar, punctuation, and format. Once the publication process of a manuscript is completed, it is published online on the journal's webpage as an ahead-of-print publication before it is included in its scheduled issue. A PDF proof of the accepted manuscript is sent to the corresponding author and their publication approval is requested within 2 days of their receipt of the proof.

Editor in Chief: Prof. Dr. Bedia Cakmakoglu

Address: Istanbul University, Aziz Sancar Institute of Experimental Medicine, Vakif Gureba Avenue, 34093, Capa, Fatih, Istanbul, Turkiye

Phone: +90 212 414 2000-33305

Fax: +90 212 532 4171

E-mail: bedia@istanbul.edu.tr

Publisher: Istanbul University Press

Address: Istanbul University Central Campus, 34452 Beyazit, Fatih / Istanbul - Turkiye

Phone: +90 212 440 0000